LARGE-SCALE THERMODYNAMIC ENVIRONMENTS FAVORING INTENSE CONVECTION: A PERSPECTIVE FROM SATELLITE OBSERVATIONS

A Dissertation

by

NANA LIU

BS, Lanzhou University, 2013
MS, Texas A&M University-Corpus Christi, 2016

Submitted in Partial Fulfillment of the Requirements for the Degree of

DOCTOR OF PHILOSOPHY

in

COASTAL AND MARINE SYSTEM SCIENCE

Texas A&M University-Corpus Christi
Corpus Christi, Texas

December 2019

December 2019

LARGE-SCALE THERMODYNAMIC ENVIRONMENTS FAVORING INTENSE CONVECTION: A PERSPECTIVE FROM SATELLITE OBSERVATIONS

A Dissertation

by

NANA LIU

This dissertation meets the standards for scope and quality of
Texas A&M University-Corpus Christi and is hereby approved.

Chuntao Liu, PhD Chair	Feiqin Xie, PhD Committee Member
Philippe Tissot, PhD Committee Member	Toshiaki Shinoda, PhD Committee Member

December 2019

ABSTRACT

Intense convective clouds play an important role in our climate system by redistribution of heat, moisture, and trace gases, as well as producing large quantities of precipitation. These clouds have been increasingly investigated in recent years due to a growing concern that they might become more frequent, longer lived, or more intense in the course of natural and anthropogenic climate change. A better understanding of the favorable thermodynamic and kinematic environments for these events may lead to a more robust description of these cloud processes in climate models.

In this dissertation, 16-years of Tropical Rainfall Measuring Mission (TRMM) observations and ERA-Interim reanalysis data are used to understand the favorable thermodynamic environments for intense thunderstorms globally as well as regionally. The results reveal that intense thunderstorms over various regions share a few common thermodynamic features, i.e. large Convective Available Potential Energy (CAPE: > 1000 J/kg), moderate convection inhibition (CIN: 50-100 J/kg), and abundant moisture convergence associated with low-level jets. However, each region has its own specific features. Over many of these regions, high mountains play an important role by initiation of convection with orographic lifting and also by associated downslope flow at mid-levels forming an inversion above low-level moist air; this substantial convective inhibition helps accumulate higher moist convective energy.

To further examine the relationships between thermodynamic environments and thunderstorm convective intensity, two different statistical models are built to reconstruct the global

distribution of thunderstorms based on the variables derived from the reanalysis data. The first model uses a Bayesian type approach and calculates the probability functions of intense thunderstorms from 16-year TRMM Convective Features and their environments from ERA-Interim. It is found that four variables, including CAPE, CIN, low-level shear, and warm cloud depth (WCD), may be used to derive a geographical distribution of intense thunderstorms that is close to the observations. The second approach utilizes a random forest model to test the relative importance of these four variables globally, as well as regionally. The strong land vs. ocean contrast in the frequency of thunderstorms and some hotspot regions can be closely reproduced with a single model based on the four variables from the reanalysis data. This suggests that the land vs. ocean contrast in convective intensity are largely derived from the fundamental differences in the thermodynamic conditions over land and ocean. The relative importance of the four variables over different regions is also analyzed and discussed using the random forest model. Although these statistic models can still to be improved by taking into account additional variables and samples, they provide a unique foundation toward building a parameterization of convective intensity at the subgrid scale for general circulation models.

This dissertation also investigates the properties of precipitation systems observed by TRMM over different regions under different El Niño–Southern Oscillation (ENSO) phases. The results reveal that pronounced effects from ENSO on deep convection (20 dBZ radar echo tops greater than 10 km) and Mesoscale Convective Systems (MCSs) (area greater than 2000 km^2) are found over specific regions, including the central Pacific, the western Maritime Continent, the eastern Maritime Continent, Gulf of Mexico, Argentina, and Australia. The shift in the spectra of both number and rainfall contribution of precipitation systems as a function of the minimum 85-GHz

Polarization Corrected Temperature during different phases of ENSO, the maximum heights of 20 dBz radar echo, and system area, all suggest that precipitation anomalies over these regions are related to the number of precipitation events, as well as the fraction of deep, intense, and large precipitation systems. These results provide insights in improving precipitation forecast during strong ENSO events in the future.

ACKNOWLEDGEMENTS

I would like to thank Dr. Chuntao Liu for his enormous support and wonderful mentorship throughout these years. I would like to express my appreciation to my committee members, Dr. Philippe Tissot, Dr. Feiqin Xie, and Dr. Toshiaki Shinoda for their guidance and support throughout the course of this research.

I would like to express my thanks to my friends and colleagues - Thomas Lavigne, Lindsey Hayden, Abishek Adhikari, Joseph Hill, Thomas Winning, and Hao Yu, for making my time at Texas A&M University-Corpus Christi an enjoyable experience. Finally, I want to thank my parents and family who were always a great source of motivation, even in face of the great distance.

This research was supported by NASA Precipitation Measurement Mission grants NNX16AD76G under the direction of Dr. Gail Jackson and NNX16AH74G under the direction of Dr. Erich Stocker. Thanks to the Precipitation Processing System (PPS) team at NASA Goddard Space Flight Center, Greenbelt, MD, for data processing assistance.

TABLE OF CONTENTS

CONTENTS PAGE

ACKNOWLEDGEMENTS vi

TABLE OF CONTENTS vii

LIST OF FIGURES ix

LIST OF TABLES xiv

INTRODUCTION 1

CHAPTER I: What are the favorable large-scale environments for the highest flash rate thunderstorms on Earth 6

Abstract 6

Introduction 7

Methods 10

Results 14

Summary and discussion 32

Acknowledgements 36

References 37

CHAPTER II: Relative importance of thermodynamic variables to the world wide variability of thunderstorms 86

Abstract 86

Introduction 87

Data and methods 91

Results 96

Discussion 109

Summary 110

Acknowledgements 113

References 114

CHAPTER III: The variation of the intensity, height and size of precipitation systems with El Niño–Southern Oscillation in the tropics and subtropics 141

Abstract 141

Introduction 142

Data and Methods 145

Results 147

Conclusion 158

Acknowledgements 162

References 163

SUMMARY 184

FUTURE WORK 188

REFERENCES 189

LIST OF FIGURES

FIGURES PAGE

Figure 1.1 Geographical distribution of the population of total CFs and percentage of CFs with different flashes (a) total CFs (b) with no flash (c) with 1-3 flashes, (d) with 3-50 flashes, (e) with > 50 flashes. The distribution is created on a 2° x 2° grid from 16-years (1998-2013) of TRMM observations. 60

Figure 1.2 Seasonal variation of CFs and intense CFs with > 50 flashes. (a) population of total CFs, (b) the percentage of intense CFs with > 50 flashes. 61

Figure 1.3 (a) Locations of CFs (orange crosses: 1-3 flashes; black crosses: > 50 flashes) and topography (color fill) over SCUS. (b) Composite 10 m wind vectors, 2 m temperature (T) (contour), and 2 m relative humidity (RH, color fill) for CFs with > 50 flashes over SCUS. (c) at 850 hPa, (d) at 700 hPa, (e) at 500 hPa, (f) composite CAPE (color fill) and CIN (contour). The bold black cross marks the composite centroid location of the CFs with > 50 flashes. Composite are made using ERA-Interim data starting at the surface pressure. The area with high terrain is left blank in the plot of 850 hPa (b) and 700 hPa (c), if the terrain reaches that level. 62

Figure 1.4 (a) Composite vertical cross-section of wind and RH (color fill) of intense CFs with > 50 flashes along the longitude where CFs occur over SCUS, (b) Difference cross section between intense and weak CFs (1-3 flashes), (c) Same as (a), but along the latitude CFs occur, (d) Same as (b), but along the latitude CFs occur. The thick black lines present the mean near surface pressure. 63

Figure 1.5 Composite profiles of different variables for CFs with different flashes over SCUS, (a) RH(solid) and SH (dashed), (b) Potential and equivalent potential temperature, (c) zonal wind (U), (d) Meridional wind (V). Note the profiles start from the mean near-surface pressure levels. 64

Figure 1.6 Same as Figure 1.3, but for HIMA. 65

Figure 1.7 Same as Figure 1.4, but for HIMA. 66

Figure 1.8 Composite profiles of RH and SH, Potential and equivalent potential temperature for CFs with different flashes in different seasons. (a) RH (solid) and SH (dashed) in spring (MAM), (b) Potential and equivalent potential temperature in MAM, (c) RH in JJA, (d) Potential and equivalent potential temperature in JJA, (e) RH in SON, (f) Potential and equivalent potential temperature in SON. 67

Figure 1.9 Same as Figure 1.3, but for ARGEN. 68

Figure 1.10 Same as Figure 1., but for ARGEN. 69

Figure 1.11 Same as Figure 1., but for ARGEN. 70

Figure 1.12 Same as Figure 1.3, but for COLUM. 71

Figure 1.13 Same as Figure 1.4, but for COLUM. 72

Figure 1.14 Same as Figure 1.5, but for COLUM. 73

Figure 1.15 Same as Figure 1., but for SAHEL. 74

Figure 1.16 Same as Figure 1., but for SAHEL. 75

Figure 1.17 Same as Figure 1., but for SAHEL. 76

Figure 1.18 Same as Figure 1., but for CONGO. 77

Figure 1.19 Same as Figure 1., but for CONGO. 78

Figure 1.20 Same as Figure 1.5, but for CONGO. 79

Figure 1.21 Same as Figure 1.3, but for NWM. 80

Figure 1.22 Same as Figure 1.4, but for NWM. 81

Figure 1.23 Same as Figure 1.5, but for NWM. 82

Figure 1.24 Composite soundings for CFs with 1-3 flashes (dashes lines) and > 50 flashes (solid lines) in different seasons over HIMA. (a) MAM, (b) JJA, (c) SON. The wind barbs are for CFs with > 50 flahes. 83

Figure 1.25 Composite soundings for CFs with 1-3 flashes (dashes lines) and > 50 flashes (solid lines) over different regions. (a) ARGEN, (b)SAHEL, (c)COLUM, (d) SCUS, (e)NWM, (f) CONGO. The wind barbs are for CFs with > 50 flahes. 84

Figure 1.26 Composite hodograph of intense CFs with > 50 flashes over different regions. 85

Figure 2.1 (a) Geographical distribution of the population of TRMM CFs. (b) Geographical distribution of the population of TRMM CFs with more than 50 flashes, (c) Geographical distribution of percentage of the TRMM CFs with more than 50 flashes. The distribution is created on a 2° x 2° grid from 16-years (1998-2013) of TRMM observations. 129

Figure 2.2 Percentage of CFs with more than 50 flashes vs. one specific thermodynamic variable. a) CAPE, b) CIN, c) $SHEAR_{1\text{-}3km}$, d) WCD. The calculations are over land (solid red), ocean (solid blue lines) and all regions (black lines) in 36°S-36°N. The dotted red (blue) lines indicate the number of TRMM CFs over land (ocean) as a function of each variable. 130

Figure 2.3 Percentage of CFs with more than 50 flashes vs. two specific thermodynamic variables jointly. (a) CAPE and CIN, (b) CAPE and $SHEAR_{1\text{-}3km}$, (c) CAPE and WCD, (d) CIN and $SHEAR_{1\text{-}3km}$. Contours represent the distribution of the population of CFs. The color fill shows the percentage of CFs with more than 50 flashes as a function of two variables. 131

Figure 2.4 Estimated geographical distribution of the percentage of intense thunderstorms based on individual environmental variables. a) CAPE, b) CIN, c) $SHEAR_{1\text{-}3km}$. The probability of intense thunderstorms is estimated using the lookup tables shown in Figure 2.2. Thermodynamic variables are derived from 6 hourly ERA-Interim reanalysis data with a 0.75°x0.75° horizontal resolutions. "All" means that land and ocean are considered together when lookup tables are created. 132

Figure 2.5 Same as Figure 2.4, but estimated with two variables. (a) CAPE and CIN, (b) CAPE and $SHEAR_{1\text{-}3km}$, (c) CIN and $SHEAR_{1\text{-}3km}$..... 133

Figure 2.6 Same as Figure 2.4, but estimated with three variables: CAPE, CIN, and $SHEAR_{1\text{-}3km}$. a) No separation of land and ocean, b) Considering land and ocean separately. 134

Figure 2.7 Same as Figures 4-6, but estimated by four variables: CAPE, CIN, $SHEAR_{1\text{-}3km}$, and WCD. a) No separation of land and ocean, b) Considering land and ocean separately. 135

Figure 2.8 Seasonal variations of the observed (solid lines) and estimated (dashed lines) percentage of severe thunderstorms over selected regions (as shown in Figure 2.1c): ARGEN, HIMA, WAFRICA, CAFRICA, and SCUS. The correlations between the observed and estimated of percentage of intense thunderstorms over different regions are shown in the legend. The estimated seasonal variations are created by four atmospheric variables: CAPE, CIN, $SHEAR_{1\text{-}3km}$, and WCD. 136

Figure 2.9 (a) Geographical distribution of the percentage of intense CFs observed by TRMM, (b-d) Estimated geographical distribution of the percentage of intense CFs by global random forest model with (a) two atmospheric variables (CAPE and CIN); (c) three atmospheric variables (CAPE, CIN and SHEAR); (d) four atmospheric variables (CAPE, CIN, SHEAR, and WCD). (e) Normalized difference between the estimation and observations. The geographical distribution of CFs is created on a 5°x5° grid. The global random forest model is created using 16-year (1998-2007) TRMM CFs. 80% of the data is used to build the model, while the remaining 20% of the 16-year CFs is used to test the model. 137

Figure 2.10 The random forest relative importance of the four environmental variables (CAPE, CIN, $SHEAR_{1\text{-}3km}$, WCD) used to predict the occurrence of thunderstorms over different regions. The error bar represents two standard deviations by running the same model 50 times. 138

Figure 2.11 (a) Geographical distribution of the population of CFs with at least one flash observed by TRMM, (b) Estimated geographical distribution of the population of CFs with at least one flash by local random forest model with four atmospheric variables (CAPE, CIN, $SHEAR_{1\text{-}3km}$ and WCD). (c) Normalized difference between the estimation and observations. The geographical distribution of CFs is created on a 10°x10° grid. The local random forest model is created from 16-years (1998-2013) of TRMM CFs. In each grid, 80% of the data is used to build the model, while the remaining 20% of the 16-year CF dataset is used to test the model. Boxes with less than 500 CFs with at least one flash are left blank. 139

Figure 2.12 The geographical distribution of the local random forest relative importance of environmental variables in the process of predicting intense CFs. (a) CAPE, (b) CIN, (c) $SHEAR_{1\text{-}3km}$, (d) WCD..... 140

Figure 3.1 Climatology of unconditional precipitation observed by TRMM PR during 1998 and 2013, (a) Unconditional precipitation (mm/dd), (b) Difference of unconditional precipitation between El Nino and La Nina periods, (c) Normalized difference between El Nino and La Nina (b divide by a), left box with unconditional precipitation less than 0.5 mm/dd as blank. The unconditional precipitation is calculated using TRMM 2A25 near surface precipitation product. The monthly Multivariate El Niño-Southern Oscillation (ENSO) Indices (MEI, Figure 3.2) have been used to separate the El Nino and La Nina conditions (see details in section 2.2). 171

Figure 3.2 Time series of MEI during 1998-2013, red dots present El Nino months, blue dots present La Nina months. Dashed lines present 0.5 and -0.5 MEI. 172

Figure 3.3 Fraction of PFs with MAXHT20 > 10 km during 1998 and 2013 in 2^o x 2^o grids. (a) During El Nino periods, (b) During La Nina periods, (c) Difference between El Nino and La Nina. 173

Figure 3.4 Same as Figure 3.3, but for PFs with area > 2000 km^2. 174

Figure 3.5 (a) Monthly correlation between the MEI and the fraction of PFs with MAXHT20 > 10 km in 2^o x 2^o grids, (b) Monthly correlation between the MEI and the fraction of PFs with area > 2000 km^2. Left boxes with samples < 1000 as blank. 175

Figure 3.6 Monthly correlation between the MEI and the fraction of deep convection and MCSs over selected regions. Fraction of deep convection and MCSs are significantly correlated with the MEI with a p-value less than 0.05. The significant correlation coefficients are marked as larger size than nonsignificant ones. 176

Figure 3.7 Comparison of various of rainfall-related parameters as a function of the maximum 85-GHz PCT (MIN85PCT), the maximum heights of 20-dBZ echo tops (MAXHT20) and size of PFs over different phases of ENSO over central Pacific (CPACI). (a) Annual mean rainfall (solid) and occurrence (dashed) as a function of MIN85PCT, (b) the number (dashed) and volumetric rainfall contribution (solid) to the total PFs as a function of MIN85PCT, (c) same as (a) but as a function of MAXHT20, (d) same as (b) but as a function of MAXHT20, (e) same as (a) but as a function of convective size, (f) same as (b) but as a function of size. 177

Figure 3.8 Same as Figure 3.7, but for Eastern Maritime Continent (EMC)..... 178

Figure 3.9 Same as Figure 3.7, but for Western Maritime Continent (WMC). 179

Figure 3.10 Same as Figure 3.7, but for the Gulf of Mexico (GM)..... 180

Figure 3.11 Same as Figure 3.7, but for Argentina (ARGEN). 181

Figure 3.12 Same as Figure 3.7, but for Australia (AUS). 182

Figure 3.13 Median length scale of PFs during El Niño (red) and La Niña (blue) periods over selected regions. PFs from the top 50% volumetric rainfall contribution to the total rainfall based on 3-year compiled dataset are used to create this figure. (a) CPACI, (b) EMC, (c) WMC, (d) (GM), (e) ARGEN, (f) AUS The length scale is defined as $L= \pm(A/\pi)^{0.5}$, where A is area of 20, 40 dBZ at different altitudes within each PF. It represents the radius of OPFs at each altitudes assuming the symmetric conical shape of region with 20,40 dBZ. The solid lines mark the average maximum heights of 20 dBZ; the dashed lines point to the average maximum heights of 40 dBZ. 183

LIST OF TABLES

TABLES PAGE

Table 1.1 The population of CFs with different flashes and mean thermodynamic and dynamic parameters of weak (intense) thunderstorms over selected regions. The low-level shear between 1 and 6 km ($SHEAR_{1\text{-}6km}$) and the lifted condensation level (LCL) is calculated above ground level. SHL donates the near-surface Specific Humidity, while RHM represents the averaged mid-level (700-500 hPa) relative humidity (RH). 59

Table 2.1 Mean and spatial correlations between the observed percentage of CFs with > 50 flashes and estimated percentage of severe thunderstorms by individual and joint atmospheric factors. 125

Table 2.2 Skill score equations. 127

Table 2.3 Populations of training and testing CFs with at least one flash and skill scores of different models. 128

Table 3.1 Average rain and occurrence, fraction and volumetric rain contribution of deep convection and MCSs during El Nino and La Nina over different regions. 170

INTRODUCTION

Clouds with intense convection play an important role in our climate system by redistribution heat, moisture, and trace gases, as well as producing large quantities of precipitation (e.g. Houze, 1989; Tao et al., 1993; Wang et al., 1995; Willison et al., 2013; Smith et al., 2017). No matter where they occur, intense convection almost always produces a significant threat to life and property. Knowing when and where there is a high potential of those events could improve weather forecasts, and help the public to be better prepared (Brooks et al., 2003). The mechanisms and the meteorological environments favorable to producing intense convection need to be fully understood in order to make numerical weather forecasts of these events more robust.

Despite the continuous improvement in observations and modeling tools, forecasting intense convection still remains a considerable challenge (Done et al., 2006). In addition to their wide range of size and lifetime (e.g. Foote and Mohr 1979; Wilson et al., 1998; Feng et al. 2016), the rarity of intense convection also limits our capability of studying these events thoroughly. Large data sets of events would be useful for the development of improved relationships between the weather events of interest and their large-scale environments.

The quantity of satellite observational data is enormous, which is essential for the investigation of these rare events. With the help of satellites, a number of studies have revealed that intense convection exhibits a strong preference over several regions, especially flat plain areas downstream of major mountains (e.g., Orville and Henderson,

1986; Liu and Zipser, 2005; Zipser et al., 2006; Liu et al, 2012; Houze et al., 2015; Liu and Liu, 2016). These favorable regions are therefore of great interest to both educators and researchers of intense convection, such as South Asia (Houze et al., 2007; Romatschke et al. 2010; Romatschke and Houze 2011), South America (Romatschke and Houze, 2010; Rasmussen and Houze 2011; Rasmussen et al. 2014), as well as Central Africa (Zuluga and Houze 2015).

These competent research efforts and their impressive results have advanced our knowledge and understanding of the large-scale environments favoring convection over these regions. However, there is still a lack of the comparison of the large-scale thermodynamic environments of intense convection among different regions. In addition to the fundamental need to characterize the large-scale processes responsible for intense convection, there is an important practical need to represent the convective intensity and subgrid scale processes in general circulation models. To address this, various thermodynamic parameters have been designed by researchers to characterize the processes that could favor the formation and development of intense convection in the past decades (details about these parameters are described in Chapter 2). In this study, a database of intense convection from 16-year satellite observations and reanalysis dataset are used to investigate and improve these relationships. Furthermore, in the past, there is a lack of study to evaluate relative importance of different thermodynamic variables in the initiation of intense convection. Here a few statistical models are tested to provide an assessment of the importance of various thermodynamic variables in describing the regional variation of intense convection.

As the dominant coupled mode of tropical variability on interannual time scales (Rasmusson and Carpenter 1982), the El Niño–Southern Oscillation (ENSO) phenomenon has been documented to exhibit the greatest influence on the interannual variability of the global climate (Webster et al. 1998). This is because the strength and location of the Walker circulation changes as a result of changes in the wind stress and sea surface temperature (e.g. Rasmusson and Carpenter 1982; Lindzen and Nigam 1987; Trenberth et al. 1998). This change may have a significant effect on the large-scale condition and the properties of intense convection.

Previous studies of favorable large-scale environments for intense convection usually focus on a specific region. Consequently, the similarities and differences among the thermodynamic and kinematic conditions over different regions have not been studied on a global scale. Examination and comparison among the environments of thunderstorms over different regions could provide us with crucial information about the responses of properties of thunderstorms to different large-scale environments. Satellites provide a unique opportunity to reach this goal because of their large spatial-temporal and near-uniform coverage of the globe.

As a joint NASA–National Space Development Agency of Japan mission, the Tropical Rainfall Measuring Mission (TRMM) has been the world's foremost satellite for the study of precipitation and its implications for climate since its launch in November 1997. With a coverage area of 36°S–36°N, TRMM carries multiple instruments including the

Precipitation Radar (PR), TRMM Microwave Imager (TMI), Visible Infrared Scanner (VIRS) and Lightning Imaging Sensor (LIS) (Kummerow et al., 1998). As the first precipitation radar in space, PR captures the three-dimensional structure of precipitation at a high horizontal and vertical resolution. TMI measures radiances that transfer to space through a precipitation cloud at multiple microwave frequency ranging from 10.7 to 85 GHz. The intensities of radiation measured by multichannel passive microwave radiometers can be used to infer the microphysical profiles of precipitating cloud along the sensor view path because of the frequency dependence of electromagnetic properties of precipitation particles. The LIS could detect the total lightning (both cloud-to-ground and intracloud), with ~70-90% detection efficiency (Boccippio et al., 2002) and ~90 s sampling duration at a time. TRMM enhances our capability to use remote sensing to gain insight into the properties of convective systems (e.g., Nesbitt and Zipser, 2003; Zipser et al., 2006; Liu et al., 2007; Houze et al., 2007; Liu and Ziper, 2009), with a legacy data set of 16+ years of observations across tropics and subtropics.

Given the profound influences of intense convection on the climate model, there are many fundamental questions that need to be answered to have an improved understanding of these events. The specific questions addressed in this dissertation include:

- What are the favorable large-scale environments of the most intense thunderstorms on Earth? What are the differences and similarities of kinematic and thermodynamic factors for intense thunderstorms over various regions all over the world?

- Could we utilize these similarities of kinematic and thermodynamic factors to build a simple statistic model to describe the regional variation of intense thunderstorms?
- How do the properties of intense convection response to the large-scale circulation–El Niño–Southern Oscillation?

Addressing these three questions, this dissertation consists of three main chapters that have led to three research journal manuscripts. The first manuscript focuses on the large-scale environments favored for intense convection (Chapter 1). The second manuscript develops two statistical models to describe the regional variation of intense thunderstorms from thermodynamic variables, in which their importance is evaluated (Chapter 2). The third manuscript presents the variation of the intensity, height and size of precipitation systems with El Niño–Southern Oscillation (Chapter 3). Given the differences in the data and methodology used to answer different questions, the data and methods are described separately in each chapter. Then, the summary and future work are included at the end.

CHAPTER I: What are the favorable large-scale environments for the highest flash rate thunderstorms on Earth

Abstract

A 16-year Tropical Rainfall Measuring Mission (TRMM) Convective Feature (CF) dataset and ERA-Interim reanalysis data are used to understand the favorable thermodynamic and kinematic environments for high flash rate thunderstorms globally as well as regionally. Such intense thunderstorms over various regions share a few common thermodynamic features, i.e. large Convective Available Potential Energy (> 1000 J/kg), moderate Convection Inhibition (CIN: 50-100 J/kg), and abundant moisture convergence associated with low-level jets. However, each region has its own specific features. Over many of these regions, high mountains play an important role by initiation of convection with orographic lifting and also by associated downslope flow at mid-levels forming an inversion above low-level moist air; this substantial convective inhibition helps accumulate higher moist convective energy. Sufficient larger-scale lifting, or orographic lifting related to major mountain ranges, is often necessary for the development of intense convection. Low-level convergence associated with drylines over south central United States, and strong sea-breezes together with orographic ascent over Columbia and North Mexico are common features for intense convection over these regions. Intense thunderstorms are often associated with a wind shear between the low and mid-troposphere over almost all the selected regions, implying that wind shear has a profound effect on the severity. It appears that multiple environmental factors acting together are necessary to facilitate most intense thunderstorms, while the dominant factors over different regions and seasons are not identical.

Introduction

Even in their rarity, severe convective phenomena often present a significant threat to life and property. Knowing where there is a high potential of severe thunderstorms could improve weather forecasting and help the public to be better prepared for such events (Brooks et al., 2003). Favorable conditions for severe convection are proposed in past studies, such as conditional instability, abundant moisture in low-level troposphere, dynamical lifting, strong wind shear between lower and upper levels (e.g., Fulks 1951; Miller 1972). Later case studies have revealed that both mesoscale and/or synoptic scale processes contribute to initial lifting prior to thunderstorms, and are usually critical in storm initiation (e.g., Carson et al. 1983; Cotton et al., 1983; Doswell 1984; Rockwood and Maddox 1988). Once storms are initiated, wind shear is believed to be particularly important in influencing storm severity and longevity (e.g., Weisman and Klemp 1982; Schoenberg Ferrier et al. 1996; Takemi 2007). Several different altitude limits for vertical wind shear exist and their relative importance is still in debate.

Despite a significant amount of research to date on the mechanisms of thunderstorms, the majority of data collected on thunderstorms are from the United States. Comprehensive knowledge of intense thunderstorms over other regions is still inadequate. In many sparsely populated and remote regions, records or reporting of severe thunderstorms are inadequate and few countries have official systems for these reports. Besides limited availability of reports, changes through time and a lack of uniformity in standards for data collection among different countries make comparisons over different regions difficult.

Satellites are one possible approach to solving the problem of different data standards, owing to their large spatial-temporal and near-uniform coverage. The Tropical Rainfall Measuring Mission (TRMM, Kummerow et al. 1998) is a satellite that has become a useful tool in the effort to explore intense convection across tropics and subtropics since its launch (Liu and Zipser 2005; Zipser et al. 2006; Houze et al. 2015). Recently, Global Precipitation Measurement (GPM) core observatory satellite (Hou et al., 2014), as the next-generation of TRMM, has extended the potential for studies of precipitation and convection to the middle and high latitudes (e.g., Liu and Zipser 2015; Liu and Liu 2016).

With the help of satellite missions, we get a more realistic picture of the worldwide distribution of thunderstorms. The wealth of satellite observations has provided opportunity in the efforts to explore intense thunderstorms globally. A number of studies have revealed that continental convective storms often have more intense convection and exhibit a strong preference over specific regions, such as in the plains area downstream of major mountains (Spencer and Stantek 1985; Orville and Henderson 1986; Alcala and Dessler 2003; Liu et al. 2012) Therefore, these favorable regions are of great interest to both educators and researchers, such as South Asia (Houze et al., 2007; Romatschke et al. 2010; Romatschke and Houze 2011), South America (Seluchi and Marengo 2000; Xie et al. 2006; Romatschke and Houze 2010; Rasmussen and Houze 2011; Rasmussen et al. 2014), central Africa, and West Africa (Nicholls and Mohr 2010; Zuluga and Houze 2015), as well as northeast China (Liu and Liu 2018). These studies have advanced our

knowledge and understanding of the frequency and characteristics of intense convection, and storm initiation over different regions.

The available information is still insufficient to specify precisely the processes that lead to intense thunderstorms. A number of processes may be involved in the formation of these systems. Detailed analysis of the large-scale fields of temperature, moisture, and wind at standard levels, would permit the identification of regions which are preferable for intense thunderstorms. This has inspired the present paper in which we investigate the favorable environments of intense thunderstorms over the zone covered by TRMM and especially the hotspots of the most intense convection on Earth demonstrated by prior studies (Mohr and Zipser 1996; Liu and Zipser 2005; Zipser et al. 2006; Cecil and Blankenship 2011; Houze et al. 2015; Liu and Liu 2016).

Lightning is one of the most dramatic aspects of intense thunderstorms and cloud-to-ground lightning flashes have been among the leading causes of weather-related fatalities (Curran et al. 2000). There has been growing public concern in recent years in the forecasting and assessment of the severity of convective storms around the world based on lightning (e.g., MacGorman and Burgess 1994; Lang and Rutledge 2002; Carey et al. 2003) To improve the accuracy forecasting of these rare events, the meteorological environment and mechanisms favorable to producing intense thunderstorms should be fully understood. Here convective intensity is inferred from the lightning flash rate observed by the TRMM Lightning Imaging Sensor (LIS). Williams (1985) proposed that the flash rate could be scaled as the fifth power of the cold cloud-top height. In spite of

the large variance of the relationship between the flash rate and the maximum storm height, this proposed scaling provides an insight into the relationship between the lightning probability and the convective intensity. Many past studies confirmed that flash rate can be related to convective intensity in thunderstorms using ground and satellite-based observation (Mohr et al. 1996; Petersen et al. 1996; Ushio et al. 2001; Liu et al. 2011).

Our objective in this study is to examine the favorable dynamic and thermodynamic conditions for the most intense thunderstorms over different regions. First, we present the geographical distribution and seasonal variations of high flash rate thunderstorms across the tropics and subtropics observed by TRMM. Then, the favorable meteorological environments of these events over selected regions are explored, with the help of Interim European Centre for Medium-Range Weather Forecast Reanalysis (ERA-Interim, Dee et al, 2011). Finally, a discussion of the similarities and differences in the favorable environments associated with these events is provided. With this objective, this paper will be arranged in the following order: data and methodology in section 2, results in section 3, followed by summary and discussion in section 4.

Methods

a. TRMM convective feature datasets for identifying intense thunderstorms

TRMM has enhanced our capability to use remote sensing to gain insight into the properties of convective systems over tropics and subtropics (from 36°S to 36°N) with multiple instruments (Kummerow et al. 1998), including the Precipitation Radar (PR),

TRMM Microwave Imager (TMI), Visible Infrared Scanner (VIRS) and LIS. LIS onboard TRMM has provided valuable observations in studying lightning (Cecil et al. 2005; Petersen et al. 2005; Pessi and Businger 2009; Xu et al. 2010). With ~70-90% detection efficiency (Boccippio et al. 2002) and ~90 s sampling duration, the total lightning rate, including both cloud-to-ground and intracloud, can be derived for each thunderstorm that TRMM samples.

In this study, 16-year (1998-2013) TRMM version 7 products from PR and LIS are used. First, Convective Features (CFs) are defined by grouping the contiguous area with convective precipitation derived with PR after Liu and Zipser (2013), using the precipitation feature approach described in Liu et al. (2008). The LIS lightning flash counts are summarized within each CF as an indicator of the convective intensity. Then, four categories of storms are classified using the flash counts: no flash, weak (1-3 flashes), moderate (3-50 flashes), and the most intense (> 50 flashes). This classification is arbitrary. In 16 years, total ~25 million CFs with at least four contiguous pixels (with size greater than ~75 km^2) are considered in this study to remove noisy data. There are more samples in the subtropical latitudes due to the +/- 35° orbit (Figure 1.1a).

b. Selected regions for the most intense thunderstorms

Although the regions with frequent intense convection have been demonstrated for more than a few decades (Spencer and Santek 1985; Zipser et al. 2006), it is still fruitful to re-examine the climatological frequency of high flash rate thunderstorms on the basis of 16-year TRMM/LIS comprehensive datasets. The percentage of the storms in different

categories are identified by the CFs with no flash 1-3, 3-50, > 50 flashes by dividing the total number of CFs in each 2°x 2° box shown in Figure 1.1. The ocean has a much higher percentage of CFs with no flash than land. Central Africa, mountains, and a few desert regions have much lower fraction of CFs with no flash. The geographical distribution of percentage of weak, moderate and intense thunderstorms are consistent with prior studies (e.g., *Orville and Henderson* 1986; *Zipser and Lutz* 1994; *Christian et al.* 2003; Liu et al. 2012). Thunderstorms are found more often over land than over the ocean. Over land, the most intense thunderstorms with more than 50 flashes, corresponding to about 33 flashes per minute, tend to occur in a few hotspot regions (Figure 1.1c). This inspires the examination of the nature of the most intense thunderstorms over these hotspots. In this study, we focus on the regions (boxes as shown in Figure 1.1c) where the most intense convection occurs the most frequently on Earth (Zipser et al. 2006). These regions include the south central United States (SCUS: 32°N - 36°N & 95°W-100°W), southwest Mexico (NWM: 27°N -29°N & 108°W-110°W), Argentina (ARGEN: 33°S -36°S & 63°W-67°W), Sahel (SAHEL: 10°N -14°N & 17°E-21°E), Congo (CONGO: 3°S -2°N & 18°E-24°E), Columbia (COLUM: 7°N -9°N & 74°W-76°W), and Himalaya (HIMA: 33°N -35°N & 72°E-74°E).

The seasonal variations of total CFs and intense CFs with more than 50 flashes are shown in Figure 1.2. It is not surprising that intense thunderstorms are found more frequently in the warm season. There is a smaller seasonal variation of both the total number and the percentage of intense CFs over CONGO than other regions. Two peaks of intense thunderstorms are found over HIMA in June and September, which is consistent with

prior studies (Qie et al. 2014). It is well known that thunderstorms are typical spring and summer phenomena (e. g., Johns et al. 1982; Uyeda et al. 2001; Qie et al. 2003; Schulz et al. 2005; Taszarek et al. 2015) due to more intense low-level atmosphere heating and higher equivalent potential temperature (Miller and Fritsch 1991). Therefore, we discuss the high flash rate thunderstorms in the most active months for each region respectively, hereafter often using this as a synonym for "intense convection", as Zipser et al. (2006) and many others have shown to be generally the case.

c. ERA-Interim reanalysis data for large-scale conditions

To derive large scale thermodynamic environments for intense thunderstorms, the ERA-Interim reanalysis data (Dee et al, 2011) are used. With 37 vertical levels and 0.75° × 0.75° horizontal resolution, the ERA-Interim reanalysis dataset is available every 6 hours. In addition to the traditional variables, e.g. temperature, geopotential height, relatively humidity, and horizontal wind components, additional parameters, i.e., convective available potential energy (CAPE); convective inhibition (CIN); potential temperature (Θ), and equivalent potential temperature (Θ_e) are derived from these basis variables. Using the location and time of each CF, a storm-centroid nearest preceding large-scale environment in ERA-Interim reanalysis are obtained for each CF. Knowing that no reanalysis is perfect, our choice of reanalysis time between 0-6 h prior to the storm is intended to minimize the possible influence of the storm itself on the analysis. Different from some earlier studies using specific longitude and latitude regions (e.g., Romatschke and Houze 2011; Rasmussen and Houze 2015; Zuluga and Houze 2015), to focus on CFs, we composite the large scale fields relative to the thunderstorm centers. The horizontal or

vertical traditional and derived parameters centered at CFs are averaged to examine the common large scale features of thunderstorms. The difference between intense and weak thunderstorms are examined by calculating anomalies of each large scale field by subtracting the composite fields of the intense CFs with 50 flashes to weak CFs with 1-3 flashes. Because sometimes weak and intense CFs may coexist in the same satellite overpasses, the orbits with intense CFs are removed from samples to calculate the large-scale condition background for weak CFs.

Results

A number of studies have revealed the synoptic conditions that are highly correlated with the occurrence of intense convection (e.g. Barnes and Newton 1986; van Delden 2001; Doswell 2001; Tuttle and Carbone 2004; Schumacher and Johnson 2005; Trier et al. 2006). Next, we examine the favorable environments of TRMM-identified intense thunderstorms for each region. Then, the similarities and differences in the dynamic and thermodynamic factors for intense thunderstorms are compared among different regions.

a. South Central United Stated (SCUS)

Thunderstorms over the southern plains of the United States have been well studied for more than half a century. As early as the 1950s (Beebe 1958; Fujita 1958), boundaries between moist air originating over the Gulf of Mexico and dry air originating over arid regions in northern Mexico, eastern New Mexico, and western Texas, or so-called drylines (e.g., Rhea 1966; Schaefer 1974), have been identified as a major focus of intense thunderstorms over SCUS. More than 40% of thunderstorms in April, May, and

June (AMJ) have been found to be associated with the drylines (e.g., Rhea 1966; Schaefer 1974; Peterson 1983). Much effort has been made to explore the drylines and their association with convection initiation in the United States (e.g., Benjamin and Carlson 1986; Bluestein et al. 1988; Ziegler and Hane 1993; Shaw et al. 1997; Atkins et al. 1998; Ziegler and Rasmussen 1998). For those reasons, this better-known region is the first one used to explore environments conducive to intense thunderstorms. Then, we apply a similar methodology to other regions to determine their preferred synoptic conditions for their intense convection.

Benjamin and Carlson (1985) suggest that a favorable environment for the formation of severe thunderstorms is frequently a product of both surface-related processes and large-scale flow patterns. Surface processes are often related to the terrain configuration (McCarthy and Koch 1982; Carlson and Ludlam 1986; Steenburgh and Mass 1994). Therefore, the locations of both weak and intense CFs, as well as the topography, are shown (Figure 1.3a) before investigating their large-scale field environments. Then, Figure 1.3b-3f present the composite ERA-Interim dynamic and thermodynamic conditions centered at the location of each intense CF in AMJ over SCUS.

The centroid of the intense thunderstorm located in front of the large-gradient of specific humidity (SH) 2 m above the surface indicates the position of the dryline in Figure 1.3b. South-southeast of the dryline brings moist air (SH > 12 g/kg) from the Gulf of Mexico into the storm center. The convergence between the warm-moist flow and the westerly dry flow behind the dryline is identifiable. The continued strong southerly wind (>10

m/s) at 850 hPa indicates the low-level jet (Figure 1.3c). At 700 hPa, south of the storm centroid, hot and dry continental air flows northeastward above moist low-level air providing large CIN (Carlson and Ludlam 1968). According to Carlson et al. (1983), convection is often suppressed by this "lid" of hot, dry air until the low-level air flows out from beneath this lid (termed "underrunning"). Farther aloft, the shortwave trough, ahead of a thermal trough, is identifiable based on the curvature in the wind field on the 500-hPa composite map (Figure 1.3e). In accordance with past studies (e.g., Rhea 1966; Hane et al. 1997; Ziegler et al. 1997), a 500 hPa trough is a frequent feature together with a dryline. Schultz et al. (2007) also noted that strong synoptic patterns contribute to the strength of the dryline. In the composite-CAPE map, the storm centroid is within the modest CAPE values (~1200 J/kg), with larger values farther south. CAPE values are nearly coincident with the region of large moisture advection near the surface (Figure 1.3b). Although there is an extensive area of large CAPE, intense storms are more likely found within modest CAPE.

Composite cross sections related to the intense thunderstorms, as well as their differences compared to the weak ones, are constructed at the storm-centroid latitude/longitude to provide further insight into the favorable properties of intense thunderstorm environments (Figure 1.4). With a shallow moist layer deepening toward the moisture source, the dryline profile is similar to the dryline structure suggested by prior studies (Rockwood and Maddox 1982). Deep southerly moist low-level jet is evident from the surface to around 700 hPa (Figure 1.4a and 4c). Low-level warm moist advection, together with the southwesterly dry flow aloft, create a potentially unstable environment. Increased

strength of the southerly wind for intense thunderstorms implies a stronger low-level jet for intense thunderstorms than for weak ones (Figure 1.4b and 4d). Near the storm centroid, a slightly higher relative humidity (RH) anomaly around 800 hPa suggests more moisture feeding into higher flash rate thunderstorms. Compared to weak thunderstorms, intense thunderstorms are associated with a drier airflow above 700 hPa (Figure 1.4b and 4d).

The vertical profiles of several selected variables related to thunderstorms with different flash rates are shown in Figure 1.5. Lower RH but higher SH in the lowest level (below 800 hPa) is associated with storms with more flashes. Decreasing with height rapidly, a common characteristic of high convective instability (Holton, 1979), Θ_e is much higher for the intense thunderstorms in the low levels (below 700 hPa). Previous studies found that the high-Θ_e air at low levels with its associated convective instability was essential (Glass et al. 1995; Moore et al. 2003). The larger zonal and meridional wind for the intense thunderstorms (Figure 1.5d) is consistent with the stronger southerly wind anomaly in Figure 1.4b and 4d.

The re-examination of the large-scale conditions of intense thunderstorms over the SCUS confirms previous studies about how large-scale patterns and the physical processes interact and create a favorable environment for the development of such events. Next, we apply similar analysis to other regions.

b. Southwest slope of Himalayas (HIMA)

Convection over the southwest of the Himalayas, with high lightning rates (e.g., Christian et al. 2003; Zipser et al. 2006; Cecil et al. 2015) and close to the world's largest mountain barrier (Murakami 1987), has been a frequent scientific topic for researchers. Asian monsoons play a critical role in the occurrence of intense convection over this region (Romatschke et al. 2010; Qie et al. 2014; Virts and Houze 2016). Most of the TRMM-identified intense CFs over the region are found in the warm season (May to September), as shown in Figure 1.2a. However, higher percentage of the intense CFs is found in May and September rather than June, July and August (Figure 1.2b). Previous studies have also revealed that convective systems in the pre-monsoon season (March-May) over this region are more intense than in other seasons, with a maximum in lightning activity (La and Pawar 2009; Ranalkar and Chaudhari 2009). We have examined the favorable environments of TRMM-identified intense thunderstorms in three seasons: spring (March, April, May (MAM)), summer (JJA), and fall (September, October, November (SON)). Only the spring synoptic pattern of intense thunderstorms is shown here over this region because of the similarities in environmental conditions found in the three seasons.

The composites of large-scale conditions of intense storms, as well as the topography and locations of weak and intense thunderstorms, are shown in Figure 1.6. There is a strong humidity gradient at near surface along the Himalayan foothills (Figure 1.6b). Southwesterly flow at low levels encounters the dry north-northwesterly air flowing from the Afghan highlands at mid troposphere over the region. The southwesterly low-level jet brings warm, moist air from the Arabian sea into the storm centroid area, which increases the convective instability. South of the storm centroid, the westerly flow from the Afghan

high land is dry from 700 hPa to 500 hPa. This hot, dry air, similar to that over the SCUS, creates a "cap" to suppress the development of convection and help to accumulate moist static energy. At 500 hPa, the storm centroid is ahead of a shortwave trough (Figure 1.6e). The large-scale ascent ahead of the trough may play a role in triggering convection over HIMA, while other vertical lifting mechanisms (e.g., orography, surface heating) may be equally important over the area (Carlson et al. 1983; Houze et al. 2007; Romatschke et al. 2010). Representative of the boundary layer moisture and temperature stratification, CAPE values are consistent with the near surface moisture distribution, as shown in Figure 1.6b. The storm centroid located within the modest CIN also suggests that thunderstorms tend to form along the lid edge, created by the hot, dry air above the low-level moist air. In spite of a large CAPE, large CIN (> 100 J/kg) southwest of the storm centroid suppresses the development of convection. Figure 1.7a and 7c demonstrate the vertical wind shear over the intense thunderstorm region. Note that intense thunderstorms have lower relative humidity at low levels than weaker thunderstorms, however, they are associated with warmer low-level air and more moisture (Figure not shown).

The composite vertical profiles of atmospheric variables for CFs with different flash counts in three seasons are shown in Figure 1.8. In spring and fall, moderate and intense thunderstorms have higher Θ and Θ_e (below 600 hPa) at the low-level troposphere. In summer, the thunderstorms are characterized by lower RH and SH than CFs with no flash. The equivalent potential temperature (Θ_e) increases rapidly with the onset of the summer monsoon in JJA (Figure 1.8d) and decreases with the retreat of the summer

monsoon in SON (Figure 1.8f). Higher equivalent potential temperature in summer than that in spring and fall implies that this region is warmer and moister during monsoon season. However, during monsoon season, convection is relatively weaker than the preseason and postseason (Xu and Zipser 2012). Schumacher (2015) demonstrates that introducing slightly drier air in the near-surface layer into the initial condition could lead to more intense convection. Note that intense thunderstorms in JJA are associated with relatively weaker moist static energy. Under this condition, it is more important to have a "cap" mechanism for moist static energy to accumulate to form an intense storm in this season. However, CIN is found to be lower in summer (32.8 J/kg) than in spring (65.8 J/kg) and fall (37.6 J/kg). In other words, higher moist static energy but smaller CIN during monsoon season is favorable for ordinary thunderstorms over HIMA, while relatively lower static energy but larger CIN in preseason and postseason is preferred for the most intense thunderstorms.

c. Argentina (ARGEN)

With a high frequency of hail production (Cecil 2009; Cecil and Blankenship 2012) and intense convection (Liu and Zipser 2005; Zipser et al. 2006; Liu and Liu 2016), Argentina until recently has been an understudied hotspot of the most intense thunderstorms in the world because of the lack of uniformity in the ground operational networks (Nascimento and Doswell 2006). Moisture-laden South America low-level jet (SALLJ) has been found to play a vital role in the development of convection over this region (Nieto Ferreira et al. 2003; Vera et al. 2006; Salio et al. 2007; Romatschke and Houze 2010). Rssmussen and Houze (2016) delineated a conceptual model in which they

synthesized key factors of convection initiation in the lee of the subtropical Andes, including lee cyclone, topography, and moisture flux. In that model, the crucial role of orographic control in convective initiation was demonstrated using simulations with the Weather Research and Forecasting Model.

This section attempts to provide a comprehensive description of the environment of TRMM-identified intense thunderstorms over ARGEN. Figure 1.9 presents the composite large-scale conditions of intense thunderstorms over ARGEN in December-February. East of the Andes and north of the Sierras de Córdoba, the wind pattern contains several key features that have some similarity to those in SCUS that help explain the occurrence of intense convection over this region. A strong low-level northerly jet at low levels, the SALLJ, brings tropical moisture toward the storm centroid (Figure 1.9b) extending from near surface to about 700 hPa. The SALLJ is enriched in moisture by evapotranspiration in the Amazon Basin (Marengo, 2005). Similarly to the situation in SCUS, the low level jet is very often capped by a stable layer separating it from dry, potentially warmer air descending in the westerly flow downstream of the Andes (Figure 1.9c-d). At 500 hPa, the storm centroid is within the strong westerly wind (Figure 1.9e). Intense thunderstorms are more likely to be found along the edge of large CAPE (>1500 J/kg) and moderate CIN. This suggests that it is critical to consider both CAPE and CIN to anticipate when and where intense convection may erupt.

Characterized by a northerly wind at low levels (below 700 hPa), the storm centroid is also normally contained within westerly wind at the upper levels (Figure 1.10a and 10c).

This sheared environment is favorable for intense convection (Altinger de Schwarzkopf and Rosso, 1982; Weisman and Klemp, 1982; Rosenfeld et al., 2006). The anomaly composite cross section shows that intense thunderstorms are associated with stronger low-level jets than weaker storms, with greater moisture convergence into the storm centroid (Figure 1.10b and 10d). The vertical profiles are shown in Figure 1.11, showing that stronger storms have both greater instability and stronger meridional low-level wind transporting moisture in the SALLJ.

d. Columbia (COLUM)

Colombia is a region known to have a high frequency of mesoscale convective systems (MCSs) (e.g., Velasco and Frisch 1987; Mohr and Zipser 1996; Zipser et al. 2006; Durkee and Mote 2009), especially along the Pacific coast west of Colombia, which is one of the rainiest places on Earth (e.g., Lopez 1966; Poveda and Mesa 2000; Sakamoto et al. 2011; Duran-Quesada et al. 2012). In addition to the copious intense rainfall, Figure 1.1 shows that the region, specifically northwest of Columbia, is another hotspot of high-frequency lightning, which is consistent with past studies (e.g., Christian et al. 2003; Zipser et al. 2006; Diaz et al. 2009). Moreover, Albrecht et al. (2011) and Cecil et al. (2015) found that portions of this region have greater flash rates than anywhere else on Earth.

The composite large-scale conditions of intense thunderstorms in summer over this region is shown in Figure 1.12 to understand the processes governing thunderstorms. COLUM is characterized by a very complex topography. Wind flows near the surface

from the south becoming westerly (known as the Chocó jet), which is associated with a strong Sea Surface Temperature (SST) gradient between the coastal region of Colombia and Ecuador–Peru cold tongue (Poveda et al. 2006). This low-level jet transports large quantities of moisture from the Pacific Ocean into this region (Poveda and Mesa 2000; Mapes et al. 2003; Sakamoto et al. 2011; Zuluaga and Houze 2015). Meanwhile, the encounter of the Chocó jet with the easterly low-level jet, known as the Caribbean low-level jet (CLLJ) (Magaña et al. 1998; Amador and Magaña 1999), forms a strong convergence in the low troposphere. Figure 1.12a also shows moisture transport into the region with the easterly wind. The south branch of the easterly low-level jet descends over the Andes Mountains and serves to provide a cap or lid over the Chocó jet. From 700 to 500 hPa, the wind is predominantly easterly and forms a strong wind shear with the near surface westerly Chocó jet. The intense convection over COLUM is characterized by a large CAPE center and exhibits relatively small CIN (~ 20 J/kg). Again, important factors including the convergence, the complex topography, and the abundant moisture in the low troposphere make this region a favorable place for the development of thunderstorms. In addition, Zuluga and Houze (2015) pointed out that the diurnal heating also plays an important role in the development of convection over this region.

With deep low-level moisture below easterly upper-level flow (Figure 1.13a and 13c) thunderstorms in this region experience appreciable easterly shear. The composite cross section also shows that the low-level jet is below 800 hPa and relatively shallower than in other regions. The differences between intense and weak thunderstorms in the

meteorological conditions are relatively small compared to those over the ARGEN and HIMA (Figure 1.13b and 13d). The difference of the vertical profiles between weak and intense storms over COLUM is weaker than in most other regions, and does not appear to be significant (Figure 1.14).

e. Sahel (SAHEL)

SAHEL, a transition zone between moist tropical regions near the Guinean coast and the precipitation-free Sahara, has received a great deal of attention because of the highly favorable meteorological conditions for the development of convection (e.g., Tetzlaff and Peters 1988; Parker et al., 2005; Lafore et al. 2011; Zuluga and Houze 2015). In Figure 1.15, the boundary between the hot, dry air from the Sahara and moist air south of the storm centroid is evident near the surface (Figure 1.15b). South of the storm centroid the flow is from the southwest. The boundary shifts northward with height. At 700 hPa, the main feature is the African easterly jet (AEJ) with strong wind shear between low levels and 700 hPa (Figure 1.15d). This low-level shear could fundamentally affect the intensity of convection, as has been emphasized by Alfaro (2017). As a result of the instability of the AEJ (Burpee 1972), African Easterly Waves (AEWs) are evident in the composite map at 700 and 500 hPa (Figure 1.15d and 15e). The role of the westward traveling AEWs over this region in the development of the convective activity is well studied (e.g., Carlson 1969; Burpee 1972; Aspliden et al. 1976; Fink and Reiner 2003; Guy and Rutledge 2012). Recent studies indicate that convection in central and eastern Africa may play a role in triggering the AEW activity (Berry and Thorncroft 2005; Mekonnen et al. 2006; Price et al. 2007). The transition region between the Sahara desert and the

vegetated region of central Africa has strong meridional gradients of CAPE and CIN (Figure 1.15f). During the active season of the West African monsoon (June to September), the moist air is beneath the relatively hot dry air from the Saharan Desert. Convection could be triggered once the potential instability is released, for example, by ascent ahead of the AEWs trough.

Wind direction changing from westerly at the low level to easterly at the upper level indicate the strong wind shear over SAHEL region when intense convection occurs (Figure 1.16a). There is a dry-air tongue in the cross-section at the middle-level troposphere (Figure 1.16a). Several studies have described the important role of dry-air intrusion in convective activity (Brown and Zhang 1997; Johnson et al. 2001; Roca et al. 2005). The high relative humidity values in whole column south of storm (Figure 1.16b) is consistent with the theory, proposal by Nicholson (2009) and other researchers (e.g., Brubaker et al. 1993; Savenije 1995; Trenberth 1999), that the moisture over West Africa is locally recycled. There is a large gradient of RH with dry air north and moist air south of the storm centroid. Except for slightly drier middle troposphere and stronger meridional RH gradient for intense thunderstorms, there is not much difference in the anomaly cross section between weak and intense thunderstorms (Figure 1.16b and 16d). The differences between intense and weak thunderstorms in the vertical profiles of these selected variables are small over SAHEL (Figure 1.17).

f. Congo (CONGO)

As one of the places that are vulnerable to climate variability and extreme events, the Congo Basin is one of the regions that experience the highest frequencies of lightning and thunderstorms (Christian et al. 2003; Zipser et al., 2006; Cecil et al. 2015). According to the global ranking of lightning flash rate density reported by Albrecht et al. (2016), half of the world's hottest spots in lightning are found in the Congo basin. The Congo Basin is also the region with a small seasonal variation in the percentage of intense thunderstorms among the selected regions in this study (Figure 1.2). Three major monsoons, the northeast, southeast and southwest monsoon described by Nicholson (1996, 2018), play a crucial role in the convection and rainfall over this region. However, the favorable large-scale environments for intense thunderstorms is not yet fully understood over this region due to very limited observations.

Located in the same longitude zone as SAHEL, there are a lot of similarities in the large-scale conditions for intense convection over CONGO and SAHEL. Three major air streams, dry air from the northeast, air from southeast at levels below 700 hPa, and moist southerly flow, are separated by two surface convergence zones (Figure 1.18b). The first one is "tropical rainbelt", termed by Nicholson (2009). The southerly monsoon confined to the lowest levels (Figure 1.18b and 18c) of the troposphere is similar to the results shown by Nicholson (2009). Sufficient moisture from the Congo rainforest makes the Congo basin unstable year-round (Reason et al., 2006). The easterly wind is dominant at the middle and upper level. Large CAPE but small CIN values (Figure 1.18f) make it easy for air to rise to the level of free convection and release the potential energy. Thermodynamic instability in warm and humid air, as well as ascent facilitated by the

surface wind convergence, make this region active with intense thunderstorms. The stronger easterly flow (Figure 1.20c), together with the drier mid-level troposphere (Figure 1.19b, 19d, 20a), is consistent with the results shown by Chaggar's (1977), that stronger easterly flow is more conducive to the development of intense thunderstorms.

g. Northwestern Mexico (NWM)

The western slope of the Sierra Madre Occidental east of the Gulf of California (Figure 1.21a), in northwestern Mexico is another hotspot of intense thunderstorms (Figure 1.1). NWM receives more than 60% of the total annual rainfall in the burst of convective activity during the North American monsoon (NAM) season (Douglas 1993), which typically begins in mid-June and finishes around the end of September (Higgins et al. 1997).

The outstanding thermodynamic feature near the surface is the surge of moisture from the Gulf of California (Figure 1.21b). Suggested by prior studies (Hales 1972; Brenner 1974; Stensrud et al. 1997), coastally trapped, northward-propagating disturbances are characterized by anomalous southerly or southeasterly moisture flow along the Gulf of California. Low-level moisture transport may play an important role in the onset of the NAM-convection, which has been emphasized in numerous studies (e.g., Green and Sellers 1964; McCllum et al. 1995; Romatschke and Houze 2010). An anticyclone is faintly identifiable at 700 hPa and becomes clear at 500 hPa (Figure 1.21d-e). The anticyclone is another well-known feature associated with the NAM-convection. Evidence shows that deep convection is related to the forming of the NAM anticyclone

(e.g., Newman and Johnson 2012; Stensrud 2013). Prior studies have also demonstrated that the convergence and upward motion associated with the passage of easterly waves or anticyclones often facilitate convective storms (Bieda et al. 2009; Finch and Jonson 2010; Newman and Johnson 2012).

In addition to the features shown, several characteristics are worth mentioning in Figure 1.21. The strong specific humidity gradient and the convergence near the coast in Figure 1.18a confirms that the Gulf of California is the major moisture source for the NAM-convection instead of the Gulf of Mexico due to the topography (Anderson and Roads 2001; Berbery 2001; Bordoni and Stevens 2006; Barron et al. 2012). Convergence between the northwesterly and southeasterly wind along the east side of the strong moisture flow is apparent near the surface. This might be related to the sea-breeze and the topography of the Sierra Madre Occidental in the afternoon and midnight. The leading edge of the sea breeze is often associated with sharp changes in temperature and moisture. It could take on characteristics similar to those of synoptic-scale cold front (e.g., Simpson et al. 1977; Miller et al. 2003). The combination of moisture from the marine air and surface heating from the land make the region particularly favorable for convection, which has been documented in an abundant literature (e.g., Byers and Rodebush 1948; Burpee 1984; Blanchard and Lopez 1985; Nicholls et al. 1991; Pielke et al. 1991. Johnson et al. 2007) showed that the onshore flow associated with the notable sea breeze along the east coast of the Gulf of California also affects the maximum convection and precipitation over the slope of the Sierra Madre Occidental. The storm centroid is found west of the maximum CAPE and CIN centers (Figure 1.21f).

Above the storm centroid, the easterly wind is relatively weak, compared to other regions (Figure 1.22a and 22b). Relatively larger middle-level RH (> 60%) for the intense thunderstorms than weak ones are found at 500 hPa (Figure 1.22b and 22d). This is consistent with Erfani and Mitchen's result (2014) of convective moistening of the mid-troposphere. The NAM intense thunderstorms have higher SH and Θ_e at low levels (Figure 1.23a and 23b), suggesting warm air surges from the gulf. The intense thunderstorms also have stronger low-level wind shear than weak ones (Figure 1.23c and 23d).

h. Similarities and differences among the thermodynamic and dynamic conditions

Up to this point, we have explored the key properties of the large-scale conditions for the TRMM-identified intense thunderstorms over seven selected regions. The large-scale conditions related to intense thunderstorms over these regions bear some similarities; however, intense thunderstorms are creations of environments whose properties may vary greatly in time and space. To demonstrate these variations, the ERA-Interim soundings at the nearest grid prior to the TRMM-observed thunderstorms are averaged to compare the similarities and differences among these favorable environments.

For example, Figure 1.24 shows the composite soundings of weak and intense thunderstorms over HIMA in three different seasons. Intense thunderstorms in spring (MAM) and fall (SON) exhibit a colder and dryer air at low levels than in summer (JJA). In MAM and SON, intense thunderstorms have warmer and moister tropospheric

environments than weak ones. Among the three seasons, JJA has the weakest upper-level westerly wind. With the onset of monsoon, the sounding in JJA is found to be associated with the largest CAPE but the smallest CIN, as well as the highest level of neutral buoyancy. Though the upper troposphere is less important in the initiation of convection, JJA intense thunderstorms have much dryer air in the mid troposphere than other two seasons. The high level of neutral buoyancy over HIMA in JJA helps to explain why the deepest convection occurs frequently there (Weston 1972; Zipser et al. 2006; Romatschke et al. 2009).

The example of spatial variation of large-scale conditions favoring intense convection is shown by composite soundings over six regions in Figure 1.25. First, except that over the ARGEN and NWM, intense thunderstorms over all other regions exhibit a drier mid troposphere compared to the weak ones. Second, a strong low-level wind shear, which is conducive to the development of thunderstorms, is found in three regions: ARGEN, SAHEL, and NWM. Subtropical regions, such as ARGEN and SCUS are characterized by a strong westerly flow in the mid troposphere, while tropical regions, including SAHEL, CONGO, COLUM and NWM, have easterly flow in the mid troposphere. An evident southerly wind at the low levels over SCUS indicates that the moisture from the Gulf of Mexico and the low-level jet play an important role in the development of intense thunderstorms. Note that not all regions have a significant larger CAPE and a dryer mid-troposphere for more intense thunderstorms.

Many observational and modeling studies have clarified the relationship between the storm longevity, propagation and the character of the hodograph associated with the vertical shear (e.g., Maddox 1976; Weisman and Klemp 1986; Thompson et al. 2007), although debate continues about the effects of the curvature on the characteristic of supercell storms (Weisman and Rotunno 1999). The hodographs related to the intense thunderstorms over seven regions are shown in Figure 1.26. Sitting under the westerly jet, the difference in the structure of hodographs over ARGEN and SCUS is distinct from other regions. Over these two regions, the composite hodograph is substantially curved in the lowest layers with large shear between low-mid layers. Over HIMA, the shear is strong but curvature is very weak. The wind shear over SAHEL, although only slightly curved is fairly strong between the surface to 700 hPa. CONGO, COLUM, and NWM are characterized by relatively small wind shear in the low levels. With different low level shear scenario, the role of shear in organizing the convection does seem to vary significantly over these regions.

To have a quantitative comparison of the favorable environments of the thunderstorms over the seven regions, the mean values of the thermodynamic and dynamic parameters and the numbers of weak and intense thunderstorms are listed in Table 1. Those parameters include CAPE, CIN, wind shear between 1 and 6 km above the ground ($SHEAR_{1\text{-}6km}$), near-surface SH (SHL), mid-level RH (RHM, 700-500 hPa), and lifting condensation level (LCL).

First, comparing environmental properties for intense thunderstorms among the seven regions, substantial CAPE and moderate CIN is present in all regions. Substantial wind shear is present for all subtropical regions and SAHEL, less in the other 3 tropical regions. In terms of surface specific humidity and the height of the LCL, the main outliers are HIMA in Spring and NWM, where effects of orography allow severe storms in rather dry surface environments with LCL about 2.5 km above the surface compared with much lower LCL in all other regions. Mid-levels are rather dry (RH in the 51-71% range) for all 7 regions.

Next, comparing the environmental properties for intense vs. weak thunderstorms in each region, there is generally more discrimination in the subtropics, with all 3 regions showing much larger CAPE, larger CIN, and modestly larger shear, compared with the tropical regions. Consistent with the larger CAPE, the subtropical regions also show larger near-surface specific humidity for intense vs. weak storms. For tropical regions, with the exception of larger CAPE for intense vs. weak storms, and slightly larger shear, the remaining parameters (humidity near surface and in mid-levels, and LCL, show very small differences, suggesting either that these parameters are poor discriminators in these tropical regions, or that the reanalyses may not be sufficiently reliable to draw conclusions.

Summary and discussion

The goal of the current study is to explore the regional variations of relationships between intense thunderstorms and their favorable thermodynamic and kinematic environments.

These environments have been documented using ERA-Interim reanalysis data for seven hotspot regions with intense TRMM-observed convective features. Based on the composite fields for high flash rate thunderstorms, we have compared these seven regions, seeking to learn whether their environments share common features, and within each region, we have also compared low vs. high flash rate storms.

There are a number of common features shared by the seven regions, although they have different quantitative values, especially between the tropical and subtropical regions. The major conclusions of this study are summarized as follows:

- The common ingredients for intense convection found in previous studies (e.g., McNulty 1978; Johns and Doswell 1992; Doswell et al. 1996), abundant low-level moisture, convective instability as indicated by large CAPE, and some lifting mechanism to permit the ascent of parcels through a layer of convective inhibition to their level of free convection, are found over all seven regions. However, some of the details, such as the magnitude of the low-mid level wind shear, low-level jets, the specific lifting mechanisms, and the role of topography, vary considerably from region to region.
- The magnitude of the low-mid-troposphere wind shear is greatest over SCUS, ARGEN, SAHEL, and HIMA, implying that its effect on the severity of storms over those regions is consistent with prior studies (e.g., Weisman and Klemp 1982; Schoenberg Ferrier et al. 1996; Takemi 2007; Tao et al., 2007). But the

intense storms over other regions, with far lower wind shear, apparently gain their intensity without this mechanism.

- Within each specific region, comparing weak vs. intense storms (i.e., low vs. high flash rate storms) gives widely differing results. The 3 subtropical regions share many similarities with the abundantly-studied south central U.S., but the tropical regions are more varied. For example, compared to weak storms, intense storms in subtropical regions have much greater CAPE and with one exception greater convective inhibition, and greater shear. In tropical regions, strong storms have greater CAPE than weak storms but the differences are not as great as those in the subtropical regions. For low-level specific humidity, mid-level relative humidity, and LCL, the differences between weak and intense storms appear to be insignificant compared to the rather strong differences between regions.
- The specific role played by topography appears to vary from region to region, although there is little question of its importance. The Rockies and Andes both provide opportunities for sinking of mid-level flow on their lee side, helping to create the cap (CIN) overlying the region of high CAPE, permitting stronger storms when the convergence associated with the low-level jet provides the required lift to assist in breaking through that cap. In HIMA, MWM, and COLUM, in contrast, the mountains appear to provide the lifting mechanism directly.

To the extent that the environment of intense storms in these regions shares conditions widely agreed to be important, the differences between weak and intense storms in some

regions, especially the tropical regions, and the variability from region to region, demands some caution in accepting these results uncritically. There are uncertainties of unknown quantity in the reanalysis datasets, making rigorous and unambiguous comparison between weak and intense storms difficult. We are uncertain of the accuracy of the ERA-Interim reanalyses in data-sparse regions, especially in regions with complex topography (COLUM, NWM, HIMA). Also, we have not considered other factors, such as the nature of atmospheric synoptic disturbances in data-sparse regions, or aerosol effects that may have an effect, so we look forward to further studies in the future, with improved datasets, before accepting these results in quantitative detail.

Acknowledgements

This research was supported by NASA Precipitation Measurement Mission grants NNX16AD76G under the direction of Dr. Gail Jackson and NNX16AH74G under the direction of Dr. Erich Stocker. Thanks to the Precipitation Processing System (PPS) team at NASA Goddard Space Flight Center, Greenbelt, MD, for data processing assistance.

References

Albrecht, R. I., S. J. Goodman, D. E. Buechler, R. J. Blakeslee, and H. J. Christian, 2016: Where are the lightning hotspots on Earth? *Bull. Amer. Meteor. Soc.*, **97**, 2051–2068, doi:https://doi.org/10.1175/BAMS-D-14-00193.1

Albrecht, R. I., S. J. Goodman, W. A. Petersen, D. E. Buechler, E. C. Bruning, R. J. Blakeslee, and H. J. Christian, 2011: The 13 years of TRMM Lightning Imaging Sensor: From individual flash characteristics to decadal tendencies. *Proc. 14th Int. Conf. on Atmospheric Electricity,* Rio de Janeiro, Brazil, International Commission of Atmospheric Electricity, M11-0203.

Alcala, C. M., and A. E. Dessler 2002: Observations of deep convection in the tropics using the tropical rainfall measuring (TRMM) precipitation radar, *J. Geophys. Res.*, **107(D24),** 4792, doi:10.1029/2002JD002457.

Alfaro, D. A., 2017: Low-tropospheric shear in the structure of squall lines: impacts on latent heating under layer-lifting ascent. *J. Atmos. Sci.* **74,** 229–248.

Altinger de Schwarzkopf, M. L., and L. C. Rosso, 1982: Severe storms and tornadoes in Argentina.Preprints, *12th Conf. on Severe Local Storms,* San Antonio, TX, Amer. Meteor. Soc., 59–62.

Amador, J. A., 1998: A climatic feature of the tropical Americas: The trade wind easterly jet. *Trop. Meteor. Oceanogr.*, **5**, 91–102.

Amador, J. A., and V. Magaña, 1999: Dynamics of the low level jet over the Caribbean Sea. Preprints, *Third Conf. on Hurricanes and Tropical Meteorology,* Dallas, TX, Amer. Meteor. Soc., 868–869.

Anderson, B. T., and J. O. Roads, 2001: Summertime moisture divergence over the southwestern US and northwestern Mexico, *Geophys. Res. Lett.,* **28**, 1973–1976, doi:10.1029/2001GL012903.

Aspliden, J. P., Y. Tourre, and J. B. Sabine, 1976: Some climatological aspects of West African disturbance lines during GATE, *Mon. Weather Rev.,* **104**, 1029 – 1035.

Atkins, N. T., R. M. Wakimoto, and C. L. Ziegler, 1998: Observations of the finescale structure of a dryline during VORTEX 95. *Mon. Wea. Rev.,* **126**, 525–550.

Ba, M.B. and S.E. Nicholson, 1998: Analysis of Convective Activity and Its Relationship to the Rainfall over the Rift Valley Lakes of East Africa during 1983–90 Using the Meteosat Infrared Channel. *J. Appl. Meteor.,* **37**, 1250–1264.

Barnes, S. L., and C. W. Newton, 1986: Thunderstorms in the synoptic setting. *Thunderstorm Morphology and Dynamics,* 2d ed., E. Kessler, Ed., University of Oklahoma Press, 75–112.

Barron, J. A. S., E. Metcalfe, and J. A. Addison, 2012: Response of the North American monsoon to regional changes in ocean surface temperature, *Paleoceanography*, **27**, PA3206, doi:10.1029/2011PA002235.

Beebe, R. G., 1958: An instability line development as observed by the tornado research airplane. *J. Meteor.*, **15**, 278–282.

Benjamin, S. G., and T. N. Carlson, 1986: Some effects of surface heating and topography on the regional severe storm environment. Part I: Three-dimensional simulations. *Mon. Wea. Rev.,* **114**, 307–329.

Berbery, E. H., 2001: Mesoscale moisture analysis of the North American monsoon. *J. Climate*, **14**, 121–137, doi:10.1175/ 1520-0442(2001)013,0121:MMAOTN.2.0.CO;2.

Berry, G.J. and C. Thorncroft, 2005: Case Study of an Intense African Easterly Wave. *Mon. Wea. Rev.,* **133**, 752–766, https://doi.org/10.1175/MWR2884.1.

Bieda, S. W., C. L. Castro, S. L. Mullen, A. C. Comrie, and E. Pytlak, 2009: The relationship of transient upper-level troughs to variability of the North American monsoon system. *J. Climate*, **22**, 4213–4227, doi:10.1175/2009JCLI2487.1.

Blanchard, D. O., and R. E. Lopez, 1985: Spatial patterns of convection in south Florida. *Mon. Wea. Rev*., **113**, 1282–1299.

Bluestein, H. B., E. W. McCaul Jr., G. P. Byrd, and G. R. Woodall, 1988: Mobile sounding observations of a tornadic storm near the dryline: The Canadian, Texas storm of 7 May 1986. *Mon. Wea. Rev.,* **116**, 1790–1804.

Boccippio, D. J., W. J. Koshak, and R. J. Blakeslee, 2002: Performance assessment of the Optical Transient Detector and Lightning Imaging Sensor. Part I: Predicted diurnal variability. *J. Atmos. Oceanic Technol.*, **19,** 1318–1332.

Bordoni, S., and B. Stevens, 2006: Principal component analysis of the summertime winds over the Gulf of California: A gulf surge index, *Mon. Weather Rev.,* **134**, 3395–3414.

Brenner, I. S., 1974: A surge of maritime tropical air—Gulf of California to the southwestern United States. *Mon. Wea. Rev.,* **102**, 375–389, doi:10.1175/1520-0493(1974)102,0375: ASOMTA.2.0.CO;2.

Brooks, H. E., C. A. Doswell III, and M. P. Kay, 2003: Climatological estimates of local daily tornado probability for the United States. *Wea. Forecasting*, **18**, 626–640, doi:10.1175/ 1520-0434(2003)018,0626:CEOLDT.2.0.CO;2.

Brown, R. G., and C. Zhang, 1997: Variability of midtropospheric moisture and its effect on cloud-top height distribution during TOGA COARE. *J. Atmos. Sci.,* **54**, 2760–2774.

Brubaker K. L., Entekhabi D, Eagleson P. S., 1993: Estimation of continental precipitation recycling. *J. Climate*, **6**, 1077–1089.

Burpee, R. W., 1972: Origin and structure of easterly waves in lower troposphere of North Africa. *J. Atmos. Sci.,* **29**, 77–90, doi:10.1175/1520-0469(1972)029,0077:TOASOE.2.0.CO;2.

Burpee, R. W., and L. N. Lahiff, 1984: Area-average rainfall variations on sea-breeze days in south Florida. *Mon. Wea. Rev.,* **112**, 520–534.

Byers, H. R., and H. R. Rodebush, 1948: Causes of thunderstorms of the Florida peninsula. *J. Meteor.*, **5**, 275–280.

Carey, L.D., W.A. Petersen, and S.A. Rutledge, 2003: Evolution of Cloud-to-Ground Lightning and Storm Structure in the Spencer, South Dakota, Tornadic Supercell of 30 May 1998. *Mon. Wea. Rev.,* **131**, 1811–1831, https://doi.org/10.1175//2566.1.

Carlson TN, Benjamin SG, Forbes GS. 1983. Elevated mixed layers in the regional severe storm environment: conceptual model and case studies. *Mon. Weather Rev.*, **111**, 1453–1473.

Carlson, T. N., 1969: Some remarks on African disturbances and their progress over tropical Atlantic. *Mon. Wea. Rev.,* **97**, 716–726, doi:10.1175/1520-0493(1969)097,0716:SROADA.2.3.CO;2.

Carlson, T. N., and F. H. Ludlam, 1968: Conditions for the occurrence of severe local storms. *Tellus*, **20,** 203–226.

Cecil, D. J., 2009: Passive microwave brightness temperatures as proxies for hailstorms. J. *Appl. Meteor. Climatol.,* **48**, 1281–1286.

Cecil, D. J., and C. B. Blankenship, 2012: Toward a global climatology of severe hailstorms as estimated by satellite passive microwave imagers. *J. Climate*, **25**, 687–703.

Cecil, D. J., S. J. Goodman, D. J. Boccippio, E. J. Zipser, and S. W. Nesbitt, 2005: Three years of TRMM precipitation features. Part I: Radar, radiometric, and lightning characteristics, *Mon. Weather Rev.*, **133**, 543–566, doi:10.1175/MWR-2876.1.

Cecil, D.J., D.E. Buechler, and R.J. Blakeslee, 2015: TRMM LIS Climatology of Thunderstorm Occurrence and Conditional Lightning Flash Rates. *J. Climate,* **28**, 6536–6547, https://doi.org/10.1175/JCLI-D-15-0124.1

Chaggar, T. S., 1977: Geographical Distribution of Monthly and Annual Mean Frequency of Thunderstorm Days Over Eastern Africa. East African Meteorological Department. Nairobi: Tech. Memo. No. 26, pp. 1-22.

Christian, H. J., et al., 2003: frequency and distribution of lightning as observed from space by the Optical Transient Detector, *J. Geophys. Res.,* **108(D1)**, 4005, doi:10.1029/2002JD002347.

Cotton, W. R., M. S. Lin, R. L. McAnelly, and C. J. Tremback, 1989: A composite model of mesoscale convective complexes. *Mon. Wea. Rev.,* **117**, 765–783.

Cotton, W. R., R. L. George, P. J. Wetzel, and R. L. McAnelly, 1983: A long-lived mesoscale convective complex. Part I: The mountain-generated component. *Mon. Wea. Rev.*, **111,** 1893–1918.

Dee, D. P., et al., 2011: The ERA-Interim reanalysis: Configuration and performance of the data assimilation system, *Q. J. R. Meteorol. Soc*., **137(656)**, 553–597, doi:10.1002/qj.828.

Diaz, L., M. Martinez, J. Ramírez, and J. Rodriguez, 2009: Actualización de la actividad de rayos en Venezuela, empleando la información del proyecto satelital de la NASA. *Congreso Venezolano de Redes y Energía Eléctrica,* Porlamar, Venezuela, Comité Nacional Venezolano de CIGRÉ, B2-223.

Doswell III, C. A., 1984: A kinematic analysis of frontogenesis associated with a nondivergent vortex.*J. Atmos. Sci.*, **41,** 1242–1248.

Doswell III, C. A., 2001: Severe convective storms—An overview. *Severe Convective Storms, Meteor. Monogr.,* No. 50, Amer. Meteor. Soc., 1–26.

Doswell, C.A., H.E. Brooks, and R.A. Maddox, 1996: Flash Flood Forecasting: An Ingredients-Based Methodology. *Wea. Forecasting,* **11**, 560–581.

Douglas, M. W., R. Maddox, K. Howard, and S. Reyes, 1993: The Mexican monsoon. *J. Climate*, **6**, 1665–1667.

Duran-Quesada, A. M., M. Reboita, and L. Gimeno, 2012: Precipitation in tropical America and the associated sources of moisture: A short review, *Hydrol. Sci. J.,* **57(4),** 612–624.

Durkee JD, Mote TL., 2009: A climatology of warm-season mesoscale convective complexes in subtropical South America. *Int. J. Climatol.* **30**, 418–431, doi: 10.1002/joc.1893.

Erfani, E., and D. Mitchell, 2014: A partial mechanistic understanding of the North American monsoon, *J. Geophys. Res. Atmos.,* **119**, 13,096–13,115, doi:10.1002/ 2014JD022038

Finch, Z. O., and R. H. Johnson, 2010: Observational analysis of an upper-level inverted trough during the 2004 North American monsoon experiment. *Mon. Wea. Rev.,* **138**, 3540–3555, doi:10.1175/2010MWR3369.1.

Fink, A. H., and A. Reiner, 2003: Spatiotemporal variability of the relation between African Easterly Waves and West African squall lines in 1998 and 1999. *J. Geophys. Res.,* **108,** 4332, doi:10.1029/2002JD002816.

Frank, W. M., 1978: The life cycles of GATE convective systems. *J. Atmos. Sci.,* **35**, 1256–1264

Fujita, T., 1958: Structure and movement of a dry front. *Bull. Amer. Meteor. Soc.,* **39**, 574–582.

Fulks, J. R., 1951: The instability line. *Compendium of Meteorology,* T. F. Malone, Ed., Amer. Meteor. Soc., 647–652.

Glass, F. H., D. L. Ferry, J. T. Moore, and S. M. Nolan, 1995: Characteristics of heavy convective rainfall events across the mid-Mississippi valley during the warm season: Meteorological conditions and a conceptual model. Preprints, *14th Conf. on Weather Analysis and Forecasting,* Dallas, TX, Amer. Meteor. Soc., 34–41.

Green, C. R., and W. D. Sellers, Eds., 1964: Arizona Climate. Tucson University of Arizona Press, 503 pp.

Guy, N., and S. A. Rutledge, 2012: Regional comparison of West African convective characteristics: A TRMM-based climatology. *Quart. J. Roy. Meteor. Soc.,* **138**, 1179–1195, doi:10.1002/qj.1865.

Hales, J. E., 1972: Surges of maritime tropical air northward over the Gulf of California. *Mon. Wea. Rev.*, **100**, 298–306.

Hane, C. E., H. B. Bluestein, T. M. Crawford, M. E. Baldwin, and R. M. Rabin. 1997: Severe thunderstorm development in relation to along-dryline variability: A case study. *Mon. Wea. Rev.*, **125**, 231–251.

Higgins, R. W., Y. Yao, and X. L. Wang, 1997: Influence of the North American monsoon system on the U.S. summer precipitation regime. *J. Climate*, **10**, 298–306, doi:10.1175/1520-0442(1997)010,2600: IOTNAM.2.0.CO;2.

Hoch, J., and P. Markowski, 2005: A climatology of springtime dryline position in the U.S. Great Plains region. *J. Climate*, **18**, 2132–2137.

Holton, J. R., 1979: *An Introduction to Dynamic Meteorology*. 3rd ed. Academic Press, 507 pp.

Hou, A. Y., R. K. Kakar, S. Neeck, A. A. Azarbarzin, C. D. Kummerow, M. Kojima, R. Oki, K. Nakamura, and T. Iguchi, 2014: The Global Precipitation Measurement mission, *Bull. Am. Meteorol. Soc.,* **95**, 701–722.

Houze, R. A., D. C. Wilton, and B. F. Smull, 2007: Monsoon convection in the Himalayan region as seen by the TRMM Precipitation Radar. *Quart. J. Roy. Meteor. Soc.,* **133,** 1389–1411, doi:10.1002/ qj.106.

Houze, R. A., Jr., K. L. Rasmussen, M. D. Zuluaga, and S. R. Brodzik 2015: The variable nature of convection in the tropics and subtropics: A legacy of 16 years of the Tropical Rainfall Measuring Mission satellite, *Rev. Geophys.,* **53**, doi:10.1002/2015RG000488.

Jackson, B., S. E. Nicholson, and D. Klotter, 2009: Mesoscale convective systems over western equatorial Africa and their relationship to large-scale circulation. *Mon. Wea. Rev.,* **137**, 1272–1294, doi:10.1175/2008MWR2525.1.

Johns, R. H., and C. A. Doswell III, 1992: Severe local storms forecasting. *Wea. Forecasting*, **7**, 588–612.

Johns, R.H., 1982: A Synoptic Climatology of Northwest Flow Severe Weather Outbreaks. Part I: Nature and Significance. *Mon. Wea. Rev.,* **110**, 1653–1663.

Johnson, R. H., P. E. Ciesielski, and J. A. Cotturone, 2001: Multiscale variability of the atmospheric mixed layer over the western Pacific warm pool. *J. Atmos. Sci.,* **58**, 2729–2750.

Johnson, R. H., P. E. Ciesielski, B. D. McNoldy, P. J. Rogers, and R. K. Taft (2007), Multiscale variability of the flow during the North American Monsoon Experiment, *J. Clim.,* **20,** 1628–1648

Kummerow, C., W. Barnes, T. Kozu, J. Shiue, and J. Simpson, 1998: The Tropical Rainfall Measuring Mission (TRMM) Sensor Package, *J. Atmos. Oceanic Technol.*, **15**, 809–817.

Lafore, J.-P., and Coauthors, 2011: Progress in understanding of weather systems in West Africa. *Atmos. Sci. Lett.*, **12**, 7–12, doi:10.1002/asl.335.

Lal, D. M., and S. D. Pawar, 2009: Relationship between rainfall and lightning over central Indian region in monsoon and premonsoon seasons. *Atmos. Res.,* **92**, 402–410, doi:10.1016/ j.atmosres.2008.12.009.

Lang, T. J., and S. A. Rutledge, 2002: Relationships between convective storm kinematics, precipitation, and lightning. *Mon. Wea. Rev.,* **130**, 2492–2506.

Lenters, J.D. and K.H. Cook, 1995: Simulation and Diagnosis of the Regional Summertime Precipitation Climatology of South America. *J. Climate,* **8**, 2988–3005.

Liu, C., and E. J. Zipser, 2015: The global distribution of largest, deepest, and most intense precipitation systems, *Geophys. Res. Lett.,* **42**, doi:10.1002/ 2015GL063776.

Liu, C., and E. Zipser, 2005: Global distribution of convection penetrating the tropical tropopause, *J. Geophys. Res.,* **110,** D23210, doi:10.1029/ 2005JD00006063.

Liu, C., D. Cecil, and E. J. Zipser, 2012: Relationships betwe en lightning flash rates and radar reflectivity vertical structures in thunderstorms over the tropics and subtropics, *J. Geophys. Res.,* **117**, D06212, doi:10.1029/2011JD017123.

Liu, C., D. J. Cecil, E. J. Zipser, K. Kronfeld, and R. Robertson 2012: Relationships between lightning flash rates and radar reflectivity vertical structures in thunderstorms over the tropics and subtropics, *J. Geophys. Res.,* **117**, D06212, doi:10.1029/2011JD017123.

Liu, N. and C. Liu, 2018: Synoptic Environments and Characteristics of Convection Reaching the Tropopause over Northeast China. *Mon. Wea. Rev.,* **146**, 745–759,https://doi.org/10.1175/MWR-D-17-0245.1.

Liu, N., and C. Liu, 2016: Global distribution of deep convection reaching tropopause in 1 year GPM observations, *J. Geophys. Res. Atmos.*, **121,** 3824–3842, doi:10.1002/ 2015JD024430.

Lopez, M. E., 1966: Cloud seeding trials in the rainy belt of western Colombia, *Water Resour. Res.*, **2**, 811–823.

MacGorman, D. R., and D. W. Burgess, 1994: Positive cloud-to-ground lightning in tornadic storms and hailstorms. *Mon. Wea. Rev.,* **122**, 1671– 1697.

Maddox, R. A., 1983: Large-scale meteorological conditions associated with midlatitude, mesoscale convective complexes. *Mon. Wea. Rev.,* **111**, 1475–1493.

Maddox, R.A., 1976: An Evaluation of Tornado Proximity Wind and Stability Data. *Mon. Wea. Rev.,* **104**, 133–142.

Mapes, B.E., T.T. Warner, M. Xu, and A.J. Negri, 2003: Diurnal Patterns of Rainfall in Northwestern South America. Part I: Observations and Context. *Mon. Wea. Rev.,* **131**,799–812, https://doi.org/10.1175/1520-0493(2003)131<0799:DPORIN>2.0.CO;2

Marengo, J. A.,, W. R. Soares, C. Saulo, and M. Nicolini, 2004: Climatology of the low level jet east of the Andes as derived from the NCEP–NCAR reanalyses: Characteristics and temporal variability. *J. Climate,* **17**, 2261–2280.

McCarthy, J., and S. E. Koch, 1982: The evolution of an Oklahoma dryline. Part I: A meso- and subsynoptic-scale analysis. *J. Atmos. Sci.*, **39**, 225–236.

McCollum, D., R. Maddox, and K. Howard, 1995: Case study of a severe mesoscale convective system in central Arizona. *Wea. Forecasting*, **10**, 643–665.

McNulty, R. P., 1978: On upper tropospheric kinematics and severe weather occurrence. *Mon. Wea. Rev.,***106,** 662–672.

Mekonnen, A., C.D. Thorncroft, and A.R. Aiyyer, 2006: Analysis of Convection and Its Association with African Easterly Waves. *J. Climate,* **19**, 5405–5421,https://doi.org/10.1175/JCLI3920.1

Miller, D. and J.M. Fritsch, 1991: Mesoscale Convective Complexes in the Western Pacific Region. *Mon. Wea. Rev.,* **119**, 2978–2992, https://doi.org/10.1175/1520-0493(1991)119<2978:MCCITW>2.0.CO;2

Miller, R., 1972: Notes on analysis and severe-storm forecasting procedures of the Air Force Global Weather Center. Air Weather Service Tech. Rep. 200, rev. ed. Air Weather Service, Scott Air Force Base, IL, 184 pp.

Miller, S. T. K., B. D. Keim, R. W. Talbot, and H. Mao, 2003: Sea breeze: Structure, forecasting, and impacts, *Rev. Geophys.,* **41**, 1011, doi:10.1029/2003RG000124, 3.

Mohr K. I, E. R. Toracinta, E. J. Zipser, and R. E. Orville, 1996: A comparison of WSR-88D reflectivities, SSM/I brightness temperatures, and lightning for mesoscale convective systems in Texas. Part II: SSM/I brightness temperatures and lightning. *J. Appl. Meteor.,***35,** 919–931.

Mohr K. I., and E. J. Zipser, 1996: Defining mesoscale convective systems by their 85-GHz ice-scattering signatures. *Bull. Am. Meteorol. Soc*. **77**, 1179–1189.

Moore, J.T., F.H. Glass, C.E. Graves, S.M. Rochette, and M.J. Singer, 2003: The Environment of Warm-Season Elevated Thunderstorms Associated with Heavy Rainfall over the Central United States. *Wea. Forecasting,* **18**, 861–878, https://doi.org/10.1175/1520-0434(2003)018<0861:TEOWET>2.0.CO;2

Murakami, T., 1987: Effects of the Tibetan Plateau. *Monsoon Meteorology,* C.-P. Chang and T. N. Krishnamurti, Eds., Oxford University Press, 235–270.

Nascimento, E. L., and C. A. Doswell III, 2006: The need for an improved documentation of severe thunderstorms and tornadoes in South America. *Symp. on the Challenges of Severe Convective Storms,*Atlanta, GA, Amer. Meteor. Soc., P1.18.

Newman, A. J., and R. H. Johnson, 2012: Mechanisms for precipitation enhancement in a North American monsoon upper-tropospheric trough. *J. Atmos. Sci.*, **69**, 1775–1792, doi:10.1175/JAS-D-11-0223.1.

Newman, A.J. and R.H. Johnson, 2013: Dynamics of a Simulated North American Monsoon Gulf Surge Event. *Mon. Wea. Rev.,* **141**, 3238–3253,https://doi.org/10.1175/MWR-D-12-00294.1

Newton, C. W., 1963: Dynamics of severe convective storms. *Severe Convective Storms, Meteor. Monogr.*, **No. 27**, Amer. Meteor. Soc., 33–58.

Nicholls, M. E., R. A. Pielke, and W. R. Cotton, 1991: A two-dimensional numerical investigation of the interaction between sea breezes and deep convection over the Florida peninsula. *Mon. Wea. Rev.*, **119**, 298–323.

Nicholls, S. D., and K. I. Mohr, 2010: An analysis of the environments of intense convective systems in West Africa in 2003. *Mon. Wea. Rev.,* **138**, 3721–3739.

Nicholson, S. E., 1996: A review of climate dynamics and climate variability in Eastern Africa. *The Limnology, Climatology and Paleoclimatology of the East African Lakes,* T. C. Johnson and E. O. Odada, Eds., Gordon and Breach, 25–56.

Nicholson, S.E., 2009: A revised picture of the structure of the “monsoon” and land ITCZ over West Africa. *Climate Dyn.,* **32**, 1155–1171, doi:10.1007/s00382-008- 0514-3.

Nicholson, S.E., 2018: The ITCZ and the Seasonal Cycle over Equatorial Africa. *Bull. Amer. Meteor. Soc.,* **99**, 337–348.

Nicholson, S.E., and J. P. Grist, 2003: The seasonal evolution of the atmospheric circulation over West Africa and equatorial Africa. *J. Climate*, **16**, 1013–1030, doi:10.1175/1520-0442(2003)0162.0.CO;2.

Nieto Ferreira, R., T. M. Rickenbach, D. L. Herdies, and L. M. V. Carvalho, 2003: Variability of South American convective cloud systems and tropospheric circulation during January– March 1998 and 1999. *Mon. Wea. Rev.,* **131**, 961–973.

Orville, R.E. and R.W. Henderson, 1986: Global Distribution of Midnight Lightning: September 1977 to August 1978. *Mon. Wea. Rev.,* **114**, 2640–2653, https://doi.org/10.1175/1520-0493(1986)114<2640:GDOMLS>2.0.CO;2.

Parker DJ, Thorncroft CD, Burton RR, Diongue-Niang A. 2005. Analysis of the African easterly jet, using aircraft observations from the JET2000 experiment. *Q. J. R. Meteorol. Soc*. **131**, 1461–1482.

Pessi, A. T., and S. Businger, 2009: Relationships among lightning, precipitation, and hydrometeor characteristics over the North Pacific Ocean, *J. Appl. Meteorol. Climatol.*, **48**, 833–848, doi:10.1175/2008JAMC1817.1.

Petersen, W. A., H. J. Christian, and S. A. Rutledge, 2005: TRMM observations of the global relationship between ice water content and lightning, *Geophys. Res. Lett.*, **32**, L14819, doi:10.1029/2005GL023236.

Petersen, W. A., S. A. Rutledge, and R. E. Orville, 1996: Cloud-to-ground lightning observations from TOGA COARE: Selected results and lightning location algorithms. *Mon. Wea. Rev.*, **124,** 602–620.

Peterson, R. E., 1983: The west Texas dryline: Occurrence and behavior. Preprints, 13th Conf. Severe Local Storms, Tulsa, OK, *Amer. Meteor. Soc*., J9–J11.

Pielke, R. A., A. Song, P. J. Michaels, W. A. Lyons, and R. W. Arritt, 1991: The predictability of sea-breeze generated thunderstorms. *Atmosfera*, **4**, 65–78.

Poveda, G., and O. J. Mesa, 2000: On the existence of Lloro (the rainiest locality on Earth): Enhanced ocean-atmosphere-land interaction by a low-level jet, *Geophys. Res. Lett*., **27**, 1675–1678.

Poveda, G., P. R. Waylen, and R. S. Pulwarty, 2006: Annual and inter-annual variability of the present climate in northern South America and southern Mesoamerica. *Palaeogeogr. Palaeoclimatol. Palaeoecol.*, **234,** 3–27.

Price, C., Y. Yair, and M. Asfur, 2007: East African lightning as a precursor of Atlantic hurricane activity*, Geophys. Res. Lett*., **34**, L09805, doi:10.1029/2006GL028884.

Qie, X., R. Toumi, and T. Yuan, 2003: Lightning activities on the Tibetan Plateau as observed by the Lightning Imaging Sensor. *J. Geophys. Res.*, **108**, 4551, doi:10.1029/2002JD003304.

Qie, X., X. Wu, T. Yuan, J. Bian, and D. Lu, 2014: Comprehensive pattern of deep convective systems over the Tibetan Plateau–South Asian monsoon region based on TRMM data. *J. Climate*, **27**, 6612–6626, doi:https://doi.org/10.1175/JCLI-D-14-00076.1.

Ranalkar, M., and H. Chaudhari, 2009: Seasonal variation of lightning activity over the Indian subcontinent. *Meteor. Atmos. Phys.,* **104**, 125–134, doi:10.1007/s00703-009-0026-7.

Rasmussen, K. L., and R. A. Houze, 2011: Orogenic convection in subtropical South America as seen by the TRMM satellite. *Mon. Wea. Rev.,* **139**, 2399–2420, doi:10.1175/MWR-D-10-05006.1.

Rasmussen, K. L., and R. Houze, 2016: Convective Initiation near the Andes in Subtropical South America. *Mon. Wea. Rev.,* **144**, 2351–2374, doi: 10.1175/MWR-D-15-0058.1.

Rasmussen, K. L., M. D. Zuluaga, and R. A. Houze, 2014: Severe convection and lightning in subtropical South America. *Geophys. Res. Lett*., **41**, 7359–7366, doi:10.1002 /2014GL061767.

Reason, C.J., W. Landman, and W. Tennant, 2006: Seasonal to Decadal Prediction of Southern African Climate and Its Links with Variability of the Atlantic Ocean. *Bull. Amer. Meteor. Soc.,* **87**, 941–955, https://doi.org/10.1175/BAMS-87-7-941.

Rhea, J. O., 1966: A study of thunderstorm formation along dry lines. *J. Appl. Meteor.,* **5**, 58– 63.

Roca, R., J. Lafore, C. Piriou, and J. Redelsperger, 2005: Extratropical Dry-Air Intrusions into the West African Monsoon Midtroposphere: An Important Factor for the Convective Activity over the Sahel. *J. Atmos. Sci.,* **62**, 390–407, https://doi.org/10.1175/JAS-3366.1

Rockwood, A. A., and R. A. Maddox, 1988: Mesoscale and synoptic interactions leading to intense convection: The case of 7 June 1982. *Wea. Forecasting,* **3,** 51–68.

Romatschke, U. and R. Houze, 2011: Characteristics of Precipitating Convective Systems in the Premonsoon Season of South Asia. *J. Hydrometeor.,* **12**, 157–180, doi: 10.1175/2010JHM1311.1.

Romatschke, U., and R. A. **Houze,** Jr., 2010: Extreme summer convection in South America. *J. Climate*, **23**, 3761-3791.

Romatschke, U., S. Medina, and R. A. Houze, 2010: Regional, seasonal, and diurnal variations of extreme convection in the South Asian region, *J. Clim.*, **23**, doi:10.1175/2009JCLI3140.1.

Rosenfeld, D., W. L. Woodley, T. W. Krauss, and V. Makitov, 2006: Aircraft microphysical documentation from cloud base to anvils of hailstorm feeder clouds in Argentina. *J. Appl. Meteor. Climatol.,* **45**, 1261–1281.

Sakamoto, M. S., T. Ambrizzi, and G. Poveda, 2011: Moisture sources and life cycle of convective systems over western Colombia, *Adv. Meteorol.,* **2011**, 1–11, doi:10.1155/2011/890759.

Salio, P., M. Nicolini, and E.J. Zipser, 2007: Mesoscale Convective Systems over Southeastern South America and Their Relationship with the South American Low-Level Jet. *Mon. Wea. Rev.,* **135**, 1290–1309, https://doi.org/10.1175/MWR3305.1.

Sanders, F., 1999: A Short-Lived Cold Front in the Southwestern United States. *Mon. Wea. Rev.,* **127**, 2395–2403, https://doi.org/10.1175/1520-0493(1999)127<2395:ASLCFI>2.0.CO;2

Savenije, H. H. G, 1995: New definitions of moisture recycling and relation with land-use changes in the Sahel. J Hydrol (Amst) 167:57–78. doi:10.1016/0022-1694(94)02632-L

Schaefer, J. T., 1974: The life cycle of the dryline. *J. Appl. Meteor.,* **13**, 444–449.

Schoenberg Ferrier, B., J. Simpson, and W.-K. Tao (1996), Factors responsible for precipitation efficiencies in midlatitude and tropical squall simulations, *Mon. Weather Rev.,* **124**, 2100 – 2125, doi:10.1175/1520- 0493(1996)1242.0.CO;2.

Schultz, D.M., C.C. Weiss, and P.M. Hoffman, 2007: The Synoptic Regulation of Dryline Intensity. *Mon. Wea. Rev.,* **135**, 1699–1709, https://doi.org/10.1175/MWR3376.1

Schulz, W., K. Cummins, G. Diendorfer, and M. Dorninger, 2005: Cloud-to-ground lightning in Austria: A 10-year study using data from a lightning location system. *J. Geophys. Res.,* **110**, D09101, doi:10.1029/2004JD005332.

Schumacher, R.S. and R.H. Johnson, 2005: Organization and Environmental Properties of Extreme-Rain-Producing Mesoscale Convective Systems. *Mon. Wea. Rev.,* **133**,961–976, https://doi.org/10.1175/MWR2899.1

Schumacher, R.S., 2015: Sensitivity of Precipitation Accumulation in Elevated Convective Systems to Small Changes in Low-Level Moisture. *J. Atmos. Sci.,* **72**, 2507–2524.

Seluchi, M., and J. Marengo, 2000: Tropical–midlatitude exchange of air masses during summer and winter in South America: Climatic aspects and extreme events. *Int. J. Climatol*, **20,** 1167–1190.

Shaw, B. L., R. A. Pielke, and C. L. Ziegler, 1997: A threedimensional numerical simulation of a Great Plains dryline. *Mon. Wea. Rev.,* **125**, 1489–1506.

Simpson J. E., D. A. Mansfield, and J. R. Milford, 1977: Inland penetration of sea-breeze fronts. *Quart. J. Roy. Meteor. Soc.,* **103**, 47–76.

Spencer, R. W., and D. A. Santek 1985: Measuring the global distribution of intense convection over land with passive microwave radiometery, *J. Appl. Meteorol.,* **24,** 860–864.

Steenburgh, W. J., and C. F. Mass, 1994: The structure and evolution of a simulated Rocky Mountains lee trough. *Mon. Wea. Rev.* **122**, 2740-2761.

Stensrud, D. J., 2013: Upscale effects of deep convection during the North American Monsoon, *J. Atmos. Sci*., **70**, 2681–2695.

Stensrud, D. J., R. L. Gall, and M. K. Nordquist, 1997: Surges over the Gulf of California during the Mexican monsoon. *Mon. Wea. Rev.,* **125**, 417–437, doi:10.1175/1520-0493(1997)125,0417: SOTGOC.2.0.CO;2.

Takemi, T., 2007: A sensitivity of squall-line intensity to environmental static stability under various shear and moisture conditions, *Atmos. Res.,* **84**, 374 – 389, doi:10.1016/j.atmosres.2006.10.001.

Tao, W.-K., X. Li, A. Khain, T. Matsui, S. Lang, and J. Simpson, 2007: Role of atmospheric aerosol concentration on deep convective precipitation: Cloud-resolving model simulations, *J. Geophys. Res.,* **112**, D24S18, doi:10.1029/2007JD008728.

Taszarek, M., B. Czernecki, and A. Kozioł, 2015: A Cloud-to-Ground Lightning Climatology for Poland. *Mon. Wea. Rev.,* **143**, 4285–4304, https://doi.org/10.1175/MWR-D-15-0206.1

Tetzlaff G, Peters M. 1988. A composite study of early summer squall lines and their environment over West Africa. *Meteorol. Atmos. Phys*. **38**, 153–163, doi: 10.1007/BF01029779.

Thompson, R.L., C.M. Mead, and R. Edwards, 2007: Effective Storm-Relative Helicity and Bulk Shear in Supercell Thunderstorm Environments. *Wea. Forecasting,* **22**,102–115, https://doi.org/10.1175/WAF969.1

Trenberth K. E., 1999: Atmospheric moisture recycling: role of advection and local evaporation. *J Clim.* **12**, 1368–1381. doi:10.1175/1520-0442(1999)012\1368:AMRROA[2.0.CO;2

Trier, S. B., C. A. Davis, D. A. Ahijevych, M. L. Weisman, and G. H. Bryan, 2006: Mechanisms supporting long-lived episodes of propagating nocturnal convection within a 7-day WRF model simulation. *J. Atmos. Sci.*, **63,** 2437–2461.

Tuttle, J. D., and Carbone, R. E., 2004: Coherent regeneration and the role of water vapor and shear in a long-lived convective episode. *Monthly Weather Review,* **132(1),** 192-208.

Ushio, T., S. Heckman, D. J. Boccippio, and H. J. Christian, 2001: A survey of thunderstorm flash rates compared to cloud top height using TRMM satellite data. *J. Geophys. Res.*, **106,** 24089–24095.

Uyeda, H., and Coauthors, 2001: Characteristics of convective clouds observed by a Doppler radar at Naqu on Tibetan Plateau during the GAME-Tibet IOP. *J. Meteor. Soc. Japan*, **79**, 463–474.

van Delden, A., 2001. The synoptic setting of thunderstorms in Western Europe. *Atmos. Res.,* **56**, 89–110.

Velasco I, Frisch M, 1987: Mesoscale convective complexes in the Americas. *J. Geophys. Res.* **92(D8)**, 9591–9613.

Virts KS, and RA Houze., 2016: Seasonal and Intraseasonal Variability of Mesoscale Convective Systems over the South Asian Monsoon Region. *Journal of the Atmospheric Sciences* **73(12):**4753-4774. doi:10.1175/JAS-D-16-0022.1

Weisman, M. L., and R. Rotunno, 2000: The use of vertical wind shear versus helicity in interpreting supercell dynamics. *J. Atmos. Sci.*, **57,** 1452–1472

Weisman, M.L. and J.B. Klemp, 1982: The Dependence of Numerically Simulated Convective Storms on Vertical Wind Shear and Buoyancy. *Mon. Wea. Rev.,* **110**, 504–520, https://doi.org/10.1175/1520-0493.

Weston, K. J., 1972: The dry-line of Northern India and its role in cumulonimbus convection. *Q.J.R. Meteorol. Soc.,* **98**, 519–531. doi:10.1002/qj.49709841704.

Williams, E. R., C. Cooke, and K. Wright, 1985: Electrical discharge propagation in and around space charge clouds. *J. Geophys. Res.*, **90**, 6059–6070.

Xie, S., H. Xu, N.H. Saji, Y. Wang, and W.T. Liu, 2006: Role of Narrow Mountains in Large-Scale Organization of Asian Monsoon Convection. *J. Climate,* **19**, 3420–3429,https://doi.org/10.1175/JCLI3777.1

Xu, W., and E. J. Zipser, 2012: Properties of deep convection in tropical continental, monsoon, and oceanic rainfall regimes, *Geophys. Res. Lett*, **39**, doi: 10.1029/2012GL051242.

Xu, W*.,* E. J. Zipser*,* C. Liu*, and* J. Jiang*,* 2010*:* On the relationships between lightning frequency and thundercloud parameters of regional precipitation systems*, J. Geophys. Res.,* **115***, D12203, doi:10.1029/2009JD013385.*

Ziegler, C. L., and C. E. Hane, 1993: An observational study of the dryline. *Mon. Wea. Rev.,* **121**, 1134–1151.

Ziegler, C. L., and E. N. Rasmussen, 1998: The initiation of moist convection at the dryline: Forecasting issues from a case study perspective. *Wea. Forecasting*, 13, 1106–1131.

Ziegler, C. L., T. J. Lee, and R. A. Pielke, 1997: Convective initiation at the dryline: A modeling study. *Mon. Wea. Rev.,* **125**, 1001–1026

Zipser, E., C. Liu, D. Cecil, S. W. Nesbitt, and S. Yorty, 2006: Where are the most intense thunderstorms on Earth? *Bull. Am. Meteorol. Soc.,* **87**, 1057–1071.

Zuluaga, M., and R. A. Houze, 2015: Extreme convection of the near-equatorial Americas, Africa, and adjoining oceans as seen by TRMM, *Mon. Weather Rev.*, **143**, 298–316.

Table 1.1 The The population of CFs with different flashes and mean thermodynamic and dynamic parameters of weak (intense) thunderstorms over selected regions. The low-level shear between 1 and 6 km ($SHEAR_{1\text{-}6km}$) and the lifted condensation level (LCL) is calculated above ground level. SHL donates the near-surface Specific Humidity, while RHM represents the averaged mid-level (700-500 hPa) relative humidity (RH).

	Regions	Numbers (#)	CAPE (J/kg)	CIN (J/kg)	$SHEAR_{1\text{-}6km}$ (m/s)	SHL (g/kg)	RHM (%)	LCL (km)
Tropics	COLUM	113(41)	1897(2611)	22(13)	7.8(8.4)	16.7(17.6)	67.2(68.1)	1.21(0.98)
	SAHEL	364(51)	1477(1738)	38(32)	10.6(11.7)	17.4(17.3)	67.5(65.2)	1.20(1.22)
	CONGO	828(105)	1677(2046)	25(20)	5.9(6.9)	18.1(18.5)	65.9(59.6)	0.71(0.69)
	NWM	169(25)	1161(1581)	46(44)	5.1(7.0)	14.6(14.4)	69.8(71.4)	2.37(2.55)
Subtropics	HIMA*	206(28)	792(1270)	63(66)	11.8(12.9)	10.0(11.8)	67.1(61.8)	2.42(2.45)
	SCUS	701(164)	494(1156)	38(58)	13.2(14.6)	11.4(14.2)	57.9(51.4)	1.08(1.43)
	ARGEN	706(124)	748(1349)	54(41)	15.6(16.8)	12.3(13.7)	61.3(61.0)	1.26(1.21)

*March, April, and May

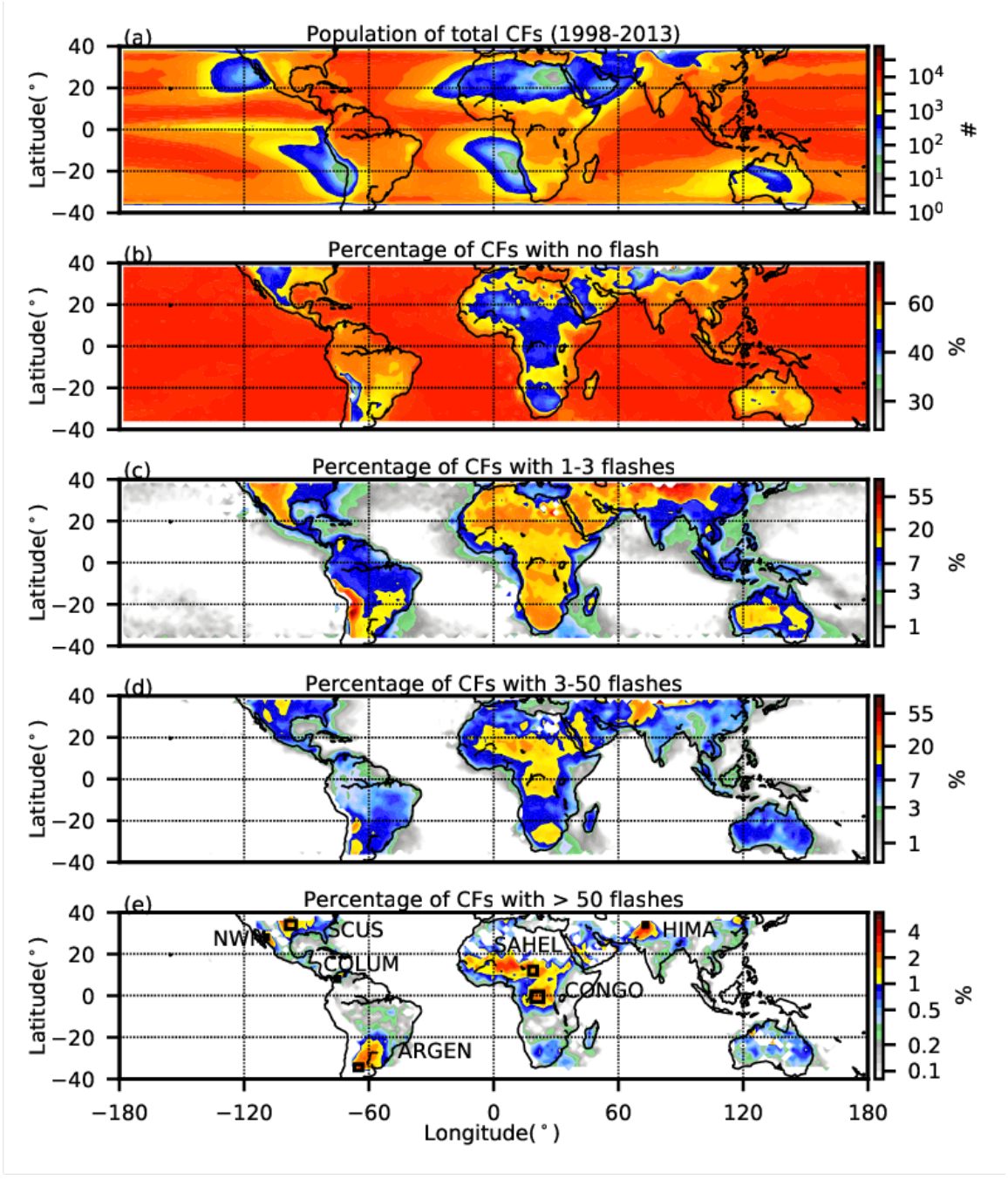

Figure 1.1 Geographical distribution of the population of total CFs and percentage of CFs with different flashes (a) total CFs (b) with no flash (c) with 1-3 flashes, (d) with 3-50 flashes, (e) with > 50 flashes. The distribution is created on a 2° x 2° grid from 16-years (1998-2013) of TRMM observations.

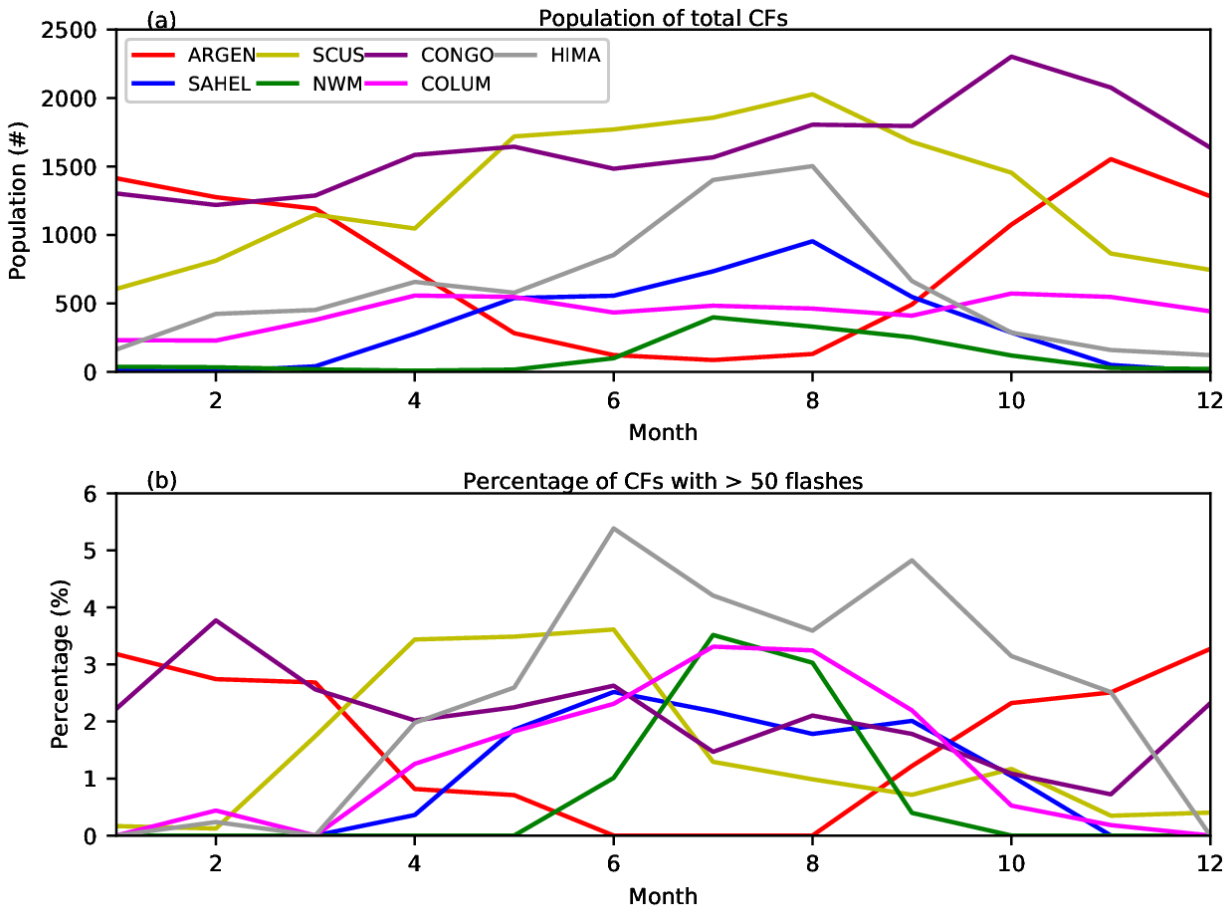

Figure 1.2 Seasonal variation of CFs and intense CFs with > 50 flashes. (a) population of total CFs, (b) the percentage of intense CFs with > 50 flashes.

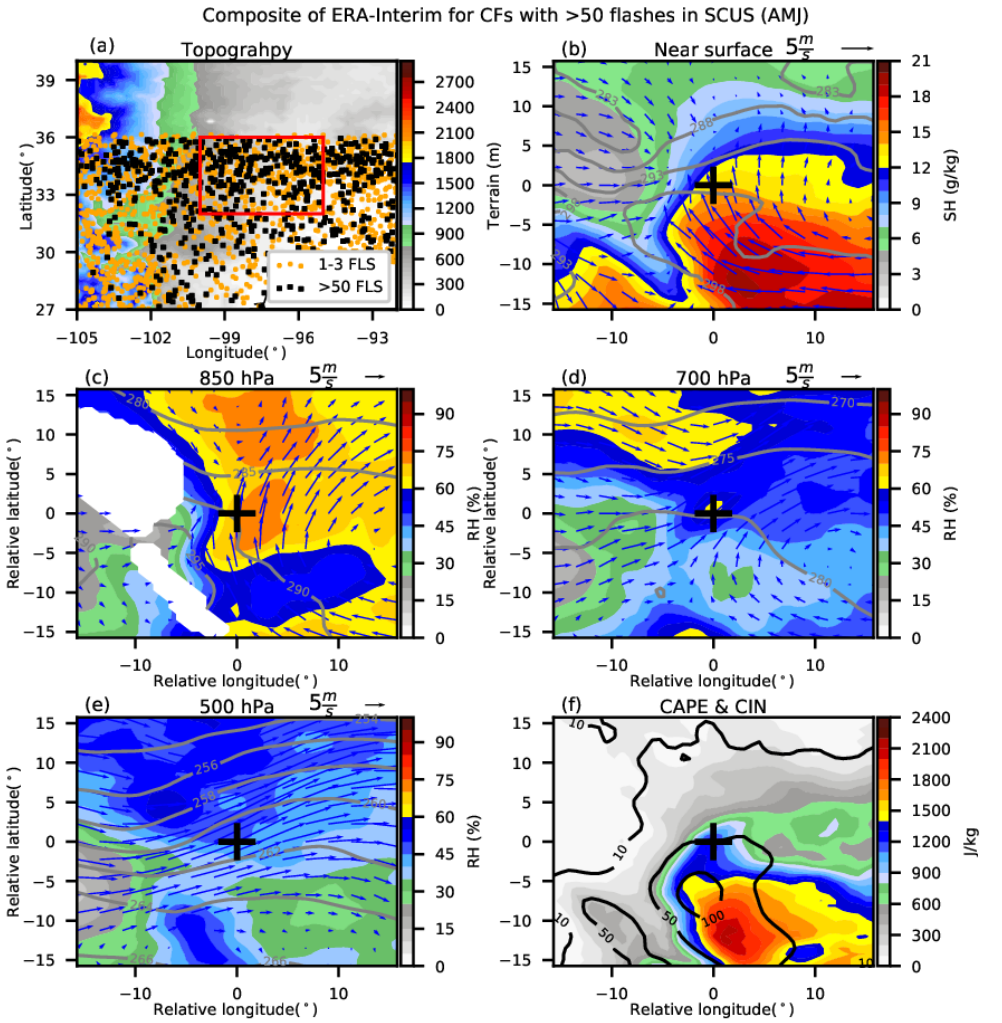

Figure 1.3 (a) Locations of CFs (orange crosses: 1-3 flashes; black crosses: > 50 flashes) and topography (color fill) over SCUS. (b) Composite 10 m wind vectors, 2 m temperature (T) (contour), and 2 m relative humidity (RH, color fill) for CFs with > 50 flashes over SCUS. (c) at 850 hPa, (d) at 700 hPa, (e) at 500 hPa, (f) composite CAPE (color fill) and CIN (contour). The bold black cross marks the composite centroid location of the CFs with > 50 flashes. Composite are made using ERA-Interim data starting at the surface pressure. The area with high terrain is left blank in the plot of 850 hPa (b) and 700 hPa (c), if the terrain reaches that level.

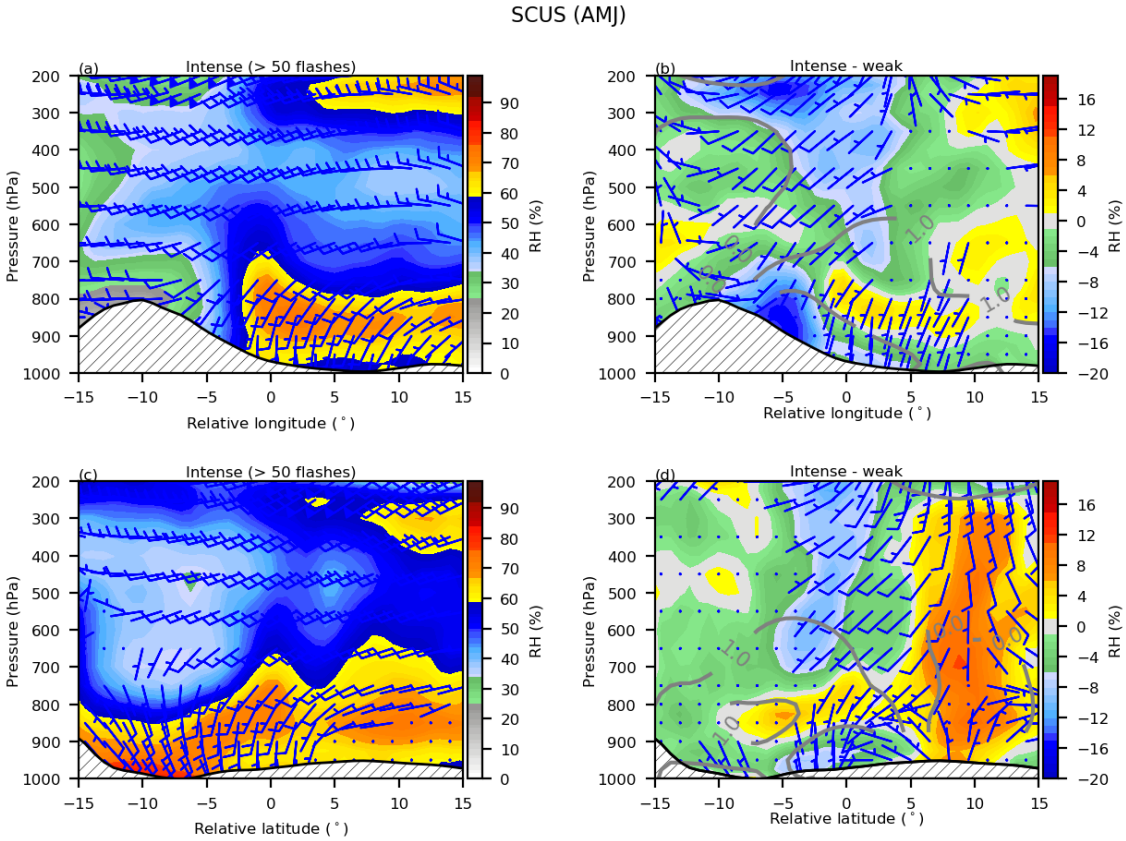

Figure 1.4 (a) Composite vertical cross-section of wind and RH (color fill) of intense CFs with > 50 flashes along the longitude where CFs occur over SCUS, (b) Difference cross section between intense and weak CFs (1-3 flashes), (c) Same as (a), but along the latitude CFs occur, (d) Same as (b), but along the latitude CFs occur. The thick black lines present the mean near surface pressure.

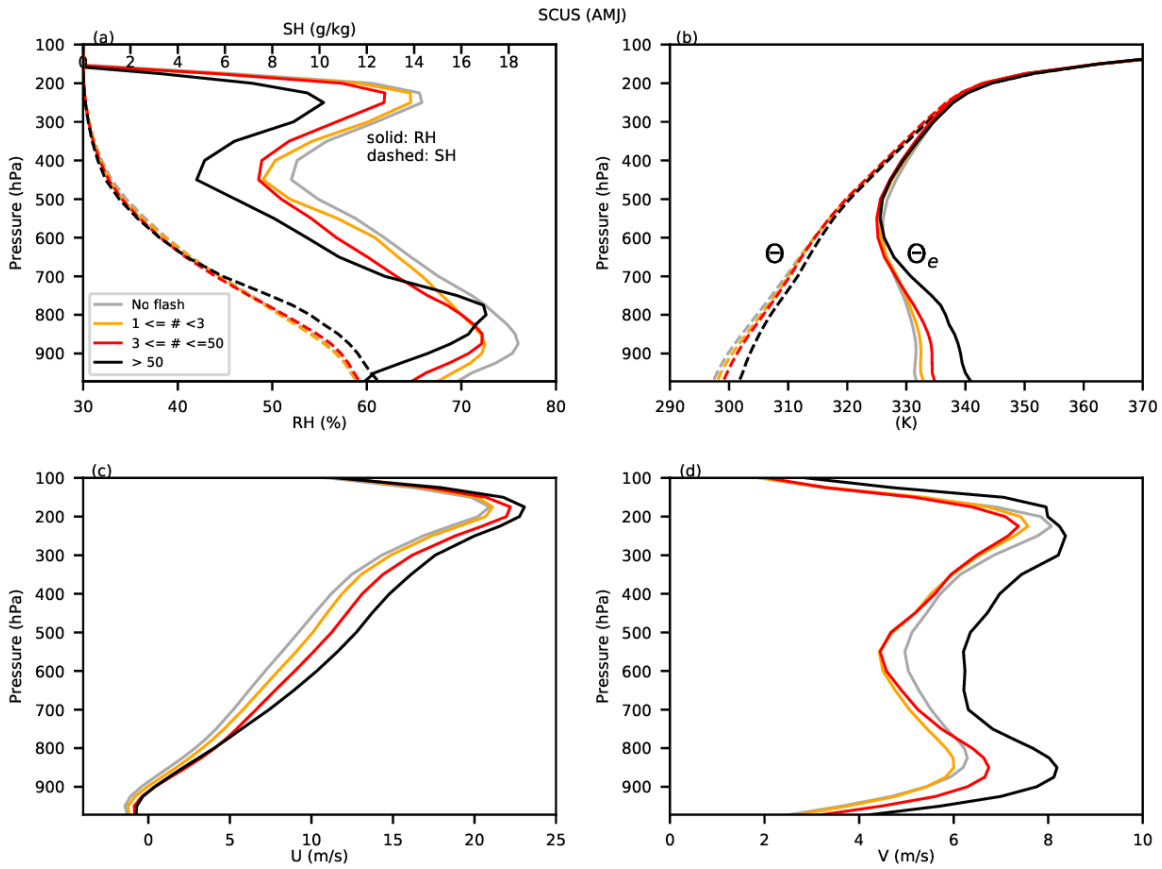

Figure 1.5 Composite profiles of different variables for CFs with different flashes over SCUS, (a) RH(solid) and SH (dashed), (b) Potential and equivalent potential temperature, (c) zonal wind (U), (d) Meridional wind (V). Note the profiles start from the mean near-surface pressure levels.

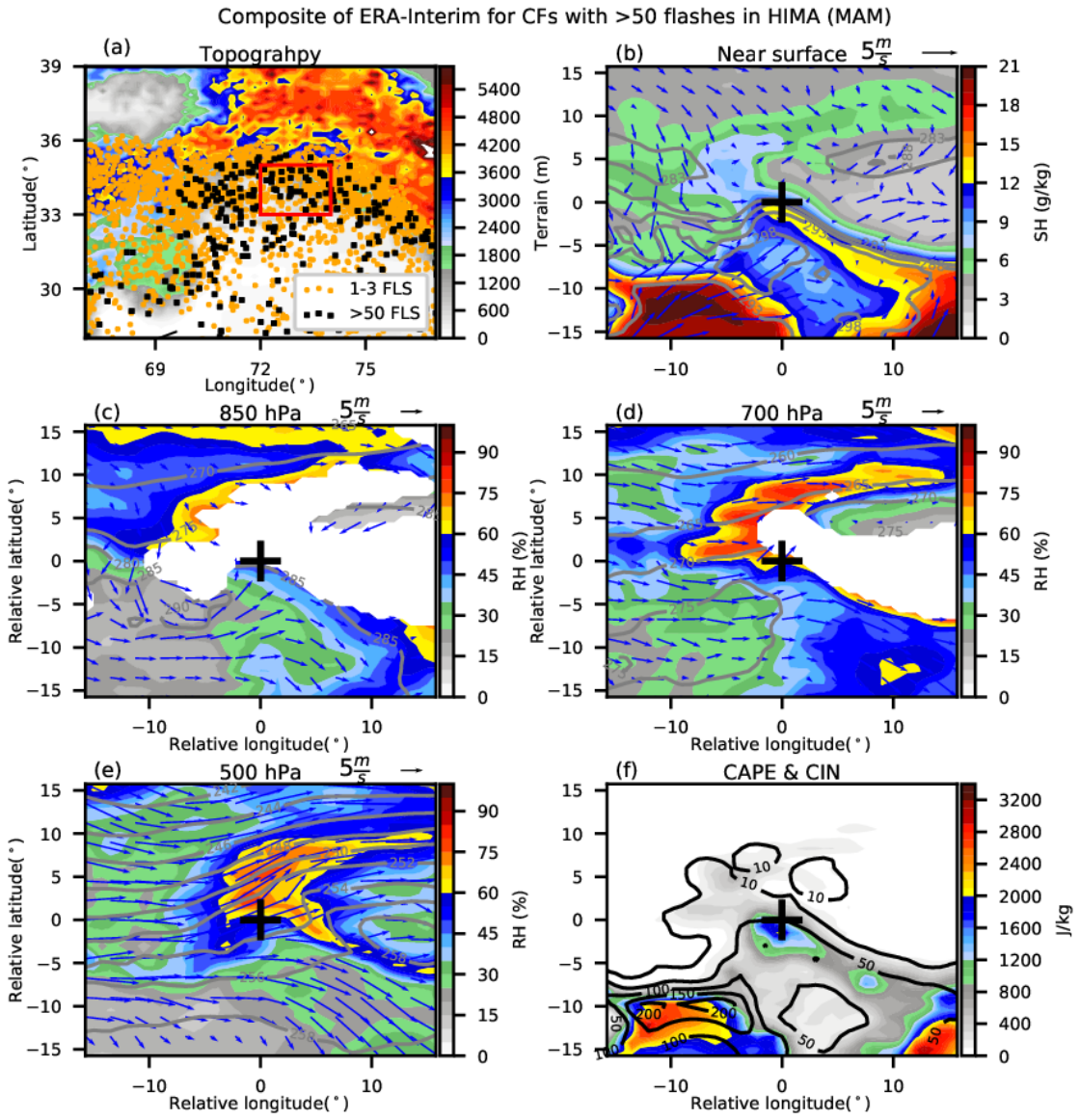

Figure 1.6 Same as Figure 1.3, but for HIMA.

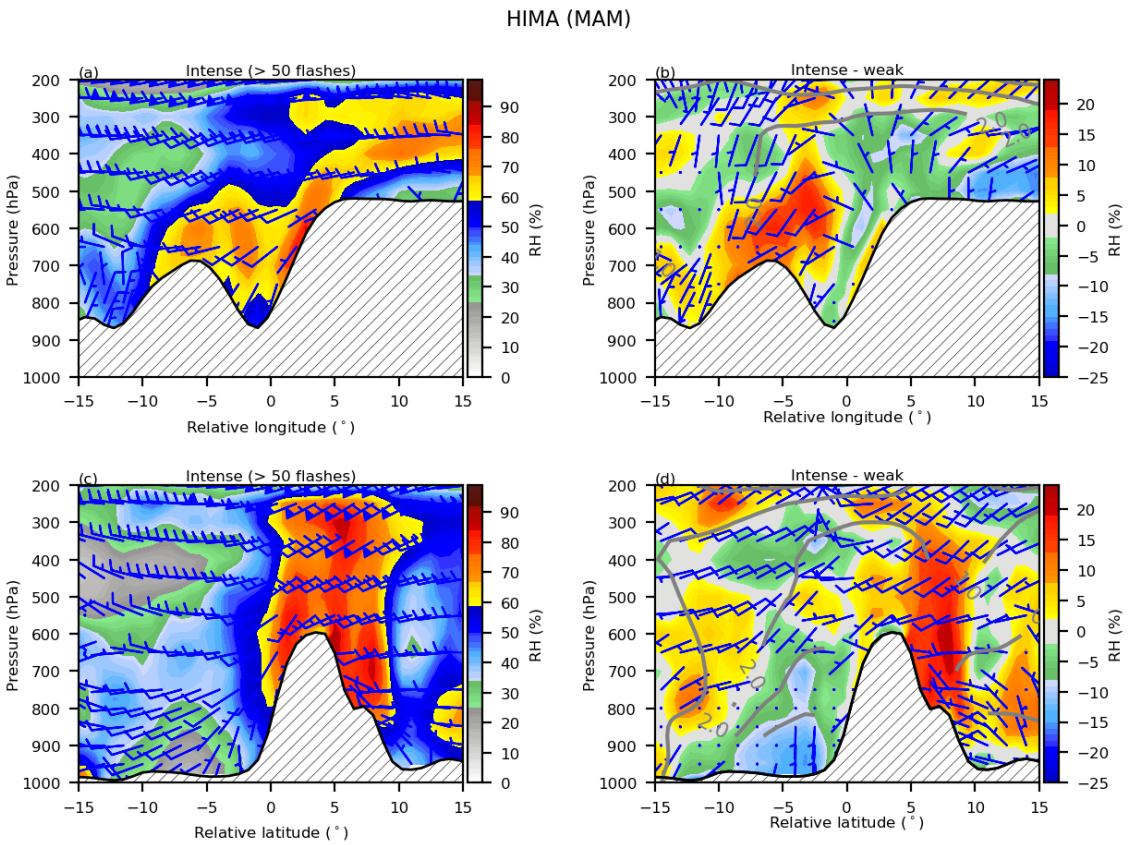

Figure 1.7 Same as Figure 1.4, but for HIMA.

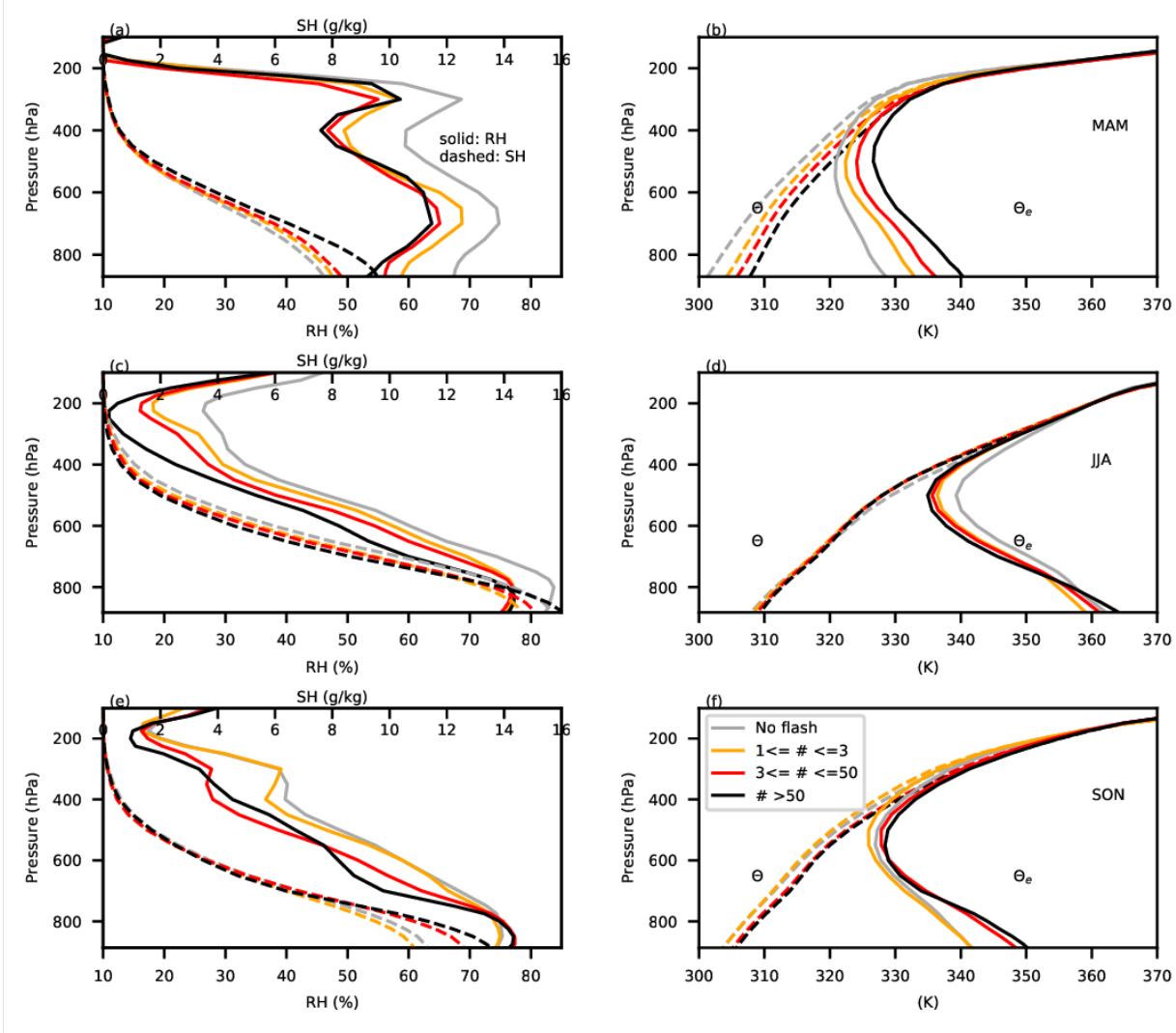

Figure 1.8 Composite profiles of RH and SH, Potential and equivalent potential temperature for CFs with different flashes in different seasons. (a) RH (solid) and SH (dashed) in spring (MAM), (b) Potential and equivalent potential temperature in MAM, (c) RH in JJA, (d) Potential and equivalent potential temperature in JJA, (e) RH in SON, (f) Potential and equivalent potential temperature in SON.

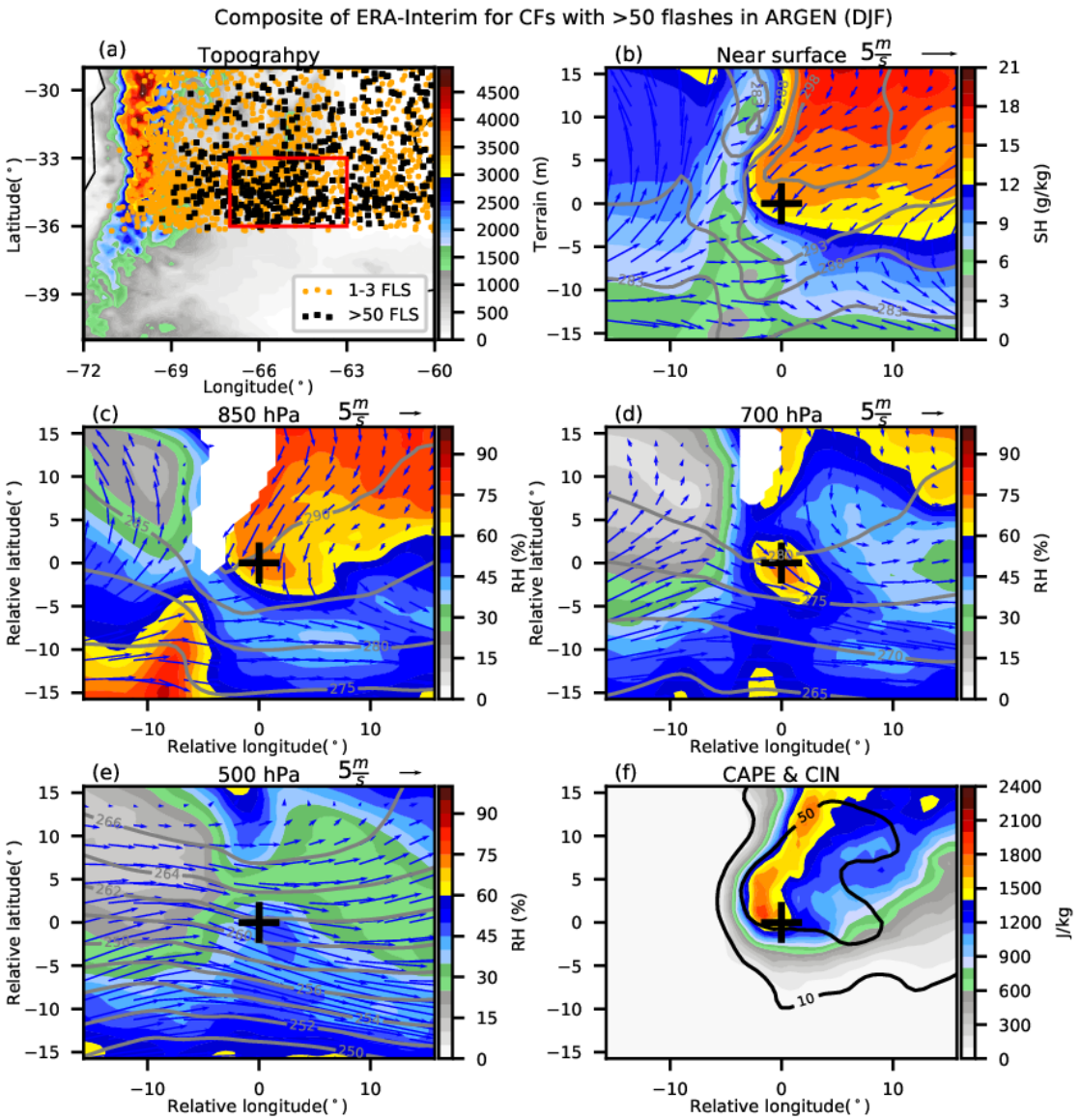

Figure 1.9 Same as Figure 1.3, but for ARGEN.

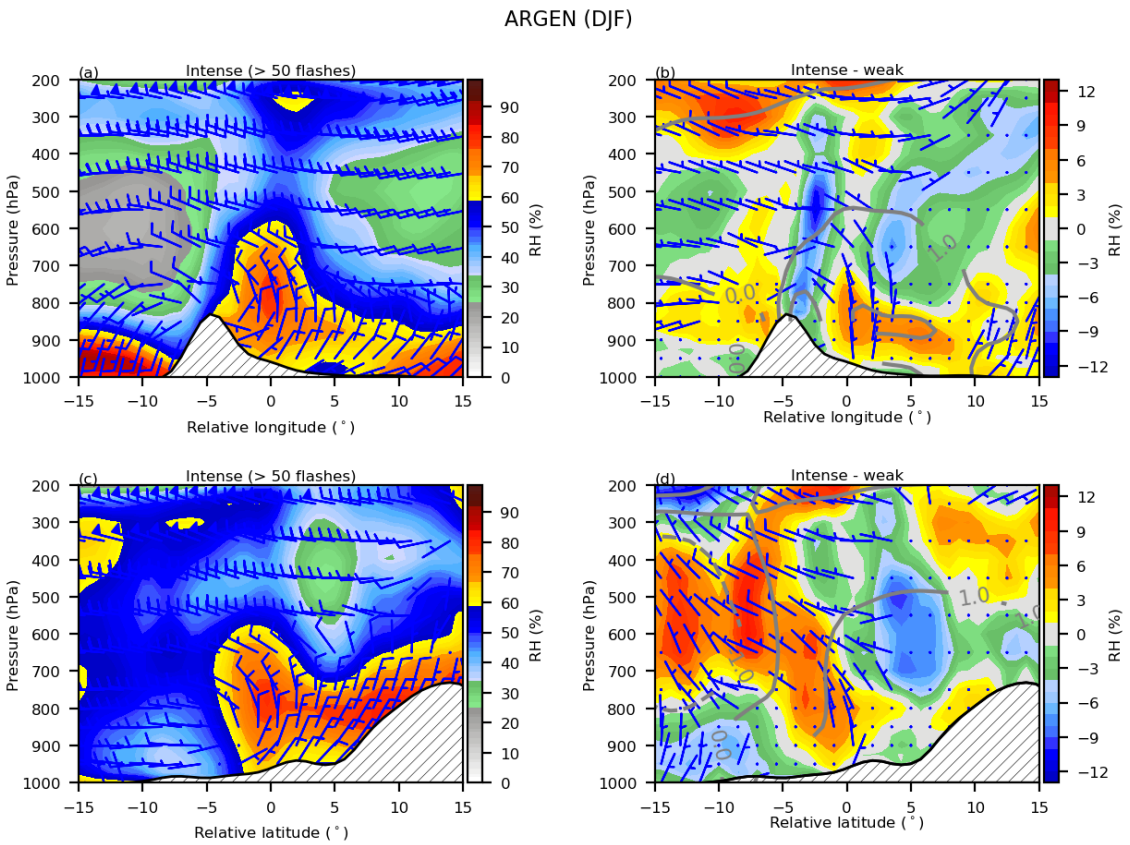

Figure 1.10 Same as Figure 1., but for ARGEN.

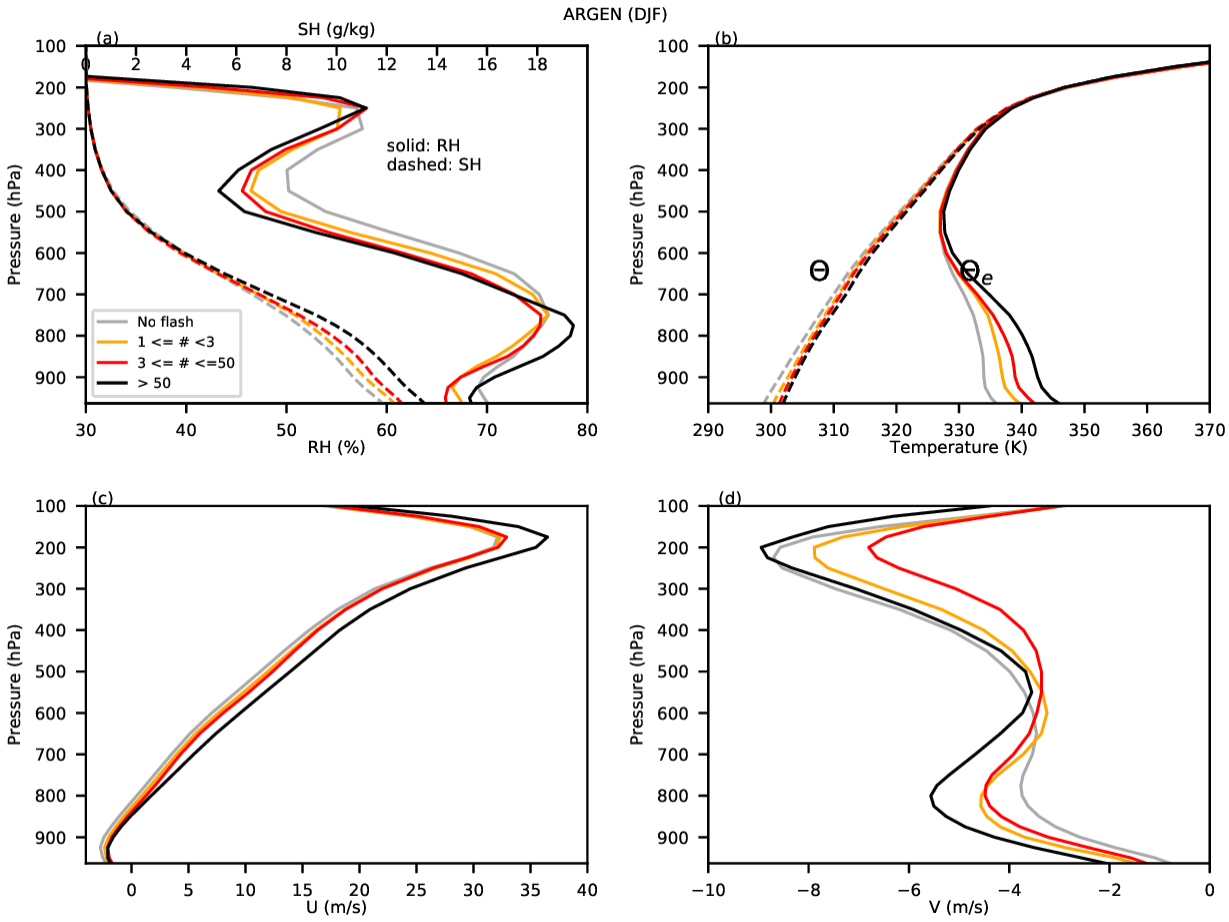

Figure 1.11 Same as Figure 1., but for ARGEN.

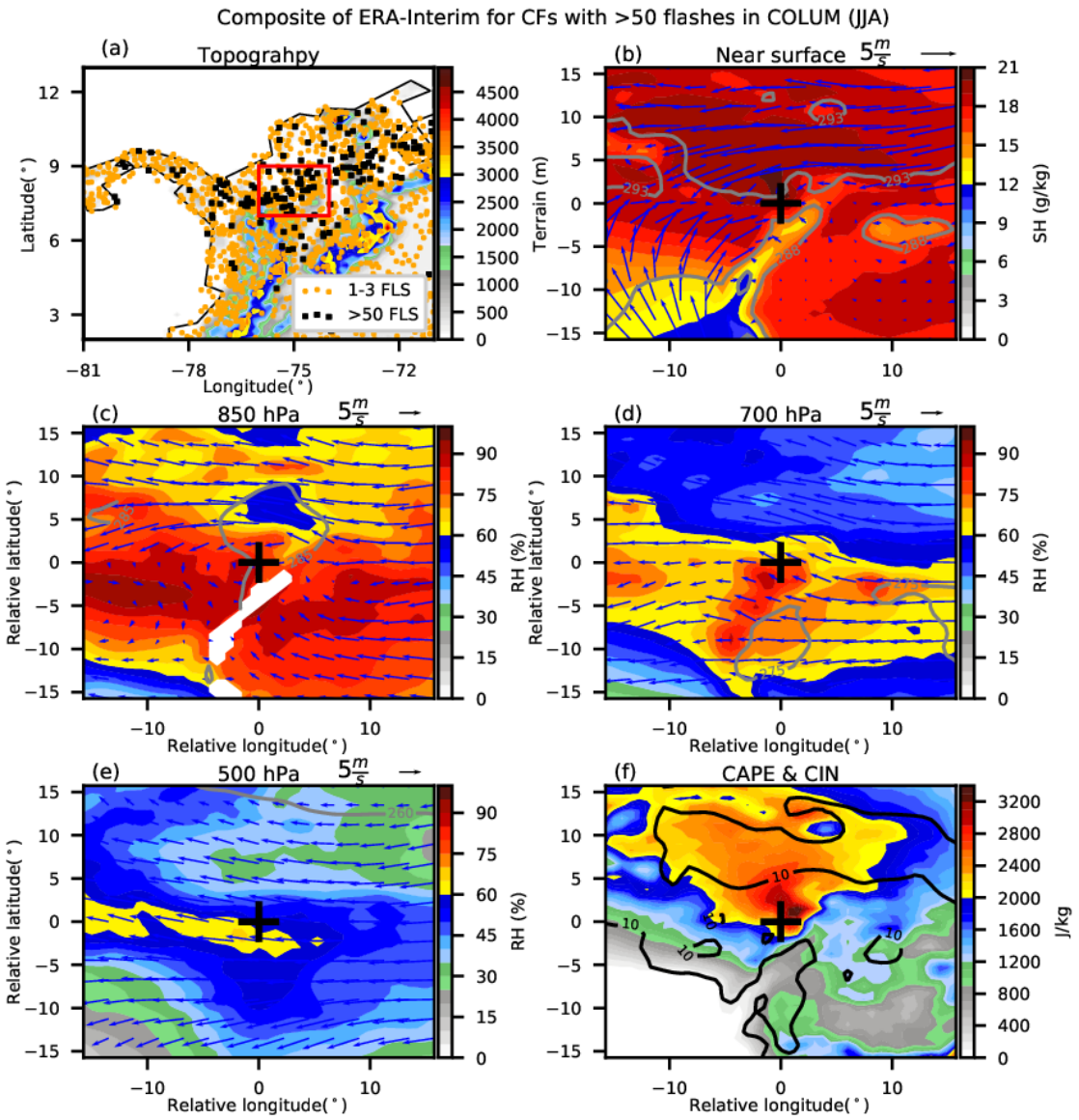

Figure 1.12 Same as Figure 1.3, but for COLUM.

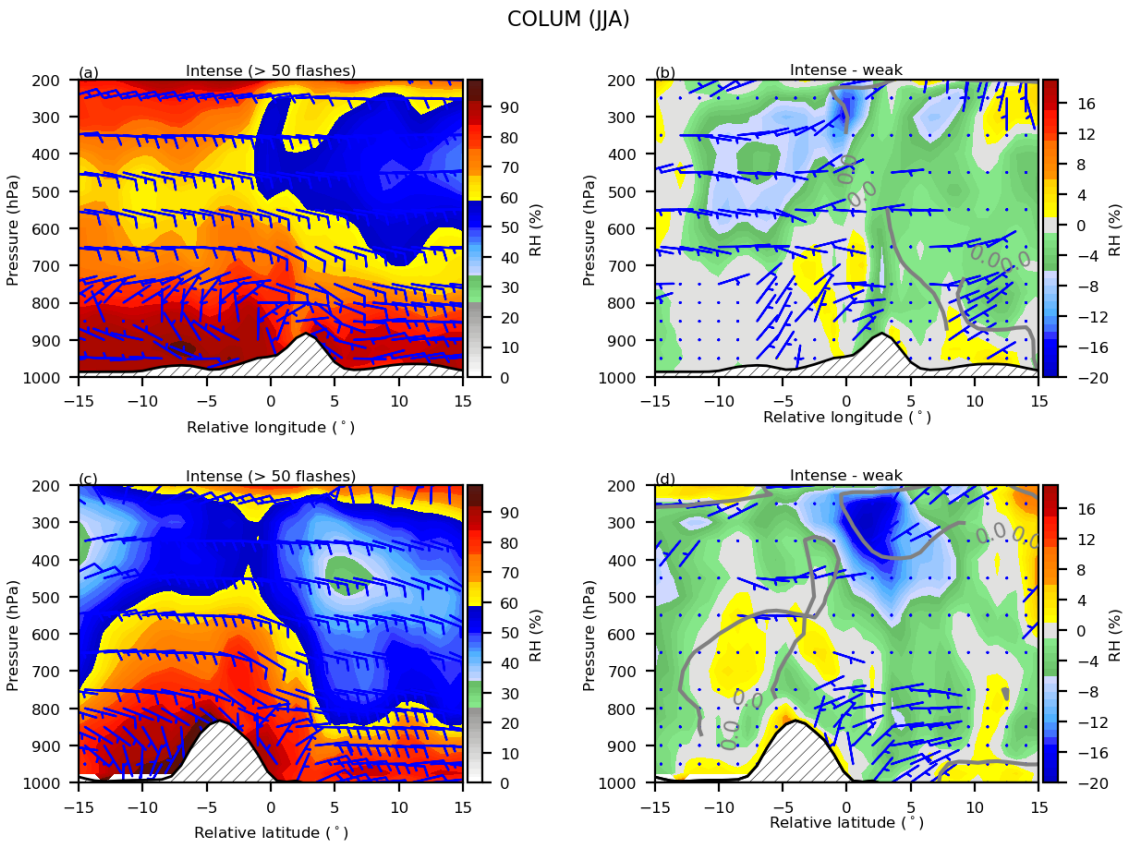

Figure 1.13 Same as Figure 1.4, but for COLUM.

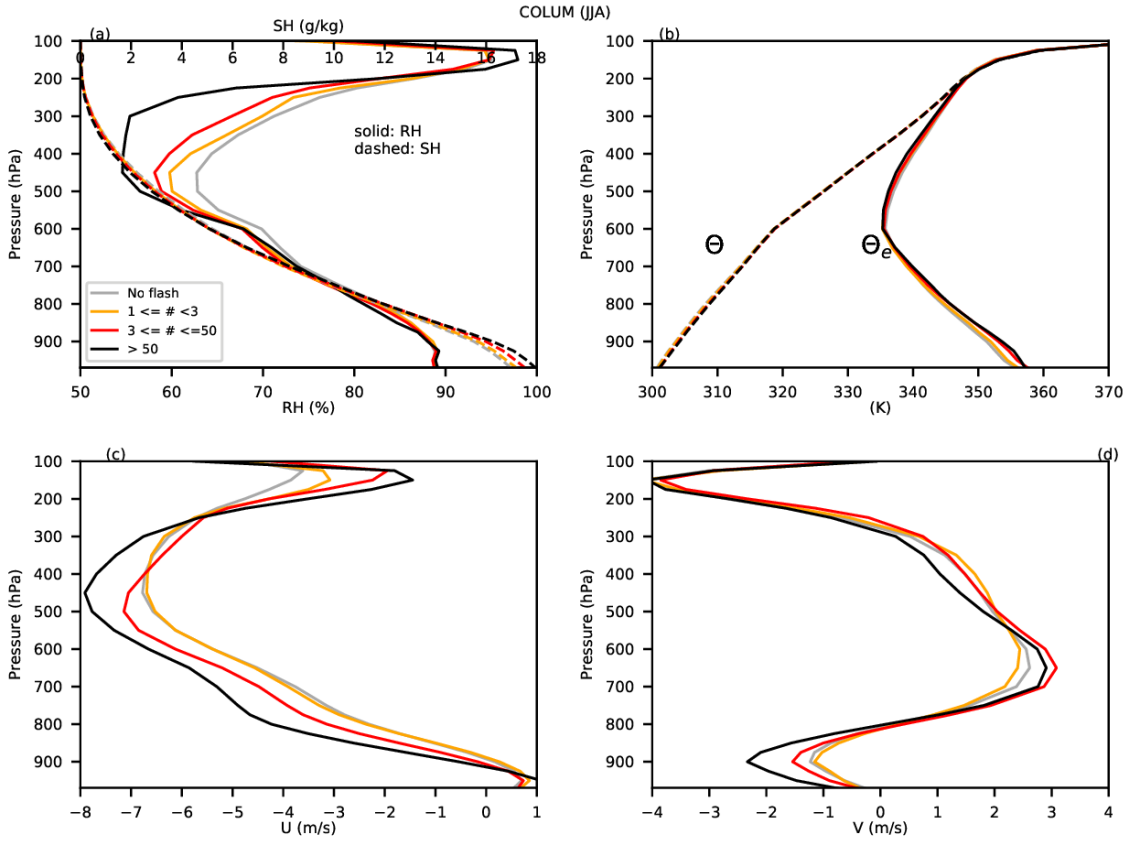

Figure 1.14 Same as Figure 1.5, but for COLUM.

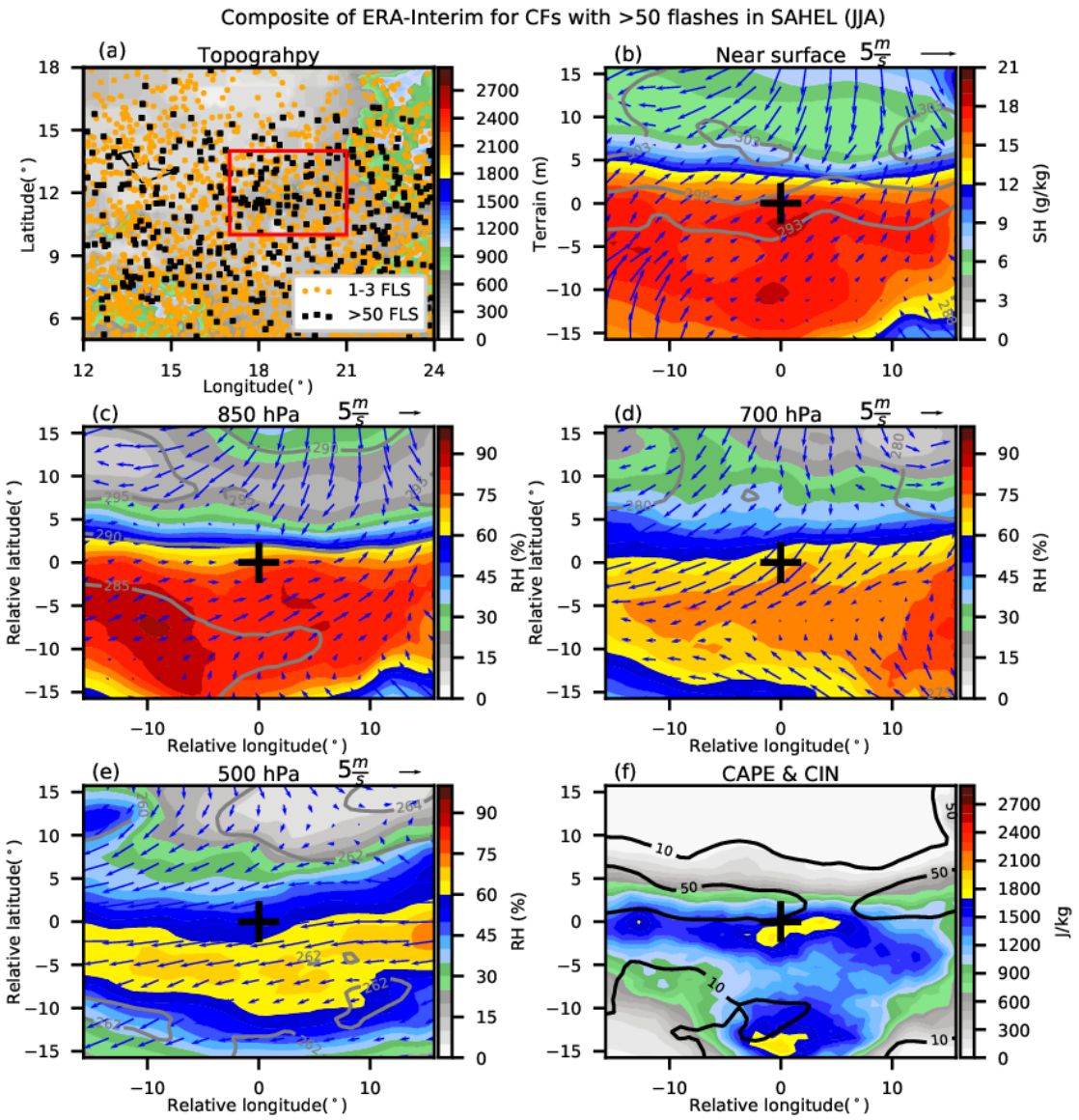

Figure 1.15 Same as Figure 1., but for SAHEL.

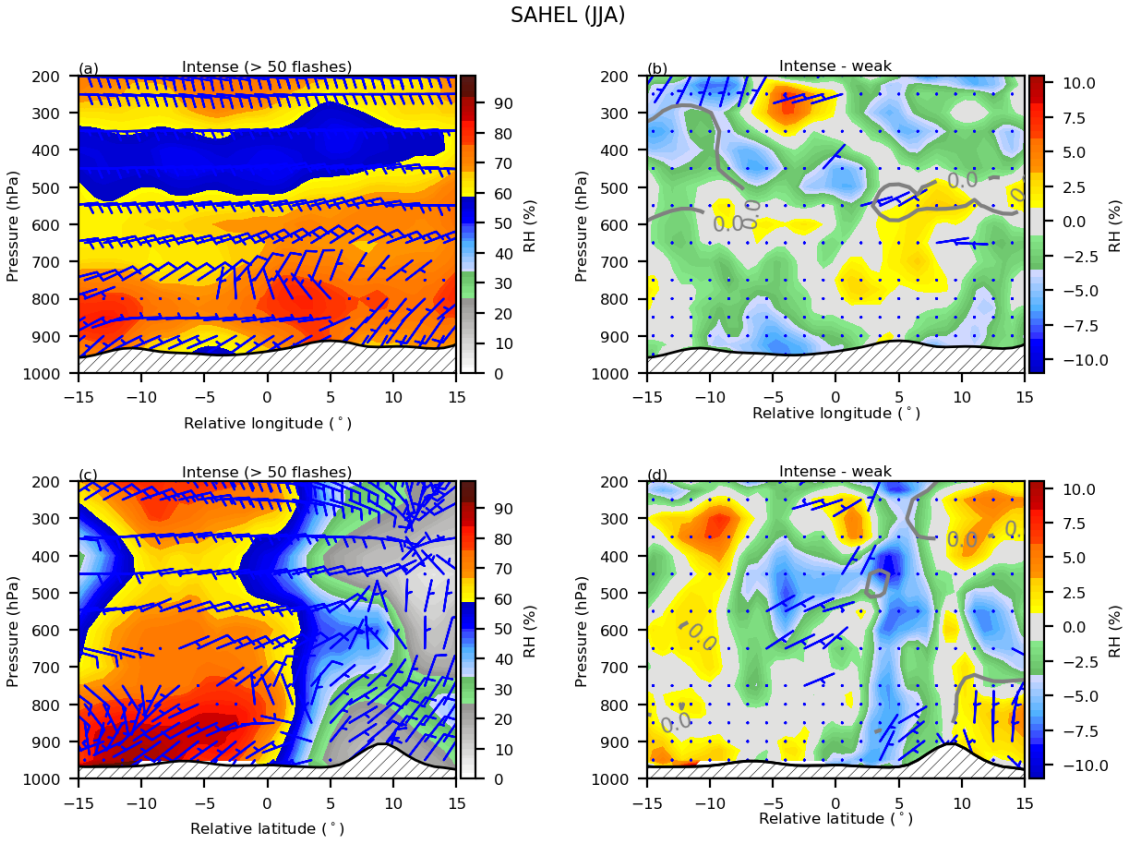

Figure 1.16 Same as Figure 1., but for SAHEL.

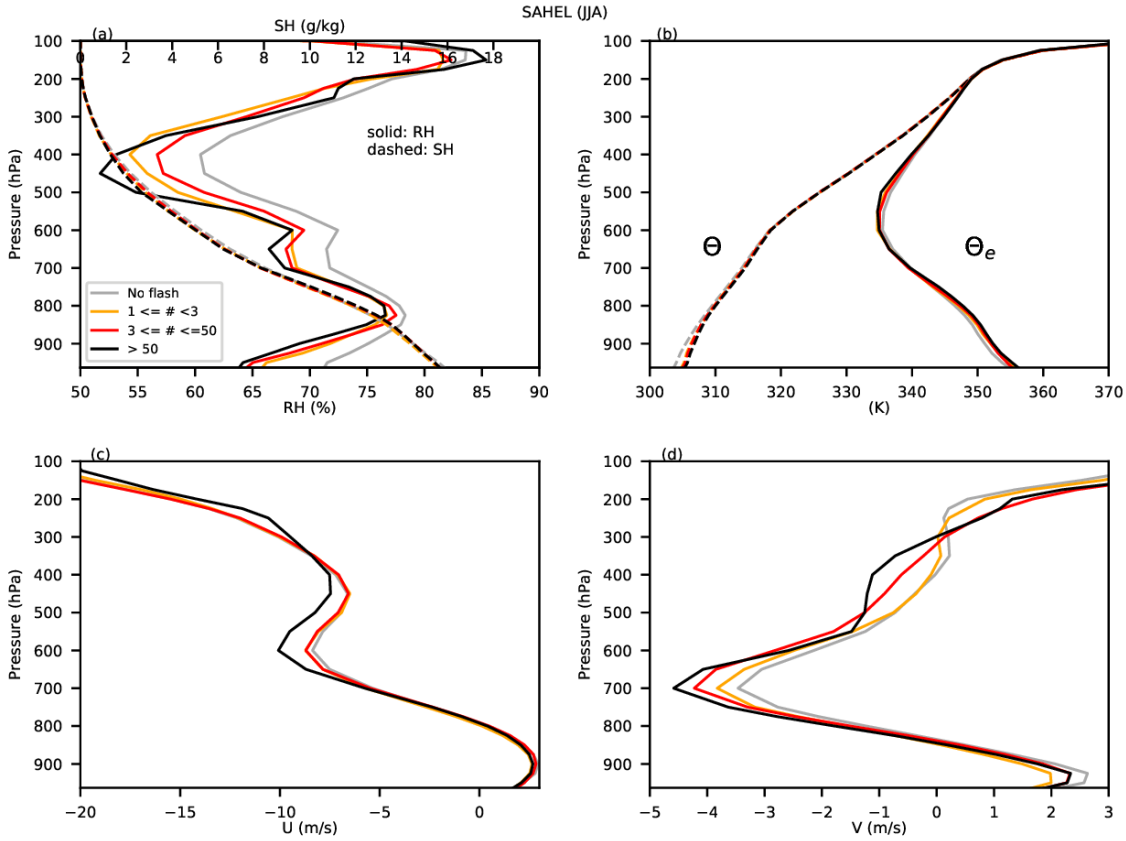

Figure 1.17 Same as Figure 1., but for SAHEL.

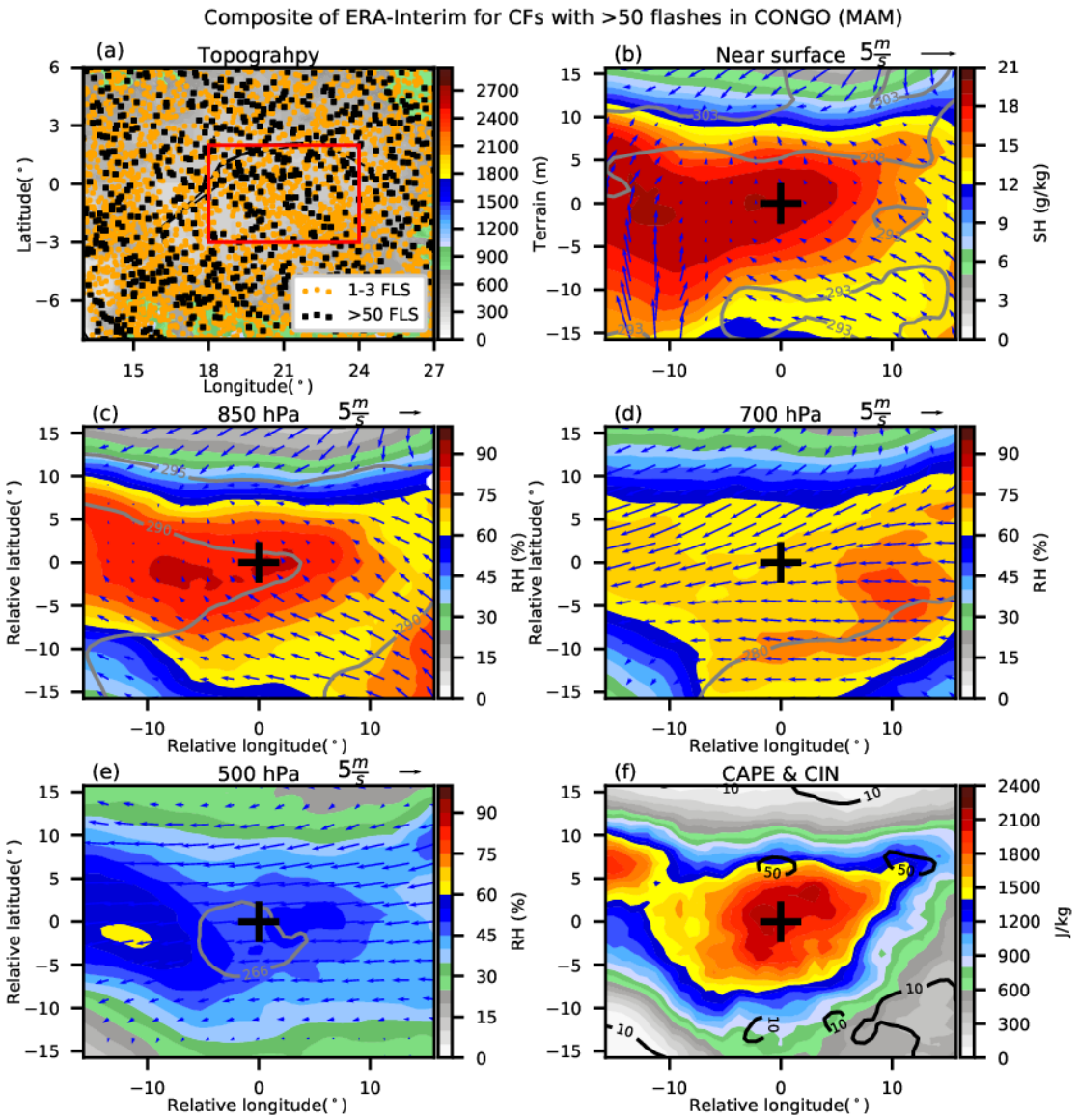

Figure 1.18 Same as Figure 1., but for CONGO.

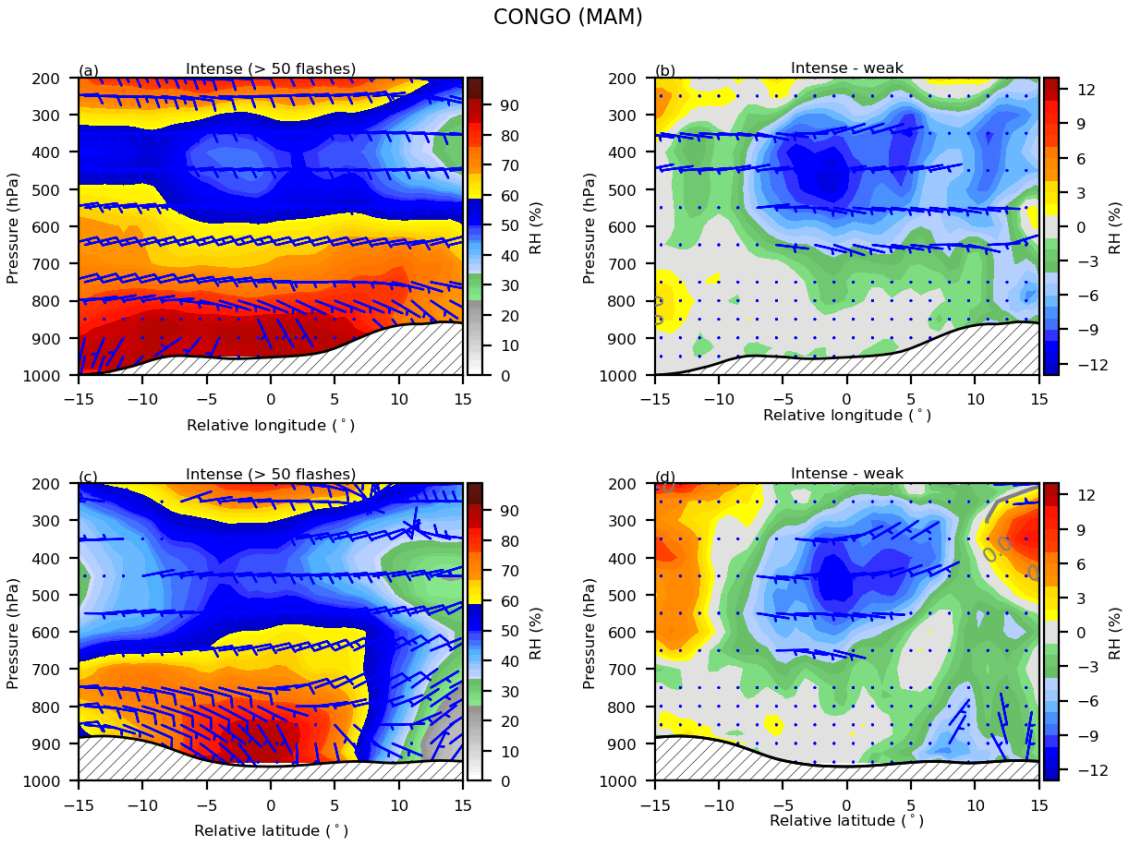

Figure 1.19 Same as Figure 1., but for CONGO.

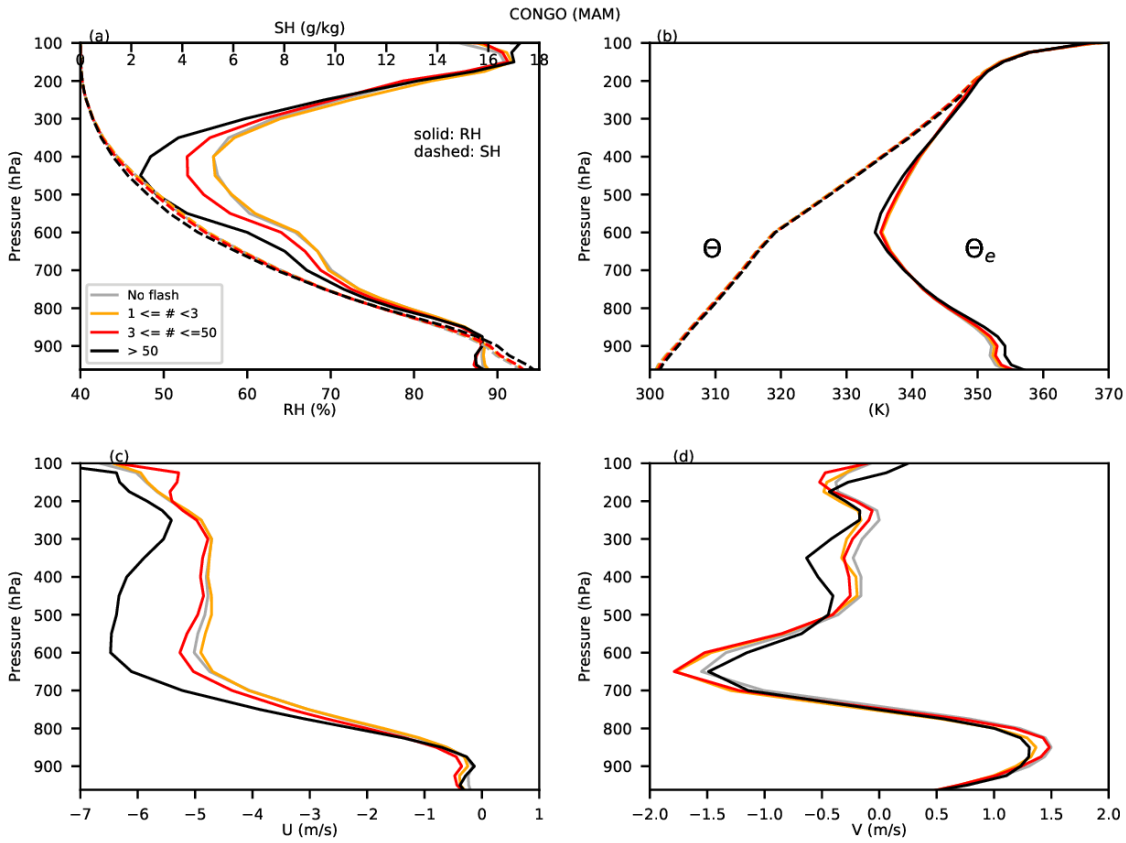

Figure 1.20 Same as Figure 1.5, but for CONGO.

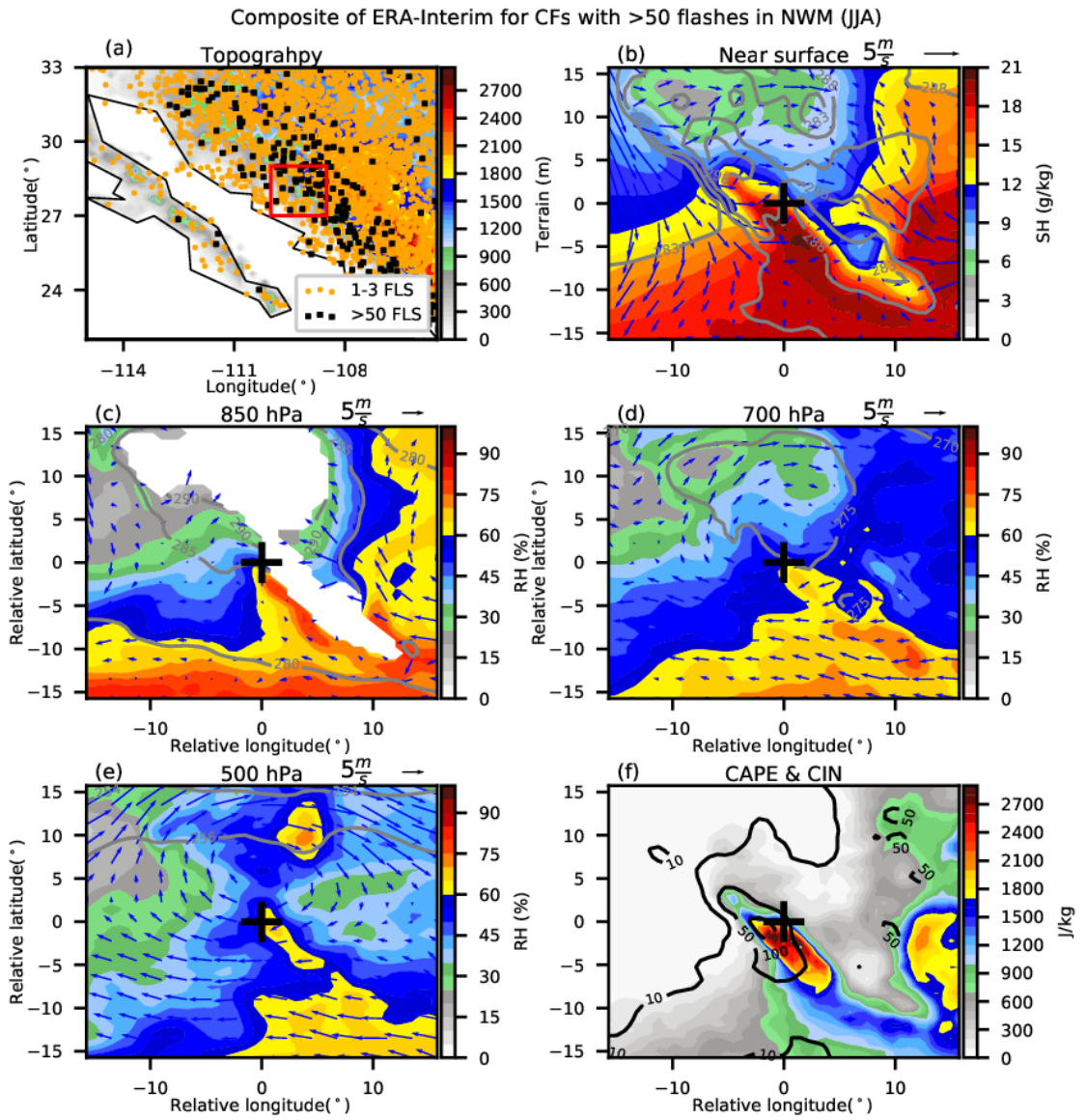

Figure 1.21 Same as Figure 1.3, but for NWM.

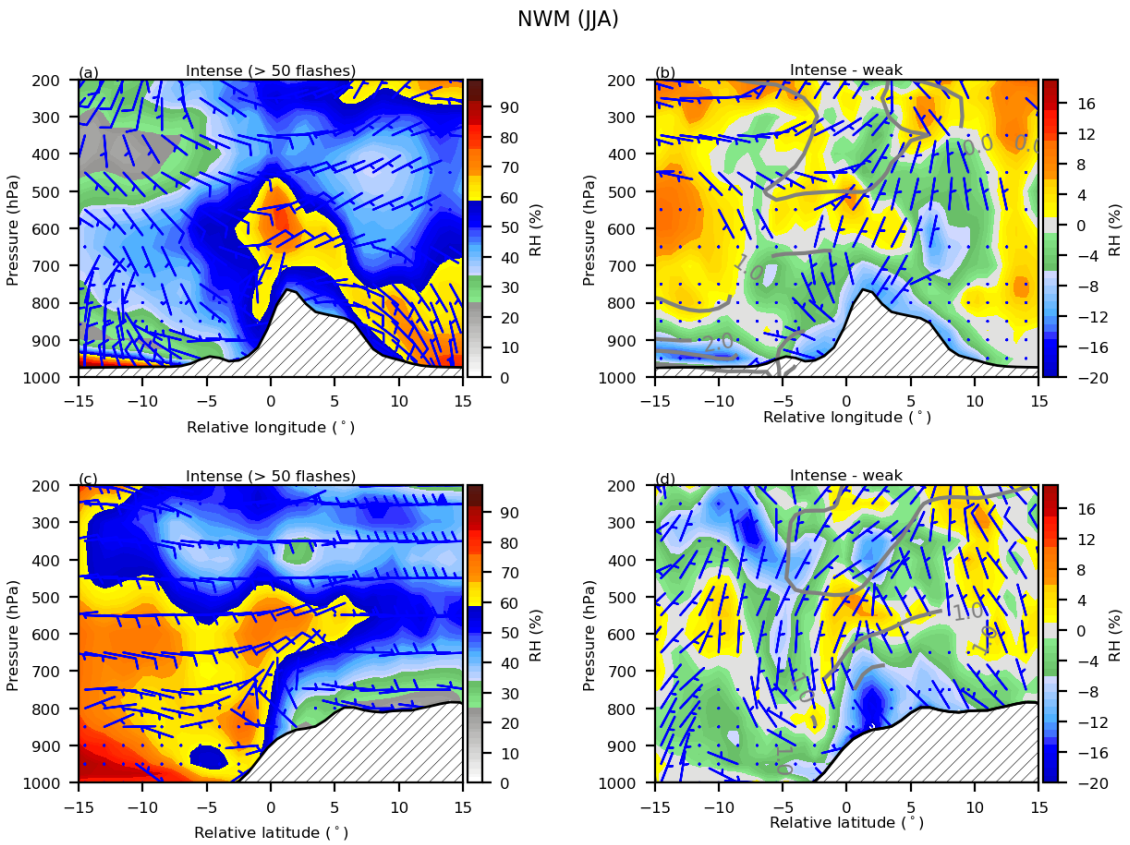

Figure 1.22 Same as Figure 1.4, but for NWM.

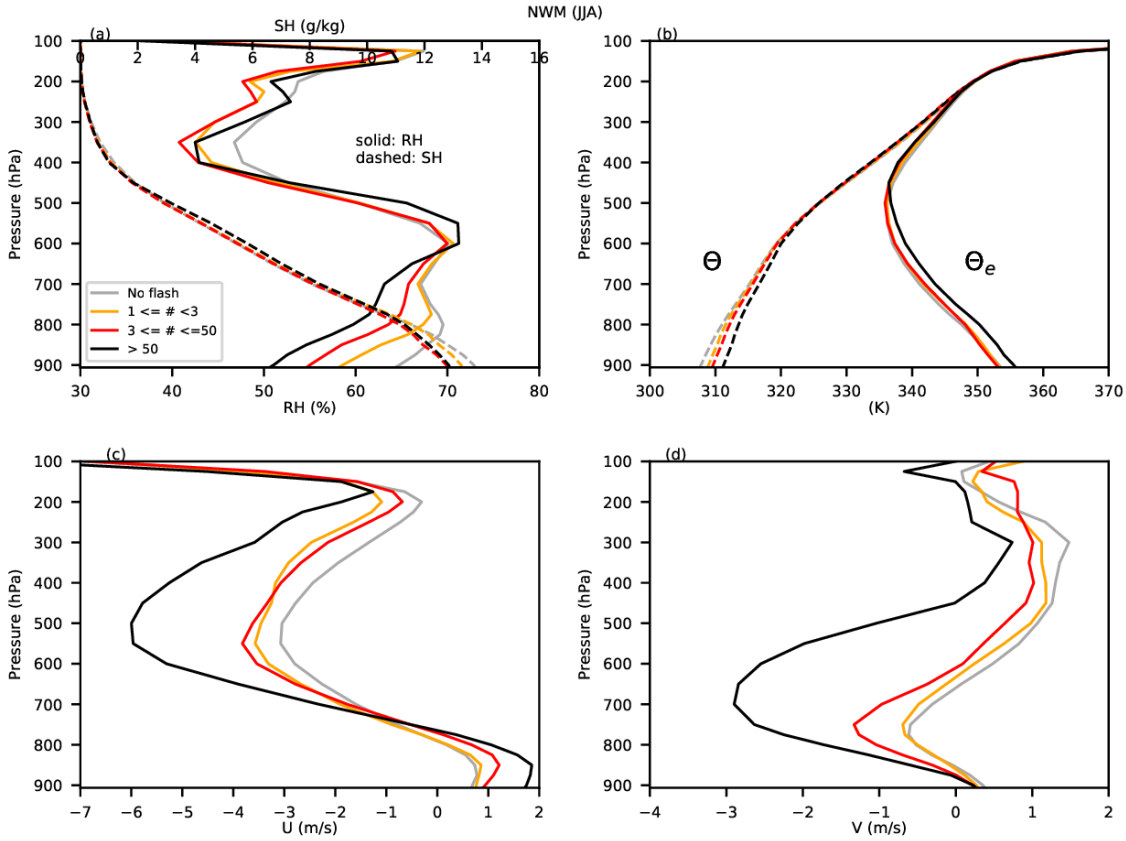

Figure 1.23 Same as Figure 1.5, but for NWM.

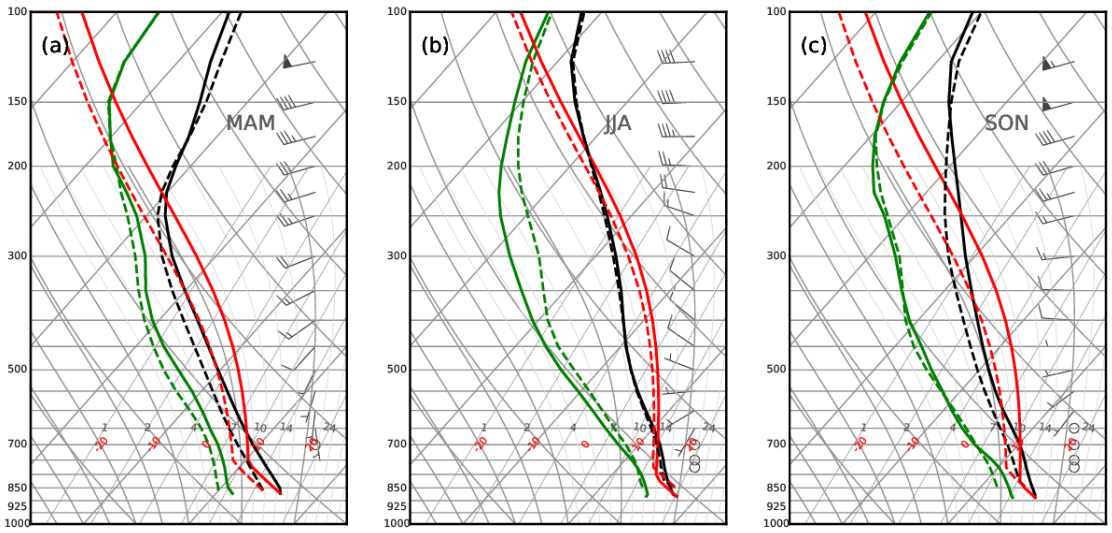

Figure 1.24 Composite soundings for CFs with 1-3 flashes (dashes lines) and > 50 flashes (solid lines) in different seasons over HIMA. (a) MAM, (b) JJA, (c) SON. The wind barbs are for CFs with > 50 flahes.

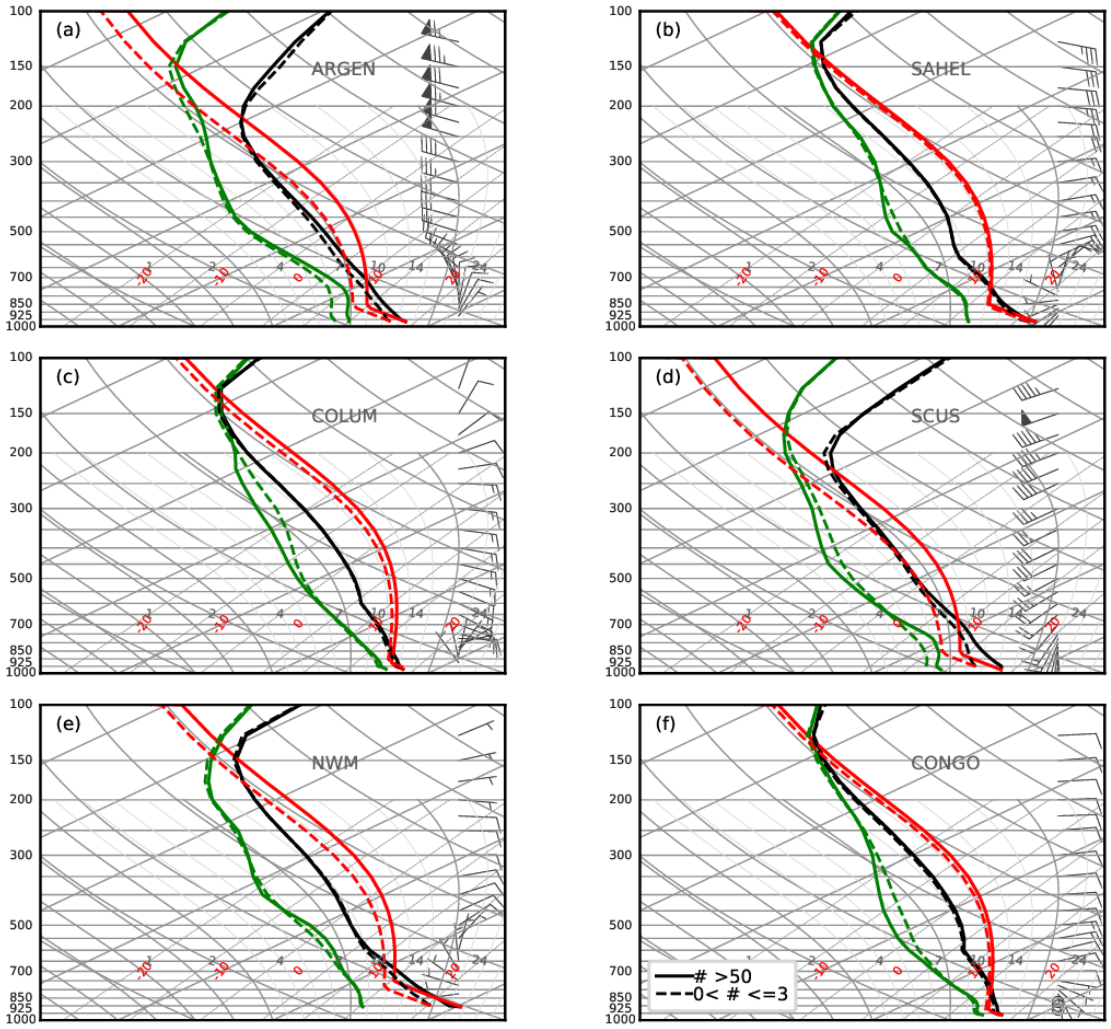

Figure 1.25 Composite soundings for CFs with 1-3 flashes (dashes lines) and > 50 flashes (solid lines) over different regions. (a) ARGEN, (b)SAHEL, (c)COLUM, (d) SCUS, (e)NWM, (f) CONGO. The wind barbs are for CFs with > 50 flahes.

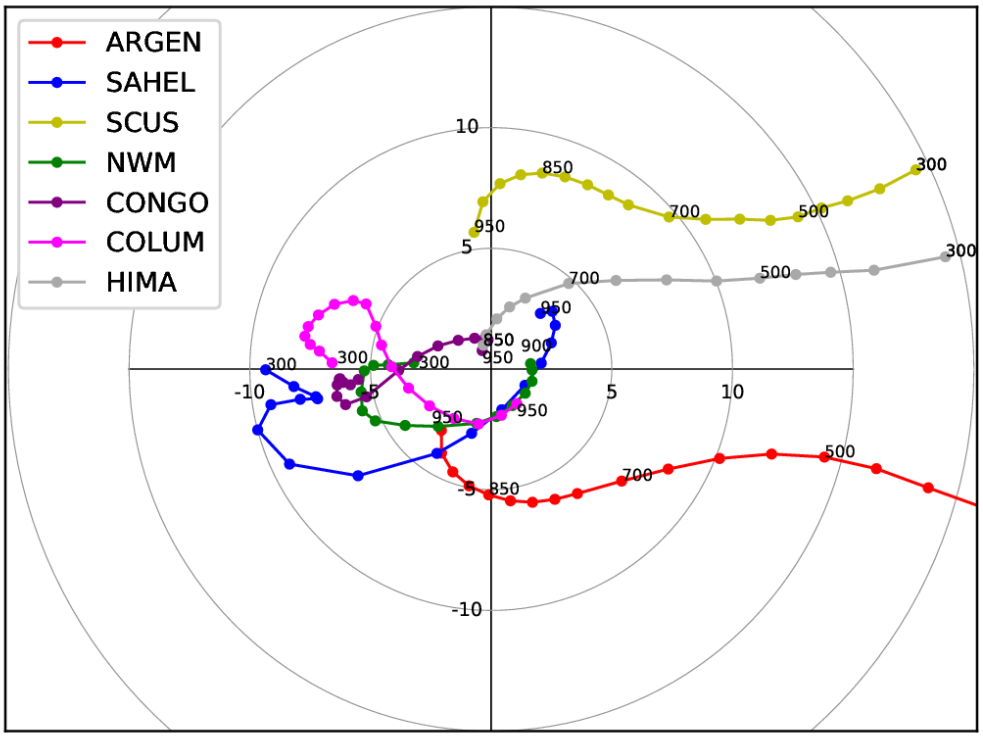

Figure 1.26 Composite hodograph of intense CFs with > 50 flashes over different regions.

CHAPTER II: Relative importance of thermodynamic variables to the world wide variability of thunderstorms

Abstract

A 16-year Tropical Rainfall Measuring Mission (TRMM) Convective Feature (CF) dataset and ERA-Interim reanalysis data is used to examine the relationships between thermodynamic environments and thunderstorm convective intensity. In this study, two statistical models are built to reconstruct the global distribution of thunderstorms only based on their environmental variables. The first model creates the probability functions of intense thunderstorms from the TRMM CFs and their environments from ERA-Interim a horizontal grid spacing of 0.75^{o}x0.75^{o}. It is found that four variables, including Convective Available Potential Energy (CAPE), Convective Inhibition (CIN), low-level shear, and warm cloud depth, may be used to derive a geographical distribution of intense thunderstorms that is close to the observations. The second approach utilizes a random forest model to test the relative importance of these four variables for a convective cloud having lightning globally, as well as regionally. The strong land-ocean contrast of frequency of thunderstorms and some hotspot regions can be closely reproduced with the random forest model only based on the four variables from the reanalysis data. This suggests that the land-ocean contrast in thunderstorms can be largely interpreted by the fundamental differences between the thermodynamic conditions over land and ocean. The investigation of the relative importance of the four environmental variables over different regions suggest that CAPE plays an important role in the lightning over central America, central Africa and the Maritime Continents. CIN is relatively more important over Amazon and a few coastal areas. Low level wind shear is more important over Argentina, southcentral United States, and eastern Sahel. Warm cloud depth is shown with a greater importance than other three variables near mountains.

Introduction

Extreme weather events are increasingly drawing our attention over the years due to a growing concern that they have a great impact on humans and societies, no matter where they occur, especially in the course of natural and anthropogenic climate change. Despite the continuous improvement in observation and modeling tools, the prediction of these events, especially of intense ones, remains a considerable challenge (Gallus et al., 2005). The prediction of extreme weather events that produce significant amount of lightning continues to be a difficult task and a fascinating scientific challenge because they may occur in a wide range of weather regimes and have various sizes and lifetimes (e.g. Foote and Mohr 1979; Wilson et al., 1998; Feng et al. 2016).

While numerical models have proven useful in improving the understanding of thunderstorms in the atmosphere, operational numerical models with a horizontal resolution of about 10 km have often failed to predict not only the location and time of convective initiation (Anquetin et al., 2005; Meißner et al., 2007), but also the type and intensity of thunderstorms (e.g. Kain et al., 2013; Mecikalski et al., 2015; Romero et al., 2015). This is largely due to the limited observational records and imperfect climate models that are not able to fully represent all the relevant physical processes involved in creating extreme events (e.g. Brooks, 2013; Kunkel et al., 2013; Fierro et al., 2014).

Alternatively, the statistical approach of meteorological covariates can be used to investigate the occurrence of these extreme events (Brown and Murphy, 1996; Brooks et al., 2003). Covariates

relate environmental conditions that are well-observed in space and time to weather events of interest. This idea has led to many of our current forecasting approaches for intense thunderstorms. For example, proximity soundings, where observations from radiosondes are taken in the vicinity of tornadoes, have been used to understand environmental conditions associated with tornadoes (Rasmussen and Blanchard, 1998). Parameters calculated from sounding data are widely used to identify the pre-convective environments that favor intense thunderstorms. These parameters and indices generally reflect the potential for the development of intense thunderstorms, making it possible to quantify the uncertainty implicit in any forecast (Murphy, 1977; Kaltenböck et al. 2009).

In the past decades, various thermodynamic and kinematic parameters have been designed to characterize the conditions that could favor the formation and development of thunderstorms. Convective Available Potential Energy (CAPE) is the most frequently used as a forecasting tool for gauging the likelihood of intense thunderstorms. This is because the relative motion of hydrometeors inside the cloud depends on the updraft speeds. The strength of updraft is directly related to the vertical profile of CAPE (Doswell and Rasmussen 1994; Blanchard, 1998; Doswell and Evans, 2003). CAPE has also been used in cumulus parameterization in general circulation models (e.g. Moncrieff and Miller, 1976; Ye et al., 1998; Washington and Parkinson, 2005) and as a predictor of lightning intensity in deep tropical convection (Williams et al., 1993). As an opposite parameter of CAPE, convection inhibition (CIN) is another variable that plays an important role in the development of intense convection (e.g. Mapes, 1998; Davies, 2004; Stensrud, 2007). Convection is often widespread but shallow in the absence of CIN (Bennett et al., 2006). The presence of the CIN (or a lid) can allow for the accumulation of heat and

moisture, creating the potential for intense convection (Keith et al., 2007). In addition to CAPE and CIN, low-level wind shear has also gained wide acceptance by the forecaster community as a parameter to identify potential intense weather (Rotunno et al. 1988; Weisman and Rotunno 2004). Weisman and Klemp (1986) suggested that the bulk Richardson number, which combines CAPE and surface to 6 km wind shear, can be used to differentiate storm type, organization and lifetime. Since then, many researchers have used proxies that combine CAPE and wind shear to model the occurrence of intense convection (e.g. Diffenbaugh et al. 2013; Sander et al. 2013; Allen et al. 2015).

Williams et al. (2005) presents that an elevated cloud base height may increase the cloud water concentration in the mixed-phase region. Because the presence of ice particles in this region is necessary for cloud electrification (e.g. Takahashi 1978; Houze 1993; MacGorman and Rust 1998). Higher cloud base height could result in less entrainment (McCarthy, 1974), stronger updrafts (Williams et al. 2005), and ultimately, higher liquid water content in the mixed-phased zone. In addition, a higher cloud base height also implies a shallower warm cloud depth (WCD), which is the distance between the cloud base height and freezing height. A shallower WCD allows less time for droplets to interact for coalescence (Pierce, 1958) and results in a higher liquid water content in the mixed-phase and charging zone from the freezing of large raindrops (Rosenfeld and Woodley 2003). Stolz et al. (2015) also confirmed that lightning density and the average height of 30 dBZ echoes are higher for storms with a shallower WCD, compared to those with a deeper WCD. In their multiple-liner regression model to predict global lightning activity, they suggested that WCD, CAPE, and cloud condensation nuclei (CCN) are among the most influential predictors accounting for the variation of convective intensity (Stolz et al. 2017).

In addition to the atmospheric factors mentioned above, the relationships between the occurrence of intense thunderstorms and other parameters such as low- and mid-level humidity, lifted index (LI_{500}) and total column water vapor (TCWV), are investigated as well. Although these parameters may influence convective activity in different ways, no parameter could characterize the state of the atmosphere on its own. Therefore, this study explores the influences of these parameters/factors individually and jointly on the probability of intense thunderstorms.

In past investigations of intense thunderstorms, satellites have provided valuable information about the global distribution of the intense convection (e.g. Spencer and Stantek, 1985; Zipser et al., 2006; Cecil and Blankenship, 2012; Liu and Liu, 2016). The near-uniform global coverage of satellites makes them continue to be the most efficient tools to advance the understanding of extreme weather events. As one of the most successful missions during the past decades, the Tropical Rainfall Measuring Mission (TRMM, Kummerow et al., 1998) has provided us a clear picture of the distribution of thunderstorms and lightning activity across the tropics and subtropics (Liu and Zipser, 2005; Zipser et al., 2006; Houze et al., 2015). In order to describe the regional variation of thunderstorms from the perspective of thermodynamic environments, here we focus on the large-scale thermodynamic environments from reanalysis datasets for intense convective systems observed by TRMM. The objective of this study is to answer the following questions:

- What are the relationships between the thermodynamic variables, such as CAPE, CIN, low-level wind shear, etc. individually as well as jointly, and the probability of intense thunderstorms?

- Can we utilize these relationships to interpret the global geographical frequency distribution of intense thunderstorms?
- What is the relative importance of these thermodynamic variables in the probability of intense thunderstorms over different regions?

To answer these questions, lightning flashes, a commonly used proxy to recognize intense thunderstorms (e.g. MacGorman and Burgess, 1994; Lang and Rutledge, 2002; Carey et al., 2003), are used to identify these rare events. The lightning flashes are observed by the Lightning Imaging Sensor (LIS) on the TRMM satellite. The LIS provided 16+ years of continuous total lightning observations with high detection efficiency across the tropics and subtropics after its launch in 1997. The 16 years of TRMM data and analysis methodology used in this study are introduced in section 2. The results are presented in section 3, which includes the relationships between several selected atmospheric factors and the occurrence of intense thunderstorms, the reconstructed geographical distribution and seasonal variation of those events by these relationships, and the relative importance of these atmospheric variables over selected regions.

Data and methods

Two data sources are used in this study to investigate the occurrence of intense thunderstorms based on their relationship to atmospheric variables. One is the database of TRMM convective features (CF) and their properties. In addition, the ERA-Interim reanalysis data (Dee et al, 2011) is used to calculate the thermodynamic variables for each CF.

1. TRMM feature datasets

The study uses a 16-year (1998-2013) CF dataset that is derived from the TRMM version 7 products, with a coverage of 36°S-36°N. A CF is defined by grouping contiguous convective precipitation pixels observed by the TRMM Precipitation Radar (PR) (Liu et al. 2008). In this analysis, only CFs with at least four contiguous pixels (with size ~75 km^2) are used in order to limit the noise. The lightning flash count from LIS is summarized for each CF. The LIS detects both cloud-to-ground and intracloud lightning activity within ~92 s overpassing time after the boost of the satellite orbit in August of 2001 (Albrech et al., 2011). Having collected lightning measurements for over 16 years, LIS has been especially useful in the effort to understand lightning activities in remote regions of the world that have limited observations (Zipser et al. 2006; Virts et al. 2013; Cecil et al. 2014).

As shown in Figure 2. 1a, the population of total ~ 25 million CFs from 16-year TRMM observations are mapped onto a latitude-longitude grid with 2°x2° resolution. The large sample size of CFs over the TRMM domain makes it possible to examine intense convection across the tropics and subtropics. With a focus on convection that produces intense weather, we define CFs with more than 50 flashes as intense thunderstorms in this study. Thunderstorms, especially intense ones, exhibit a strong preference for formations near major mountain ranges, such as the east of Rockies and Andes, south of Himalayas, and the west of Mitumba mountain (Figure 2. 1b). This is similar to the climatology map of intense thunderstorms depicted by prior studies (e.g., Mohr and Zipser, 1996; Zipser et al., 2006; Cecil and Blankenship, 2012). Considering the population of the intense CFs varies with the total number of CFs, we use the percentage of intense CFs instead of the population in this study. The percentage of intense CFs is defined as the number of CFs with more than 50 flashes divided by the total number of CFs, multiplied by

100 (%). The geographical distribution of the percentage of intense CFs (those with more than 50 flashes) is shown in Figure 2. 1c. Similar to the population distribution in Figure 2. 1b, a higher percentage of intense CFs is found over land than over ocean, with a strong preference over several specific regions, such as Argentina, Congo, Northern Pakistan, and the south central United States.

2. Thermodynamic environments from ERA-Interim reanalysis dataset

The ERA-Interim reanalysis data (Dee et al, 2011) are used to provide the large-scale thermodynamic environments for each TRMM-identified intense CF. The three-dimensional 6 hourly reanalysis data are obtained at 0.75^{o}x0.75^{o} horizontal resolution, at 37 pressure levels, and for the same TRMM data period. The atmospheric fields of ERA-Interim reanalysis used in this study include temperature (T), horizontal wind (u and v), geopotential heights, relative humidity (RH), 2 m temperature, and the total column water vapor.

CAPE and CIN are computed using the algorithms outlined by Emanuel (1994). The low-level wind shear ($SHEAR_{1\text{-}3km}$) is defined as the difference in the horizontal wind between 1 and 3 km above ground level. The WCD is calculated by subtracting the lifting condensation level (LCL) from the freezing level (height of the 0^{o}C isotherm). The specific humidity at the near surface (SHL) is calculated from the 2 m temperature and pressure, while the relative humidity at the middle level (RHM) is averaged over the 700-500 hPa layer. Then, these parameters are temporally and spatially interpolated to the time and location of each CF. Because the percentage of intense CFs are analyzed in this study, the information of precipitation at the reanalysis grids

is required. Here 3 hourly 0.25°x0.25° TRMM 3B42 products (Huffman et al. 2007) are downgraded to the ERA-Interim grids to provide the precipitation background.

All of these arbitrarily selected variables reflect certain corresponding physical processes, though some of them are more often employed in data analysis, while others are more often employed in modeling contexts, mostly due to historical as well as practical reasons. Note that all of these variables can be both calculated from observations, if the relevant atmospheric variables are properly measured, or can be obtained from the model outputs.

3. Statistical Models to describe the regional variation of thunderstorms

    a. Bayesian model

In the Bayesian model, the probability of intense thunderstorms can be denoted as P(A|B), where A is a predictor variable, such as CAPE, CIN, etc. and B are the cases to be taken into account. The approach is used to calculate the probability of intense thunderstorms with equation (1).

$$P(C) = \frac{P(C|A)}{P(C|B)} \qquad (1)$$

where P is the probability of intense thunderstorms under the condition (C) with a value of a certain predictor variable. P(C|A) is the number of CFs with more than 50 flashes under the condition C, while P(C|B) is the number of total CFs under the same condition (C). Here the condition C refers to a grid point with surface precipitation and a specific large scale environments, such as a value of CAPE, CIN, etc., or a combination of two or more variables as a condition associated with the probability of intense thunderstorms. Here, two methods are considered. The first one explores the relationship between atmospheric variables and the probability of intense CFs based on CFs over the whole TRMM domain (36°S-36°N), including

both land and ocean. The second considers the land and ocean separately for the analysis. Then, the probability of intense thunderstorms calculated by the Bayesian model is used to reconstruct their geographical distribution from atmospheric variables from ERA-Interim to better understand the regional and seasonal variation of these events.

b. Random forest model

A new and powerful statistical classifier, random forests use bootstrap samples to construct multiple decision trees (Breiman, 2011). Each decision tree is grown with a random subset of predictors to its maximum size. Random forests are trained by fitting a decision tree to each randomly sampled subset of the training data and aggregating the predictors. The random sampling adds more diversity and leads to a more robust model. In the process of each tree growing in the random forest model, the Gini impurity is calculated, which is a measurement of the likelihood of incorrect classification of a new instance of a random variable. For each variable, the sum of the Gini decreases across every tree of the forest is accumulated each time when that variable is chosen to split a node. The importance is defined as the sum of Gini over the number of trees. Note that in general, a variable with a relatively larger dynamic range in the selection tree would yield a larger importance value. Then, the relevance is normalized so that the sum of all the relative importance is 1. To perform the prediction using the trained random forest model, we pass the test features through each randomly created tree. Each predicted target vote is calculated for the same feature. Then, the most frequently predicted class by the individual trees, also known as a majority vote, is considered the final prediction.

To build the random forest model, the open source Python sklearn.ensemble.RandomForestClassifier package from scikitlearn （https://scikit-learn.org/stable/) is used in this study. One drawback of random forest method is the requirement of large samples. Even with 16 years of data, we are only able to apply the method to the CFs with lightning vs. CFs without lightning. Here, we label CFs with at least one flash as class 1 and CFs with no flashes as class 2. 16-year (1998-2013) TRMM CFs and their four environmental variables (CAPE, CIN, Shear, and WCD), derived from ERA-Interim reanalysis data, are used to build the random forest model. 80% of the 16-year dataset is used as training data to build the random forest model. In addition, thunderstorms are relatively rare events, making up only ~4% of all the CFs over the whole TRMM domain. To minimize the overall error rate related to the unbalanced dataset, the model uses the values of the target to automatically adjust weights inversely proportional to class frequencies to balance the dataset. Then, the environmental variables from the remaining 20% of the ERA-Interim reanalysis data are used to classify whether a CF is a thunderstorm event or not and test the performance of the random forest model. To test the robustness of the random forest model, we randomly split samples and rerun the model 50 times and derived the standard deviations from results. Note that in this approach, only the thermodynamic variables are used, and no precondition of precipitation information is needed.

Results

1. Relationships between thermodynamic variables and probability of intense CFs

The relationship between one specific atmospheric variable and the percentage of CFs with more than 50 flashes is shown in Figure 2. 2. These rare events, especially the intense ones (with more

than 50 flashes), show a higher probability over land than over ocean. The probability of intense convection remains relatively low when there is a low CAPE (< 1000 J/kg) (Figure 2. 2a). Then, the probability increases rapidly with increasing CAPE until sample sizes (dotted lines) become small (CAPE > 4000 J/kg), so that the estimates might be inaccurate. With a peak with CIN values between 120 to 200 J/kg, the probability of intense CFs associated with CIN increases with the increasing CIN, and then starts to decrease when the value exceeds 200 J/kg (Figure 2. 2b). Over the ocean, the variation in the probability of intense thunderstorms associated with CIN is small. This is because the magnitude of CIN is relatively smaller over ocean than over land (Williams and Renno 1993). Over land, high CIN could allow CAPE to build up rapidly through a suppression of entrainment under conditions of surface heating and boundary layer growth (Parker, 2002). Convection tends to be widespread but shallow over the ocean under low CIN conditions. The probability of intense events as it relates to wind shear shows a bimodal dependence on the shear (Figure 2. 3c), which has also been suggested in a prior study (Westermayer et al., 2016). They have explained this bimodal distribution of the probability of thunderstorms related to wind shear by a combination of two effects. First, towering cumulus clouds are not tilted and are more likely to develop into intense thunderstorms in a weak shear environment than in a strong shear one. On the other hand, strong wind shear usually occurs in the vicinity of fronts or jets, which could help initiate and maintain the well-organized systems once they form. However, moderate wind shear is detrimental to the isolated storms and is not sufficient to initiate organized convection by the frontal systems. The pattern of the probability of intense thunderstorms as a function of WCD shows a peak when WCD values are between 2 and 3 km, though most of the CFs have WCD deeper then 3.5 km. In addition to the indicator of "warm rain" process, WCD also represents the low level relative humidity. There have been

studies suggesting that a slight dry air at near surface layer would help enhance the storm intensity (e.g. Schumacher 2015).

Figure 2. 3 shows the population of total CFs (contours) and probability of intense CFs (color fill) as a function of two environmental variables, based on CFs over the whole TRMM domain. The number of samples is sufficiently large, as shown in gray contours. These represent the two dimensional histogram of population of CFs as a function of two of the four variables: CAPE, CIN, $SHEAR_{1\text{-}3km}$ and WCD. Environments with small CAPE (< 1000 J/kg) are not favorable for intense thunderstorms (Figure 2. 3a). In environments with moderate CAPE (1000-2500 J/kg), the probability of intense CFs associated with moderate CIN (100-200 J/kg) is higher than that associated with zero CIN. This implies that CIN may help accumulate the moist static energy and increase the potential for intense thunderstorms in environments with moderate CAPE. When CAPE is large enough (> 3000 J/kg), intense storms can develop even with relatively small CIN (< 100 J/kg). As a widely accepted factor for identifying intense weather days, larger low-level wind shear is associated with a higher probability of intense CFs for a constant value of CAPE (Figure 2. 3b). Under an unstable environment with CAPE > 2000 J/kg, shallower WCD is favorable for intense thunderstorms (Figure 2. 3c). This is consistent with the results shown by Stolz et al. (2015) that the total lightning density increases with decreasing WCD. With moderate CIN (100-200 J/kg), an environment with stronger low-level wind shear is more favorable for intense thunderstorms than an environment with weaker wind shear (Figure 2. 3d).

2. Reconstruct the probability of intense thunderstorms from thermodynamic variables

As shown in Figure 2. 2 and 3, the relationships between the probability of intense thunderstorms and their environmental variables have major implications for understanding which environments are supportive for intense thunderstorms. This allows us to examine the regional variation of intense thunderstorms based on lookup tables created using these relationships.

a. Using one thermodynamic variable

The probability of intense thunderstorms is estimated after applying the relationships between the occurrence of intense CFs and environmental variables (Figure 2. 2 and 3). The thermodynamic variables are derived from 6 hourly ERA-Interim reanalysis data with a 0.75^{o}x0.75^{o} horizontal resolution. Note that the probability of intense CFs is conditional in Figure 2. 2. In other words, it is the probability of intense thunderstorms under the condition that a CF occurs. The TRMM 3B42 (v7) 3 hourly, 0.25^{o}x0.25^{o} precipitation products are interpolated into 0.75^{o}x0.75^{o} to be consistent with the ERA-Interim dataset. Then, we consider rainfall greater than 0 (mm/hour) as the precondition to apply the relationship, and estimate the probability of intense thunderstorms. To further explore how the probability of intense thunderstorms is related to environmental conditions, the geographical distribution of intense thunderstorms is reconstructed. The average of the 16-year (1998-2013) estimation of the probability of intense thunderstorms is calculated on each 2^{o} x 2^{o} grid and shown in Figure 2. 4 and 5.

Figure 2. 4 shows the reconstructed geographical distribution of the probability of intense thunderstorms from one environmental variable, based on the lookup table created for the whole TRMM domain without consideration of land vs. ocean in Figure 2. 2. Unsurprisingly, the

performance is poor when sole environmental factor is considered to estimate the probability of intense thunderstorms. The geographical distribution in Figure 2. 4a reveals that regions with higher probability of intense thunderstorms estimated from CAPE, such as the Gulf of Mexico, the Amazon, central Africa and the Maritime Continents, are associated with higher potential energy. However, these regions are not favorable for intense thunderstorms as shown in Figure 2. 1c. This implies that an atmosphere with high moist potential energy alone is insufficient for intense convection. Regions with relative high probability of intense thunderstorms estimated by CIN are found over land, especially downstream of major mountain ranges. This indicates that large topography may play an important role in creating CIN (e.g. Peckham and Wicker 2000; Hanley et al. 2011; Rasmussen and Houze 2016). Low-level wind shear alone is not capable of estimating the probability of intense thunderstorms (Figure 2. 4c). That is why the combination of CAPE and shear is commonly used to identify the potential of intense weather (e.g., Sander et al. 2013; Diffenbaugh et al. 2013; Allen et al. 2015).

b. Using two thermodynamic variables

The percentages of intense thunderstorm as function of two thermodynamic variables in Figure 2. 3 are used as lookup tables to estimate the probability of intense thunderstorms. There is a clear improvement in the performance of the estimation when a combination of two environmental variables is used to reconstruct the geographical distribution of intense thunderstorms (Figure 2. 5). A combination of CAPE and CIN can reproduce the probability of intense thunderstorms over a few specific regions, such as the vicinity of the Himalayas, west Africa, and central Africa. The underestimation over west Africa and Argentina by CAPE and CIN indicates the important role of other factors, such as wind shear, in the probability of intense

thunderstorms (Figure 2. 5a). Figure 2. 5b shows that the probability of intense thunderstorms tends to be underestimated downstream of major mountain ranges when CIN is not considered. This confirms the results shown in previous studies (e.g. Houze et al., 2007; Romatschke and Houze, 2010; Rasmussen and Houze 2011) that dry warm air flowing off the mountains provides a cap; therefore, the high moist energy air has more CIN to overcome. In this case, convective instability can be stored and accumulated in the environment. Under these conditions, intense convection is more likely to develop once the accumulated instability can be released explosively. It is worth noting that the distinct difference of the probability of intense thunderstorms between land and ocean can be separated by only two environmental variables, though still overestimating over ocean.

c. Probability of intense thunderstorms using CAPE, CIN and $SHEAR_{1\text{-}3km}$

Prior studies (e.g., Weisman and Klemp, 1986; Mapes, 1997; Raymond and Herman 2011), have made efforts to estimate the occurrence of intense thunderstorms from a few environmental factors, individually and by using two of them jointly. Here, the sufficiently large number of samples from 16-yr TRMM observations enables us to add more information to estimate the probability of intense thunderstorms. With the similar approach, lookup tables using three variables have been created and the geographical distribution of intense thunderstorms has been estimated with these lookup tables using ERA-Interim fields. The best results are obtained from the combination of CAPE, CIN and $SHEAR_{1\text{-}3km}$ (Figure 2. 6). Compared to the observations in Figure 2. 1c, the geographical distribution of percent of thunderstorms is closely reproduced both in the magnitude and the general distribution pattern. For example, Argentina, another hotspot for intense thunderstorms, starts to stand out by adding the third factor (Figure 2. 6a). However,

it is still overestimated over ocean. When lookup tables of land and ocean are used separately, the estimated probability of intense thunderstorms over ocean is close to the observations shown in Figure 2. 1c. In addition, the combination of these three factors gives a good discrimination of the favorable environment for intense thunderstorms over the southwest United States and Colombia, locations shown to be favorable for intense thunderstorms.

d. Consideration of four thermodynamic variables

Pushing the limit of samples further, a fourth factor is added in the process of reproducing the distribution of intense thunderstorms. We tested several variables including LCL, SHL, RHM, LI500, TCWV, and WCD. Here, the one with the best performance (WCD) is displayed in Figure 2. 7. The combination of these four factors in Figure 2. 7a captures these hotpots of intense thunderstorms with more than 50 flashes shown in Figure 2. 1c despite some overestimation over the Arabian Sea. When we apply the lookup Table 2.that considers the land and ocean separately, further improvement is seen over oceans, the south central United States, and Argentina.

Together with the combination of CAPE, CIN and $SHEAR_{1\text{-}3km}$, the best performance of the fourth factor is from WCD. In this study, we use lightning flashes as a proxy to identify intense thunderstorms, which involves storm electrification. Electrification has been suggested to be associated with the mass of cloud ice particles in the appropriate temperature range of $0^{o}C$ to $-40^{o}C$ in models (e.g., Baker et al., 1995; Sherwood et al., 2006). WCD, the difference between the LCL and the freezing height, is directly related to the warm rain process and amount of water

being lifted to the mixed phase levels, this could be the reasons of why WCD is helpful in the estimation of thunderstorms with more lightning flashes.

In summary, Table 2.1 lists the mean and spatial correlations between the observed percentage of CFs with more than 50 flashes and the estimated percentage of intense thunderstorms by individual and joint thermodynamic variables. The spatial correlations between the observed and estimated probability of intense thunderstorms tend to increase when more factors are considered. The best performance is from the combination of CAPE, CIN, $SHEAR_{1\text{-}3km}$ and WCD, which is reflected in the highest spatial correlation over land between the observed and the estimated probability of intense thunderstorms. The second highest spatial correlation between the observation and estimation is associated with best three and SHL. This indicates that the low-level moisture, which has been emphasized in modeling contexts (e.g., Droegemeier and Wilhelmson, 1985; Reap and MacGorman, 1989; Yano et al., 2013), is another important factor in the estimation of intense thunderstorms. In addition, the relatively high spatial correlations for LCL and RHM suggest that they are also useful in the prediction of intense thunderstorms. TCWV, a useful predictor for large precipitating systems (Chen et al., 2016), with the combination of CAPE, CIN and $SHEAR_{1\text{-}3km}$, does not show good performance in the estimation of intense thunderstorms with the highest flashes. The spatial correlation related to LI_{500} is relatively low, compared to other variables. One reason for this is because instability information has been included in the analysis by using CAPE. Although both LI_{500} and CAPE have been used as measures of instability, CAPE often provides a better overall profile of instability than LI500, which uses a single atmospheric layer.

3. The seasonal variation of intense thunderstorms over selected regions.

Because the relationship between intense thunderstorms and large-scale environments could vary in different seasons, efforts are made here to determine the seasonal variation of the intense thunderstorms from the four thermodynamic variables and their correlation with the observations over selected regions. These regions include Argentina (ARGEN), Himalaya (HIMA), west Africa (WAFRICA), central Africa (CAFRICA) and the South Central United States (SCUS) (boxes shown in Figure 2. 1c). The seasonal variation of intense thunderstorms over ARGEN is smaller than that over the other selected regions. Over CAFRICA, the reconstructed seasonal variation is in agreement with the observations. With two peaks in spring and fall, the estimated seasonal variation of intense thunderstorms is consistent with the observation over HIMA and WAFRICA. The underestimation (overestimation) of the second peak in September for HIMA (WAFRICA) confirms that the favorable environments for intense thunderstorms varies in different seasons, even in the same region. Over SCUS, more than 40% of thunderstorms during April, May, and June (AMJ) are found to be associated with drylines (e.g. Rhea, 1966; Schaefer, 1974; Peterson, 1983), boundaries between moist air from the Gulf of Mexico and dry air from arid regions in northern Mexico, eastern New Mexico and western Texas. However, none of the variables used here are good representative parameters for these boundaries. This might be one of the reasons that the peak of intense thunderstorms is found in summer (June, July and August) by thermodynamic variables while the observed peak of intense thunderstorms occurs in spring and early summer (April, May and June).

4. A random forest model for thunderstorms using the four thermodynamic variables

Due to the requirement of large sample size by random forest, we use thunderstorms, defined as CFs with at least one flash, as the predictions target. This leads to an inconsistency in the prediction targets between this model and the Bayesian approach discussed earlier. Also, the roles of the thermodynamic variables could be different when considering all thunderstorms rather than just the thunderstorms with high lightning rates. Nevertheless, it is still interesting to examine the importance of these variables correlated to the thunderstorms in general. In the global random forest model, the whole 16-year TRMM CFs and their environmental variables, derived from ERA-Interim reanalysis data is randomly split. 80% of the data is used to train the model. The remaining 20% of the dataset is used to test the performance of the model.

Figure 2. 9a presents the geographical distribution of thunderstorms at least with one flash from the testing data set. Even with 20% of the whole data set, the general geographical distribution of thunderstorms is consistent with the well-documented climatology of thunderstorms (e.g. Boccippio et al. 2000; Christian et al. 2003; Liu et al. 2012). The global picture of thunderstorms reveals a strong land dominance, which has been related to the surface properties and aerosol effects (Williams et al. 2004). With an exception over central Africa and Maritime Continents, the general overestimation from random forest model by using two atmospheric variables indicates that CAPE and CIN have limited skill to reproduce thunderstorms (Figure 2. 9b). Compared to the estimation by using CAPE and CIN, the performance of the model improves by adding the low level wind shear into the global random forest model (Figure 2. 9c. Consistent with the observation, more thunderstorms are found over land than over ocean. However, the random forest model by using CAPE, CIN and $SHEAR_{1\text{-}3km}$ still tends to overestimate the frequency of thunderstorms over ocean. When considering four thermodynamic

variables from the reanalysis data (Figure 2. 9d and 9e), the strong land and ocean contrast in the frequency of thunderstorms can be closely reproduced with the global random forest model. This suggests that the land-ocean contrast in convective intensity can be largely interpreted by the fundamental differences between the thermodynamic conditions over land and ocean.

5. Regional variation of relative importance of thermodynamic variables for thunderstorms

As shown in the previous section, the relationships between thunderstorms and thermodynamic variables could vary regionally and seasonally. This implies that even with some common features, the favorable environments for thunderstorms over different regions may have their own individual characteristics. Therefore, the relative influence of the four environmental variables for thunderstorms is investigated by using the random forest models created over selected regions. The relative importance is calculated by training and testing with samples over selected regions separately.

As listed in Table 2.3, the large sample size of training and testing datasets make it possible to build a robust model not only globally, but also over the selected regions. The prediction skill scores of the models over different regions are also shown in Table 2.3, including the Probability of Detection (POD), False Alarm Rate (FAR), Critical Success Index (CSI), and Heidlke Skill Score (HSS). As a commonly used skill score for assessing the accuracy of thunderstorms forecasts (e.g., Huntrieser et al., 1997; Michell et al., 1998; Mazur et al., 2009), the Critical Success Index (CSI) measures the ratio of hits to the total number of hits (a), false alarms (b) and misses (c). In other words, it is a combined measurement of the accuracy of thunderstorms warnings and includes both misses and false alarms as defined in Table 2.2. The HSS compares

the proportion of correct forecasts to a no skill forecast. While not impressive the regional HSSs range between 0.11 for CAFRICA and 0.29 for HIMA clear evidence of a skillful model. It is also important to point out that the geographical distribution of thunderstorms is well captured by these models with spatial correlation coefficients of 0.88 between the percentages of observed and RF predicted CFs (Figure 2.s 9a and 9d).

Figure 2. 10 illustrates the relative importance of the four environmental variables for the prediction of thunderstorms over different regions. In the global random forest model, the relative importance of CAPE is the highest among these four variables. However, the relative importance of these four atmospheric variables varies by region. For example, ARGEN and CAFRICA have CAPE as the most important predictor; WCD is more important over SCUS and HIMA. Over the whole TRMM domain, the relative influence of CIN and $SHEAR_{1\text{-}3km}$ on the prediction of thunderstorms is relatively weak compared to CAPE and WCD. Though an important factor in the development of intense convection (e.g. Weisman and Klemp, 1982; Weisman and Trapp 2003; Diffenbaugh et al. 2013; Sander et al. 2013), $SHEAR_{1\text{-}3km}$ is found to have the lowest relative importance among these four variables. Note that here all the CFs with at least one flash are the targets, which include numerous weak thunderstorms with low lightning rates. The low-level shear is known to be important for organized and intense thunderstorms. Therefore, it is not a surprise that shear does not stand out in this case.

The Bayesian and global random forest model, as well as the variation of the relative importance of the four environmental variables over these selected regions, confirm that thermodynamic environments favored by thunderstorms have their own specific features over different regions.

Therefore, the geographical distribution of thunderstorms is reconstructed from the four atmospheric variables using the local random forest models in 10^{o}x10^{o} grids. In each grid, 80% of the data is used as a training dataset while the remaining 20% is considered as a testing dataset. In this process, only the grids with sufficient target samples (> 500 samples) are analyzed and shown. The 20% of the observations and prediction of thunderstorms using 10^{o}x10^{o} local random forest models are shown in Figure 2. 11. Overall, there is a slight overestimation of thunderstorms by the local models. In addition to the general pattern of the geographical distribution, the hotspot regions of intense thunderstorms, such as CAFIRCA, WAFICA, HIMA, SCUS and ARGEN, can also be closely reproduced. The overestimation of thunderstorms is found to be more pronounced over coastal regions.

The regional variation of the relative importance of the four environmental variables is shown in Figure 2. 12. Higher relative importance values in CAPE are found over the Amazon, central Africa and the Maritime Continents, as well as the coastal regions (Figure 2. 12a). For example, the Gulf of Guinea is characterized by higher relative importance of CAPE than that of the other three variables. The Bay of Bengal, which is the site of the highest mean precipitation of the entire Asian monsoon region (Zuidema, 2003), is also found to have the highest relative importance of CAPE. In general, the relative importance of CIN is smaller than other variables (Figure 2. 12b). However, higher relative importance of CIN over the Amazon, southeast United States and the Maritime Continents indicates its influence on thunderstorms is more pronounced over these regions. These land regions have more abundant moisture and are close to oceanic scenario. CIN is needed to accumulate the moisture potential energy. Hotspot regions of thunderstorms, such as SCUS, ARGEN and the Sahel, are characterized by higher relative

importance of $SHEAR_{1\text{-}3km}$ than other regions (Figure 2. 12c). WCD is relatively more important over mountain regions and their west downstream (Figure 2. 12d). It is interesting to note that compared to CIN and low-level shear, WCD is relatively more important for a cloud to have lightning over many land regions, such as southcentral US, west Indian, northern Australian, and southeast China. We speculate that these regions have convective systems of different types of weather regimes that WCD, or low-level relative humidity can be used as a good indicator. Note that in all these estimates, CFs of all seasons are included. Therefore, relative importance shown in Figure 2. 14 also represents the seasonal and regional variation of the dynamic range of each variable for thunderstorms. All above regional variations indicate that the role of these environmental variables in the development of thunderstorms can vary in a small-scale regionally.

Discussion

Caution must be taken in interpreting the results here. First, ERA-Interim reanalysis data have uncertainties resulting from the forecast model, data assimilation, and data sources used (Courtier et al. 1994; Uppala et al. 2008; Dee et al. 2011). The calculation of CAPE is still open to debate because of the various assumptions about the parcel level of origin, characteristics of parcel moisture and temperature, ascent path, and the presence or absence of the ice phase (Williams and Renno 1993; Doswell and Rasmussen 1994; Emanuel 1994; Craven et al. 2002). Also, it is known that the potential energy would be released almost instantaneously once it is triggered by sufficient lifting, such as synoptic ascent, low-level convergence, and orography lifting (e.g. Berry and Thorncroft, 2005; Mekonnen et al., 2006; Houze et al., 2007; Rasmussen and Houze 2016). Second, here we have discussed the convective precipitation with high

lightning rates, which involves electrification process. Though we refer these samples as convectively intense, the relationships to thermodynamic variables might vary for intense convective clouds if differently identified, such as by high radar echoes at high altitudes etc. Consideration should be given in the application to different types of systems. For example, TCWV has been suggested to be strongly associated with the large-size precipitation systems (Zhou et al. 2013; Chen et al. 2016). Third, the effects of aerosol in the estimation of intense thunderstorms are not considered in this study because of the considerable uncertainty of their role in deep convection and lightning (e.g. Williams and Stanfill, 2002; Lee, 2012; Koren et al., 2012; Wall et al., 2014). In addition, even if the environment is favorable for an intense thunderstorm, it does not mean one would occur. For example, here we have not discussed the mechanism of initiation of convection. Even with these limitations, the investigation in this study demonstrates that it is possible to utilize the satellite observed historical events and reanalysis data to understand the relationships between large scale environments and subgrid scale convective processes. The approach used here can be developed further to parameterize proxies for intense thunderstorms in climate models, reanalysis, and numerical weather prediction models.

Summary

The analysis of a 16-yr TRMM CFs dataset has shown that the probability of intense thunderstorms is related to their thermodynamic and kinematic environmental variables. Those environmental variables, derived from the ERA-Interim reanalysis data, include CAPE, CIN, $SHEAR_{1\text{-}3km}$, WCD, LCL, TCWV, SHL, RHM, and LI500. Each of them corresponds to certain physical processes. In order to examine the relationships between thermodynamic environments

and thunderstorm convective intensity, two statistical models are built to reconstruct the global distribution of normal and intense thunderstorms based only on the variables derived from the reanalysis data.

The first model examines the relationships from single, as well as a combination of two or more environmental variables, to the probability of intense thunderstorms with more than 50 flashes. Two types of lookup tables have been built based on the relationship between the probability of intense thunderstorms and the environmental conditions. One considers the whole TRMM domain including both land and ocean, while the other considers land and ocean separately. Then, those lookup tables have been used to reconstruct the geographical distribution of intense thunderstorms across the tropics and subtropics. The general pattern of the geographical distribution of intense thunderstorms derived from a combination of the four variables CAPE, CIN, $SHEAR_{1\text{-}3km}$, and WCD agrees well with the TRMM observations. The estimated seasonal variation of intense thunderstorms from these four variables over various selected regions captures the two peaks in the seasonal variation of intense thunderstorms occurring in June and September over HIMA and WAFRICA, and small variations over CAFRICA and ARGEN. There is an overestimation (underestimation) in September over WAFRICA (HIMA).

The second approach utilizes a random forest model to test the relative importance of these four variables for a convective precipitation system to have lightning globally and regionally. The land-ocean contrast in thunderstorms is closely reproduced by the global random forest model, suggesting the fundamental differences between the thermodynamic conditions over land and ocean in producing lightning. The relative importance of the four environmental variables are

examined at 10^{o}x10^{o} grids. CAPE plays an important role in the occurrence of thunderstorms over Amazon, central Africa, the maritime continents, and the coastal regions. WCD, the difference between the LCL and freezing height, is helpful in the prediction of intense thunderstorms with more than 50 flashes. It is a more important indicator for a convective cloud to have lightning. The importance of four variables are shown to vary significantly in different regions and likely in seasons. Although these models could still to be improved by taking into account additional variables and samples, they provide a unique foundation toward building a parameterization of convective intensity at the sub-grid scale for general circulation models.

Acknowledgements

This research was supported by NASA Precipitation Measurement Mission grants NNX16AD76G under the direction of Dr. Gail Jackson and NNX16AH74G under the direction of Dr. Erich Stocker. Thanks to the Precipitation Processing System (PPS) team at NASA Goddard Space Flight Center, Greenbelt, MD, for data processing assistance.

References

Allen, J. T., M. K. Tippett, and A. H. Sobel, 2015: An empirical model relating U.S. monthly hail occurrence to large-scale meteorological environment, *J. Adv. Model. Earth Syst.*, **7**, 226–243, doi:10.1002/2014MS000397.

Anquetin, S., and Coauthors, 2005: The 8 and 9 September 2002 flash flood event in France: A model intercomparison. *Nat. Hazards Earth Syst.*, **5,** 741–754.

Baker, M. B., H. J. Christian, and J. Latham, 1995: A computational study of the relationships linking lightning frequency and other thundercloud parameters, *Q. J. R. Meteorol. Soc.,***121**, 1525–1548.

Bennett, L. J., K. A. Browning, A. M. Blyth, D. J. Parker, and P. A. Clark, 2006: A review of the initiation of precipitating convection in the United Kingdom. *Quart. J. Roy. Meteor. Soc.*, **132,** 1001–1020.

Berry, G.J. and C. Thorncroft, 2005: Case Study of an Intense African Easterly Wave. *Mon. Wea. Rev.,* **133**, 752–766, https://doi.org/10.1175/MWR2884.1.

Blanchard D., 1998: Assessing the vertical distribution of CAPE. *Weather and Forecasting,* **13,** 870–877.

Boccippio, D.J., S.J. Goodman, and S. Heckman, 2000: Regional Differences in Tropical Lightning Distributions. *J. Appl. Meteor.,* **39**, 2231–2248.

Brooks, H. E., 2013: Intense thunderstorms and climate change. *Atmos. Res.*, **123**, 129–138, doi:https://doi.org/10.1016/j.atmosres.2012.04.002.

Brooks, H. E., J. W. Lee, and J. P. Craven, 2003: The spatial distribution of intense thunderstorm and tornado environments from global reanalysis data, *Atmos. Res*., **67 – 68**, 73 – 94.

Brown, B. G., and A. H. Murphy, 1996: Verification of aircraft icing forecasts: The use of standard measures and meteorological covariates. Preprints, *13th Conf. on Probability and Statistics in the Atmospheric Sciences,* San Francisco, CA, Amer. Meteor. Soc., 251–252.

Browning, K. A., and Coauthors, 2007: The Convective Storm Initiation Project. *Bull. Amer. Meteor. Soc.*, **88**, 1939–1955, doi:10.1175/ BAMS-88-12-1939.

Carey, L.D. and K.M. Buffalo, 2007: Environmental Control of Cloud-to-Ground Lightning Polarity in Severe Storms. *Mon. Wea. Rev.,* **135**, 1327–1353.

Carey, L.D., W.A. Petersen, and S.A. Rutledge, 2003: Evolution of Cloud-to-Ground Lightning and Storm Structure in the Spencer, South Dakota, Tornadic Supercell of 30 May 1998. *Mon. Wea. Rev.,* **131**, 1811–1831, https://doi.org/10.1175//2566.1.

Cecil, D. J., and C. B. Blankenship, 2012: Toward a global climatology of intense hailstorms as estimated by satellite passive microwave imagers, *J. Clim.*, **25**, 687–703.

Cecil, D. J., D. E. Buechler, and R. J. Blakeslee, 2014: Gridded lightning climatology from TRMM-LIS and OTD: Dataset description. *Atmos. Res.,* **135–136,** 404–414.

Craven, J., R. Jewell, and H. Brook, 2002: Comparison between observed convective cloud-base heights and lifting condensation level for two different lifted parcels. *Wea. Forecasting*, **17,** 885–890.

Courtier, P., J-N. Thépaut, and A. Hollingsworth, 1994: A strategy for operational implementation of 4D-Var, using an incremental approach. *Quart. J. Roy. Meteor. Soc*, **120,** 1367–1387.

Davies, J. M., 2004: Estimations of CIN and LFC associated with tornadic and non-tornadic supercells. *Wea. Forecasting*, **19,** 714–726.

Dee, D. P., et al., 2011: The ERA-Interim reanalysis: Configuration and performance of the data assimilation system, *Q. J. R. Meteorol. Soc*., **137(656)**, 553–597, doi:10.1002/qj.828.

Diffenbaugh, N. S., M. Scherer, and R. J. Trapp, 2013: Robust increases in intense thunderstorm environments in response to greenhouse forcing. *Proc. Natl. Acad. Sci. USA*, **110,** 16 361–16 366, doi:10.1073/pnas.1307758110.

Doswell, C. A., III, and E. N. Rasmussen, 1994: The effect of neglecting the virtual temperature correction on CAPE calculations. *Wea. Forecasting*, **9**, 625–629.

Doswell III, C. A., and J. S. Evans, 2003: Proximity sounding analysis for derechos and supercells: An assessment of similarities and differences. *Atmos. Res.*, **67–68,** 117–133.

Droegemeier, K.K. and R.B. Wilhelmson, 1985: Three-Dimensional Numerical Modeling of Convection Produced by Interacting Thunderstorm Outflows. Part I: Control Simulation and Low-Level Moisture Variations. *J. Atmos. Sci.,* **42**, 2381–2403.

Emanuel, K. A., 1994: *Atmospheric Convection*, Oxford Univ. Press, N. Y.

Feng, Z., L. R. Leung, S. Hagos, R. A. Houze, C. D. Burleyson, and K. Balaguru, 2016: More frequent intense and long-lived storms dominate the springtime trend in central US rainfall. *Nat. Commun.*, **7**, 13429.

Fierro, A. O., J. Gao, C. L. Ziegler, E. R. Mansell, D. R. MacGorman, and S. R. Dembek, 2014: Evaluation of a cloud-scale lightning data assimilation technique and a 3DVAR method for the analysis and short-term forecast of the 29 June 2012 derecho event. *Mon. Wea. Rev.*, **142**, 183–202, doi:https://doi.org/10.1175/MWR-D-13-00142.1.

Foote, G. B., and C. G. Mohr, 1979: Results of a randomized hail suppression experiment in northeast Colorado. Part VI: Post hoc stratification by storm type and intensity. *J. Appl. Meteor*, **18,** 1589–1600.

Gallus, W.A., J. Correia, and I. Jankov, 2005: The 4 June 1999 Derecho Event: A Particularly Difficult Challenge for Numerical Weather Prediction. *Wea. Forecasting,* **20**,705–728.

Houze, R. A., 1993: *Cloud Dynamics.* Academic Press, 573 pp.

Houze, R. A., D. C. Wilton, and B. F. Smull, 2007: Monsoon convection in the Himalayan region as seen by the TRMM Precipitation Radar. *Quart. J. Roy. Meteor. Soc.,* **133,** 1389–1411, doi:10.1002/ qj.106.

Houze, R. A., Jr., K. L. Rasmussen, M. D. Zuluaga, and S. R. Brodzik, 2015: The variable nature of convection in the tropics and subtropics: A legacy of 16 years of the Tropical Rainfall Measuring Mission satellite, *Rev. Geophys.,* **53**, doi:10.1002/2015RG000488.

Huffman, G.J., D.T. Bolvin, E.J. Nelkin, D.B. Wolff, R.F. Adler, G. Gu, Y. Hong, K.P. Bowman, and E.F. Stocker, 2007: The TRMM Multisatellite Precipitation Analysis (TMPA): Quasi-Global, Multiyear, Combined-Sensor Precipitation Estimates at Fine Scales. *J. Hydrometeor.,* **8**, 38–55.

Huntrieser, H., H. H. Schiesser, W. Schmid, and A. Waldvogel, 1997: Comparison of traditional and newly developed thunderstorm indices for Switzerland. *Wea. Forecasting*, **12**, 108–125.

Kain, J.S., M.C. Coniglio, J. Correia, A.J. Clark, P.T. Marsh, C.L. Ziegler, V. Lakshmanan, S.D. Miller, S.R. Dembek, S.J. Weiss, F. Kong, M. Xue, R.A. Sobash, A.R. Dean, I.L. Jirak, and C.J. Melick, 2013: A Feasibility Study for Probabilistic Convection Initiation Forecasts Based on Explicit Numerical Guidance. *Bull. Amer. Meteor. Soc.,* **94**,1213–1225, https://doi.org/10.1175/BAMS-D-11-00264.1.

Kaltenböck, R., G. Diendofer, and N. Dotzek, 2009: Evaluation of thunderstorm indices from ECMWF analyses, lightning data and intense storms reports. *Atmos. Res.*, **93**, 381–396.

Koren, I., O. Altaratz, L. A. Remer, G. Feingold, J. Vanderlei Martins, and R. H. Heiblum, 2012: Aerosol-induced intensification of rain from the tropics to the midlatitudes, Nat. Geosci., 5, 118–122, doi:10.1038/ngeo1364

Kummerow, C., W. Barnes, T. Kozu, J. Shiue, and J. Simpson, 1998: The Tropical Rainfall Measuring Mission (TRMM) Sensor Package, *J. Atmos. Oceanic Technol.,* **15**, 809–817.

Kunkel, K. E., and Coauthors, 2013: Monitoring and understanding trends in extreme storms: State of knowledge. *Bull. Amer. Meteor. Soc.,* **94,** 499–514.

Lang, T. J., and S. A. Rutledge, 2002: Relationships between convective storm kinematics, precipitation, and lightning. *Mon. Wea. Rev.,* **130**, 2492–2506.

Liu, N., and C. Liu, 2016: Global distribution of deep convection reaching tropopause in 1 year GPM observations, *J. Geophys. Res. Atmos.*, **121,** 3824–3842, doi:10.1002/ 2015JD024430.

Liu, C., D. J. Cecil, E. J. Zipser, K. Kronfeld, and R. Robertson, 2012: Relationships between lightning flash rates and radar reflectivity vertical structures in thunderstorms over the tropics and subtropics. *J. Geophys. Res.*, **117**, D06212.

Liu, C., and E. Zipser, 2005: Global distribution of convection penetrating the tropical tropopause, *J. Geophys. Res.,* **110,** D23210, doi:10.1029/ 2005JD00006063.

Lee, S. S., 2012: Effect of aerosol on circulations and precipitation in deep convective clouds, *J. Atmos. Sci.,* 69, 1957–1974, doi:10.1175/ JAS-D-11-0111.1.

MacGorman, D. R., and W. D. Rust, 1998: *The Electrical Nature of Storms*. Oxford University Press, 422 pp.

MacGorman, D. R., and D. W. Burgess, 1994: Positive cloud-to-ground lightning in tornadic storms and hailstorms. *Mon. Wea. Rev.,* **122**, 1671– 1697.

Mapes, B. E., 1997: Equilibrium vs. activation control of large-scale variations of tropical deep convection. *The Physics and Parameterization of Moist Atmospheric Convection,* R. K. Smith, Ed., Kluwer Academic, 321–358.

Mapes, B., 1998: The large-scale part of tropical mesoscale convective system circulations. *Journal of the Meteorological Society of Japan Series II*, **76**, 29–55.

Mazur, R. J., J. F. Weaver, and T. H. Vonder Haar, 2009: A preliminary statistical study of correlations between inflow feeder clouds, supercell or multicell thunderstorms, and severe weather. *Wea. Forecasting,* **24**, 921–934.

McCarthy, J., 1974: Field verification of the relationship between entrainment rate and cumulus cloud diameter. *J. Atmos. Sci.*, **31**, 1028–1039.

Mecikalski, J.R., J.K. Williams, C.P. Jewett, D. Ahijevych, A. LeRoy, and J.R. Walker, 2015: Probabilistic 0–1-h Convective Initiation Nowcasts that Combine Geostationary Satellite Observations and Numerical Weather Prediction Model Data. *J. Appl. Meteor. Climatol.,* **54**, 1039–1059.

Meißner, C., N. Kalthoff, M. Kunz, G. Adrian, 2007: Initiation of shallow convection in the Black Forest mountains. *Atmos. Res.,* **86,** 42–60.

Mekonnen, A., C.D. Thorncroft, and A.R. Aiyyer, 2006: Analysis of Convection and Its Association with African Easterly Waves. *J. Climate,* **19**, 5405–5421,https://doi.org/10.1175/JCLI3920.1.

Mitchell, E. D., S. V. Vasiloff, G. J. Stumpf, A. Witt, M. D. Eilts, J. T. Johnson, and K. W. Thomas, 1998: The National Severe Storms Laboratory tornado detection algorithm. *Wea. Forecasting*, **13**, 352–366.

Moncrieff, M.W., Miller, M., 1976: The dynamics and simulation of tropical cumulonimbus and squall lines. *Q. J. R. Meteorol. Soc*. **102**, 373–394.

Mohr, K. I., and E. J. Zipser, 1996: Defining mesoscale convective systems by their ice scattering signature, *Bull. Am. Meteorol. Soc.,* **77,** 1179–1189.

Mohr, K. I. and C. D., Thorncroft, 2006: Intense convective systems in West Africa and their relationship to the African easterly jet. *Q.J.R. Meteorol. Soc.,* **132:** 163-176. doi:10.1256/qj.05.55.

Murphy, A. H., 1977: The value of climatological, categorical and probabilistic forecasts in the cost–loss ratio situation. *Mon. Wea. Rev.*, **105**, 803–816.

Parker, D. J., 2002: The response of CAPE and CIN to tropospheric thermal variations. *Quart. J. Roy. Meteor. Soc.*, **128**, 119–130.

Peterson, R. E., 1983: The west Texas dryline: Occurrence and behavior. Preprints, 13th Conf. Intense Local Storms, Tulsa, OK, *Amer. Meteor. Soc.,* J9–J11.

Pierce, E. T., 1958: Some topics in atmospheric electricity. *Recent Advances in Atmospheric Electricity,*Pergamon, 5–16.

Rasmussen, E. N., and D. O. Blanchard, 1998: A baseline climatology of sounding-derived supercell and tornado forecast parameters. *Wea. Forecasting*, **13,** 1148–1164.

Rasmussen, K. L., and R. A. Houze, 2011: Orogenic convection in subtropical South America as seen by the TRMM satellite. *Mon. Wea. Rev.,* 139, 2399–2420, doi:10.1175/MWR-D-10-05006.1.

Rasmussen, K.L. and R.A. Houze, 2016: Convective Initiation near the Andes in Subtropical South America. *Mon. Wea. Rev.,* **144**, 2351–2374.

Raymond, D. J., and M. J. Herman, 2011: Convective quasi-equilibrium reconsidered, *J. Adv. Model. Earth Syst.*, **3**, M08003, doi:10.1029/2011MS000079.

Reap, R.M. and D.R. MacGorman, 1989: Cloud-to-Ground Lightning: Climatological Characteristics and Relationships to Model Fields, Radar Observations, and Intense Local Storms. *Mon. Wea. Rev.,* **117**, 518–535.

Rhea, J. O., 1966: A study of thunderstorm formation along dry lines. *J. Appl. Meteor.,* **5**, 58–63.

Romero, R., C. Ramis, and V. Homar, 2015: On the intense convective storm of 29 October 2013 in the Balearic Islands: Observational and numerical study, *Q. J. R. Meteorol. Soc.*, **141**, 1208–1222, doi:10.1002/qj.2429.

Romatschke, U., S. Medina, and R. A. Houze, 2010: Regional, seasonal, and diurnal variations of extreme convection in the South Asian region, *J. Clim.*, **23**, doi:10.1175/2009JCLI3140.1.

Rosenfeld, D. and W. L. Woodley., 2003: Closing the 50-year circle: From cloud seeding to space and back to climate change through precipitation physics. *Cloud Systems, Hurricanes, and the Tropical Rainfall Measuring Mission (TRMM), Meteor. Monogr.*, No. 51, Amer. Meteor. Soc., 59–80.

Rotunno, R., J.B. Klemp, and M.L. Weisman, 1988: A Theory for Strong, Long-Lived Squall Lines. *J. Atmos. Sci.,* **45**, 463–485.

Sander, J., J. F. Eichner, E. Faust, and M. Steuer, 2013: Rising variability in thunderstorm-related U.S. losses as a reflection of changes in large-scale thunderstorm forcing, *Weather Clim. Soc.*, **5**, 317–331, doi: 10.1175/WCAS-D-12-00023.1.

Schaefer, J. T., 1974: The life cycle of the dryline. *J. Appl. Meteor.,* **13**, 444–449.

Schumacher, C., S. N. Stevenson, and C. R. Williams, 2015: Vertical motions of the tropical convective cloud spectrum over Darwin, Australia. *Quart. J. Roy. Meteor. Soc.*, **141**, 2277–2288.

Sherwood, S. C., V. T. J. Phillips, and J. S. Wettlaufer, 2006: Small ice crystals and the climatology of lightning, *Geophys. Res. Lett.*, **33**, L05804, doi:10.1029/2005GL025242.

Spencer, R. W., and D. A. Santek, 1985: Measuring the global distribution of intense convection over land with passive microwave radiometery, *J. Appl. Meteorol.,* **24,** 860–864.

Stackpole, J. D., 1967: Numerical analysis of atmospheric soundings. *J. Appl. Meteor.*, **6,** 464–467.

Stensrud, D. J., 2007: *Parameterization Schemes: Keys to Understanding Numerical Weather Prediction Models*. Cambridge University Press, 459 pp.

Stolz, D. C., S. A. Rutledge, and J. R. Pierce, 2015: Simultaneous influences of thermodynamics and aerosols on deep convection and lightning in the tropics, *J. Geophys. Res. Atmos.*, **120**, 6207–6231.

Stolz, D. C., S. A. Rutledge, J. R. Pierce, and S. C. van den Heever, 2017: A global lightning parameterization based on statistical relationships among environmental factors, aerosols, and convective clouds in the TRMM climatology, *J. Geophys. Res. Atmos.*, 122, 7461–7492.

Takahashi, T., 1978: Riming electrification as a charge generation mechanism in thunderstorms, *J. Atmos. Sci.*, **35**, 1536–1548.

Uppala, S. M., D. Dee, S. Kobayashi, and A. Simmons, 2008: Evolution of reanalysis at ECMWF.*Extended Abstracts, Third WCRP Int. Conf. on Reanalysis,* Tokyo, Japan, University of Tokyo, 6 pp.

Virts, K.S., J.M. Wallace, M.L. Hutchins, and R.H. Holzworth, 2013: Highlights of a New Ground-Based, Hourly Global Lightning Climatology. *Bull. Amer. Meteor. Soc.,* **94**,1381–1391.

Wall, C., E. J. Zipser, and C. Liu, 2014: An investigation of the aerosol indirect effect on convective intensity using satellite observations, J. Atmos. Sci., 71, 430–447.

Washington, W. M., and C. L. Parkinson, 2005: An Introduction to Three-dimensional Climate Modeling, Univ. Science Books, Sausalito, Calif.

Weisman, M.L. and J.B. Klemp, 1982: The Dependence of Numerically Simulated Convective Storms on Vertical Wind Shear and Buoyancy. *Mon. Wea. Rev.,* **110**, 504–520.

Weisman, M. L., and J. B. Klemp, 1986: Characteristics of isolated convective storms. *Mesoscale Meteorology and Forecasting,* P. S. Ray, Ed., Amer. Meteor. Soc., 331–358.

Weisman, M.L. and R. Rotunno, 2004: "A Theory for Strong Long-Lived Squall Lines" Revisited. *J. Atmos. Sci.,* **61**, 361–382.

Weisman, M.L. and R.J. Trapp, 2003: Low-Level Mesovortices within Squall Lines and Bow Echoes. Part I: Overview and Dependence on Environmental Shear. *Mon. Wea. Rev.,* **131**, 2779–2803.

Westermayer, A. T., P. Groenemeijer, G. Pistotnik, R. Sausen, and E. Faust, 2016: Identification of favorable environments for thunderstorms in reanalysis data. *Meteor. Z.*, **26**, 59–70, doi:https://doi.org/10.1127/metz/2016/0754.

Williams, E., and N. Renno, 1993: An analysis of the conditional stability of the tropical atmosphere.*Mon. Wea. Rev.*, **121,** 21–36.

Williams, E. R., and S. Stanfill, 2002: The physical origin of the land–ocean contrast in lightning activity. *Comp. Rendus Phys.*, **3,** 1277–1292.

Williams, E., T., Chan, and D., Boccippio, 2004: Islands as miniature continents: Another look at the land-ocean lightning contrast, *J. Geophys. Res.*, **109**, D16206.

Williams, E. R., T. V. Mushtak, D. Rosenfeld, S. Goodman, and D. Boccippio, 2005: Thermodynamic conditions favorable to superlative thunderstorm updraft, mixed phase microphysics and lightning flash rate, *Atmos. Res.*, **76**, 288–306.

Wilson, J. W., N. A. Crook, C. K. Mueller, J. Sun, and M. Dixon, 1998: Nowcasting thunderstorms: A status report, *Bull. Am. Meteorol. Soc.*, **79**, 2079–2099.

Yano, J.-I., M. Bister, v. Fuchs, L. Gerard, V. T. J. Phillips, S. Barkidija, and J.-M. Piriou, 2013: Phenomenology of convection-parameterization closure. *Atmos. Chem. Phys.,* **13,** 4111–4131.

Ye, B., A.D. Del Genio, and K.K. Lo, 1998: CAPE Variations in the Current Climate and in a Climate Change. *J. Climate,* **11**, 1997–2015.

Zipser, E., C. Liu, D. Cecil, S. W. Nesbitt, and S. Yorty, 2006: Where are the most intense thunderstorms on Earth? *Bull. Am. Meteorol. Soc.,* **87**, 1057–1071.

Zhou, Y., W. K. M. Lau, and C. Liu, 2013: Rain characteristics and large-scale environments of precipitation objects with extreme rain volumes from TRMM observations, *J. Geophys. Res. Atmos.*, **118**, 9673–9689.

Zuidema, P., 2003: Convective Clouds over the Bay of Bengal. *Mon. Wea. Rev.,* **131**, 780–798, https://doi.org/10.1175/1520-0493(2003)131<0780:CCOTBO>2.0.CO;2

Table 2.1 Mean and spatial correlations between the observed percentage of CFs with > 50 flashes and estimated percentage of severe thunderstorms by individual and joint atmospheric factors.

		Land & Ocean separately				Land & Ocean together			
		Land		Ocean		Land		Ocean	
	Atmospheric factors	Mean	R	Mean	R	Mean	R	Mean	R
	Observations	0.53		0.10					
One	CAPE	0.26	0.38	0.03	0.29	0.09	0.29	0.07	0.25
	CIN	0.33	0.52	0.03	0.32	0.14	0.51	0.09	0.31
	$SHEAR_{1\text{-}3km}$	0.40	0.27	0.04	0.30	0.12	0.23	0.10	0.21
Two	CAPE+CIN	0.30	0.56	0.03	0.35	0.19	0.55	0.07	0.36
	$CAPE+SHEAR_{1\text{-}3km}$	0.30	0.54	0.03	0.38	0.14	0.48	0.08	0.35
	$CIN+SHEAR_{1\text{-}3km}$	0.37	0.63	0.04	0.38	0.17	0.64	0.10	0.40
Three	$CAPE+CIN+SHEAR_{1\text{-}3km}$	0.31	0.59	0.03	0.41	0.21	0.59	0.07	0.41
Four	$CAPE+CIN+SHEAR_{1\text{-}3km}+TCWV$	0.39	0.61	0.06	0.44	0.29	0.60	0.10	0.42
	$CAPE+CIN+SHEAR_{1\text{-}3km}+LCL$	0.47	0.63	0.06	0.43	0.41	0.62	0.09	0.44
	CAPE+CIN+	0.42	0.63	0.07	0.53	0.31	0.64	0.09	0.54

	$SHEAR_{1-3km}$+SHL							
	CAPE+CIN+							
	$SHEAR_{1-3km}$+RHM	0.45	0.63	0.07	0.45	0.34	0.61	0.11	0.44
	CAPE+CIN+$SHEAR_{1-3km}$+LI500	0.66	0.50	0.07	0.33	0.51	0.49	0.16	0.36
	CAPE+CIN+$SHEAR_{1-3km}$+WCD	0.41	0.66	0.06	0.53	0.30	0.65	0.08	0.53

Table 2.2 Skill score equations.

		Prediction	
		Yes	No
Observation	Yes	a (hits)	c (misses)
	No	b (false alarm)	d (Null)

Skill Scores	POD= a/(a+c) FAR=b/(b+d) CSI= a/(a+b+c) HSS= 2(ad-bc)/((a+b)(b+d)+(a+c)(c+d))

Table 2.3 Populations of training and testing CFs with at least one flash and skill scores of different models.

		Global	ARGEN	CAFRICA	SCUS	HIMA	WAFRICA
	CFs (#)	18154483	21188	35636	21145	28455	19625
Training: 0.8	>0 flashes (#)	723368	5291	12344	5139	11404	5541
Testing:	CFs (#)	4538612	5297	8909	5287	7114	4907
0.2	>0 flashes (#)	147578	1389	3047	1295	2966	1139
	POD	0.26	0.44	0.50	0.46	0.67	0.59
Skill	FAR	0.68	0.61	0.60	0.63	0.44	0.61
Scores	CSI	0.17	0.26	0.29	0.26	0.44	0.31
	HSS	0.26	0.19	0.11	0.19	0.29	0.21

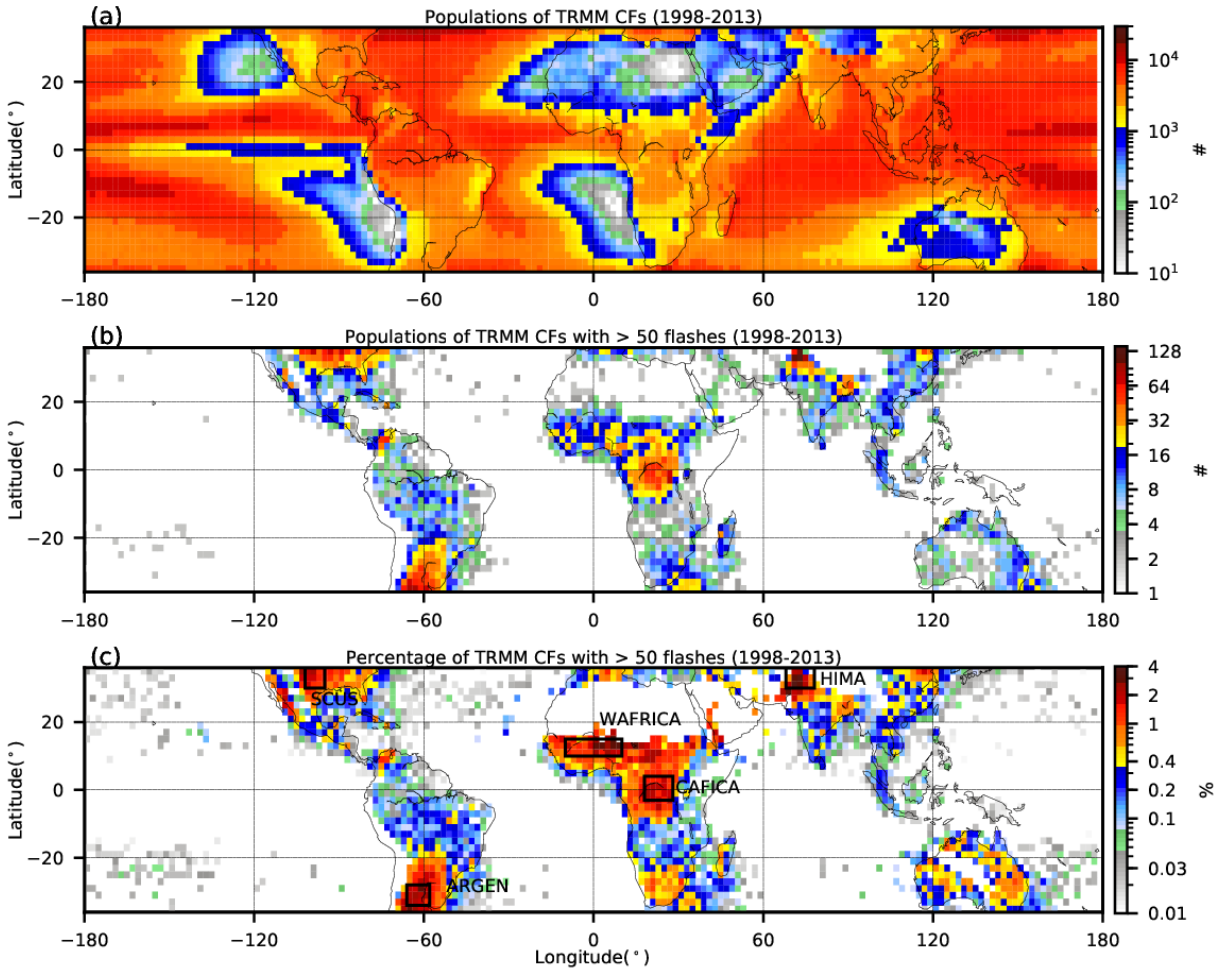

Figure 2.1 (a) Geographical distribution of the population of TRMM CFs. (b) Geographical distribution of the population of TRMM CFs with more than 50 flashes, (c) Geographical distribution of percentage of the TRMM CFs with more than 50 flashes. The distribution is created on a 2° x 2° grid from 16-years (1998-2013) of TRMM observations.

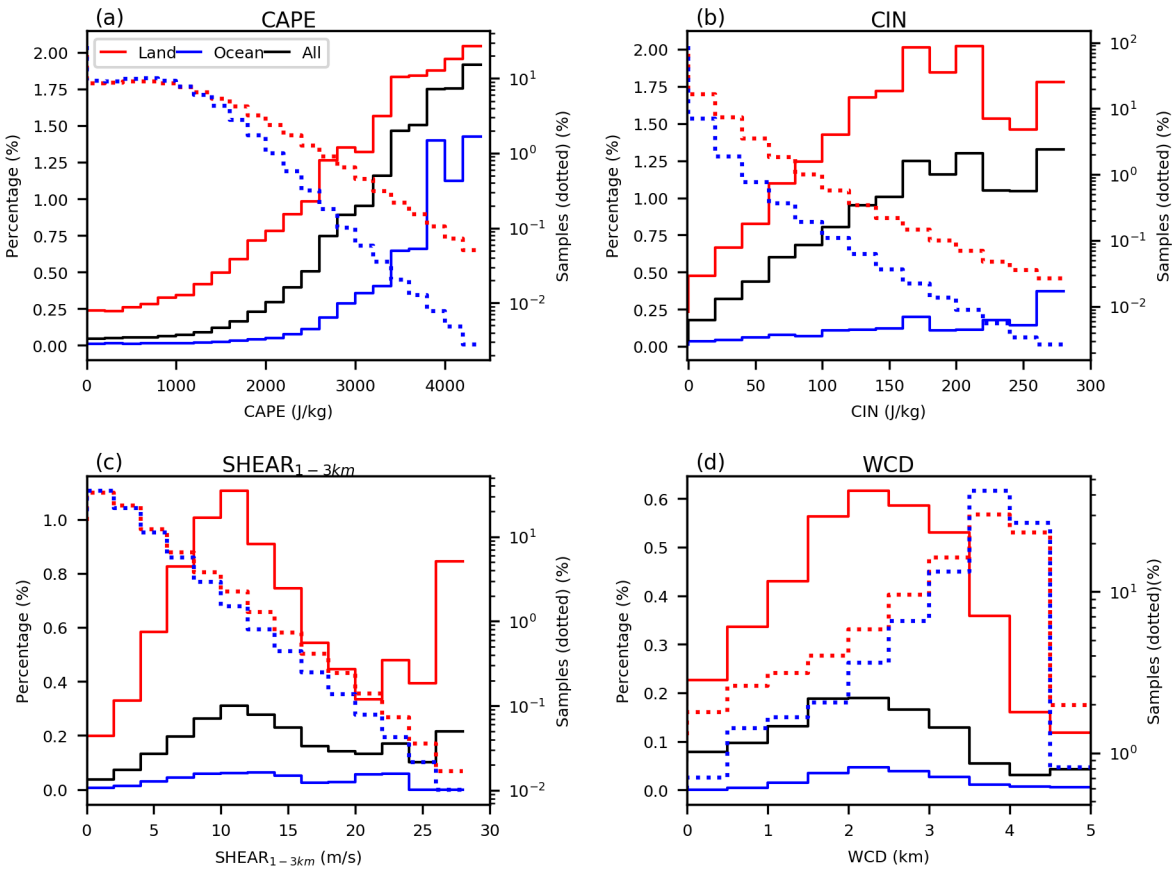

Figure 2.2 Percentage of CFs with more than 50 flashes vs. one specific thermodynamic variable. a) CAPE, b) CIN, c) SHEAR$_{1\text{-}3km}$, d) WCD. The calculations are over land (solid red), ocean (solid blue lines) and all regions (black lines) in 36°S-36°N. The dotted red (blue) lines indicate the number of TRMM CFs over land (ocean) as a function of each variable.

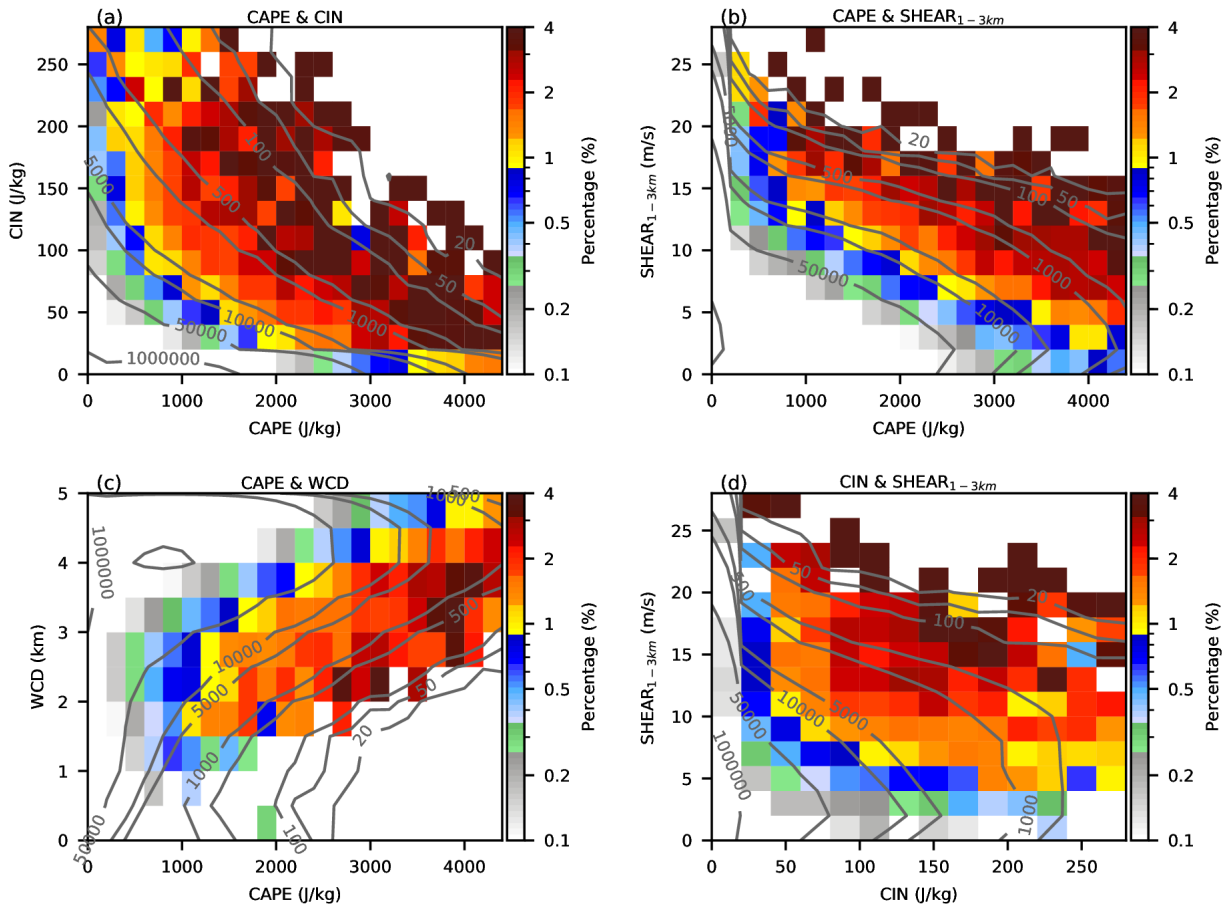

Figure 2.3 Percentage of CFs with more than 50 flashes vs. two specific thermodynamic variables jointly. (a) CAPE and CIN, (b) CAPE and $SHEAR_{1\text{-}3km}$, (c) CAPE and WCD, (d) CIN and $SHEAR_{1\text{-}3km}$. Contours represent the distribution of the population of CFs. The color fill shows the percentage of CFs with more than 50 flashes as a function of two variables.

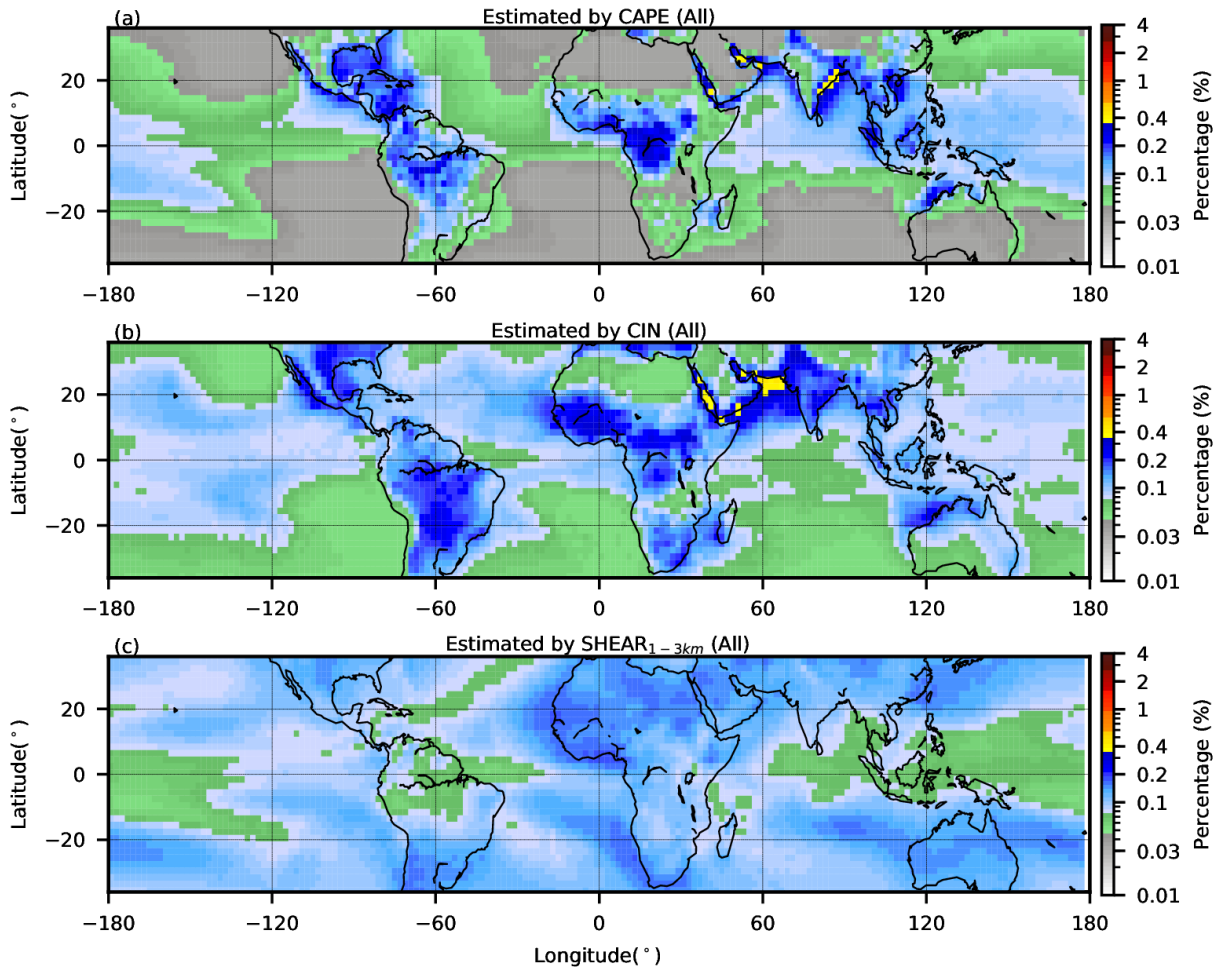

Figure 2.4 Estimated geographical distribution of the percentage of intense thunderstorms based on individual environmental variables. a) CAPE, b) CIN, c) $SHEAR_{1\text{-}3km}$. The probability of intense thunderstorms is estimated using the lookup tables shown in Figure 2.2. Thermodynamic variables are derived from 6 hourly ERA-Interim reanalysis data with a 0.75°x0.75° horizontal resolutions. "All" means that land and ocean are considered together when lookup tables are created.

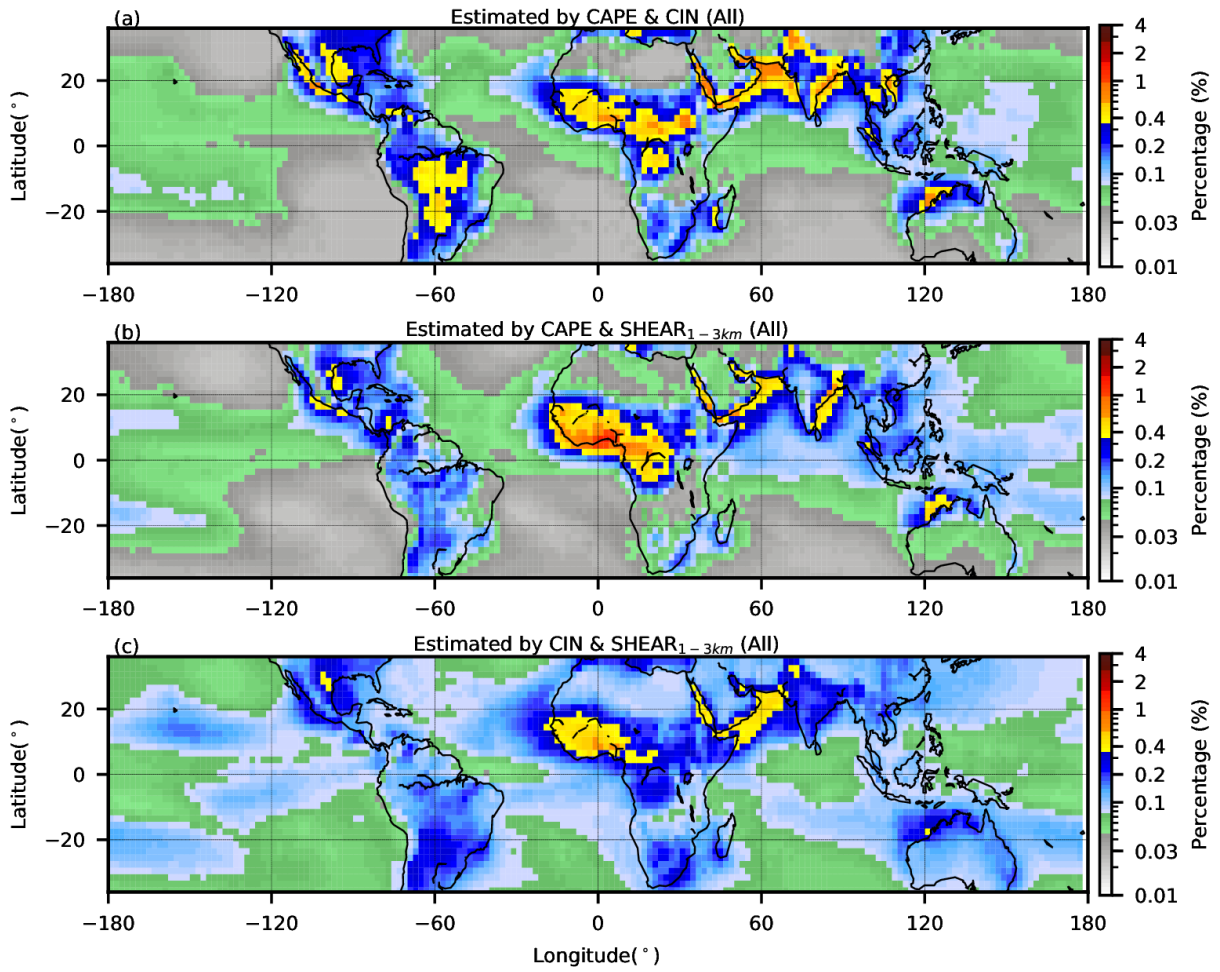

Figure 2.5 Same as Figure 2.4, but estimated with two variables. (a) CAPE and CIN, (b) CAPE and $SHEAR_{1\text{-}3km}$, (c) CIN and $SHEAR_{1\text{-}3km}$.

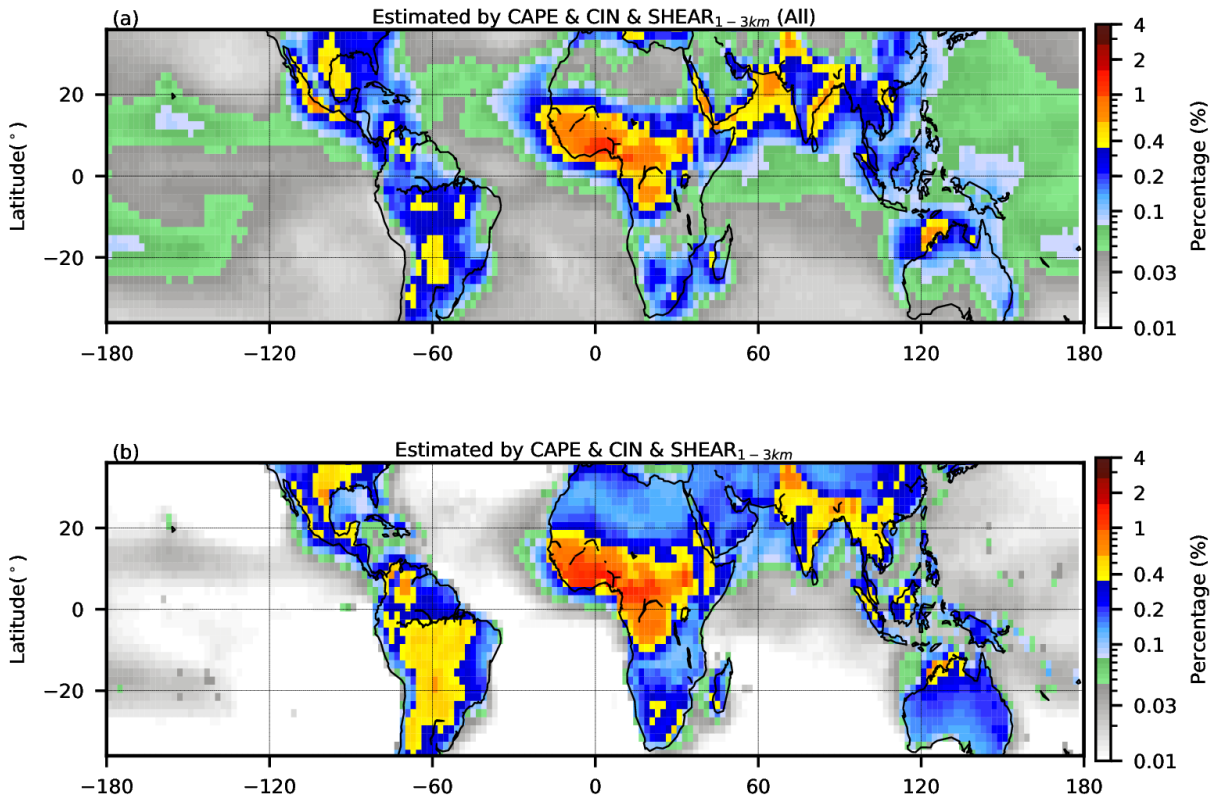

Figure 2.6 Same as Figure 2.4, but estimated with three variables: CAPE, CIN, and $SHEAR_{1\text{-}3km}$.

a) No separation of land and ocean, b) Considering land and ocean separately.

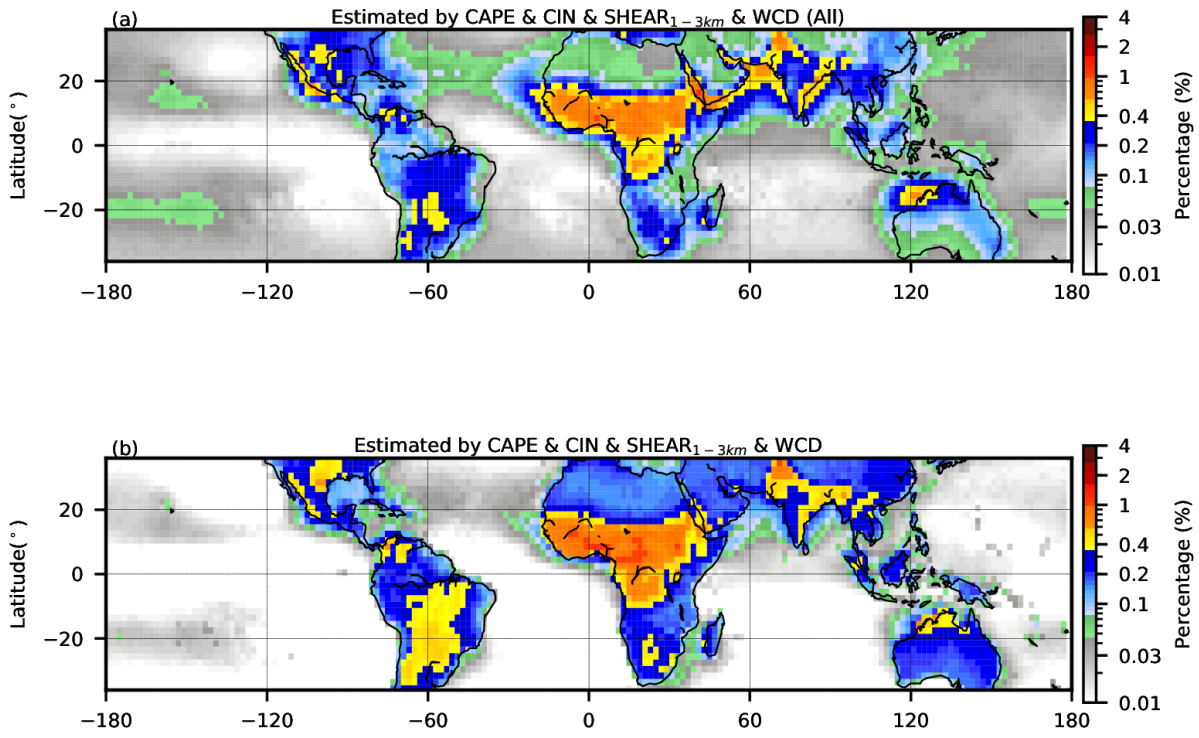

Figure 2.7 Same as Figures 4-6, but estimated by four variables: CAPE, CIN, $SHEAR_{1\text{-}3km}$, and WCD. a) No separation of land and ocean, b) Considering land and ocean separately.

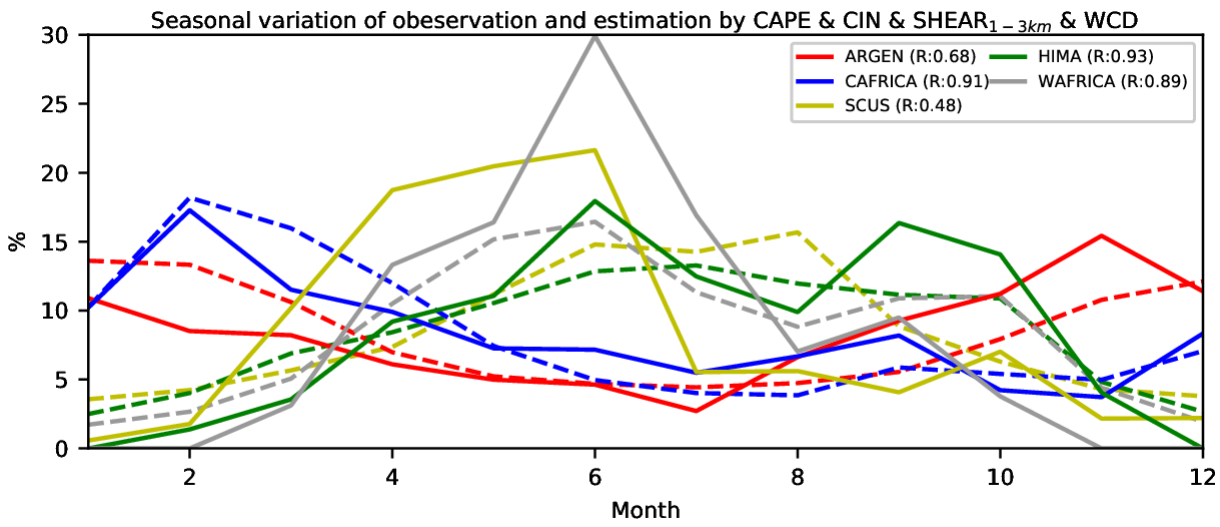

Figure 2.8 Seasonal variations of the observed (solid lines) and estimated (dashed lines) percentage of severe thunderstorms over selected regions (as shown in Figure 2.1c): ARGEN, HIMA, WAFRICA, CAFRICA, and SCUS. The correlations between the observed and estimated of percentage of intense thunderstorms over different regions are shown in the legend. The estimated seasonal variations are created by four atmospheric variables: CAPE, CIN, $SHEAR_{1\text{-}3km}$, and WCD.

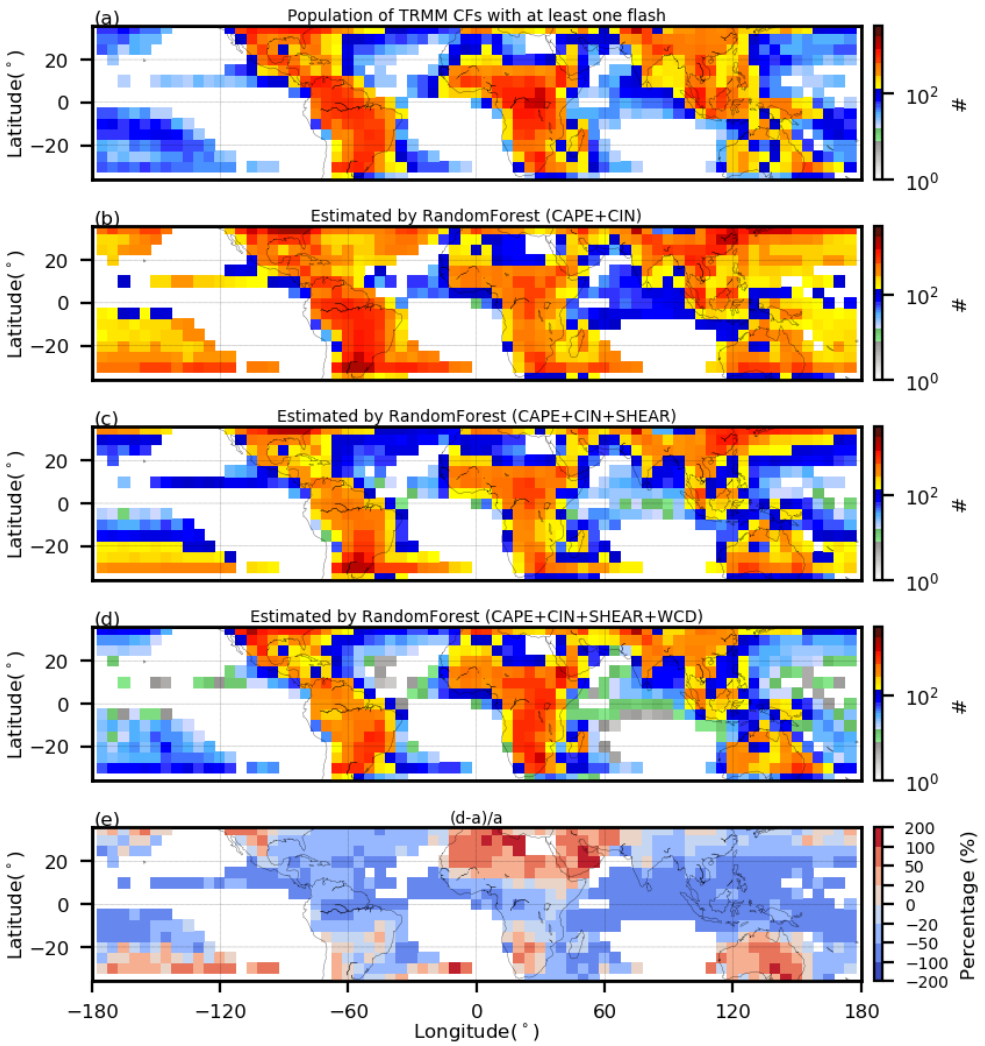

Figure 2.9 (a) Geographical distribution of the percentage of intense CFs observed by TRMM, (b-d) Estimated geographical distribution of the percentage of intense CFs by global random forest model with (a) two atmospheric variables (CAPE and CIN); (c) three atmospheric variables (CAPE, CIN and SHEAR); (d) four atmospheric variables (CAPE, CIN, SHEAR, and WCD). (e) Normalized difference between the estimation and observations. The geographical distribution of CFs is created on a 5°x5° grid. The global random forest model is created using 16-year (1998-2007) TRMM CFs. 80% of the data is used to build the model, while the remaining 20% of the 16-year CFs is used to test the model.

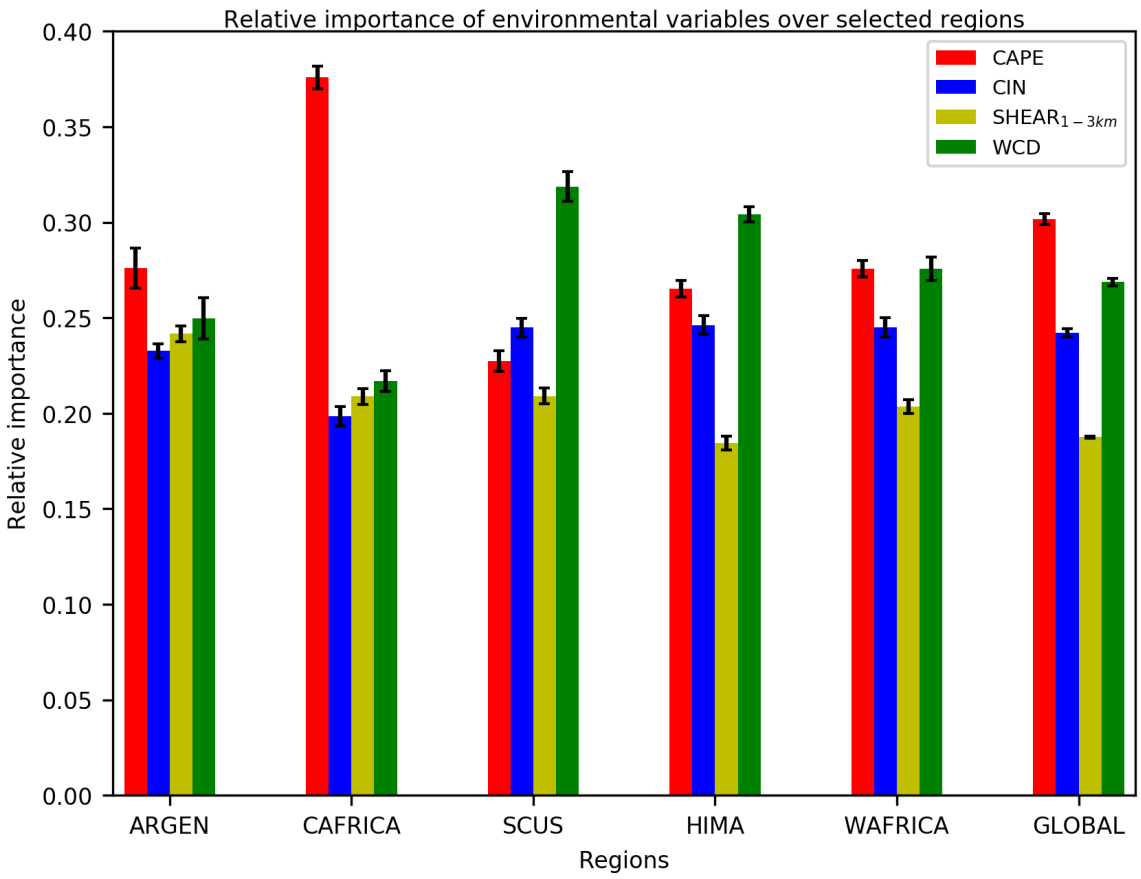

Figure 2.10 The random forest relative importance of the four environmental variables (CAPE, CIN, $SHEAR_{1\text{-}3km}$, WCD) used to predict the occurrence of thunderstorms over different regions. The error bar represents two standard deviations by running the same model 50 times.

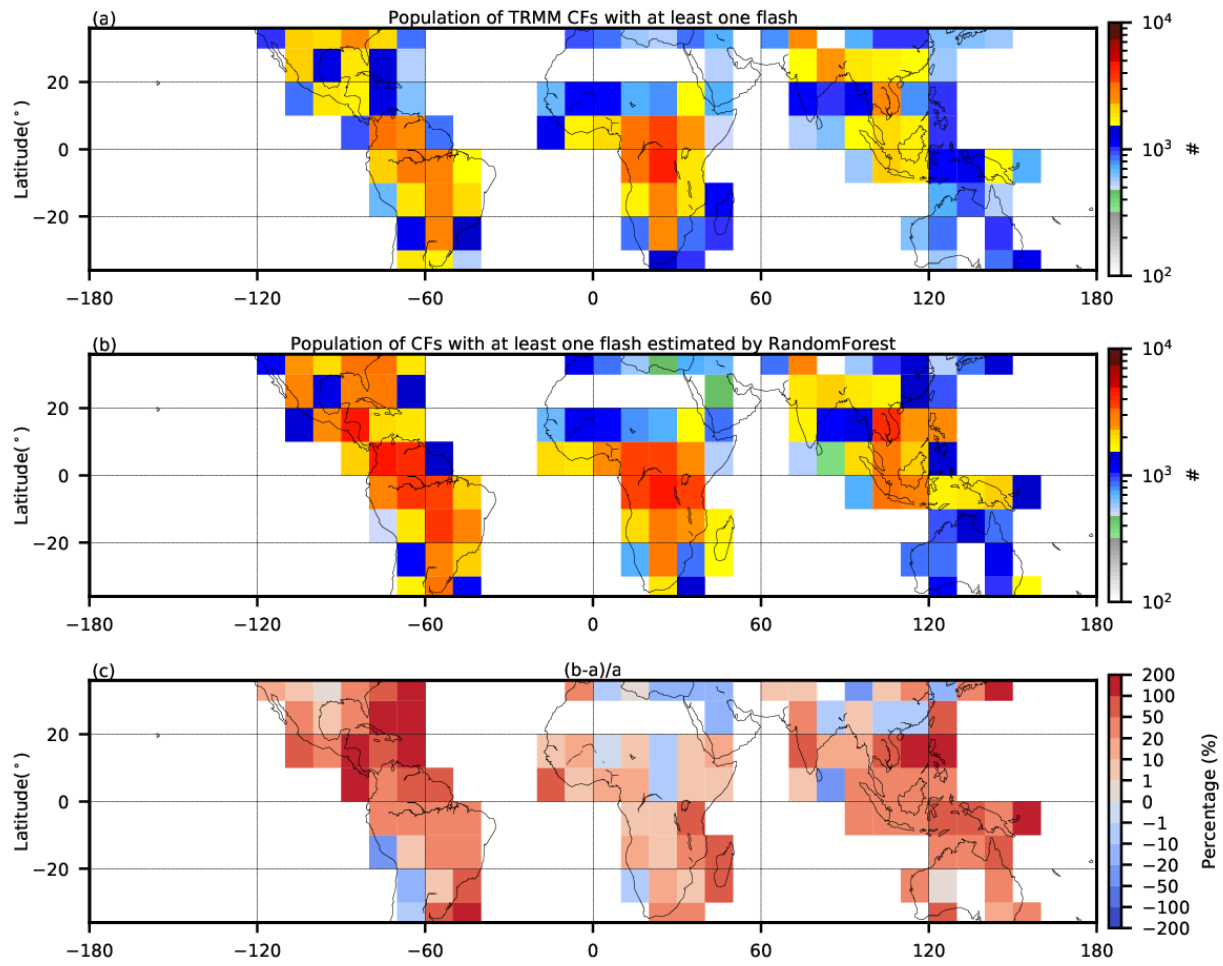

Figure 2.11 (a) Geographical distribution of the population of CFs with at least one flash observed by TRMM, (b) Estimated geographical distribution of the population of CFs with at least one flash by local random forest model with four atmospheric variables (CAPE, CIN, $SHEAR_{1\text{-}3km}$ and WCD). (c) Normalized difference between the estimation and observations. The geographical distribution of CFs is created on a 10°x10° grid. The local random forest model is created from 16-years (1998-2013) of TRMM CFs. In each grid, 80% of the data is used to build the model, while the remaining 20% of the 16-year CF dataset is used to test the model. Boxes with less than 500 CFs with at least one flash are left blank.

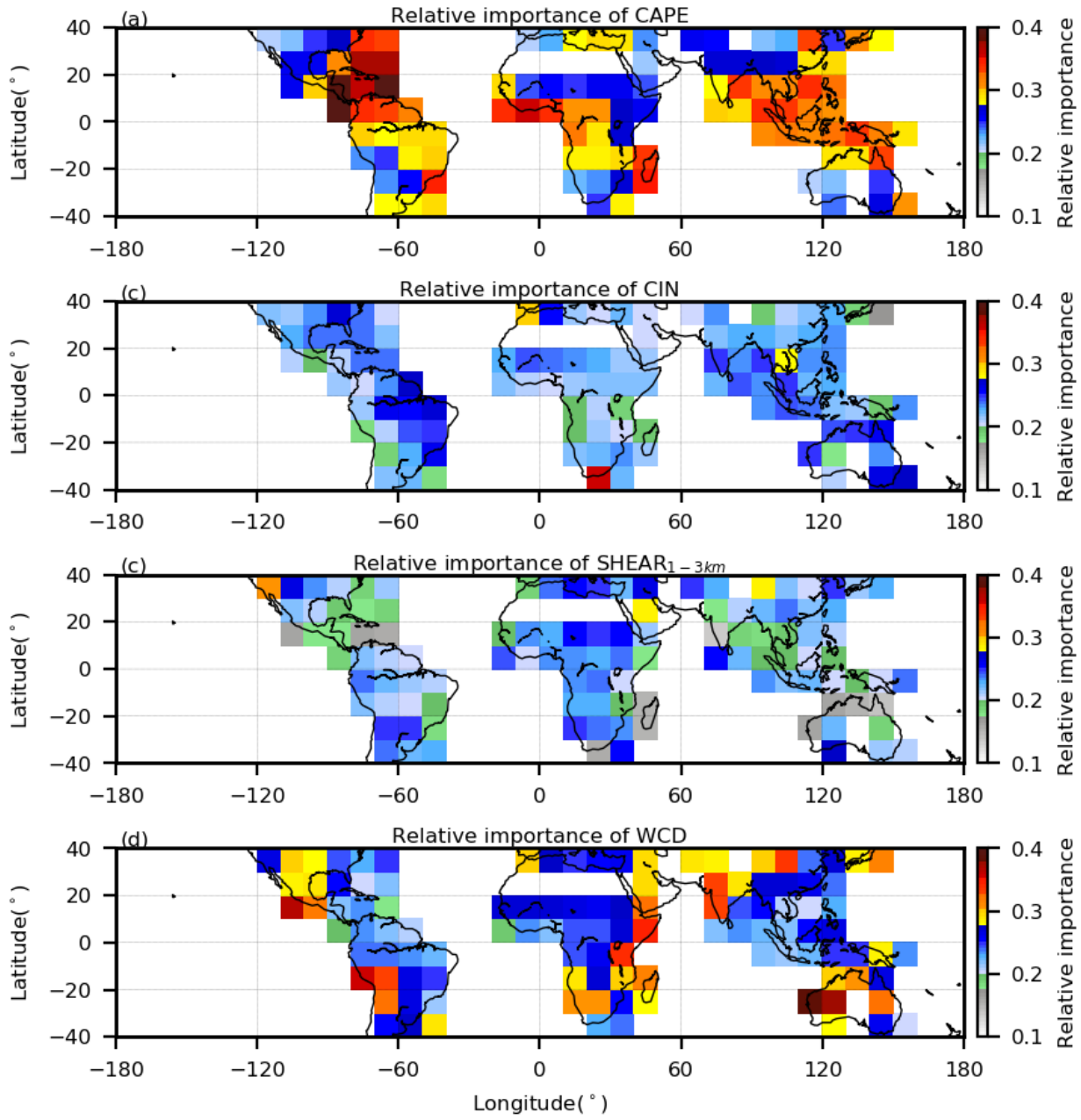

Figure 2.12 The geographical distribution of the local random forest relative importance of environmental variables in the process of predicting intense CFs. (a) CAPE, (b) CIN, (c) $SHEAR_{1\text{-}3km}$, (d) WCD.

CHAPTER III: The variation of the intensity, height and size of precipitation systems with El Niño–Southern Oscillation in the tropics and subtropics

Abstract

A 16-year (1998-2013) Tropical Rainfall Measuring Mission (TRMM) Precipitation Feature (PF) database is used to examine the impacts of the El Niño–Southern Oscillation (ENSO) on the characteristics of precipitation systems in the tropics and subtropics. Noticeable differences in the fractions of deep systems (20 dBZ radar echo tops greater than 10 km) and Mesoscale Convective Systems (MCSs) (an area greater than 2000 km^2) between different phases of ENSO are found over specific regions, including the central Pacific (CPACI), the western Maritime Continent (WMC), the eastern Maritime Continent (EMC), Gulf of Mexico (GM), Argentina (ARGEN), and Australia (AUS). The coefficients of determination (R^2) between the Multivariate ENSO Index (MEI) and the population fractions of deep convection and MCSs are analyzed seasonally over these regions. The responses from these precipitation systems to the ENSO are found more pronounced in the winter half-year than the summer half-year. An increase of rainfall during the El Niño periods over the CPACI, GM, and ARGEN is found associated with more precipitation-events and a higher fraction of intense, deep, and large precipitation systems. AUS has fewer precipitation events and a higher fraction of shallow and small precipitation systems during El Niño conditions. Both EMC and WMC have a higher fraction of MCSs during La Niña than El Niño conditions. The EMC observes a higher fraction of deep convection during La Niña conditions. However, the WMC has a higher fraction of deep convection during El Niño conditions, possibly related to the effect of the Indian Ocean Dipole.

Introduction

As a dominant coupled mode of tropical variability on interannual time scales (Rasmusson and Carpenter 1982), the El Niño–Southern Oscillation (ENSO) phenomenon has been accounted for climate anomalies since the early years of the last century (Walker 1925). The effect of extreme phases of ENSO on the precipitation variation is well documented, especially over the equatorial Pacific. Knowledge of ENSO-precipitation over the tropical Pacific spawned many efforts to document the role of ENSO in the climate anomaly over other regions. For example, Rasmusson and Carpenter (1983) showed that the ENSO events may impact the Asian-Australian monsoon, and these atmosphere circulation changes during ENSO events could have an influence on the storm frequency and intensity (Williams 2005). Leigh and Kuhnel (2001) suggested that severe thunderstorms in Australia are related to certain ENSO cycles (Yeo 2005; Leigh and Kuhnel 2001). A number of studies also established that North America contains a significant ENSO signal in extreme precipitation (e.g., Gershunov 1998; Cayan et al. 1999; Jong et al. 2016).

Unprecedented efforts have also been put into the examination of which characteristics of precipitation-convection best corresponds to the precipitation variation over different regions. Zolman et al. (2000) presents that the tropical anomalous precipitation is not explained by the area distribution and median intensity of tropical Mesoscale Convective Systems (MCSs), using two-years of 85-GHz brightness temperature data of the Special Sensor Microwave Imager (SSM/I). Mohr et al. (2009) indicated the stability of area and intensity in the CFDs of precipitation systems during different phases of ENSO years in west Africa and the western Pacific tropical cyclone basin. Over the warm pool region, Mapes and Houze (1993) observed a

noticeable difference in the cumulative fraction of cold clouds (< 235 K) between warm and cold ENSO events, based on the analysis of IR cloud clusters. In addition, the size distribution of 208 and 198 K cloud clusters indicates that cloud clusters are dominated by small clusters, with 50% (80%) of clusters smaller than 300 (1000) km^2. Therefore, the area distribution of clusters is not always revealing of the relative importance of cluster with various sizes, especially with a limited sample.

Is the ENSO-related anomalous precipitation explained by more precipitation events, or larger and/or more intense precipitation events? The answer to this question is still not clear. This study expands previous studies by investigating which characteristic of precipitation systems best corresponds to the precipitation variation over different regions, with a consistent methodology and dataset. The coverage of the Tropical Rainfall Measuring Mission (TRMM) allows the investigation of the characteristics of precipitation across the tropics and subtropics (35^oN-35^oS) from the launch of the satellite in November 1997 to mid-2014 (Kummerow et al. 1998). Launched in early 2014, the Global Precipitation Measurements core satellite (Hou et al., 2014), as the next generation of TRMM, has extended the studies of precipitation to the middle and high latitudes (Liu and Zipser, 2015). However, given the short period observations from GPM and the uncertainty by combining observations from different satellites, only the long time period observations from TRMM are used in this study. The ability of the Precipitation Radar (PR) onboard TRMM to see the three-dimensional structure of the precipitation at high horizontal and vertical resolution provides a unique vision of ENSO-precipitation relationship.

The climatology of unconditional precipitation observed by the TRMM PR in Figure 3.1a, shows a robust statistics of precipitation using 16-years observations. The unconditional precipitation is defined as total precipitation accumulation, including both precipitation and non-precipitation time periods, and calculated by dividing the total PR precipitation with the total PR samples. Using 16-years of TRMM records, we are able to subset the samples and create robust statistics of precipitation under strong warm and cold ENSO phases (Figure 3.2, details in section 2). Figure 3.1b shows the difference of precipitation between the warm and cold phase of ENSO. The results follow the well-documented ENSO-related anomalous precipitation (Ropelewski and Halpert 1987; Kiladis and Diaz 1989; Dai and Wigley 2000; Lyon and Barnston 2005; Yang and DelSole 2012), with enhanced precipitation over the eastern and central Pacific, and reduced rainfall over Maritime Continent during El Niño years and vice versa during La Niña years. The effects on the anomaly of rainfall in the Indian Ocean and Atlantic Ocean are less pronounced than the tropical Pacific and Maritime Continent. The fractional anomaly in total precipitation (Figure 3.1c) shows almost 3-times the precipitation over the central Pacific in the warm versus cold phase of ENSO periods (Figure 3.1c). Zolman et al. (2000) also shows that the number of MCSs in winter (summer) over the equatorial central Pacific during El Niño is 4 times (3 times) of that during La Niña year.

The goal of this study is to revisit the question of whether the ENSO-related anomalous precipitation is associated with the variation of the intensity, area, and heights of convective systems, with much larger samples than previous studies. This particular study will describe the data and methodology in section 2. Section 3 presents the effect of ENSO as a potential factor for

the characteristics of convective systems. Finally, the conclusion and summary will be provided in section 4.

Data and Methods

Our effort is to extend the understanding of anomalous precipitation through the analysis of the characteristics of precipitation systems based on the use of long-term records (1998-2013) of TRMM rainfall products obtained from the PR and the TRMM Microwave Imager (TMI). The data source is obtained from the precipitation features (PFs) (Nesbitt et al. 2000; Liu et al. 2008), derived from the TRMM version 7 rainfall products. PFs are defined by grouping contiguous pixels with near surface rainfall derived from the TRMM PR (Iguchi et al. 2000, 2009). Various parameters are used in this study to explore the properties of precipitation systems, including PF area, the maximum height of 20 dBZ radar reflectivity (MAXHT20), and the minimum 85-GHz Polarization Corrected Temperature (Spencer et al. 1989; MIN85PCT). Directly associated with the ice scattering signature in the column, 85-GHz PCT have been commonly used as a proxy of convective intensity (e.g. Cecil and Zipser 1999; Nesbitt and Zipser 2003; Liu and Zipser 2005; Mohr et al. 2009). Therefore, the minimum 85-GHz PCT of each PF is used to examine the different intensity of convective systems under warm and cold phases of ENSO. The general size distribution of cloud clusters, dominated by small clusters, inspires us to pay particular attention to the heavy-tailed nature of the precipitation from the deepest and the largest systems. Deep convective systems are defined as PFs with the MAXHT20 greater than 10 km. With only 10-20% of the population but more than 70% contribution of the rainfall (Mohr et al. 1999; Nesbitt et al. 2000), MCSs are defined as PFs with area greater than 2000 km^2. Here, two terms related

to the deep/tall or large precipitation systems have also been defined to characterize the properties of precipitation systems in this study. One is occurrence, which is defined as the total pixels of PFs divided by total sampled pixels in the PR swath, multiplied by 100 (%). The second term is fraction, which is defined as the number of PFs divided by the total number of PFs for the entire time period, multiplied by 100 (%). To remove the noise, only PFs with at least 4 pixels (about 80 km^2) are used in this analysis.

The variability associated with ENSO is represented by the Multivariate ENSO Index (MEI) (Wolter and Timlin 2011). The MEI index is defined as the first un-rotated principal component of six observed atmosphere-ocean variables (sea level pressure, zonal and meridional components of the surface wind, sea surface temperature, surface air temperature and total cloud-fraction of the sky) over the tropical Pacific (30°N-30°S & 100°E-70°W). Consistent with the past studies (e.g. Andrew et al., 2003; Kiem, and Franks, 2001; Shrestha and Kostaschuk, 2005), months with values greater than +0.5 are considered as El Niño conditions, while months with values less than -0.5 are considered as La Niña conditions (Figure 3.2). Because there is uneven number of months determined as El Niño and La Niña in each season during the TRMM era, the direct comparison between the averages of El Niño and La Niña monthly properties would be biased. Therefore, two different approaches have been used to address this. The first approach is used to create the mean properties of precipitation systems with equation (1).

$$P = \frac{1}{12}\sum_{n=1}^{12}\frac{\sum p_n}{\sum S_n} \qquad (1)$$

Where P is the mean property of precipitation system, n is the month; p_n presents the property of precipitation systems (volumetric rain, number of deep convection and number of MCSs) in the specific month n; S_n is total number of sampled pixels (Figure 3.1b, 1c) or total number of PFs

(Figure 3.3, 4, 5, 6) in month n under the El Niño or La Niña conditions. For the following analysis in this study, Figure 3.1, 3, 4, 5, 6 are created using this method.

The second approach is to test which characteristics of convective systems correspond to the variation of precipitation in different phases of ENSO, the three strongest El Niño (red dots) and La Niña (blue dots) years are chosen for each month, totaling three-years of data, as shown in Figure 3.2. It is important to note that May, June and July did not observe 3 years of La Niña conditions of less than -0.5 during the TRMM timespan. For these months, the three strongest La Niña years with the lowest MEI values are chosen, and all of these months are negative on the MEI index, indicating they are still slight La Niña conditions. Another important caveat to note is that this 3-year compiled dataset of the strongest years of each month is not continuous, and the limited ENSO events during the TRMM time period could possibly affect the results. Figure 3.7-12 of the study are produced using this second approach.

Results

a. Variation of deep precipitation systems during ENSO

Figure 3.3 illuminates the geographical distribution of the fraction of deep precipitation systems with 20 dBZ echo tops exceeding 10 km over the two phases of ENSO. To create this plot, we divide the numbers of PFs with maximum height of 20 dBZ greater than 10 km, by the total number of PFs in each $2^{o}x2^{o}$ grid box. In general, the geographical distribution of the fraction of deep convection over these two periods show a similar spatial correspondence with past studies (Mohr and Zipser 1999; Liu and Zipser 2005; Zipser et al. 2006; Liu and Liu 2016). These studies identified that more deep convection are found over land than over ocean, with a

preference over some specific regions, such as central Africa, Maritime Continent and Columbia. There is also a relatively larger fraction of deep convection over the Inter Tropical Convergence Zone (ITCZ) and tropical Atlantic. To make the comparison of deep convection between the two phases of ENSO, the difference of the fraction of deep convection over these two periods is shown in Figure 3.3c. Similar with the anomalous precipitation, there is a larger fraction (e.g. ~2.6% larger over central Pacific) of deep convection in the central and eastern tropical Pacific and Indian Ocean during the warm phase in comparison to the cold phase of ENSO. The small variation (~2.6%) in the fraction of deep convection could result in ~27% difference in the rain contribution over central Pacific. A larger fraction (~1.2% larger) of deep convection, accounting for ~5.5% higher rain contribution, is found over the Western Maritime Continent (WMC: 95°-115°E & 5°S-5°N) during El Niño years than that during La Niña periods. The Eastern Maritime Continent (EMC: 115°-135°E & 0°-13°N) is found to have a smaller fraction (~1.3% smaller) and lower rain contribution (~3.2 % lower) of deep convection during El Niño periods. Over the areas that are favorable for deep convection, such as North America, Argentina, Central Africa and Columbia, the difference in the fraction of deep convection between these two phases of ENSO is also significant (e.g. ~10.3% during the El Niño periods and ~8.7% during the La Niña periods over ARGEN).

b. Variation of size during ENSO

Figure 3.4 presents the geographical distribution of the fraction of MCSs during the two phases of ENSO. The general shapes of the distributions in Figure 3.4 follow the well-established pattern by various studies (e.g. Laing and Fritsch 1997; Nesbitt and Zipser 2000; Yuan and Houze 2010), with a tendency of a larger concentration over some particular regions (mid-

latitude South America, central Africa, south central United States and southern China). The larger fraction of MCSs during El Niño conditions than that of during La Niña in the central Pacific is consistent with the anomalous precipitation shown in Figure 3.1b. The increase /decrease of the population fraction of MCSs over the WMC under El Niño condition is consistent with the increase/decrease of precipitation in the region. This indicates that the variation of population of MCSs may play an important role in the precipitation anomaly over the WMC.

c. Geographical correlation between MEI and height/size of PFs

To further examine the linkage between the ENSO to the size and height of convection, the Pearson Correlation (r-value) between the monthly MEI values and the monthly fractions of PFs from deep systems and MCSs are analyzed on a 2^{o}x2^{o} grid. As shown in Figure 3.5, the effect of ENSO on the heights and size of convective systems over the areas directly linked to ENSO, are more pronounced than those areas with an indirect link. The largest correlation over the tropical Pacific and Maritime Continent provide supportive evidence. Regions of the world with a direct link to ENSO are considered as immediately touching the Pacific Walker Circulation region, which extends from the west coast of North America, westward to the Maritime Continent and Southeast Asia (Julian and Chervin 1978). All other regions of the globe that are not directly touching the Pacific Walker Circulation region are considered as indirectly linked to ENSO. The areas with the largest correlation of ENSO variability to both storm height and horizontal size, lie inside the region defined as having a direct link to ENSO variability. The positive correlation over the WMC is consistent with the difference in the fraction of deep convection between El Niño and La Niña periods (Figure 3.3c).

The impacts of ENSO on the fraction of deep and large systems over the Maritime Continent region are unique, and provide evidence that the phase of ENSO indeed plays an important role in influencing the properties of precipitation systems over this region, which is consistent with some earlier studies (Wang and Rui 1990; Hamid et al. 2001, Xie et al. 2009). Figure 3.5a shows that the EMC observes a positive correlation between the MEI and the fraction of deep convection. In contrast, the WMC observes negative correlation between the MEI and the fraction of deep convection. Figure 3.5b shows that the entire Maritime Continent has more uniform negative correlation between the MEI and the fraction of MCSs. This is consistent with the ENSO precipitation anomaly in the region, providing evidence that in the region, MCSs play an important role in the anomalous precipitation during different phases of ENSO events.

Since there are distinct differences in the fraction of deep and large convection between the two phases of ENSO, especially over some particular regions, six regions (enclosed by the black box in Figure 3.5b), including central Pacific (CPACI: 150°-180°W & 8°S-5°N), WMC, EMC, the Gulf of Mexico (GM: 85°-95° W & 21°-30°N), Argentina (ARGEN: 53°-65°W & 28°-35°S), and Australia (AUS: 140°-160°E & 15°-20°S), are chosen to investigate the seasonal effect of ENSO on the characteristics of precipitation systems in this study. Then, the mean volumetric rainfall occurrence and contribution of rainfall to the total rainfall over these regions are examined further.

d. Seasonal variability in the correlation between ENSO and different systems

It is well known that the properties of precipitation systems vary seasonally (Romatschke et al. 2010). Thus, the seasonal variations of the coefficient determination (R^2) between the MEI and the fraction of deep convection and MCSs are summarized in Figure 3.6. Symbols with a larger size indicate a significant correlation between the MEI and the fraction of either the height or horizontal size of the precipitation systems, with a p-value less than 0.05.

The CPACI, which lies on the equator, has a relatively higher coefficient of determination seasonal variability of correlations between MEI and the fraction of deep and large precipitation systems than other regions throughout the year. The CPACI, with the exception of April, show a significant correlation between the MEI and the fraction of tall storms (Figure 3.6a) in almost all months, with the exception of Mar, April, and June. This indicates that the presence of El Niño conditions is correlated to the fraction of deep storms throughout the entire year. The CPACI also observed a significant correlation between the MEI and the fraction of horizontal storm size in all seasons except the Northern Hemispheric (NH) summer months of June, July, August (JJA), and September. In all other months, the results show that the fraction of MCSs over the region are associated with the ENSO events.

The Maritime Continent region shows uniquely different characteristics of precipitation systems on the eastern and westerns portions, during the two phases of ENSO. This is also observed in the seasonality of this region. First, more months are found correlated with the fractions of deep convection and MCSs over the EMC than that over the WMC (red and green symbols in Figure 3.6). This indicates that ENSO events have larger influences on the properties of convection over the eastern portion of the Maritime Continent, compared to the western portion. Second, the

correlation between the MEI and the fraction of deep convection in the WMC is significant in September and October, coincident with the peak phase of the Indian Ocean Dipole (IOD), often September –October (Saji et al. 1999), while it is not true in the EMC in September and October. Independent of the ENSO in the Pacific Ocean, the IOD is an oscillatory mode of coupled ocean-atmosphere variability in the Indian Ocean (Webster et al. 1999).

Over AUS, the fraction of deep convection is found significantly correlated ($R^2 > 0.35$) with the MEI in October and December. In addition to April and December, significant correlations ($p < 0.05$) between the MEI and the fraction of MCSs are also found during boreal fall (September-November), which is consistent with previous studies (McBride and Nicholls, 1983; Ropelewski and Halpert, 1987). The fraction of MCSs is significantly correlated ($R^2> 0.4$) to the MEI in the GM in July, and December, while the coefficient of determination between the fraction of deep storms and the MEI is greater than 0.35 in November and December. The only extended period of time that the fraction of deep storms in ARGEN noticeably correlated ($R^2 > 0.35$) to the MEI is in October. Overall, the directly linked regions (CPACI, EMC and WMC) showed much higher correlation between the MEI and the fraction of deep and large systems than the indirectly linked regions.

e. Precipitation contribution inside the Pacific Walker Circulation

To compare the properties of PFs during two ENSO phases, the histogram of PFs as a function of different parameters is created using the 3-year compiled dataset. Figure 3.7 shows the histograms of PFs and their rainfall contributions as a function of the MIN85PCT, MAXHT20 and area during the two phases of ENSO over the CPACI region. In general, there are more

precipitation events (dashed lines in Figure 3.7a, 7c and 7e) that occurred over the CPACI, during El Niño than during La Niña periods. Another evident feature is the peak located at the heavy end of the mean rainfall distribution during the El Niño periods. Precipitation systems that are deep (>12 km), large (>10000 km^2) and intense (MIN85PCT < 200 K) have much larger (~110.4 mm/year, 27.6 mm/year, 42.3mm/year more) mean annual rainfall during the warm phase of ENSO over the CPACI when compared to that during the cold phase. The difference between the two phases of ENSO in the population and rainfall fraction of PFs as a function of intensity is shown in Figure 3.7b, 7d, 7f. The largest portion of precipitation events is contributed from warm features, with the minimum 85-GHZ PCT greater than 270 K during both periods. In terms of the percentage of both the number and volumetric rainfall, the distribution is shifted to more intense PFs with colder 85 GHz PCT during El Niño than the La Niña distribution. When examining the distribution as a function of MAXHT20 and area, the number and rainfall fraction shift to the deeper, larger and more intense end of the distribution during the warm phase of ENSO relative to the distribution during the cold phase of ENSO in the CPACI. In other words, precipitation systems tend to be deeper, larger and more intense during El Niño periods in the CPACI. A small number portion of PFs with MAXHT20 greater than 10 km (2.7%) and area greater 5000 km^2 (1.1%) produces a significant total rainfall (~52% and 51%) (Figure not shown). While shallow (< 6 km) and small systems (< 1000 km^2) contribute only about 19% and 29% to the total rainfall with a much higher percentage of total PFs (78% and 94%). Therefore, a slight shift on the heavy end of the distribution of precipitation systems could lead to a large difference in the total rainfall.

The opposite is true for the anomalous precipitation over the EMC as shown in Figure 3.8. Specifically, there are more precipitation events and a larger mean annual rainfall, as well as higher occurrence of intense precipitation systems (MIN85PCT < 200 K), during La Niña than during El Niño periods. Figure 3.8d shows a slight shift towards deeper systems taking place in the EMC during La Niña periods. Meanwhile, more large-area precipitation systems (> 10000 km^2) are found over the EMC. The increase of intense, deep and large precipitation systems over the EMC during the La Niña periods is consistent with the enhanced Walker Circulation (Lindzen and Nigam 1987). More precipitation events and a larger mean annual rainfall, as well as more large-area precipitation systems (> 10000 km^2) are also found over the WMC during La Niña intervals (Figure 3.9). However, a slight shift towards deeper systems during the El Niño periods are found over the EMC. This indicates a higher faction of deep convection during the warm phase of ENSO occurring over this region (Figure 3.9d).

These results suggest that the warm and cold phases of ENSO can indeed influence the types of precipitation events (i.e. deep convection, or MCSs) at a regional scale. Specifically, in the Maritime Continent, the eastern portion receives an increase in the fraction of intense/deeper systems and MCSs during La Niña periods. In spite of the increase in the fraction of MCSs, the western portion does not have the same increase in the occurrence of deep systems during La Niña periods, which is consistent with past work that showed that Indonesia observed an increase in lightning activity, accompanied by a decrease in precipitation during the strong El Niño event of 1997-98 (e.g. Hamid et al. 2001). Higher annual rainfall and occurrence of MCSs are found both over the eastern and western portion of the Maritime Continent. However, the difference between the two phases of ENSO is smaller over the WMC than that over the EMC (Figure 3.8e

and Figure 3.9e). According to Meyers et al. (2006), a positive temperature anomaly was found in the western portion of the Maritime Continent, during the negative IOD year (with warm sea surface temperature (SST) anomaly in the eastern Indian Ocean) with no ENSO event occurring. This provides supportive evidence that the variation of precipitation in the Maritime Continent is not only affected by ENSO but also influenced by the IOD, consistent with previous studies (e.g. Saji et al. 1999; Webster et al. 1999; Ashok et al. 2003).

f. Precipitation contribution outside the Pacific Walker Circulation

The precipitation systems described above over the areas that are directly related to ENSO provide insight into the properties of the anomalous precipitation observed in those regions in response to ENSO. The similar Figure 3.s are created for another three regions, with an indirect link to ENSO, including the GM, ARGEN, and AUS. Figure 3.10 shows distinct differences exists among the two phases of ENSO over the GM. Larger occurrence of PFs and mean annual rainfall are found during El Niño years, especially for the intense (MIN85PCT < 150 K), deep (> 10 km) and large systems (>10000 km^2). This indicates that El Niño also can shift the number and volumetric rainfall distribution toward deeper, larger and more intense events over the GM, similar to that over the CPACI region.

As one of the favorite regions of deep convection (Liu et a. 2007; Romatschke and Houze 2010; Liu and Liu 2018) and MCSs (e.g. Mohr and Zipser 1996; Nesbitt et al. 2006; Salio et al. 2007) on Earth, ARGEN is worth our particular attention on the different effects of the different phases of ENSO on the properties of precipitation systems. First, there is a higher frequency and larger mean rainfall of intense, deep and large precipitation systems found over ARGEN during the

warm phase of ENSO than that during the cold phase of ENSO (Figure 3.11a, 11c and 11e). Second, the shift to the heavy end of the distribution of PFs as a function of MIN85PCT, MAXHT20 and area is more prominent over ARGEN during El Niño conditions than that during La Niña conditions, compared to the three regions mentioned above. It implies that ENSO cycles do have an effect on the properties of precipitation systems over ARGEN.

Precipitation anomalies in Australian has been associated with the strong influence of ENSO (e.g. Ropelewski and Halpert 1987; Power et al. 1998; Kiem and Franks 2004). Risbey et al. (2009) suggest that rainfall in the east of Australia has the strongest relationship with ENSO, where El Niño (La Niña) events are associated with decreased (increased) rainfall. Therefore, a similar analysis with other regions is applied to the AUS to further explore the variations in the properties of the precipitation systems (Figure 3.12). Higher number fraction of intense convection (MIN85PCT < 200 K) is found during La Niña conditions than that during El Niño conditions (Figure 3.12b). Higher mean rainfall is consistent with the increasing precipitation during the La Niña conditions over the AUS (Figure 3.12c and 12e). The difference in the occurrence between the two phases of ENSO indicates that the precipitation anomaly is associated with variation in the population of precipitation events. Higher volumetric rain contribution from shallow (< 6 km) and small (< 1000 km^2) precipitation systems is found during the El Niño periods, while higher population fraction of deep (> 10 km) and large-size (> 1000 km^2) precipitation systems is found during the La Niña periods (Figure 3.12d and 12f). In other words, a decrease of ENSO-related rainfall over the AUS is a result of fewer precipitation events and a higher fraction of shallow and small precipitation systems occurring during the El Niño periods.

g. Properties of precipitation systems under two ENSO phases over specific regions

In summary, the regional average rain and occurrence, fraction of PFs, and volumetric rainfall contribution of deep convection and MCSs during each phase of ENSO are listed in Table 3.1. Almost 4-times the average rainfall is observed over the CPACI in the warm versus cold phase of ENSO periods. This is consistent with the results shown in Figure 3.1c. Even with a low occurrence (< 6%) and small fraction of deep convection and MCSs (< 10 %), these deep and large precipitation systems can contribute more than 60% to the total rainfall, which is consistent with previous studies (e.g. Nesbitt et al., 2006). The EMC and AUS displays a lower occurrence, fraction and volumetric rainfall contribution of deep convection and MCSs during the warm phase of ENSO, while the reverse is true over other selected regions, including the CPACI and ARGEN. With a lower occurrence during the El Niño periods than that of during La Niña periods, deep convection over the WMC exhibit a higher fraction and contribute more to the total rainfall. It is important to note that in the WMC, deep convection exhibits a larger occurrence in La Niña periods but a higher fraction in El Nino periods. This indicates that although there is a shift towards a taller distribution during El Nino, this does not necessarily indicate that a larger occurrence of deep systems will be observed. The higher observed occurrence and fraction of MCSs, as well as higher fraction of deep convection, can cause more average rainfall in the warm phase of ENSO than that of the cold phase. The difference of occurrence, fraction and volumetric rainfall contribution of deep and large precipitation systems during different phases of ENSO provide supportive evidence that the ENSO-related anomalous precipitation is not only related to the number of events, but also associated with the depth, intensity and area of events.

It is typical that the precipitation systems are dominated by shallow (MAXHT20 < 6 km) and small (< 1000 km^2) systems (Figure not shown). However, the small fraction of the deep and large systems account for a large proportion of the total rainfall (Table 3.1). To highlight the role of deep and large precipitation systems, we create the median profile of 20 and 40 dBZ area in PFs over each region, using only the PFs with large volumetric rainfall (e.g. CPACI PFs > 63110 km^2 mm/hr during the El Niño periods (Figure 3.13a)) that account for the 50% of the total volumetric rainfall. In the CPACI (Figure 3.13a), higher MAXHT20, larger size of 40 dBZ and 20 dBZ are found during El Niño periods, which indicates a shift toward deeper, more intense and larger PFs during the warm phase of ENSO relative to the cold phase distribution. Opposite patterns are observed in storm size for both the EMC and WMC (Figure 3.13b and 13c), with larger size of 20 dBZ at low levels (< 6km) being observed during La Niña. Together with the larger population fraction of MCSs during La Niña periods (Figure 3.4), the larger size of MCSs in both the EMC and WMC indicates that the size of the precipitations systems may also play an important role in the anomalous rainfall throughout the regions (Figure 3.13b and 13c). Even with relative small correlation R-values (Figure 3.5, 6), the difference in characteristics of PFs over GM and ARGEN is significant among the different phases of ENSO. The profiles of 20 and 40 dBZ area (Figure 3.13d and 13e) during El Niño and La Niña periods suggest that ENSO has a significant influence on the intensity, heights and size of convection systems over the GM and ARGEN. A larger size of 20 dBZ at low levels is observed over the AUS is consistent with the higher population fraction of large-size precipitation systems during La Niña periods (Figure 3.13f).

Conclusion

Based on 16-years of TRMM observations, distinct differences in the annual mean rainfall between different phases of ENSO are consistent with the well-documented anomalous precipitation over various regions (e.g. Ropelewski and Halpert 1987; Dai and Wigley 2000; Yang and DelSole 2012). This study examines the variations of properties of precipitation systems over different regions that result in the anomalous precipitation under warm and cold ENSO phases. First, two types of precipitation systems are focused. Deep convection is defined as precipitation systems with 20 dBZ echo top greater than 10 km while MCSs are defined with precipitation systems having an area larger than 2000 km^2. The fraction of these two types of precipitation systems during different phases of ENSO, as well as their correlations with the MEI, are examined over regions across the tropics and subtropics. The results reveal that pronounced effects from ENSO on the deep convection and MCSs are found over specific regions, including the central Pacific (CPACI), the western Maritime Continent (WMC), the eastern Maritime Continent (EMC), Gulf of Mexico (GM), Argentina (ARGEN), and Australia (AUS).

The seasonal variations of influences from ENSO are further explored. The coefficient of determination is more pronounced in the NH winter half-year in comparison to the summer half-year over CPACI, the Maritime Continent, and AUS. The fraction of deep convection is found strongly correlated ($R^2 > 0.6$) to the MEI in October-December, and January over CPACI, while it is true in January-March over EMC. The effect of ENSO on deep convection and MCSs over GM and ARGEN is less pronounced in coefficient of determination ($R^2 < 0.2$), compared to other selected regions.

The shift of the spectra of PFs in both number and rainfall contribution during different phases of ENSO, as a function of MIN85PCT, MAXHT20, and area, suggests that precipitation anomaly over these regions are related to the number of precipitation events, as well as the fraction of deep, intense and large precipitation systems. In other words, ENSO not only could affect the number of precipitation events but also could shift the spectrum of precipitation systems of various properties. Therefore, an increase of rainfall during the El Niño periods over CPACI, GM, ARGEN is a result of more precipitation events and a higher fraction of intense, deep, large precipitation systems. The opposite is true for AUS. The Maritime Continent is a unique region because of the effect of both the IOD and ENSO. A higher contribution from small-size precipitation systems (< 1000 km^2) is found in both eastern and western portion of the Maritime Continent during El Niño conditions than that during La Niña conditions. However, in terms of both the number and volumetric rainfall contribution, a higher fraction of deep convection (>12 km) over WMC is found during El Niño conditions, while a higher fraction of deep convection over EMC is found during La Niña conditions.

Though ENSO episodes vary with institution and methods employed to define an episode, the 3-years of data used to investigate the effectiveness of ENSO over selected regions, constituted by the three strongest ENSO months for each month during 1998-2013, lead to similar categorization as that based on other ENSO indices, such as Niño 3.4. Nevertheless, this study suggests the importance of ENSO variability on the relatively small number of intense, deep, and large precipitation systems (approximately 1.5-9%) in certain regions of the globe. Although these systems are small in number, they contribute the majority of rainfall in these regions. When

excluding the vast majority of PFs that are small and shallow, clear regional shifts towards deeper, larger, and more intense systems can be observed during different phases of ENSO. The shifts are associated with changes in the strength and location of the Walker circulation, as a result of changes in the wind stress and sea surface temperature (e.g. Rasmusson and Carpenter 1982; Lindzen and Nigam 1987; Trenberth et al. 1998). In addition, a stronger westerly at 200 hPa level is found during the warm phase of ENSO over GM (Arkin, 1982), coincidence with a tendency for more frequent storms and precipitation over this region (Ropelewski and Halpert 1988). Hill et al. (2009) found the highest rainfall occurred during the El Niño periods in South America due to the strengthening of the South American Low-Level Jet, based on an Atmospheric General Circulation Model. Therefore, ENSO plays a vital role in the precipitation anomaly by modulating the size and intensity of precipitation systems. The difference in rain occurrence, volumetric rainfall contribution from PFs of various intensity, depth and size during the warm and cold phases of ENSO may help provide a better insight into precipitation anomaly trends in the future.

Acknowledgements

The authors thank three anonymous reviewers for their valuable comments and suggestions to help improve this manuscript significantly. This research was supported by NASA Precipitation Measurement Mission grants NNX16AD76G under the direction of Dr. Gail Jackson and NNX16AH74G under the direction of Dr. Erich Stocker. Thanks to the Precipitation Processing System (PPS) team at NASA Goddard Space Flight Center, Greenbelt, MD, for data processing assistance.

References

Andrews, E.D., R.C. Antweiler, P.J. Neiman, and F.M. Ralph, 2004: Influence of ENSO on Flood Frequency along the California Coast. *J. Climate,* **17**, 337–348.

Arkin, P.A., 1982: The Relationship Between Interannual Variability in the 200 mb Tropical Wind Field and the Southern Oscillation. *Mon. Wea. Rev.,* **110**, 1393–1404.

Ashok, K., Z. Guan, and T. Yamagata, 2003: Influence of the Indian Ocean Dipole on the Australian winter rainfall, *Geophys. Res. Lett.*, **30**, 1821.

Cayan, D. R., K. T. Redmond, and L. G. Riddle, 1999: ENSO and hydrologic extremes in the western United States. *J. Clim.*, **12**, 2881–2893, doi:10.1175/1520-0442.

Cecil, D. J., and E. J. Zipser, 1999: Relationships between Tropical Cyclone Intensity and Satellite-Based Indicators of Inner Core Convection: 85-GHz Ice-Scattering Signature and Lightning. *Mon. Weather Rev.*, **127**, 103–123, doi:10.1175/1520-0493.

Dai, A., and T. M. L. Wigley, 2000: Global patterns of ENSO induced precipitation. *Geophys. Res. Lett.*, **27,** 1283–1286.

Gershunov, A., 1998: ENSO influence on intraseasonal extreme rainfall and temperature frequencies in the contiguous United States: Implications for long-range predictability. *J. Clim.*, **11**, 3192–3203, doi:10.1175/1520-0442.

Jong, B.-T., M. Ting, and R. Seager, 2016: El Niño impact on California precipitation: Seasonality, regionality, and El Niño intensity. *Environ. Res. Lett.*, **11**, 054021, doi:https://doi.org/10.1088/1748-9326/11/5/054021.

Julian, P.R. and R.M. Chervin, 1978: A Study of the Southern Oscillation and Walker Circulation Phenomenon. *Mon. Wea. Rev.,* **106**, 1433–1451, https://doi.org/10.1175/1520-0493.

Hamid, E. Y., Z.-I. Kawasaki, and R. Mardiana, 2001: Impact of the 1997 – 98 El Nin˜o event on lightning activity over Indonesia, *Geophys. Res. Lett*., **28(1),** 147 – 150, doi:10.1029/2000GL011374.

Hill, K. J., A. S. Taschetto, and M. H. England, 2011: Sensitivity of South American summer rainfall to tropical Pacific Ocean SST anomalies. *Geophys. Res. Lett.*, **38**, L01701.

Hou, A. Y., R. K. Kakar, S. Neeck, A. A. Azarbarzin, C. D. Kummerow, M. Kojima, R. Oki, K. Nakamura, and T. Iguchi, 2014: The Global Precipitation Measurement mission, *Bull. Am. Meteorol. Soc.,* **95**, 701–722.

Iguchi, T., T. Kozu, R. Meneghini, J. Awaka, and K. Okamoto, 2000: Rain-profiling algorithm for the TRMM precipitation radar. *J. Appl. Meteor.*, **39**, 2038-2052.

Iguchi, T., T. Kozu, J. Kwiatkowski, R. Meneghini, J. Awaka, and K. Okamoto, 2009: Uncertainties in the rain profiling algorithm for the TRMM precipitation radar. *J. Meteor. Soc. Japan*, **87**,1 1-30.

Kiem, A. S., and S. W. Franks, 2004: Multidecadal variability of drought risk, eastern Australia. *Hydrol. Processes*, **18,** 2039–2050.

Kiem, A. S., and S. W. Franks, 2001: On the identification of ENSO-induced rainfall and runoff variability: A comparison of methods and indices, *Hydrol. Sci. J.*, **46**, 715–727.

Kiladis, G. N., and H. F. Diaz, 1989: Global climate anomalies associated with extremes in the Southern Oscillation. *J. Climate*, **2**, 1069–1090.

Kummerow, C., W. Barnes, T. Kozu, J. Shiue, and J. Simpson, 1998: The Tropical Rainfall Measuring Mission (TRMM) sensor package. *J. Atmos. Ocean. Technol.*, **15**, 809–817, doi:10.1175/1520-0426.

Laing, A. G. and J. G. Fritsch. 1997. The global population of mesoscale convective complexes. *Quart. J. Roy. Meteor. Soc*. **123**, 389–405.

Leigh, R., and I. Kuhnel, 2001: Hailstorm loss modelling and risk assessment in the Sydney Region, Australia. *Nat. Hazards*, **24**, 171–185, doi:10.1023/A:1011855801345.

Lindzen, R.S. and S. Nigam, 1987: On the Role of Sea Surface Temperature Gradients in Forcing Low-Level Winds and Convergence in the Tropics. *J. Atmos. Sci.,* **44**,2418–2436.

Liu, C., and E. J. Zipser, 2005: Global distribution of convection penetrating the tropical tropopause. *J. Geophys. Res. Atmos.*, **110**, 1–12, doi:10.1029/2005JD006063.

Liu, C., and E. J. Zipser, D. J. Cecil, S. W. Nesbitt, and S. Sherwood, 2008: A cloud and precipitation feature database from nine years of TRMM observations. *J. Appl. Meteorol. Climatol.*, **47**, 2712–2728, doi:10.1175/2008JAMC1890.1.

Liu, C., E.J. Zipser, and S.W. Nesbitt, 2007: Global Distribution of Tropical Deep Convection: Different Perspectives from TRMM Infrared and Radar Data. *J. Climate,* **20**,489–503,

Liu, N., and C. Liu, 2016: Global distribution of deep convection reaching tropopause in 1 year GPM observations. *J. Geophys. Res.*, **121**, 3824–3842, doi:10.1002/2015JD024430.

Liu, N. and C. Liu, 2018: Synoptic Environments and Characteristics of Convection Reaching the Tropopause over Northeast China. *Mon. Wea. Rev.,* **146**, 745–759.

Lyon, B. and A.G. Barnston, 2005: ENSO and the Spatial Extent of Interannual Precipitation Extremes in Tropical Land Areas. *J. Climate,* **18**, 5095–5109.

Mapes, B. E., and R. A. Houze, 1993: Cloud Clusters and Superclusters over the Oceanic Warm Pool. *Mon. Weather Rev.*, **121**, 1398–1416, doi:10.1175/1520-0493.

McBride, J. L., and N. Nicholls, 1983: Seasonal relationships between Australian rainfall and the Southern Oscillation. *Mon. Wea. Rev.,***111,** 1998–2004.

Meyers, G., P. McIntosh, L. Pigot, and M. Pook, 2007: The Years of El Niño, La Niña, and Interactions with the Tropical Indian Ocean. *J. Climate,* **20**, 2872–2880.

Mohr, K.I. and E.J. Zipser, 1996: Mesoscale Convective Systems Defined by Their 85-GHz Ice Scattering Signature: Size and Intensity Comparison over Tropical Oceans and Continents. *Mon. Wea. Rev.,* **124**, 2417–2437.

Mohr, K. I., J. S. Famiglietti, and E. J. Zipser, 1999: The Contribution to Tropical Rainfall with respect to Convective System Type, Size, and Intensity Estimated from the 85-GHz Ice-Scattering Signature. *J. Appl. Meteorol.*, **38**, 596–606, doi:10.1175/1520-0450.

Mohr, K. I., J. Molinari, and C. D. Thorncroft, 2009: The interannual stability of cumulative frequency distributions for convective system size and intensity. *J. Clim.*, **22**, 5218–5231, doi:10.1175/2009JCLI2940.1.

Nesbitt, S. W., and E. J. Zipser, 2000: A census of precipitation features in the tropics using TRMM: Radar, ice scattering, and lightning observations. *J. Clim.*, **13**, 4087–4106, doi:10.1175/1520-0442.

Nesbitt, S. W., and E. J. Zipser, 2003: The diurnal cycle of rainfall and convective intensity according to three years of TRMM measurements. *J. Clim.*, **16**, 1456–1475, doi:10.1175/1520-0442-16.10.1456.

Nesbitt, S. W., R. Cifelli, and S. A. Rutledge, 2006: Storm morphology and rainfall characteristics of TRMM precipitation features. *Mon. Wea. Rev.,* **134,** 2702–2721.

Power, S. B., F. Tseitkin, S. Torok, B. Lavery, R. Dahni, and B. McAvaney, 1998: Australian temperature, Australian rainfall and the Southern Oscillation, 1910–1992: Coherent variability and recent changes. *Aust. Meteor. Mag.*, **47,** 85–101.

Rasmusson, E. M., and T. H. Carpenter, 1982: Variations in Tropical Sea Surface Temperature

and Surface Wind Fields Associated with the Southern Oscillation/El Niño. *Mon. Weather Rev.*, **110**, 354–384, doi:10.1175/1520-0493.

Rasmusson, E. M., and T. H. Carpenter, 1983: The relationship between the eastern equatorial Pacific sea surface temperatures and rainfall over India and Sri Lanka. *Mon. Wea. Rev.*, **111**, 517–528.

Romatschke, U. and R.A. Houze, 2010: Extreme Summer Convection in South America. *J. Climate,* **23**, 3761–3791.

Ropelewski, C.F. and M.S. Halpert, 1986: North American Precipitation and Temperature Patterns Associated with the El Niño/Southern Oscillation (ENSO). *Mon. Wea. Rev.,* **114**, 2352–2362.

Ropelewski, C. F., and M. H. Halpert, 1987: Global and regional scale precipitation patterns associated with the El Niño– Southern Oscillation. *Mon. Wea. Rev.,* **115**, 1606–1626.

Saji, H. N., and B. N. Goswami, P. N. Vinayachandran, and T. Yamagata, 1999: A dipole mode in the tropical Indian Ocean. *Nature*, **401**, 360–363.

Salio, P., M. Nicolini, and E.J. Zipser, 2007: Mesoscale Convective Systems over Southeastern South America and Their Relationship with the South American Low-Level Jet. *Mon. Wea. Rev.,* **135**, 1290–1309.

Shrestha, A., and R. Kostaschuk, 2005: El Niño/Southern Oscillation (ENSO)-related variablity in mean-monthly streamflow in Nepal. *J. Hydrol.*, **308**, 33–49.

Spencer, R. W., H. M. Goodman, and R. E. Hood, 1989: Precipitation Retrieval over Land and Ocean with the SSM/I: Identification and Characteristics of the Scattering Signal. *J. Atmos. Ocean. Technol.*, **6**, 254–273, doi:10.1175/1520-0426.

Trenberth, K. E., G. W. Branstator, D. Karoly, A. Kumar, N-C. Lau,

and C. Ropelewski, 1998: Progress during TOGA in understanding and modeling global teleconnections associated with tropical sea surface temperatures. *J. Geophys. Res.*, **103,** 14291–14324.

Walker, 1925: Correalation in seasoanl variations of weather - a further study of world weather. *Mon. Weather Rev.*, **X**, 252–254, doi:10.1175/1520-0493.

Wang, B., and H. Rui, 1990: Synoptic climatology of transient tropical intraseasonal convection anomalies: 1975–1985. *Meteor. Atmos. Phys*, **44,** 43–61.

Webster, P. J., A. Moore, J. Loschnigg, and M. Leban, 1999: Coupled ocean–atmosphere dynamics in the Indian Ocean during 1997–98. *Nature,* **401**, 356–360.

Williams, E. R., 2005: Lightning and climate: A review. *Atmos. Res.*, **76,** 272–287.

Wolter, K., and M. S. Timlin, 2011: El Niño/Southern Oscillation behaviour since 1871 as diagnosed in an extended multivariate ENSO index (MEI.ext). *Int. J. Climatol.*, **31**, 1074–1087, doi:10.1002/joc.2336.

Xie, S., K. Hu, J. Hafner, H. Tokinaga, Y. Du, G. Huang, and T. Sampe, 2009: Indian Ocean Capacitor Effect on Indo–Western Pacific Climate during the Summer following El Niño. *J. Climate,* **22**, 730–747.

Yamagata, T., S. K. Behera, J.-J. Luo, S. Masson, M. Jury, and S. A. Rao, 2004: Coupled ocean–atmosphere variability in the tropical Indian Ocean. *Earth Climate: The Ocean–Atmosphere Interaction, Geophys. Monogr.*, No. 147, Amer. Geophys. Union, 189– 212.

Yang, X., and T. DelSole, 2012: Systematic comparison of ENSO teleconnection patterns between models and observations. *J. Climate*, **25,** 425–446, doi:10.1175/JCLI-D-11-00175.1.

Yeo, C. S., 2005: Severe thunderstorms in the Brisbane region and a relationship to the El Niño

Southern Oscillation. *Aust. Meteorol. Mag.*, **54**, 197–202.

Yuan, J., and R. A. Houze, 2010: Global variability of mesoscale convective system anvil structure from A-train satellite data. *J. Clim.*, **23**, 5864–5888, doi:10.1175/2010JCLI3671.1.

Zolman, J. L., E. J. Zipser, and K. I. Mohr, 2000: A comparison of tropical mesoscale convective systems in El Nino and La Nina. *J. Clim.*, **13**, 3314–3326, doi:10.1175/1520-0442.

Table 3.1 Average rain and occurrence, fraction and volumetric rain contribution of deep convection and MCSs during El Nino and La Nina over different regions.

	Rain (mm/yr) EL (LA)	Deep (20 dBZ echo top > 10 km)			MCSs (area > 2000 km^2)		
		Occur (%)	Fract (%)	Con (%)	Occur (%)	Fract (%)	Con (%)
CPACI	1663 (389)	2.6 (0.4)	3.5 (1.9)	62.8 (35.4)	3.3 (0.6)	3.6 (2.4)	71.2 (46.7)
EMC	1730 (2576)	2.6 (4.6)	5.8 (7.1)	61.9 (67.1)	3.3 (5.7)	4.5 (5.3)	68.7 (73.2)
WMC	2463 (2615)	4.0 (4.5)	10.6 (9.4)	71.4 (68.2)	4.8 (6.0)	6.9 (7.8)	75.2 (78.9)
GM	1114 (734)	1.4 (1.0)	7.2 (7.6)	65.0 (59.6)	2.0 (1.3)	4.9 (4.7)	78.9 (70.2)
ARGEN	1113 (911)	2.0 (1.4)	10.3 (8.7)	74.6 (65.4)	3.1 (2.6)	9.6 (9.2)	92.7 (90.2)
AUS	712 (1172)	1.0 (1.8)	2.6 (3.9)	54.1 (58.8)	1.5 (2.8)	3.5 (4.6)	71.1 (76.5)

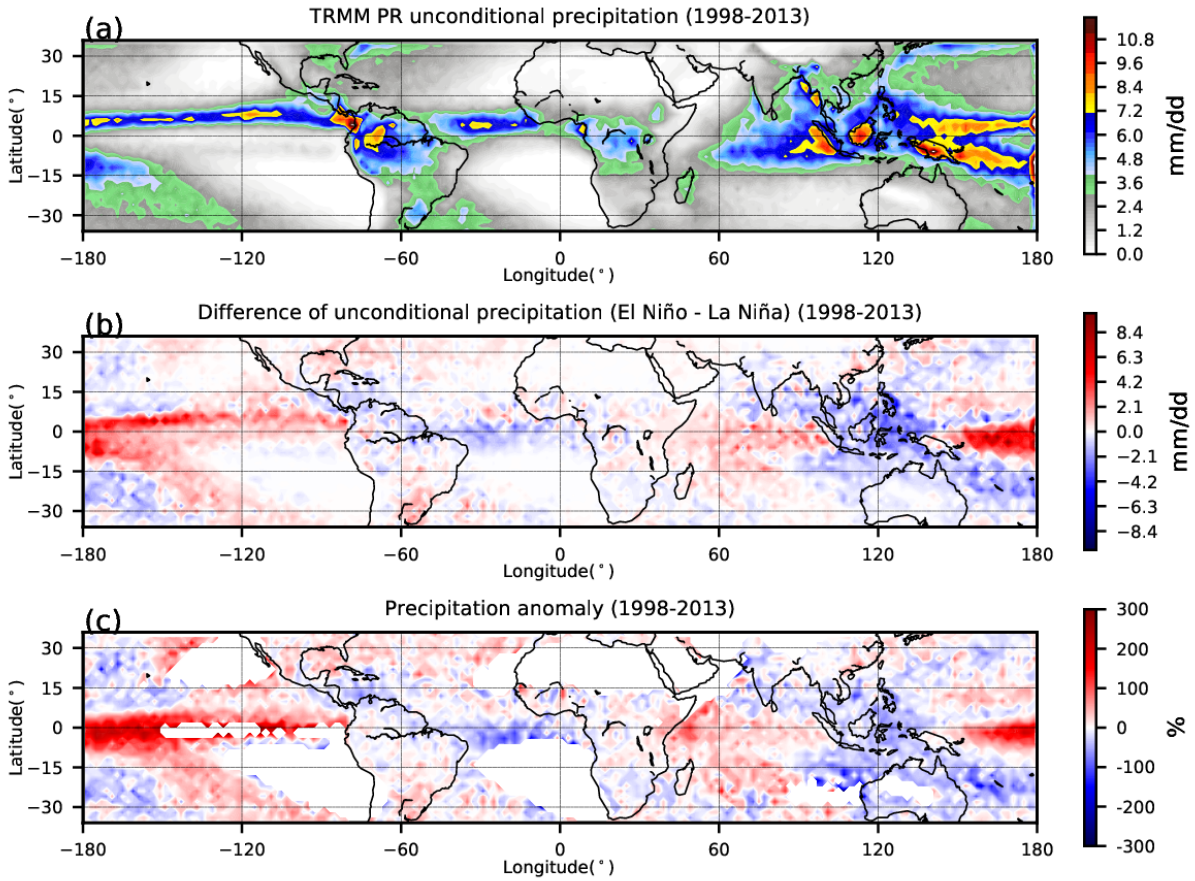

Figure 3.1 Climatology of unconditional precipitation observed by TRMM PR during 1998 and 2013, (a) Unconditional precipitation (mm/dd), (b) Difference of unconditional precipitation between El Nino and La Nina periods, (c) Normalized difference between El Nino and La Nina (b divide by a), left box with unconditional precipitation less than 0.5 mm/dd as blank. The unconditional precipitation is calculated using TRMM 2A25 near surface precipitation product. The monthly Multivariate El Niño-Southern Oscillation (ENSO) Indices (MEI, Figure 3.2) have been used to separate the El Nino and La Nina conditions (see details in section 2.2).

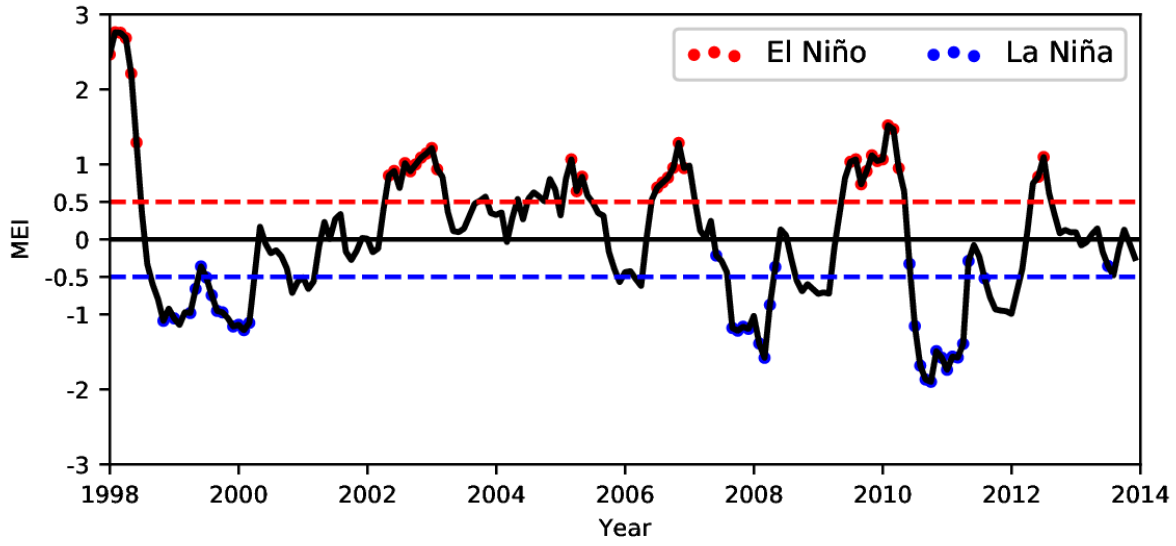

Figure 3.2 Time series of MEI during 1998-2013, red dots present El Nino months, blue dots present La Nina months. Dashed lines present 0.5 and -0.5 MEI.

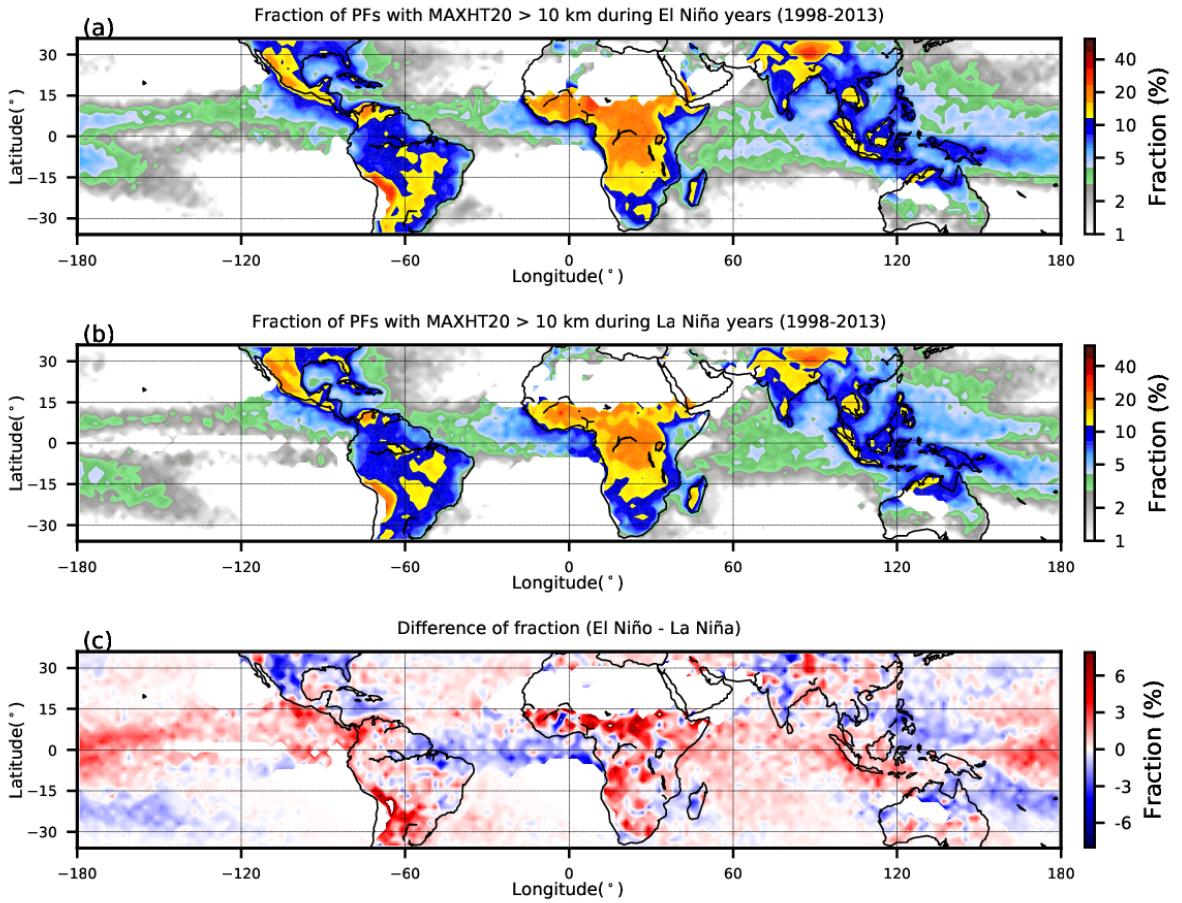

Figure 3.3 Fraction of PFs with MAXHT20 > 10 km during 1998 and 2013 in 2^{o} x 2^{o} grids. (a) During El Nino periods, (b) During La Nina periods, (c) Difference between El Nino and La Nina.

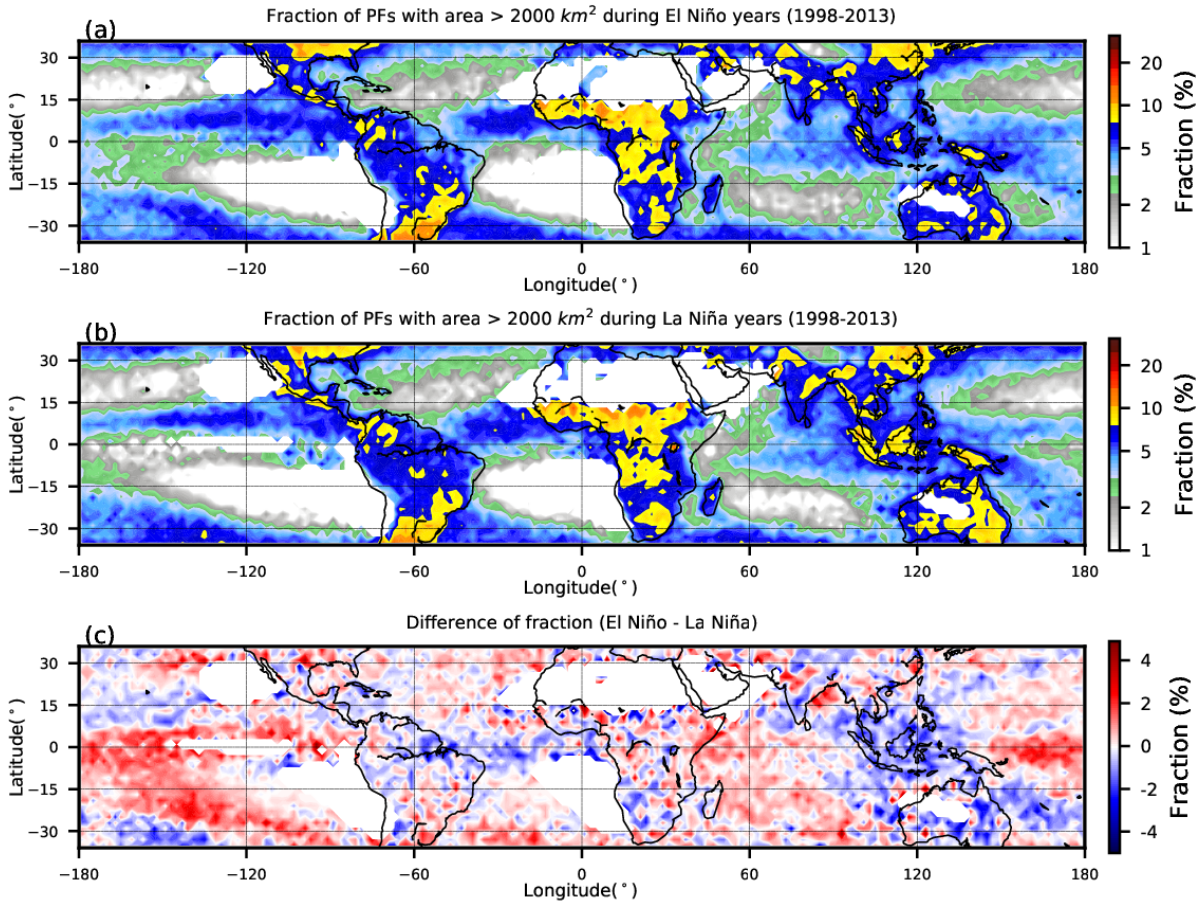

Figure 3.4 Same as Figure 3.3, but for PFs with area > 2000 km^2.

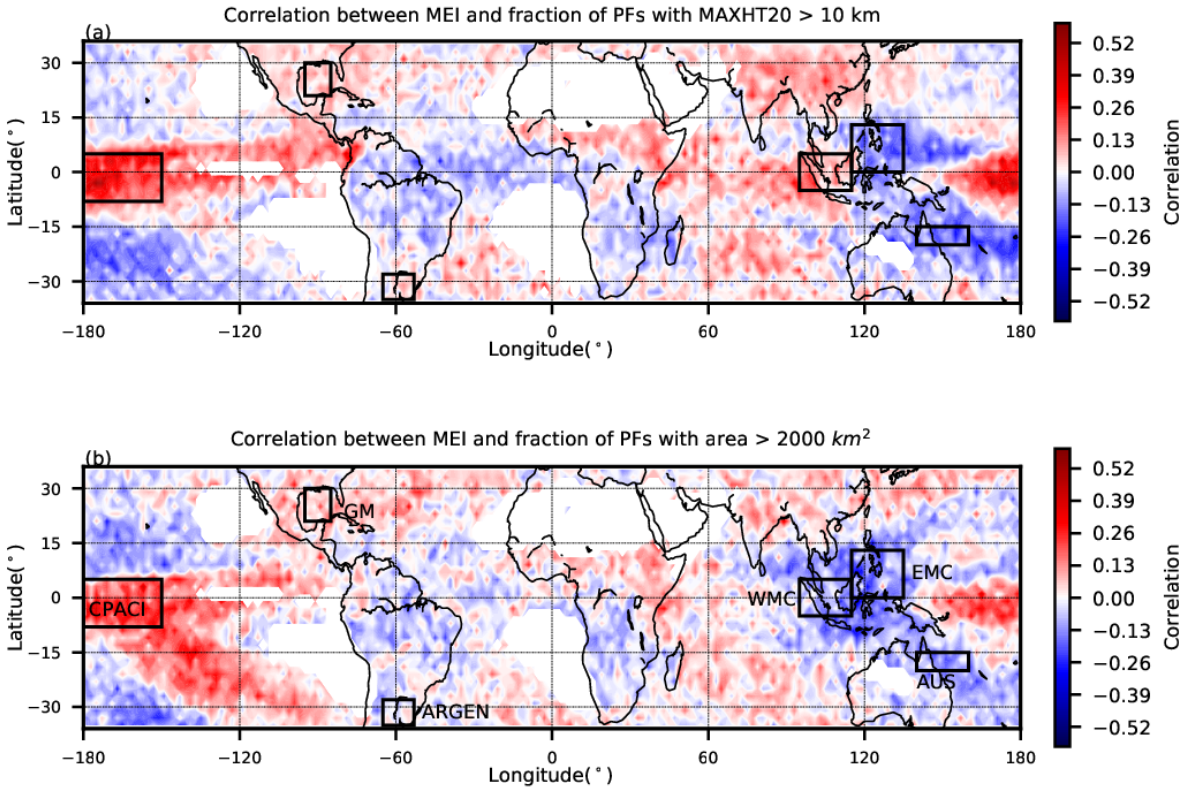

Figure 3.5 (a) Monthly correlation between the MEI and the fraction of PFs with MAXHT20 > 10 km in 2^o x 2^o grids, (b) Monthly correlation between the MEI and the fraction of PFs with area > 2000 km^2. Left boxes with samples < 1000 as blank.

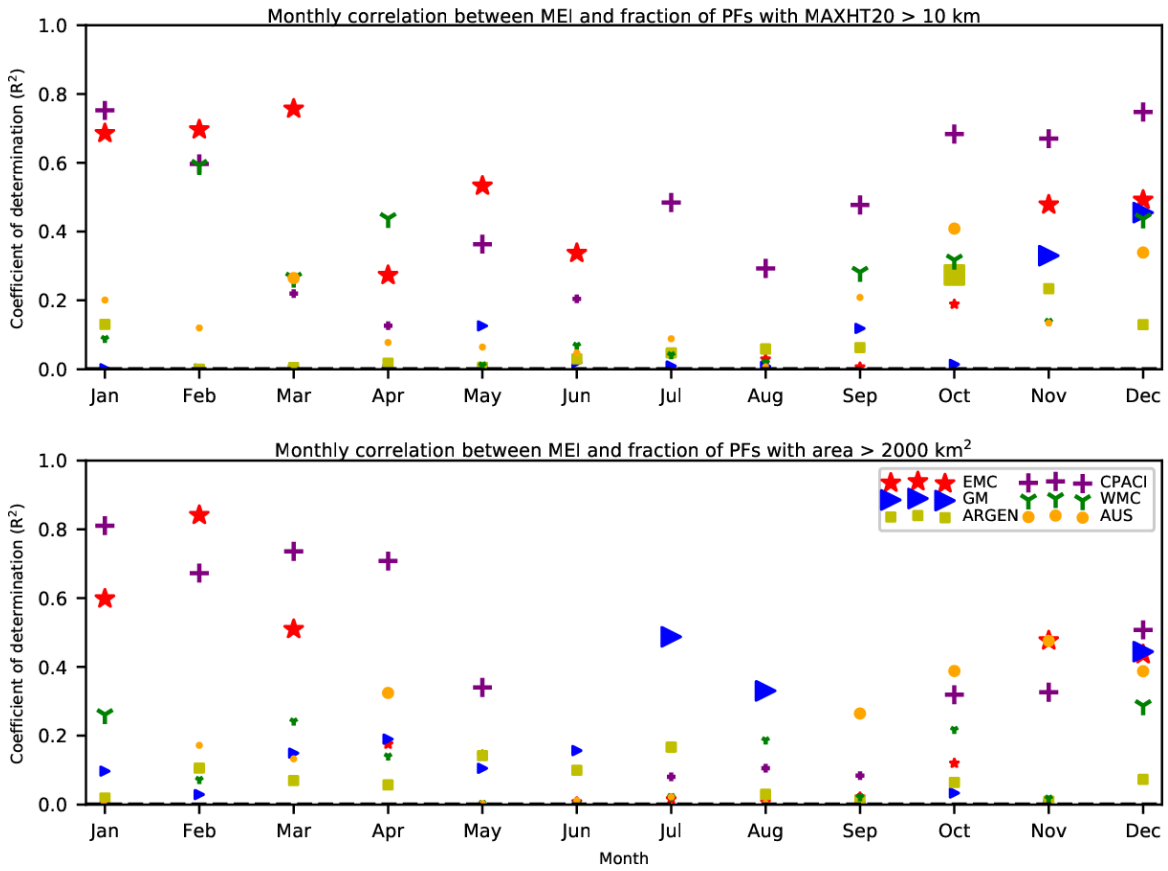

Figure 3.6 Monthly correlation between the MEI and the fraction of deep convection and MCSs over selected regions. Fraction of deep convection and MCSs are significantly correlated with the MEI with a p-value less than 0.05. The significant correlation coefficients are marked as larger size than nonsignificant ones.

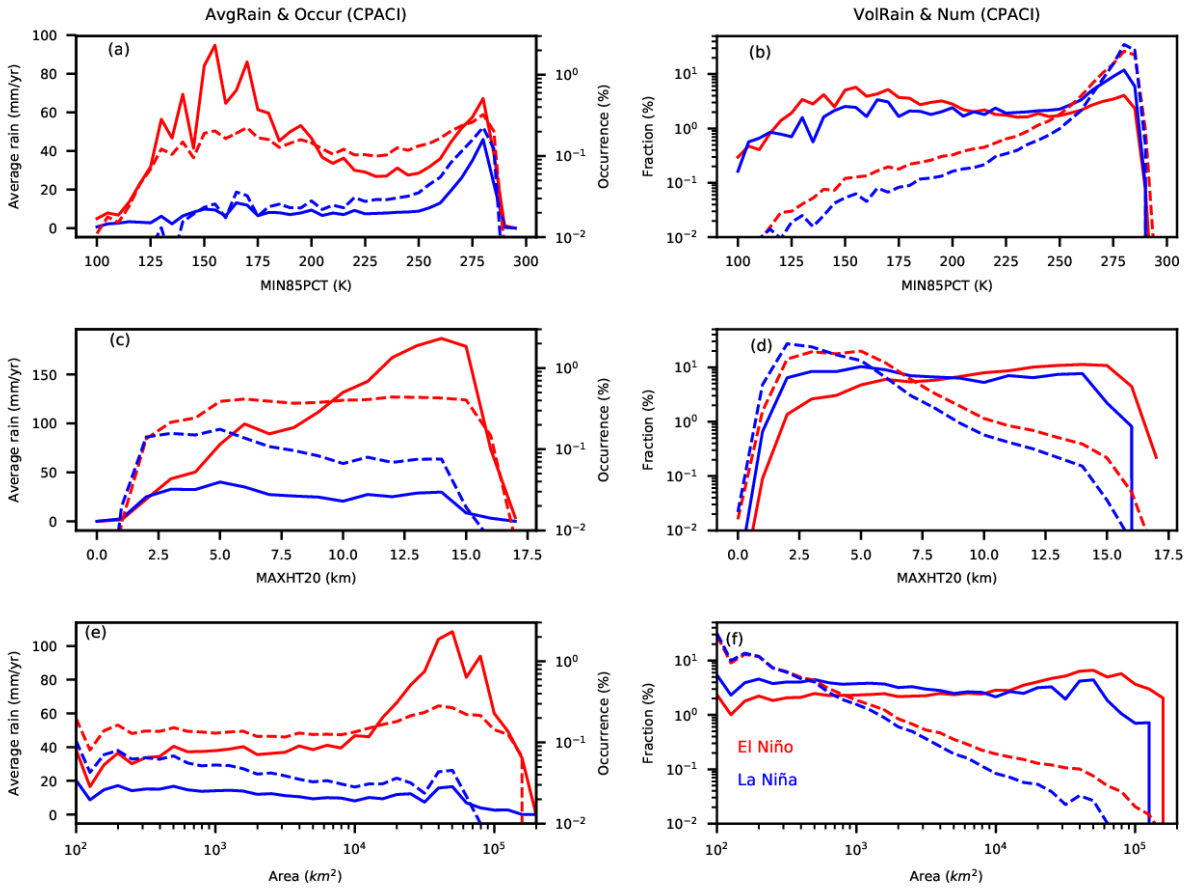

Figure 3.7 Comparison of various of rainfall-related parameters as a function of the maximum 85-GHz PCT (MIN85PCT), the maximum heights of 20-dBZ echo tops (MAXHT20) and size of PFs over different phases of ENSO over central Pacific (CPACI). (a) Annual mean rainfall (solid) and occurrence (dashed) as a function of MIN85PCT, (b) the number (dashed) and volumetric rainfall contribution (solid) to the total PFs as a function of MIN85PCT, (c) same as (a) but as a function of MAXHT20, (d) same as (b) but as a function of MAXHT20, (e) same as (a) but as a function of convective size, (f) same as (b) but as a function of size.

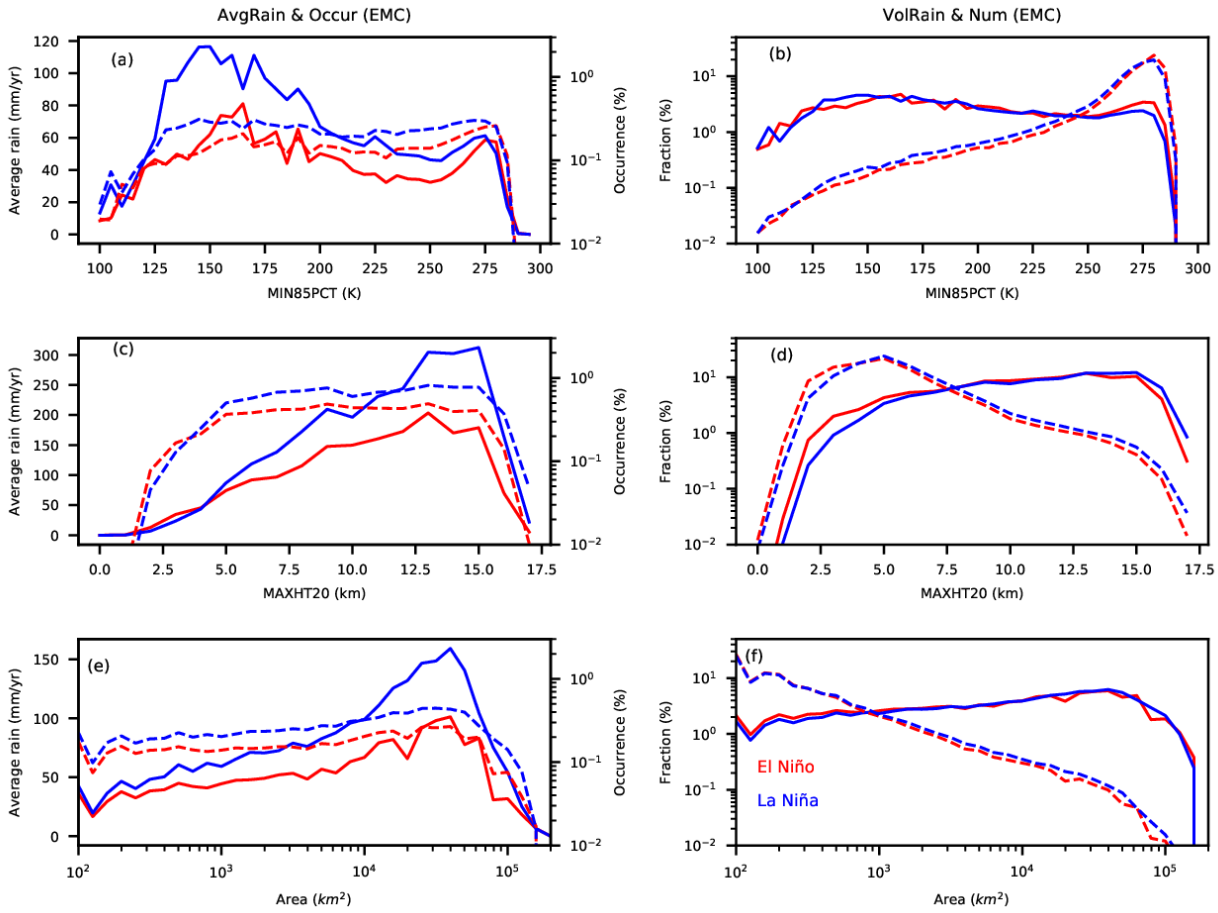

Figure 3.8 Same as Figure 3.7, but for Eastern Maritime Continent (EMC).

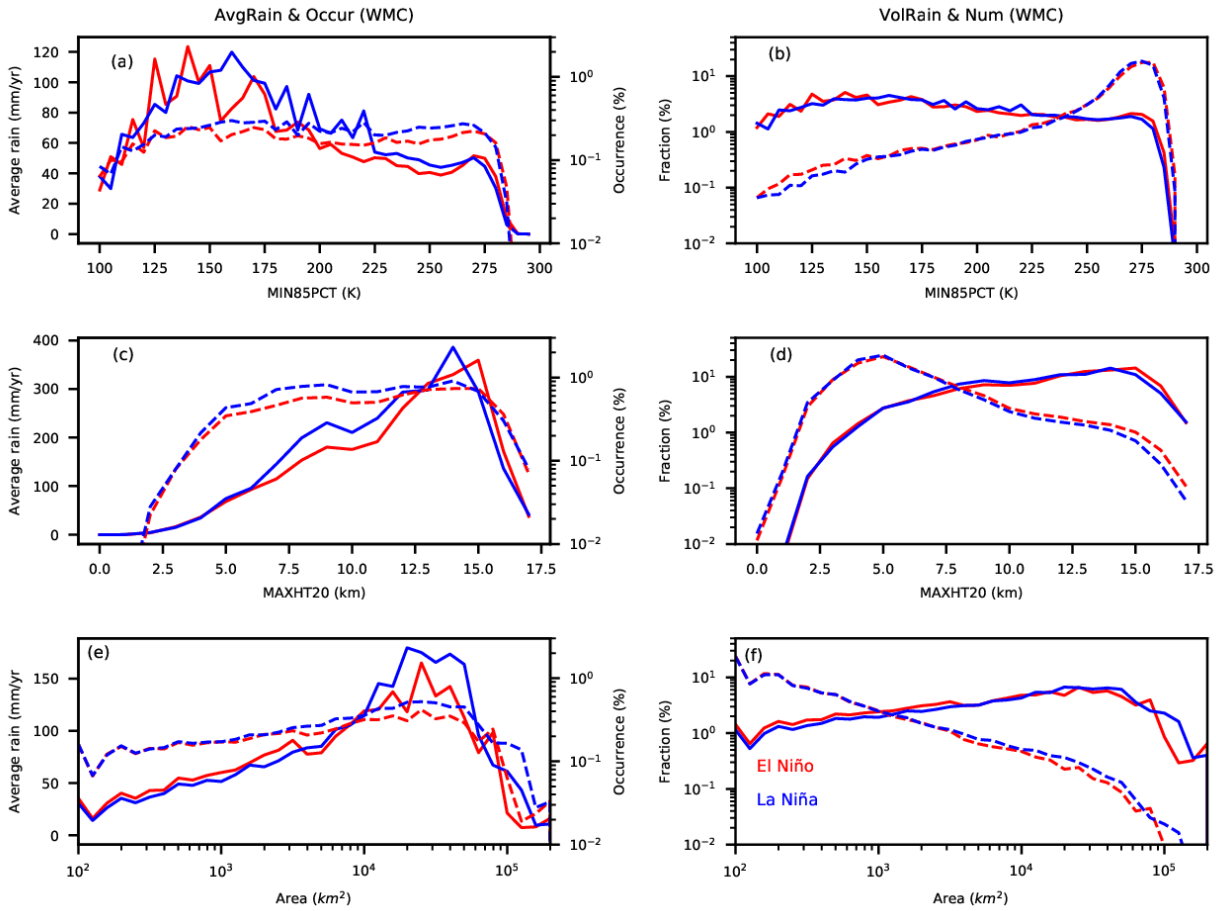

Figure 3.9 Same as Figure 3.7, but for Western Maritime Continent (WMC).

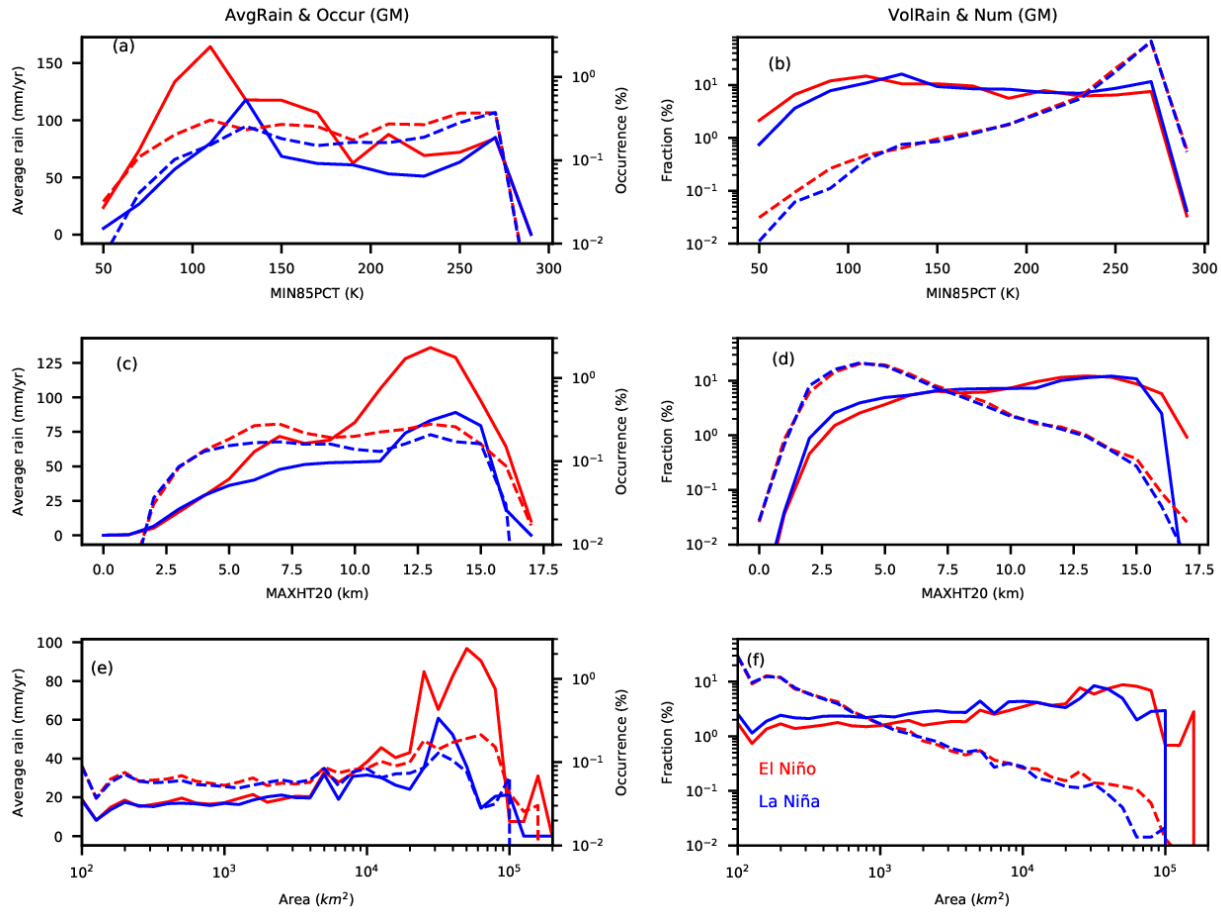

Figure 3.10 Same as Figure 3.7, but for the Gulf of Mexico (GM).

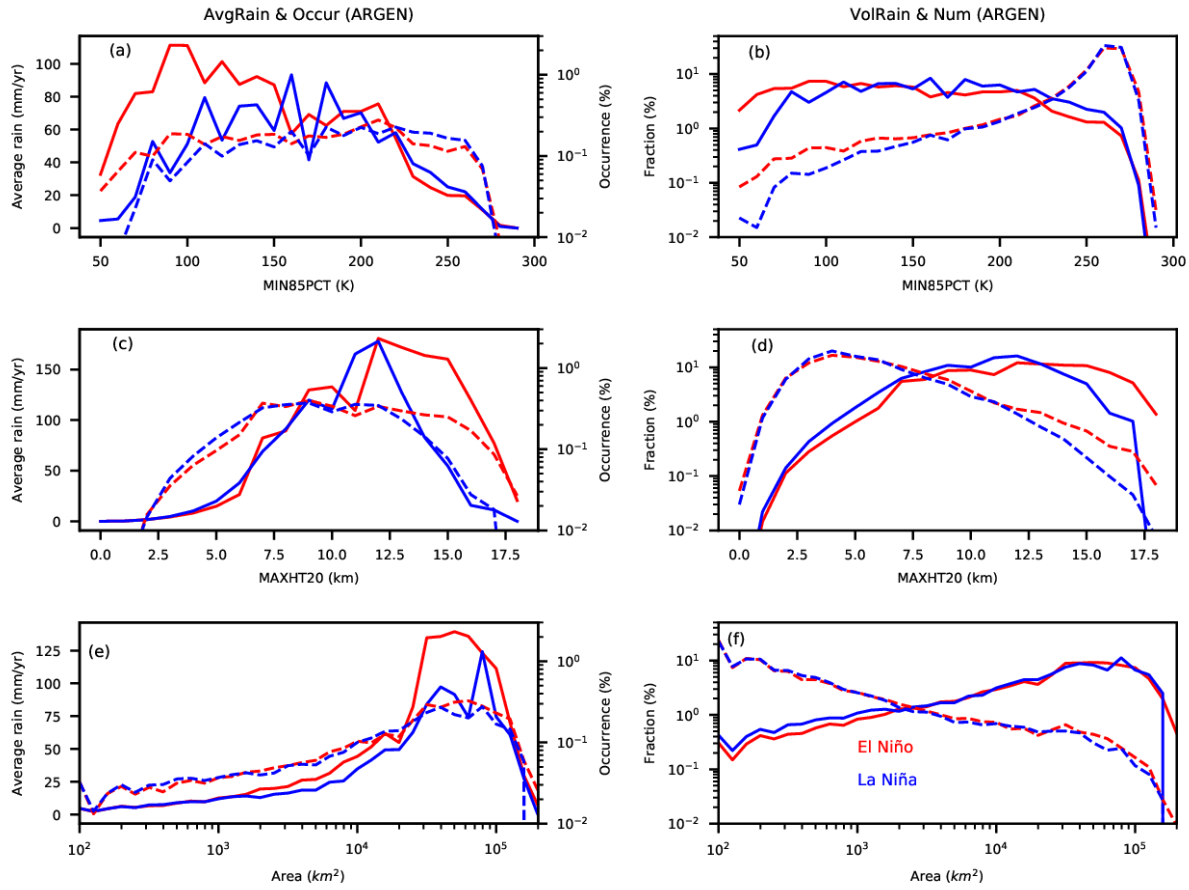

Figure 3.11 Same as Figure 3.7, but for Argentina (ARGEN).

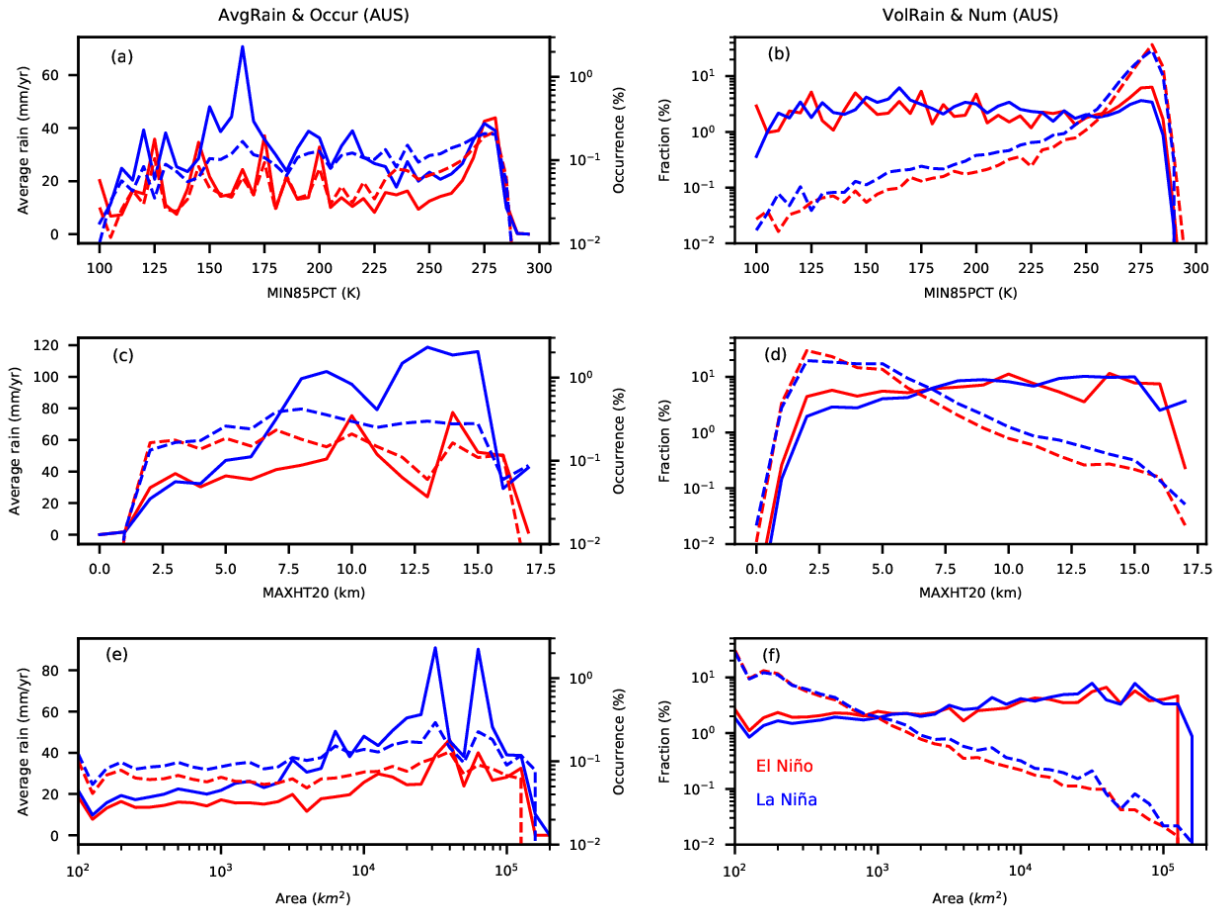

Figure 3.12 Same as Figure 3.7, but for Australia (AUS).

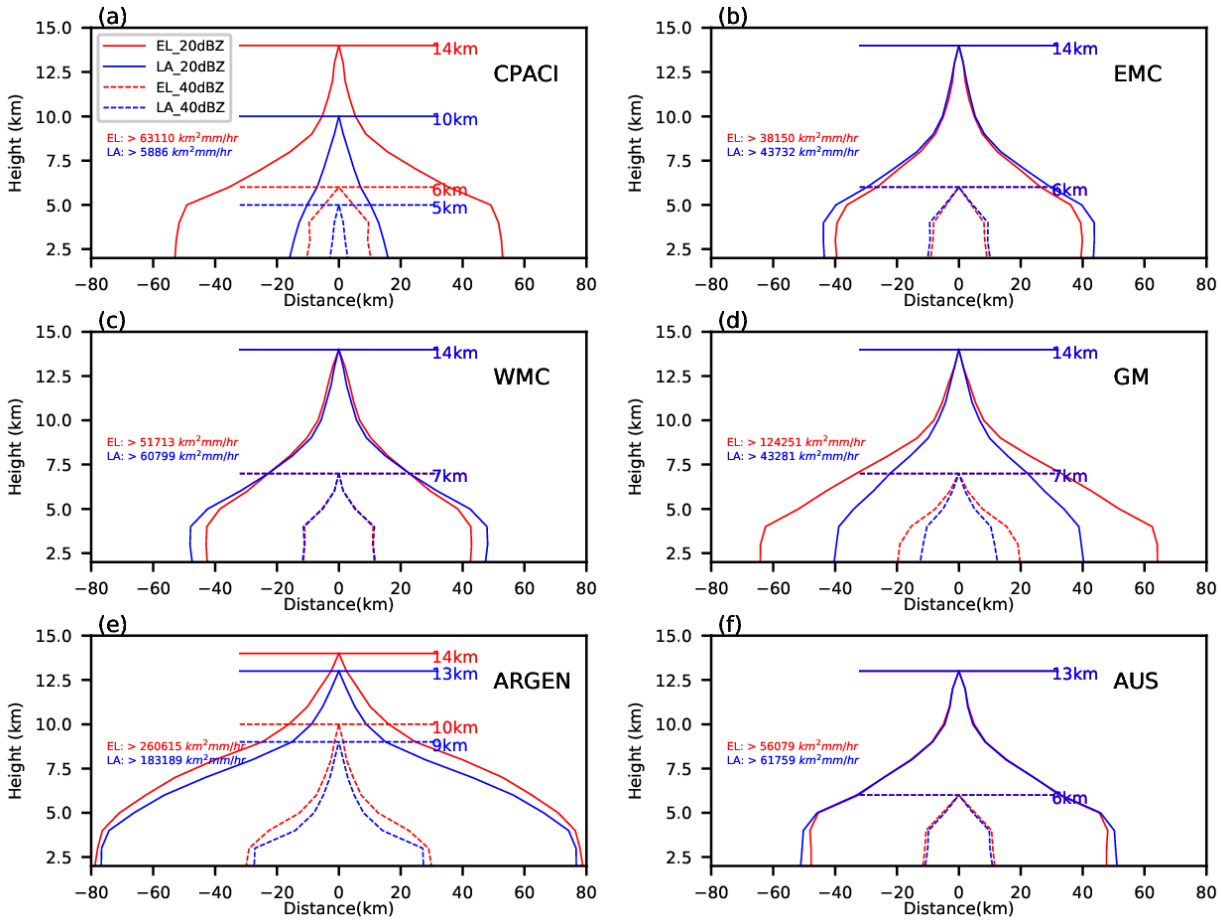

Figure 3.13 Median length scale of PFs during El Niño (red) and La Niña (blue) periods over selected regions. PFs from the top 50% volumetric rainfall contribution to the total rainfall based on 3-year compiled dataset are used to create this figure. (a) CPACI, (b) EMC, (c) WMC, (d) (GM), (e) ARGEN, (f) AUS The length scale is defined as $L = \pm(A/\pi)^{0.5}$, where A is area of 20, 40 dBZ at different altitudes within each PF. It represents the radius of OPFs at each altitudes assuming the symmetric conical shape of region with 20,40 dBZ. The solid lines mark the average maximum heights of 20 dBZ; the dashed lines point to the average maximum heights of 40 dBZ.

SUMMARY

Thunderstorms, especially intense ones, have been documented to be tendency of land-dominant phenomena, with a strong preference over specific regions. However, the rarity of these events has limited the understanding of their mechanisms. The launch of the TRMM satellites has allowed an unprecedented mapping of intense thunderstorms across the tropics and subtopics. This dissertation has investigated why these events prefer certain regions. This is accomplished by examining the favorable thermodynamic environments for intense thunderstorms globally as well as regionally, using 16-years TRMM observations and ERA-Interim reanalysis data. Then, the common thermodynamic features of the large-scale environments favoring intense thunderstorms are summarized to describe the thunderstorm convective intensity using two statistical models. The dissertation has also investigated the response of the properties of intense thunderstorms to the ENSO events.

The investigation of thunderstorm environments reveals that the environments for intense convection share a few common thermodynamic features. First, the common ingredients for intense convection found by previous studies (McNulty, 1978; Johns and Doswell, 1992; Doswell et al., 1996), including abundant low-level moisture and convective instability, and the ascent of parcels to their level of free convection by some lifting mechanism, are confirmed in the characteristic synoptic-scale patterns over all selected regions. Second, major mountains play an important role over selected regions by initiation of convection with orographic lifting, and providing a source of warm dry air advection to build a stable inversion layer on top of low-level moist air to accumulate moist convective energy. Intense thunderstorms over almost all the selected regions are found to be associated with strong wind shear between the low and mid-

troposphere. Those common features can be simply summarized in several thermodynamic parameters. In other words, large CAPE (> 1000 J/kg), moderate CIN (50-100 J/kg), and low-level wind shear are conducive for intense thunderstorms over these regions.

Aside from these common features, each region has its unique characteristics. The upward forcing can be realized in a different way over different regions, such as synoptic ascent ahead of trough waves over SAHEL, orography lifting over HIMA and ARGEN, low-level convergence associated with drylines over SCUS, and sea breezes over COLOM and NWM. Larger CAPE value is not always conducive for the formation and development of intense thunderstorms. For example, a higher fraction of intense thunderstorms over HIMA in spring and fall than that in summer is associated with a relatively smaller CAPE value but larger CIN in these seasons. These similarities and differences among these favorable environments add to our understanding of the formation mechanisms of intense thunderstorms over different regions.

Then, two different statistical models are built to reconstruct the global distribution of thunderstorms based on the differences and similarities of these thermodynamic features. The first model uses a Bayesian type approach and creates the probability functions of intense thunderstorms from TRMM observations and their environments from ERA-Interim reanalysis data. Four variables, including CAPE, CIN, low-level shear, and WCD, are capable of deriving a geographical distribution of intense thunderstorms that is close to the observations. The second approach utilizes a random forest model to test the relative importance of these four variables globally, as well as regionally. The strong land-ocean contrast of frequency of thunderstorms and some hotspot regions can be closely reproduced with a model only based on the four variables

from the reanalysis data. This provides valuable indications that the land-ocean contrast in convective intensity can be largely interpreted by the fundamental differences between the thermodynamic conditions over land and ocean. The investigation of the relative importance of the four environmental variables over different regions suggest that CAPE plays an important role in the occurrence of thunderstorms over Amazon, central Africa and the Maritime Continents, as well as the coastal regions, while CIN is found to be relatively more important near the major mountain regions. The random forest relative importance of these variables over different regions also provide a unique foundation toward building a parameterization of convective intensity at the subgrid scale for general circulation models.

As one of the products of intense thunderstorms, heavy precipitations also have a significant influence on life and property. Therefore, this dissertation also examines the variations of properties of precipitation systems over different regions under different ENSO phases. The results reveal that pronounced effects from ENSO on the deep convection and MCSs are found over specific regions, including the central Pacific, the western Maritime Continent, the eastern Maritime Continent, Gulf of Mexico, Argentina, and Australian. The seasonal variations of influences from ENSO suggest that the coefficients of determination are more pronounced in the Northern Hemisphere winter half-year in comparison to the summer half-year over central Pacific, the Maritime Continent, and Australia. The shift of the spectra of precipitation systems in both number and rainfall contribution during different phases of ENSO, as a function of the minimum 85 GHz PCT, the maximum heights of 20 dBz radar echo, and area, suggests that precipitation anomaly over these regions are related to the number of precipitation events, as well as the fraction of deep, intense and large precipitation systems. The relationships between

rain occurrence, volumetric rainfall contribution from precipitation systems of various intensity, depth and size and the warm and cold phases of ENSO may help provide a better estimate of precipitation in strong ENSO events.

FUTURE WORK

In this dissertation, only a few favorable environmental conditions for intense thunderstorms are explored. Many other factors, such as aerosols and atmospheric waves, that could also play a role in the processes associated with these events. All these factors mentioned above, as well as the higher resolution of reanalysis data and observations can be used to further investigation their role in the development of intense thunderstorms. The statistical models built for the events identified in this dissertation involve storm electrification (Lightning flash). Different models are still needed to describe other characteristics of systems (e.g. radar echo strength, size, etc.). These statistical models can be adapted to predict the interannual variations of general characteristics of precipitation systems, such as during different phases of ENSO. The ultimate goal of this work is toward building tools to diagnose the behavior of the intense convective storms using the simulations of climate models. This will be an efficient way to understand how severe weather would vary under the changing climate.

REFERENCES

Albrecht, R. I., S. J. Goodman, D. E. Buechler, R. J. Blakeslee, and H. J. Christian, 2016: Where are the lightning hotspots on Earth? *Bull. Amer. Meteor. Soc.*, **97**, 2051–2068, doi:https://doi.org/10.1175/BAMS-D-14-00193.1

Albrecht, R. I., S. J. Goodman, W. A. Petersen, D. E. Buechler, E. C. Bruning, R. J. Blakeslee, and H. J.Christian, 2011: The 13 years of TRMM Lightning Imaging Sensor: From individual flash characteristics to decadal tendencies. *Proc. 14th Int. Conf. on Atmospheric Electricity,* Rio de Janeiro, Brazil, International Commission of Atmospheric Electricity, M11-0203.

Alcala, C. M., and A. E. Dessler 2002: Observations of deep convection in the tropics using the tropical rainfall measuring (TRMM) precipitation radar, *J. Geophys. Res.*, **107(D24),** 4792, doi:10.1029/2002JD002457.

Alfaro, D.A., 2017: Low-tropospheric shear in the structure of squall lines: impacts on latent heating under layer-lifting ascent. *J. Atmos. Sci.* **74,** 229–248.

Allen, J. T., M. K. Tippett, and A. H. Sobel, 2015: An empirical model relating U.S. monthly hail occurrence to large-scale meteorological environment, *J. Adv. Model. Earth Syst.*, **7**, 226–243, doi:10.1002/2014MS000397.

Altinger de Schwarzkopf, M. L., and L. C. Rosso, 1982: Severe storms and tornadoes in Argentina.Preprints, *12th Conf. on Severe Local Storms,* San Antonio, TX, Amer. Meteor. Soc., 59–62.

Amador, J. A., 1998: A climatic feature of the tropical Americas: The trade wind easterly jet. *Trop. Meteor. Oceanogr.*, **5**:91–102.

Amador, J. A., and V. Magaña, 1999: Dynamics of the low level jet over the Caribbean Sea.

Preprints, *Third Conf. on Hurricanes and Tropical Meteorology,* Dallas, TX, Amer. Meteor. Soc., 868–869.

Anderson, B. T., and J. O. Roads, 2001: Summertime moisture divergence over the southwestern US and northwestern Mexico, *Geophys. Res. Lett.,* **28**, 1973–1976, doi:10.1029/2001GL012903.

Anquetin, S., and Coauthors, 2005: The 8 and 9 September 2002 flash flood event in France: A model intercomparison. *Nat. Hazards Earth Syst.*, **5,** 741–754.

Arkin, P.A., 1982: The Relationship Between Interannual Variability in the 200 mb Tropical Wind Field and the Southern Oscillation. *Mon. Wea. Rev.,* **110**, 1393–1404.

Ashok, K., Z. Guan, and T. Yamagata, 2003: Influence of the Indian Ocean Dipole on the Australian winter rainfall, *Geophys. Res. Lett.*, **30**, 1821.

Aspliden, J. P., Y. Tourre, and J. B. Sabine, 1976: Some climatological aspects of West African disturbance lines during GATE, *Mon. Weather Rev.,* **104**, 1029 – 1035.

Atkins, N. T., R. M. Wakimoto, and C. L. Ziegler, 1998: Observations of the finescale structure of a dryline during VORTEX 95. *Mon. Wea. Rev.,* **126**, 525–550.

Ba, M.B. and S.E. Nicholson, 1998: Analysis of Convective Activity and Its Relationship to the Rainfall over the Rift Valley Lakes of East Africa during 1983–90 Using the Meteosat Infrared Channel. *J. Appl. Meteor.,* **37**, 1250–1264.

Baker, M. B., H. J. Christian, and J. Latham, 1995: A computational study of the relationships linking lightning frequency and other thundercloud parameters, *Q. J. R. Meteorol. Soc.,***121**, 1525–1548.

Barnes, S. L., and C. W. Newton, 1986: Thunderstorms in the synoptic setting. *Thunderstorm Morphology and Dynamics,* 2d ed., E. Kessler, Ed., University of Oklahoma Press, 75–112.

Barron, J. A. S., E. Metcalfe, and J. A. Addison, 2012: Response of the North American monsoon to regional changes in ocean surface temperature, *Paleoceanography*, **27**, PA3206, doi:10.1029/2011PA002235.

Beebe, R. G., 1958: An instability line development as observed by the tornado research airplane. *J. Meteor.*, **15**, 278–282.

Benjamin, S. G., and T. N. Carlson, 1986: Some effects of surface heating and topography on the regional severe storm environment. Part I: Three-dimensional simulations. *Mon. Wea. Rev.,* **114**, 307–329.

Bennett, L. J., K. A. Browning, A. M. Blyth, D. J. Parker, and P. A. Clark, 2006: A review of the initiation of precipitating convection in the United Kingdom. *Quart. J. Roy. Meteor. Soc.*, **132,** 1001–1020.

Berbery, E. H., 2001: Mesoscale moisture analysis of the North American monsoon. *J. Climate*, **14**, 121–137, doi:10.1175/ 1520-0442(2001)013,0121:MMAOTN.2.0.CO;2.

Berry, G.J. and C. Thorncroft, 2005: Case Study of an Intense African Easterly Wave. *Mon. Wea. Rev.,* **133**, 752–766, https://doi.org/10.1175/MWR2884.1.

Bieda, S. W., C. L. Castro, S. L. Mullen, A. C. Comrie, and E. Pytlak, 2009: The relationship of transient upper-level troughs to variability of the North American monsoon system. *J. Climate*, **22**, 4213–4227, doi:10.1175/2009JCLI2487.1.

Blanchard D., 1998: Assessing the vertical distribution of CAPE. *Weather and Forecasting,* **13,** 870–877.

Blanchard, D. O., and R. E. Lopez, 1985: Spatial patterns of convection in south Florida. *Mon. Wea. Rev.*, **113**, 1282–1299.

Bluestein, H. B., E. W. McCaul Jr., G. P. Byrd, and G. R. Woodall, 1988: Mobile sounding observations of a tornadic storm near the dryline: The Canadian, Texas storm of 7 May 1986. *Mon. Wea. Rev.,* **116**, 1790–1804.

Boccippio, D. J., W. J. Koshak, and R. J. Blakeslee, 2002: Performance assessment of the Optical Transient Detector and Lightning Imaging Sensor. Part I: Predicted diurnal variability. *J. Atmos. Oceanic Technol.*, **19,** 1318–1332.

Boccippio, D.J., S.J. Goodman, and S. Heckman, 2000: Regional Differences in Tropical Lightning Distributions. *J. Appl. Meteor.,* **39**, 2231–2248.

Bordoni, S., and B. Stevens, 2006: Principal component analysis of the summertime winds over the Gulf of California: A gulf surge index, *Mon. Weather Rev.,* **134**, 3395–3414.

Brenner, I. S., 1974: A surge of maritime tropical air—Gulf of California to the southwestern United States. *Mon. Wea. Rev.,* **102**, 375–389, doi:10.1175/1520-0493(1974)102,0375: ASOMTA.2.0.CO;2.

Brooks, H. E., 2013: Intense thunderstorms and climate change. *Atmos. Res.*, **123**, 129–138, doi:https://doi.org/10.1016/j.atmosres.2012.04.002.

Brooks, H. E., C. A. Doswell III, and M. P. Kay, 2003: Climatological estimates of local daily tornado probability for the United States. *Wea. Forecasting*, **18**, 626–640.

Brooks, H. E., J. W. Lee, and J. P. Craven, 2003: The spatial distribution of intense thunderstorm and tornado environments from global reanalysis data, *Atmos. Res*., **67 – 68**, 73 – 94.

Brown, B. G., and A. H. Murphy, 1996: Verification of aircraft icing forecasts: The use of standard measures and meteorological covariates. Preprints, *13th Conf. on Probability and Statistics in the Atmospheric Sciences,* San Francisco, CA, Amer. Meteor. Soc., 251–252.

Brown, R. G., and C. Zhang, 1997: Variability of midtropospheric moisture and its effect on cloud-top height distribution during TOGA COARE. *J. Atmos. Sci.,* **54**, 2760–2774.

Browning, K. A., and Coauthors, 2007: The Convective Storm Initiation Project. *Bull. Amer. Meteor. Soc.*, **88**, 1939–1955, doi:10.1175/ BAMS-88-12-1939.

Brubaker K. L., Entekhabi D, Eagleson P. S., 1993: Estimation of continental precipitation recycling. *J. Climate*, **6**, 1077–1089.

Burpee, R. W., 1972: Origin and structure of easterly waves in lower troposphere of North Africa. *J. Atmos. Sci.,* **29**, 77–90, doi:10.1175/1520-0469(1972)029,0077:TOASOE.2.0.CO;2.

Burpee, R. W., and L. N. Lahiff, 1984: Area-average rainfall variations on sea-breeze days in south Florida. *Mon. Wea. Rev.,* **112**, 520–534.

Byers, H. R., and H. R. Rodebush, 1948: Causes of thunderstorms of the Florida peninsula. *J. Meteor.*, **5**, 275–280.

Carey, L.D. and K.M. Buffalo, 2007: Environmental Control of Cloud-to-Ground Lightning Polarity in Severe Storms. *Mon. Wea. Rev.,* **135**, 1327–1353.

Carey, L.D., W.A. Petersen, and S.A. Rutledge, 2003: Evolution of Cloud-to-Ground Lightning and Storm Structure in the Spencer, South Dakota, Tornadic Supercell of 30 May 1998. *Mon. Wea. Rev.,* **131**, 1811–1831, https://doi.org/10.1175//2566.1.

Carlson TN, Benjamin SG, Forbes GS. 1983: Elevated mixed layers in the regional severe storm environment: conceptual model and case studies. *Mon. Weather Rev.*, **111**, 1453–1473.

Carlson, T. N., 1969: Some remarks on African disturbances and their progress over tropical Atlantic. *Mon. Wea. Rev.,* **97**, 716–726, doi:10.1175/1520-0493(1969)097,0716:SROADA.2.3.CO;2.

Carlson, T. N., and F. H. Ludlam, 1968: Conditions for the occurrence of severe local storms. *Tellus*, **20,** 203–226.

Cayan, D. R., K. T. Redmond, and L. G. Riddle, 1999: ENSO and hydrologic extremes in the western United States. *J. Clim.*, **12**, 2881–2893, doi:10.1175/1520-0442.

Cecil, D. J., 2009: Passive microwave brightness temperatures as proxies for hailstorms. J. *Appl. Meteor. Climatol.,* **48**, 1281–1286.

Cecil, D. J., and C. B. Blankenship, 2012: Toward a global climatology of severe hailstorms as estimated by satellite passive microwave imagers. *J. Climate*, **25**, 687–703.

Cecil, D. J., and E. J. Zipser, 1999: Relationships between Tropical Cyclone Intensity and Satellite-Based Indicators of Inner Core Convection: 85-GHz Ice-Scattering Signature and Lightning. *Mon. Weather Rev.*, **127**, 103–123, doi:10.1175/1520-0493.

Cecil, D. J., D. E. Buechler, and R. J. Blakeslee, 2014: Gridded lightning climatology from TRMM-LIS and OTD: Dataset description. *Atmos. Res.,* **135–136,** 404–414.

Cecil, D. J., S. J. Goodman, D. J. Boccippio, E. J. Zipser, and S. W. Nesbitt, 2005: Three years of TRMM precipitation features. Part I: Radar, radiometric, and lightning characteristics, *Mon. Weather Rev.*, **133**, 543–566, doi:10.1175/MWR-2876.1.

Cecil, D.J., D.E. Buechler, and R.J. Blakeslee, 2015: TRMM LIS Climatology of Thunderstorm Occurrence and Conditional Lightning Flash Rates. *J. Climate,* **28**, 6536–6547, https://doi.org/10.1175/JCLI-D-15-0124.1

Chaggar, T. S., 1977: Geographical Distribution of Monthly and Annual Mean Frequency of Thunderstorm Days Over Eastern Africa. East African Meteorological Department. Nairobi: Tech. Memo. No. 26, pp. 1-22.

Christian, H. J., et al., 2003: frequency and distribution of lightning as observed from space by the Optical Transient Detector, *J. Geophys. Res.,* **108(**D1**)**, 4005, doi:10.1029/2002JD002347.

Cotton, W. R., M. S. Lin, R. L. McAnelly, and C. J. Tremback, 1989: A composite model of mesoscale convective complexes. *Mon. Wea. Rev.,* **117**, 765–783.

Cotton, W. R., R. L. George, P. J. Wetzel, and R. L. McAnelly, 1983: A long-lived mesoscale convective complex. Part I: The mountain-generated component. *Mon. Wea. Rev.*, **111,** 1893–1918.

Courtier, P., J-N. Thépaut, and A. Hollingsworth, 1994: A strategy for operational implementation of 4D-Var, using an incremental approach. *Quart. J. Roy. Meteor. Soc*, **120,** 1367–1387.

Craven, J., R. Jewell, and H. Brook, 2002: Comparison between observed convective cloud-base heights and lifting condensation level for two different lifted parcels. *Wea. Forecasting*, **17,** 885–890.

Dai, A., and T. M. L. Wigley, 2000: Global patterns of ENSO induced precipitation. *Geophys. Res. Lett.*, **27,** 1283–1286.

Davies, J. M., 2004: Estimations of CIN and LFC associated with tornadic and non-tornadic supercells. *Wea. Forecasting*, **19,** 714–726.

Dee, D. P., et al., 2011: The ERA-Interim reanalysis: Configuration and performance of the data assimilation system, *Q. J. R. Meteorol. Soc*., **137(656)**, 553–597, doi:10.1002/qj.828.

Diaz, L., M. Martinez, J. Ramírez, and J. Rodriguez, 2009: Actualización de la actividad de rayos en Venezuela, empleando la información del proyecto satelital de la NASA. *Congreso Venezolano de Redes y Energía Eléctrica,* Porlamar, Venezuela, Comité Nacional Venezolano de CIGRÉ, B2-223.

Diffenbaugh, N. S., M. Scherer, and R. J. Trapp, 2013: Robust increases in intense thunderstorm environments in response to greenhouse forcing. *Proc. Natl. Acad. Sci. USA*, **110,** 16 361–16 366, doi:10.1073/pnas.1307758110.

Done, J. M., G. C. Craig, S. L. Gray, P. A. Clark, and M. E. B. Gray, 2006: Mesoscale simulations of organized convection: Importance of convective equilibrium. *Quart. J. Roy. Meteor. Soc.*, **132,** 737–756.

Doswell III, C. A., 1984: A kinematic analysis of frontogenesis associated with a nondivergent vortex.*J. Atmos. Sci.*, **41,** 1242–1248.

Doswell III, C. A., 2001: Severe convective storms—An overview. *Severe Convective Storms, Meteor. Monogr.,* No. 50, Amer. Meteor. Soc., 1–26.

Doswell III, C. A., and J. S. Evans, 2003: Proximity sounding analysis for derechos and supercells: An assessment of similarities and differences. *Atmos. Res.*, **67–68,** 117–133.

Doswell, C. A., III, and E. N. Rasmussen, 1994: The effect of neglecting the virtual temperature correction on CAPE calculations. *Wea. Forecasting*, **9**, 625–629.

Doswell, C.A., H.E. Brooks, and R.A. Maddox, 1996: Flash Flood Forecasting: An Ingredients-Based Methodology. *Wea. Forecasting,* **11**, 560–581.

Douglas, M. W., R. Maddox, K. Howard, and S. Reyes, 1993: The Mexican monsoon. *J. Climate*, **6**, 1665–1667.

Droegemeier, K.K. and R.B. Wilhelmson, 1985: Three-Dimensional Numerical Modeling of Convection Produced by Interacting Thunderstorm Outflows. Part I: Control Simulation and Low-Level Moisture Variations. *J. Atmos. Sci.,* **42**, 2381–2403.

Duran-Quesada, A. M., M. Reboita, and L. Gimeno, 2012: Precipitation in tropical America and the associated sources of moisture: A short review, *Hydrol. Sci. J.,* **57(4),** 612–624.

Durkee JD, Mote TL., 2009: A climatology of warm-season mesoscale convective complexes in subtropical South America. *Int. J. Climatol.* **30**, 418–431, doi: 10.1002/joc.1893.

Emanuel, K. A., 1994: *Atmospheric Convection*, Oxford Univ. Press, N. Y.

Erfani, E., and D. Mitchell, 2014: A partial mechanistic understanding of the North American monsoon, *J. Geophys. Res. Atmos.,* **119**, 13,096–13,115, doi:10.1002/ 2014JD022038

Feng, Z., L. R. Leung, S. Hagos, R. A. Houze, C. D. Burleyson, and K. Balaguru, 2016: More frequent intense and long-lived storms dominate the springtime trend in central US rainfall. *Nat. Commun.*, **7**, 13429.

Fierro, A. O., J. Gao, C. L. Ziegler, E. R. Mansell, D. R. MacGorman, and S. R. Dembek, 2014: Evaluation of a cloud-scale lightning data assimilation technique and a 3DVAR method for the analysis and short-term forecast of the 29 June 2012 derecho event. *Mon. Wea. Rev.*, **142**, 183–202, doi:https://doi.org/10.1175/MWR-D-13-00142.1.

Finch, Z. O., and R. H. Johnson, 2010: Observational analysis of an upper-level inverted trough during the 2004 North American monsoon experiment. *Mon. Wea. Rev.,* **138**, 3540–3555, doi:10.1175/2010MWR3369.1.

Fink, A. H., and A. Reiner, 2003: Spatiotemporal variability of the relation between African Easterly Waves and West African squall lines in 1998 and 1999. *J. Geophys. Res.,* **108,** 4332, doi:10.1029/2002JD002816.

Foote, G. B., and C. G. Mohr, 1979: Results of a randomized hail suppression experiment in northeast Colorado. Part VI: Post hoc stratification by storm type and intensity. *J. Appl. Meteor*, **18,** 1589–1600.

Frank, W. M., 1978: The life cycles of GATE convective systems. *J. Atmos. Sci.,* **35**, 1256–1264

Fujita, T., 1958: Structure and movement of a dry front. *Bull. Amer. Meteor. Soc.,* **39**, 574–582.

Fulks, J. R., 1951: The instability line. *Compendium of Meteorology,* T. F. Malone, Ed., Amer. Meteor. Soc., 647–652.

Gallus, W.A., J. Correia, and I. Jankov, 2005: The 4 June 1999 Derecho Event: A Particularly Difficult Challenge for Numerical Weather Prediction. *Wea. Forecasting,* **20**,705–728.

Gershunov, A., 1998: ENSO influence on intraseasonal extreme rainfall and temperature frequencies in the contiguous United States: Implications for long-range predictability. *J. Clim.*, **11**, 3192–3203, doi:10.1175/1520-0442.

Glass, F. H., D. L. Ferry, J. T. Moore, and S. M. Nolan, 1995: Characteristics of heavy convective rainfall events across the mid-Mississippi valley during the warm season: Meteorological conditions and a conceptual model. Preprints, *14th Conf. on Weather Analysis and Forecasting,* Dallas, TX, Amer. Meteor. Soc., 34–41.

Green, C. R., and W. D. Sellers, Eds., 1964: Arizona Climate. Tucson University of Arizona Press, 503 pp.

Guy, N., and S. A. Rutledge, 2012: Regional comparison of West African convective characteristics: A TRMM-based climatology. *Quart. J. Roy. Meteor. Soc.,* **138**, 1179–1195, doi:10.1002/qj.1865.

Hales, J. E., 1972: Surges of maritime tropical air northward over the Gulf of California. *Mon. Wea. Rev.*, **100**, 298–306.

Hamada, A. and Y.N. Takayabu, 2016: Improvements in Detection of Light Precipitation with the Global Precipitation Measurement Dual-Frequency Precipitation Radar (GPM DPR). *J. Atmos. Oceanic Technol.,* **33**, 653–667.

Hamid, E. Y., Z.-I. Kawasaki, and R. Mardiana, 2001: Impact of the 1997 – 98 El Nin˜o event on lightning activity over Indonesia, *Geophys. Res. Lett*., **28(1),** 147 – 150, doi:10.1029/2000GL011374.

Hane, C. E., H. B. Bluestein, T. M. Crawford, M. E. Baldwin, and R. M. Rabin. 1997: Severe thunderstorm development in relation to along-dryline variability: A case study. *Mon. Wea. Rev.*, **125**, 231–251.

Higgins, R. W., Y. Yao, and X. L. Wang, 1997: Influence of the North American monsoon system on the U.S. summer precipitation regime. *J. Climate*, **10**, 298–306, doi:10.1175/1520-0442(1997)010,2600: IOTNAM.2.0.CO;2.

Hill, K. J., A. S. Taschetto, and M. H. England, 2011: Sensitivity of South American summer rainfall to tropical Pacific Ocean SST anomalies. *Geophys. Res. Lett.*, **38**, L01701.

Hoch, J., and P. Markowski, 2005: A climatology of springtime dryline position in the U.S. Great Plains region. *J. Climate*, **18**, 2132–2137.

Holton, J. R., 1979: *An Introduction to Dynamic Meteorology*. 3rd ed. Academic Press, 507 pp.

Hou, A. Y., R. K. Kakar, S. Neeck, A. A. Azarbarzin, C. D. Kummerow, M. Kojima, R. Oki, K. Nakamura, and T. Iguchi, 2014: The Global Precipitation Measurement mission, *Bull. Am. Meteorol. Soc.,* **95**, 701–722.

Houze Jr., R. A., 1989: Observed structure of mesoscale convective systems and implications for large-scale heating. *Quart. J. Roy. Meteor. Soc.*, **115,** 425–461.

Houze, R. A., 1993: *Cloud Dynamics.* Academic Press, 573 pp.

Houze, R. A., D. C. Wilton, and B. F. Smull, 2007: Monsoon convection in the Himalayan region as seen by the TRMM Precipitation Radar. *Quart. J. Roy. Meteor. Soc.,* **133,** 1389–1411, doi:10.1002/ qj.106.

Houze, R. A., Jr., K. L. Rasmussen, M. D. Zuluaga, and S. R. Brodzik 2015: The variable nature of convection in the tropics and subtropics: A legacy of 16 years of the Tropical Rainfall Measuring Mission satellite, *Rev. Geophys.,* **53**, doi:10.1002/2015RG000488.

Huntrieser, H., H. H. Schiesser, W. Schmid, and A. Waldvogel, 1997: Comparison of traditional and newly developed thunderstorm indices for Switzerland. *Wea. Forecasting*, **12**, 108–125.

Iguchi, T., T. Kozu, J. Kwiatkowski, R. Meneghini, J. Awaka, and K. Okamoto, 2009: Uncertainties in the rain profiling algorithm for the TRMM precipitation radar. *J. Meteor. Soc. Japan*, **87**,1 1-30.

Iguchi, T., T. Kozu, R. Meneghini, J. Awaka, and K. Okamoto, 2000: Rain-profiling algorithm for the TRMM precipitation radar. *J. Appl. Meteor.*, **39**, 2038-2052.

Jackson, B., S. E. Nicholson, and D. Klotter, 2009: Mesoscale convective systems over western equatorial Africa and their relationship to large-scale circulation. *Mon. Wea. Rev.,* **137**, 1272–1294, doi:10.1175/2008MWR2525.1.

Johns, R. H., and C. A. Doswell III, 1992: Severe local storms forecasting. *Wea. Forecasting*, **7**, 588–612.

Johns, R.H., 1982: A Synoptic Climatology of Northwest Flow Severe Weather Outbreaks. Part I: Nature and Significance. *Mon. Wea. Rev.,* **110**, 1653–1663.

Johnson, R. H., P. E. Ciesielski, and J. A. Cotturone, 2001: Multiscale variability of the atmospheric mixed layer over the western Pacific warm pool. *J. Atmos. Sci.,* **58**, 2729–2750.

Johnson, R. H., P. E. Ciesielski, B. D. McNoldy, P. J. Rogers, and R. K. Taft (2007), Multiscale variability of the flow during the North American Monsoon Experiment, *J. Clim.,* **20,** 1628–1648

Jong, B.-T., M. Ting, and R. Seager, 2016: El Niño impact on California precipitation: Seasonality, regionality, and El Niño intensity. *Environ. Res. Lett.*, **11**, 054021, doi:https://doi.org/10.1088/1748-9326/11/5/054021.

Julian, P.R. and R.M. Chervin, 1978: A Study of the Southern Oscillation and Walker Circulation Phenomenon. *Mon. Wea. Rev.,* **106**, 1433–1451, https://doi.org/10.1175/1520-0493.

Kain, J.S., M.C. Coniglio, J. Correia, A.J. Clark, P.T. Marsh, C.L. Ziegler, V. Lakshmanan, S.D. Miller, S.R. Dembek, S.J. Weiss, F. Kong, M. Xue, R.A. Sobash, A.R. Dean, I.L. Jirak, and C.J. Melick, 2013: A Feasibility Study for Probabilistic Convection Initiation Forecasts Based on Explicit Numerical Guidance. *Bull. Amer. Meteor. Soc.,* **94**,1213–1225, https://doi.org/10.1175/BAMS-D-11-00264.1.

Kaltenböck, R., G. Diendofer, and N. Dotzek, 2009: Evaluation of thunderstorm indices from ECMWF analyses, lightning data and intense storms reports. *Atmos. Res.*, **93**, 381–396.

Kiem, A. S., and S. W. Franks, 2001: On the identification of ENSO-induced rainfall and runoff variability: A comparison of methods and indices, *Hydrol. Sci. J.*, **46**, 715–727.

Kiem, A. S., and S. W. Franks, 2004: Multidecadal variability of drought risk, eastern Australia. *Hydrol. Processes*, **18,** 2039–2050.

Kiladis, G. N., and H. F. Diaz, 1989: Global climate anomalies associated with extremes in the Southern Oscillation. *J. Climate*, **2**, 1069–1090.

Koren, I., O. Altaratz, L. A. Remer, G. Feingold, J. Vanderlei Martins, and R. H. Heiblum, 2012: Aerosol-induced intensification of rain from the tropics to the midlatitudes, Nat. Geosci., 5, 118–122, doi:10.1038/ngeo1364

Kummerow, C., W. Barnes, T. Kozu, J. Shiue, and J. Simpson, 1998: The Tropical Rainfall Measuring Mission (TRMM) Sensor Package, *J. Atmos. Oceanic Technol.*, **15**, 809–817.

Kunkel, K. E., and Coauthors, 2013: Monitoring and understanding trends in extreme storms: State of knowledge. *Bull. Amer. Meteor. Soc.,* **94,** 499–514.

Lafore, J.-P., and Coauthors, 2011: Progress in understanding of weather systems in West Africa. *Atmos. Sci. Lett.*, **12**, 7–12, doi:10.1002/asl.335.

Laing, A. G. and J. G. Fritsch. 1997. The global population of mesoscale convective complexes. *Quart. J. Roy. Meteor. Soc*. **123**, 389–405.

Lal, D. M., and S. D. Pawar, 2009: Relationship between rainfall and lightning over central Indian region in monsoon and premonsoon seasons. *Atmos. Res.,* **92**, 402–410, doi:10.1016/ j.atmosres.2008.12.009.

Lang, T. J., and S. A. Rutledge, 2002: Relationships between convective storm kinematics, precipitation, and lightning. *Mon. Wea. Rev.,* **130**, 2492–2506.

Lee, S. S., 2012: Effect of aerosol on circulations and precipitation in deep convective clouds, *J. Atmos. Sci.,* 69, 1957–1974, doi:10.1175/ JAS-D-11-0111.1.

Leigh, R., and I. Kuhnel, 2001: Hailstorm loss modelling and risk assessment in the Sydney Region, Australia. *Nat. Hazards*, **24**, 171–185, doi:10.1023/A:1011855801345.

Lenters, J.D. and K.H. Cook, 1995: Simulation and Diagnosis of the Regional Summertime Precipitation Climatology of South America. *J. Climate,* **8**, 2988–3005.

Lindzen, R.S. and S. Nigam, 1987: On the Role of Sea Surface Temperature Gradients in Forcing Low-Level Winds and Convergence in the Tropics. *J. Atmos. Sci.,* **44**,2418–2436.

Liu, C. and E.J. Zipser, 2009: "Warm Rain" in the Tropics: Seasonal and Regional Distributions Based on 9 yr of TRMM Data. *J. Climate,* **22**, 767–779.

Liu, C., and E. J. Zipser, 2005: Global distribution of convection penetrating the tropical tropopause. *J. Geophys. Res. Atmos.*, **110**, 1–12, doi:10.1029/2005JD006063.

Liu, C., and E. J. Zipser, 2015: The global distribution of largest, deepest, and most intense precipitation systems. *Geophys. Res. Lett.*, **42**, 3591–3595.

Liu, C., and E. J. Zipser, D. J. Cecil, S. W. Nesbitt, and S. Sherwood, 2008: A cloud and precipitation feature database from nine years of TRMM observations. *J. Appl. Meteorol. Climatol.*, **47**, 2712–

2728, doi:10.1175/2008JAMC1890.1.

Liu, C., and E. Zipser, 2005: Global distribution of convection penetrating the tropical tropopause, *J. Geophys. Res.,* **110,** D23210, doi:10.1029/ 2005JD00006063.

Liu, C., D. J. Cecil, E. J. Zipser, K. Kronfeld, and R. Robertson 2012: Relationships between lightning flash rates and radar reflectivity vertical structures in thunderstorms over the tropics and subtropics, *J. Geophys. Res.,* **117**, D06212, doi:10.1029/2011JD017123.

Liu, C., E.J. Zipser, and S.W. Nesbitt, 2007: Global Distribution of Tropical Deep Convection: Different Perspectives from TRMM Infrared and Radar Data. *J. Climate,* **20**,489–503,

Liu, N. and C. Liu, 2018: Synoptic Environments and Characteristics of Convection Reaching the Tropopause over Northeast China. *Mon. Wea. Rev.,* **146**, 745–759.

Liu, N., and C. Liu, 2016: Global distribution of deep convection reaching tropopause in 1 year GPM observations. *J. Geophys. Res.*, **121**, 3824–3842, doi:10.1002/2015JD024430.

Lopez, M. E., 1966: Cloud seeding trials in the rainy belt of western Colombia, *Water Resour. Res.*, **2**, 811–823.

Lyon, B. and A.G. Barnston, 2005: ENSO and the Spatial Extent of Interannual Precipitation Extremes in Tropical Land Areas. *J. Climate,* **18**, 5095–5109.

MacGorman, D. R., and D. W. Burgess, 1994: Positive cloud-to-ground lightning in tornadic storms and hailstorms. *Mon. Wea. Rev.,* **122**, 1671– 1697.

MacGorman, D. R., and W. D. Rust, 1998: *The Electrical Nature of Storms*. Oxford University Press, 422 pp.

Maddox, R. A., 1983: Large-scale meteorological conditions associated with midlatitude, mesoscale convective complexes. *Mon. Wea. Rev.,* **111**, 1475–1493.

Maddox, R.A., 1976: An Evaluation of Tornado Proximity Wind and Stability Data. *Mon. Wea. Rev.,* **104**, 133–142.

Mapes, B. E., 1997: Equilibrium vs. activation control of large-scale variations of tropical deep convection. *The Physics and Parameterization of Moist Atmospheric Convection,* R. K. Smith, Ed., Kluwer Academic, 321–358.

Mapes, B. E., and R. A. Houze, 1993: Cloud Clusters and Superclusters over the Oceanic Warm Pool. *Mon. Weather Rev.*, **121**, 1398–1416, doi:10.1175/1520-0493.

Mapes, B., 1998: The large-scale part of tropical mesoscale convective system circulations. *Journal of the Meteorological Society of Japan Series II*, **76**, 29–55.

Mapes, B.E., T.T. Warner, M. Xu, and A.J. Negri, 2003: Diurnal Patterns of Rainfall in Northwestern South America. Part I: Observations and Context. *Mon. Wea. Rev.,* **131**,799–812, https://doi.org/10.1175/1520-0493(2003)131<0799:DPORIN>2.0.CO;2

Marengo, J. A., W. R. Soares, C. Saulo, and M. Nicolini, 2004: Climatology of the low level jet east of the Andes as derived from the NCEP–NCAR reanalyses: Characteristics and temporal variability. *J. Climate,* **17**, 2261–2280.

Mazur, R. J., J. F. Weaver, and T. H. Vonder Haar, 2009: A preliminary statistical study of correlations between inflow feeder clouds, supercell or multicell thunderstorms, and severe weather. *Wea. Forecasting,* **24**, 921–934.

McBride, J. L., and N. Nicholls, 1983: Seasonal relationships between Australian rainfall and the Southern Oscillation. *Mon. Wea. Rev.,***111,** 1998–2004.

McCarthy, J., 1974: Field verification of the relationship between entrainment rate and cumulus cloud diameter. *J. Atmos. Sci.*, **31**, 1028–1039.

McCarthy, J., and S. E. Koch, 1982: The evolution of an Oklahoma dryline. Part I: A meso- and subsynoptic-scale analysis. *J. Atmos. Sci.*, **39**, 225–236.

McCollum, D., R. Maddox, and K. Howard, 1995: Case study of a severe mesoscale convective system in central Arizona. *Wea. Forecasting*, **10**, 643–665.

McNulty, R. P., 1978: On upper tropospheric kinematics and severe weather occurrence. *Mon. Wea. Rev.,***106,** 662–672.

Mecikalski, J.R., J.K. Williams, C.P. Jewett, D. Ahijevych, A. LeRoy, and J.R. Walker, 2015: Probabilistic 0–1-h Convective Initiation Nowcasts that Combine Geostationary Satellite Observations and Numerical Weather Prediction Model Data. *J. Appl. Meteor. Climatol.,* **54**, 1039–1059.

Meißner, C., N. Kalthoff, M. Kunz, G. Adrian, 2007: Initiation of shallow convection in the Black Forest mountains. *Atmos. Res.,* **86,** 42–60.

Mekonnen, A., C.D. Thorncroft, and A.R. Aiyyer, 2006: Analysis of Convection and Its Association with African Easterly Waves. *J. Climate,* **19**, 5405–5421,https://doi.org/10.1175/JCLI3920.1

Meyers, G., P. McIntosh, L. Pigot, and M. Pook, 2007: The Years of El Niño, La Niña, and Interactions with the Tropical Indian Ocean. *J. Climate,* **20**, 2872–2880.

Miller, D. and J.M. Fritsch, 1991: Mesoscale Convective Complexes in the Western Pacific Region. *Mon. Wea. Rev.,* **119**, 2978–2992, https://doi.org/10.1175/1520-0493(1991)119<2978:MCCITW>2.0.CO;2

Miller, R., 1972: Notes on analysis and severe-storm forecasting procedures of the Air Force Global Weather Center. Air Weather Service Tech. Rep. 200, rev. ed. Air Weather Service, Scott Air Force Base, IL, 184 pp.

Miller, S. T. K., B. D. Keim, R. W. Talbot, and H. Mao, 2003: Sea breeze: Structure, forecasting, and impacts, *Rev. Geophys.,* **41**, 1011, doi:10.1029/2003RG000124, 3.

Mitchell, E. D., S. V. Vasiloff, G. J. Stumpf, A. Witt, M. D. Eilts, J. T. Johnson, and K. W. Thomas, 1998: The National Severe Storms Laboratory tornado detection algorithm. *Wea. Forecasting*, **13**, 352–366.

Mohr, K. I. and C. D., Thorncroft, 2006: Intense convective systems in West Africa and their relationship to the African easterly jet. *Q.J.R. Meteorol. Soc.,* **132:** 163-176. doi:10.1256/qj.05.55.

Mohr, K. I., and E. J. Zipser, 1996: Defining mesoscale convective systems by their ice scattering signature, *Bull. Am. Meteorol. Soc.,* **77,** 1179–1189.

Mohr, K. I., J. Molinari, and C. D. Thorncroft, 2009: The interannual stability of cumulative frequency distributions for convective system size and intensity. *J. Clim.*, **22**, 5218–5231, doi:10.1175/2009JCLI2940.1.

Mohr, K. I., J. S. Famiglietti, and E. J. Zipser, 1999: The Contribution to Tropical Rainfall with respect to Convective System Type, Size, and Intensity Estimated from the 85-GHz Ice-Scattering Signature. *J. Appl. Meteorol.*, **38**, 596–606, doi:10.1175/1520-0450.

Mohr, K.I. and E.J. Zipser, 1996: Mesoscale Convective Systems Defined by Their 85-GHz Ice Scattering Signature: Size and Intensity Comparison over Tropical Oceans and Continents. *Mon. Wea. Rev.,* **124**, 2417–2437.

Moncrieff, M.W., Miller, M., 1976: The dynamics and simulation of tropical cumulonimbus and squall lines. *Q. J. R. Meteorol. Soc*. **102**, 373–394.

Moore, J.T., F.H. Glass, C.E. Graves, S.M. Rochette, and M.J. Singer, 2003: The Environment of Warm-Season Elevated Thunderstorms Associated with Heavy Rainfall over the Central United

States. *Wea. Forecasting,* **18**, 861–878, https://doi.org/10.1175/1520-0434(2003)018<0861:TEOWET>2.0.CO;2

Murakami, T., 1987: Effects of the Tibetan Plateau. *Monsoon Meteorology,* C.-P. Chang and T. N. Krishnamurti, Eds., Oxford University Press, 235–270.

Murphy, A. H., 1977: The value of climatological, categorical and probabilistic forecasts in the cost–loss ratio situation. *Mon. Wea. Rev.*, **105**, 803–816.

Nascimento, E. L., and C. A. Doswell III, 2006: The need for an improved documentation of severe thunderstorms and tornadoes in South America. *Symp. on the Challenges of Severe Convective Storms,*Atlanta, GA, Amer. Meteor. Soc., P1.18.

Nesbitt, S. W., and E. J. Zipser, 2000: A census of precipitation features in the tropics using TRMM: Radar, ice scattering, and lightning observations. *J. Clim.*, **13**, 4087–4106, doi:10.1175/1520-0442.

Nesbitt, S. W., R. Cifelli, and S. A. Rutledge, 2006: Storm morphology and rainfall characteristics of TRMM precipitation features. *Mon. Wea. Rev.,* **134,** 2702–2721.

Nesbitt, S.W. and E.J. Zipser, 2003: The Diurnal Cycle of Rainfall and Convective Intensity according to Three Years of TRMM Measurements. *J. Climate,* **16**, 1456–1475.

Newman, A. J., and R. H. Johnson, 2012: Mechanisms for precipitation enhancement in a North American monsoon upper-tropospheric trough. *J. Atmos. Sci.*, **69**, 1775–1792, doi:10.1175/JAS-D-11-0223.1.

Newman, A.J. and R.H. Johnson, 2013: Dynamics of a Simulated North American Monsoon Gulf Surge Event. *Mon. Wea. Rev.,* **141**, 3238–3253,https://doi.org/10.1175/MWR-D-12-00294.1

Newton, C. W., 1963: Dynamics of severe convective storms. *Severe Convective Storms, Meteor. Monogr.*, **No. 27**, Amer. Meteor. Soc., 33–58.

Nicholls, M. E., R. A. Pielke, and W. R. Cotton, 1991: A two-dimensional numerical investigation of the interaction between sea breezes and deep convection over the Florida peninsula. *Mon. Wea. Rev.*, **119**, 298–323.

Nicholls, S. D., and K. I. Mohr, 2010: An analysis of the environments of intense convective systems in West Africa in 2003. *Mon. Wea. Rev.,* **138**, 3721–3739.

Nicholson, S. E., 1996: A review of climate dynamics and climate variability in Eastern Africa. *The Limnology, Climatology and Paleoclimatology of the East African Lakes,* T. C. Johnson and E. O. Odada, Eds., Gordon and Breach, 25–56.

Nicholson, S. E., 2009: A revised picture of the structure of the "monsoon" and land ITCZ over West Africa. *Climate Dyn.,* **32**, 1155–1171, doi:10.1007/s00382-008- 0514-3.

Nicholson, S. E., and J. P. Grist, 2003: The seasonal evolution of the atmospheric circulation over West Africa and equatorial Africa. *J. Climate*, **16**, 1013–1030, doi:10.1175/1520-0442(2003)0162.0.CO;2.

Nicholson, S.E., 2018: The ITCZ and the Seasonal Cycle over Equatorial Africa. *Bull. Amer. Meteor. Soc.,* **99**, 337–348.

Nieto Ferreira, R., T. M. Rickenbach, D. L. Herdies, and L. M. V. Carvalho, 2003: Variability of South American convective cloud systems and tropospheric circulation during January– March 1998 and 1999. *Mon. Wea. Rev.,* **131**, 961–973.

Orville, R.E. and R.W. Henderson, 1986: Global Distribution of Midnight Lightning: September 1977 to August 1978. *Mon. Wea. Rev.,* **114**, 2640–2653.

Parker DJ, Thorncroft CD, Burton RR, Diongue-Niang A. 2005. Analysis of the African easterly jet, using aircraft observations from the JET2000 experiment. *Q. J. R. Meteorol. Soc*. **131**, 1461–1482.

Parker, D. J., 2002: The response of CAPE and CIN to tropospheric thermal variations. *Quart. J. Roy. Meteor. Soc.*, **128**, 119–130.

Pessi, A. T., and S. Businger, 2009: Relationships among lightning, precipitation, and hydrometeor characteristics over the North Pacific Ocean, *J. Appl. Meteorol. Climatol.*, **48**, 833–848, doi:10.1175/2008JAMC1817.1.

Petersen, W. A., H. J. Christian, and S. A. Rutledge, 2005: TRMM observations of the global relationship between ice water content and lightning, *Geophys. Res. Lett.*, **32**, L14819, doi:10.1029/2005GL023236.

Petersen, W. A., S. A. Rutledge, and R. E. Orville, 1996: Cloud-to-ground lightning observations from TOGA COARE: Selected results and lightning location algorithms. *Mon. Wea. Rev.*, **124,** 602–620.

Peterson, R. E., 1983: The west Texas dryline: Occurrence and behavior. Preprints, 13th Conf. Severe Local Storms, Tulsa, OK, *Amer. Meteor. Soc*., J9–J11.

Pielke, R. A., A. Song, P. J. Michaels, W. A. Lyons, and R. W. Arritt, 1991: The predictability of sea-breeze generated thunderstorms. *Atmosfera*, **4**, 65–78.

Pierce, E. T., 1958: Some topics in atmospheric electricity. *Recent Advances in Atmospheric Electricity,*Pergamon, 5–16.

Poveda, G., and O. J. Mesa, 2000: On the existence of Lloro (the rainiest locality on Earth): Enhanced ocean-atmosphere-land interaction by a low-level jet, *Geophys. Res. Lett*., **27**, 1675–1678.

Poveda, G., P. R. Waylen, and R. S. Pulwarty, 2006: Annual and inter-annual variability of the present climate in northern South America and southern Mesoamerica. *Palaeogeogr. Palaeoclimatol. Palaeoecol.*, **234,** 3–27.

Power, S. B., F. Tseitkin, S. Torok, B. Lavery, R. Dahni, and B. McAvaney, 1998: Australian temperature, Australian rainfall and the Southern Oscillation, 1910–1992: Coherent variability and recent changes. *Aust. Meteor. Mag.*, **47,** 85–101.

Price, C., Y. Yair, and M. Asfur, 2007: East African lightning as a precursor of Atlantic hurricane activity*, Geophys. Res. Lett.*, **34**, L09805, doi:10.1029/2006GL028884.

Qie, X., R. Toumi, and T. Yuan, 2003: Lightning activities on the Tibetan Plateau as observed by the Lightning Imaging Sensor. *J. Geophys. Res.*, **108**, 4551, doi:10.1029/2002JD003304.

Qie, X., X. Wu, T. Yuan, J. Bian, and D. Lu, 2014: Comprehensive pattern of deep convective systems over the Tibetan Plateau–South Asian monsoon region based on TRMM data. *J. Climate*, **27**, 6612–6626, doi:https://doi.org/10.1175/JCLI-D-14-00076.1.

Ranalkar, M., and H. Chaudhari, 2009: Seasonal variation of lightning activity over the Indian subcontinent. *Meteor. Atmos. Phys.,* **104**, 125–134, doi:10.1007/s00703-009-0026-7.

Rasmussen, E. N., and D. O. Blanchard, 1998: A baseline climatology of sounding-derived supercell and tornado forecast parameters. *Wea. Forecasting*, **13,** 1148–1164.

Rasmussen, K. L., and R. A. Houze, 2011: Orogenic convection in subtropical South America as seen by the TRMM satellite. *Mon. Wea. Rev.,* **139**, 2399–2420, doi:10.1175/MWR-D-10-05006.1.

Rasmussen, K. L., M. D. Zuluaga, and R. A. Houze, 2014: Severe convection and lightning in subtropical South America. *Geophys. Res. Lett*., **41**, 7359–7366, doi:10.1002 /2014GL061767.

Rasmussen, K.L. and R.A. Houze, 2016: Convective Initiation near the Andes in Subtropical South America. *Mon. Wea. Rev.,* **144**, 2351–2374.

Rasmusson, E. M., and T. H. Carpenter, 1982: Variations in Tropical Sea Surface Temperature and Surface Wind Fields Associated with the Southern Oscillation/El Niño. *Mon. Weather Rev.*, **110**, 354–384, doi:10.1175/1520-0493.

Rasmusson, E. M., and T. H. Carpenter, 1983: The relationship between the eastern equatorial Pacific sea surface temperatures and rainfall over India and Sri Lanka. *Mon. Wea. Rev.*, **111**, 517–528.

Raymond, D. J., and M. J. Herman, 2011: Convective quasi-equilibrium reconsidered, *J. Adv. Model. Earth Syst.*, **3**, M08003, doi:10.1029/2011MS000079.

Reap, R.M. and D.R. MacGorman, 1989: Cloud-to-Ground Lightning: Climatological Characteristics and Relationships to Model Fields, Radar Observations, and Intense Local Storms. *Mon. Wea. Rev.,* **117**, 518–535.

Reason, C.J., W. Landman, and W. Tennant, 2006: Seasonal to Decadal Prediction of Southern African Climate and Its Links with Variability of the Atlantic Ocean. *Bull. Amer. Meteor. Soc.,* **87**, 941–955, https://doi.org/10.1175/BAMS-87-7-941.

Rhea, J. O., 1966: A study of thunderstorm formation along dry lines. *J. Appl. Meteor.,* **5**, 58– 63.

Risbey, J. S., M. J. Pook, P. C. McIntosh, M. C. Wheeler, and H. H. Hendon, 2009: On the remote drivers of rainfall variability in Australia. Mon. Wea. Rev., 137, 3233–3253.

Roca, R., J. Lafore, C. Piriou, and J. Redelsperger, 2005: Extratropical Dry-Air Intrusions into the West African Monsoon Midtroposphere: An Important Factor for the Convective Activity over the Sahel. *J. Atmos. Sci.,* **62**, 390–407, https://doi.org/10.1175/JAS-3366.1

Rockwood, A. A., and R. A. Maddox, 1988: Mesoscale and synoptic interactions leading to intense convection: The case of 7 June 1982. *Wea. Forecasting,* **3,** 51–68.

Romatschke, U. and R. Houze, 2011: Characteristics of Precipitating Convective Systems in the Premonsoon Season of South Asia. *J. Hydrometeor.,* **12**, 157–180.

Romatschke, U. and R.A. Houze, 2010: Extreme Summer Convection in South America. *J. Climate,* **23**, 3761–3791.

Romatschke, U., S. Medina, and R. A. Houze, 2010: Regional, seasonal, and diurnal variations of extreme convection in the South Asian region, *J. Clim.*, **23**, doi:10.1175/2009JCLI3140.1.

Romero, R., C. Ramis, and V. Homar, 2015: On the intense convective storm of 29 October 2013 in the Balearic Islands: Observational and numerical study, *Q. J. R. Meteorol. Soc.*, **141**, 1208–1222, doi:10.1002/qj.2429.

Ropelewski, C. F., and M. H. Halpert, 1987: Global and regional scale precipitation patterns associated with the El Niño– Southern Oscillation. *Mon. Wea. Rev.,* **115**, 1606–1626.

Ropelewski, C.F. and M.S. Halpert, 1986: North American Precipitation and Temperature Patterns Associated with the El Niño/Southern Oscillation (ENSO). *Mon. Wea. Rev.,* **114**, 2352–2362.

Rosenfeld, D. and W. L. Woodley., 2003: Closing the 50-year circle: From cloud seeding to space and back to climate change through precipitation physics. *Cloud Systems, Hurricanes, and the Tropical Rainfall Measuring Mission (TRMM), Meteor. Monogr.*, No. 51, Amer. Meteor. Soc., 59–80.

Rosenfeld, D., W. L. Woodley, T. W. Krauss, and V. Makitov, 2006: Aircraft microphysical documentation from cloud base to anvils of hailstorm feeder clouds in Argentina. *J. Appl. Meteor. Climatol.,* **45**, 1261–1281.

Saji, H. N., and B. N. Goswami, P. N. Vinayachandran, and T. Yamagata, 1999: A dipole mode in the tropical Indian Ocean. *Nature*, **401**, 360–363.

Sakamoto, M. S., T. Ambrizzi, and G. Poveda, 2011: Moisture sources and life cycle of convective systems over western Colombia, *Adv. Meteorol.,* **2011**, 1–11, doi:10.1155/2011/890759.

Salio, P., M. Nicolini, and E.J. Zipser, 2007: Mesoscale Convective Systems over Southeastern South America and Their Relationship with the South American Low-Level Jet. *Mon. Wea. Rev.,* **135**, 1290–1309.

Sander, J., J. F. Eichner, E. Faust, and M. Steuer, 2013: Rising variability in thunderstorm-related U.S. losses as a reflection of changes in large-scale thunderstorm forcing, *Weather Clim. Soc.*, **5**, 317–331, doi: 10.1175/WCAS-D-12-00023.1.

Sanders, F., 1999: A Short-Lived Cold Front in the Southwestern United States. *Mon. Wea. Rev.,* **127**, 2395–2403, https://doi.org/10.1175/1520-0493(1999)127<2395:ASLCFI>2.0.CO;2

Savenije, H. H. G, 1995: New definitions of moisture recycling and relation with land-use changes in the Sahel. J Hydrol (Amst) 167:57–78. doi:10.1016/0022-1694(94)02632-L

Schaefer, J. T., 1974: The life cycle of the dryline. *J. Appl. Meteor.,* **13**, 444–449.

Schoenberg Ferrier, B., J. Simpson, and W.-K. Tao (1996), Factors responsible for precipitation efficiencies in midlatitude and tropical squall simulations, *Mon. Weather Rev.,* **124**, 2100 – 2125.

Schultz, D.M., C.C. Weiss, and P.M. Hoffman, 2007: The Synoptic Regulation of Dryline Intensity. *Mon. Wea. Rev.,* **135**, 1699–1709, https://doi.org/10.1175/MWR3376.1

Schulz, W., K. Cummins, G. Diendorfer, and M. Dorninger, 2005: Cloud-to-ground lightning in Austria: A 10-year study using data from a lightning location system. *J. Geophys. Res.,* **110**, D09101, doi:10.1029/2004JD005332.

Schumacher, R.S. and R.H. Johnson, 2005: Organization and Environmental Properties of Extreme-Rain-Producing Mesoscale Convective Systems. *Mon. Wea. Rev.,* **133**,961–976, https://doi.org/10.1175/MWR2899.1

Schumacher, R.S., 2015: Sensitivity of Precipitation Accumulation in Elevated Convective Systems to Small Changes in Low-Level Moisture. *J. Atmos. Sci.,* **72**, 2507–2524.

Seluchi, M., and J. Marengo, 2000: Tropical–midlatitude exchange of air masses during summer and winter in South America: Climatic aspects and extreme events. *Int. J. Climatol*, **20,** 1167–1190.

Shaw, B. L., R. A. Pielke, and C. L. Ziegler, 1997: A threedimensional numerical simulation of a Great Plains dryline. *Mon. Wea. Rev.,* **125**, 1489–1506.

Sherwood, S. C., V. T. J. Phillips, and J. S. Wettlaufer, 2006: Small ice crystals and the climatology of lightning, *Geophys. Res. Lett.*, **33**, L05804, doi:10.1029/2005GL025242.

Shrestha, A., and R. Kostaschuk, 2005: El Niño/Southern Oscillation (ENSO)-related variablity in mean-monthly streamflow in Nepal. *J. Hydrol.*, **308**, 33–49.

Simpson J. E., D. A. Mansfield, and J. R. Milford, 1977: Inland penetration of sea-breeze fronts. *Quart. J. Roy. Meteor. Soc.,* **103**, 47–76.

Smith, J. B., et al., 2017: A case study of convectively sourced water vapor observed in the overworld stratosphere over the United States, *J. Geophys. Res. Atmos.*, **122**, 9529– 9554,

Spencer, R. W., and D. A. Santek 1985: Measuring the global distribution of intense convection over land with passive microwave radiometery, *J. Appl. Meteorol.,* **24,** 860–864.

Spencer, R. W., H. M. Goodman, and R. E. Hood, 1989: Precipitation Retrieval over Land and Ocean with the SSM/I: Identification and Characteristics of the Scattering Signal. *J. Atmos. Ocean. Technol.*, **6**, 254–273, doi:10.1175/1520-0426.

Stackpole, J. D., 1967: Numerical analysis of atmospheric soundings. *J. Appl. Meteor.*, **6,** 464–467.

Steenburgh, W. J., and C. F. Mass, 1994: The structure and evolution of a simulated Rocky Mountains lee trough. *Mon. Wea. Rev.* **122**, 2740-2761.

Stensrud, D. J., 2007: *Parameterization Schemes: Keys to Understanding Numerical Weather Prediction Models*. Cambridge University Press, 459 pp.

Stensrud, D. J., 2013: Upscale effects of deep convection during the North American Monsoon, *J. Atmos. Sci*., **70**, 2681–2695.

Stensrud, D. J., R. L. Gall, and M. K. Nordquist, 1997: Surges over the Gulf of California during the Mexican monsoon. *Mon. Wea. Rev.,* **125**, 417–437, doi:10.1175/1520-0493(1997)125,0417: SOTGOC.2.0.CO;2.

Stolz, D. C., S. A. Rutledge, and J. R. Pierce, 2015: Simultaneous influences of thermodynamics and aerosols on deep convection and lightning in the tropics, *J. Geophys. Res. Atmos.*, **120**, 6207–6231.

Stolz, D. C., S. A. Rutledge, J. R. Pierce, and S. C. van den Heever, 2017: A global lightning parameterization based on statistical relationships among environmental factors, aerosols, and convective clouds in the TRMM climatology, *J. Geophys. Res. Atmos.*, 122, 7461–7492.

Takahashi, T., 1978: Riming electrification as a charge generation mechanism in thunderstorms, *J. Atmos. Sci.*, **35**, 1536–1548.

Takemi, T., 2007: A sensitivity of squall-line intensity to environmental static stability under various shear and moisture conditions, *Atmos. Res.,* **84**, 374 – 389, doi:10.1016/j.atmosres.2006.10.001.

Tao, W-K., S-T. Soong, C-H. Sui, B. Ferrier, S. Lang, J. Scala, M-D. Chou, and K. Pickering, 1993: Heating, moisture, and water budgets of tropical and midlatitude squall lines: Comparison and sensitivity to longwave radiation. *J. Atmos. Sci.*, **50,** 673–690.

Tao, W.-K., X. Li, A. Khain, T. Matsui, S. Lang, and J. Simpson, 2007: Role of atmospheric aerosol concentration on deep convective precipitation: Cloud-resolving model simulations, *J. Geophys. Res.,* **112**, D24S18, doi:10.1029/2007JD008728.

Taszarek, M., B. Czernecki, and A. Kozioł, 2015: A Cloud-to-Ground Lightning Climatology for Poland. *Mon. Wea. Rev.,* **143**, 4285–4304, https://doi.org/10.1175/MWR-D-15-0206.1

Tetzlaff G, Peters M. 1988. A composite study of early summer squall lines and their environment over West Africa. *Meteorol. Atmos. Phys*. **38**, 153–163, doi: 10.1007/BF01029779.

Thompson, R.L., C.M. Mead, and R. Edwards, 2007: Effective Storm-Relative Helicity and Bulk Shear in Supercell Thunderstorm Environments. *Wea. Forecasting,* **22**,102–115, https://doi.org/10.1175/WAF969.1

Trenberth K. E., 1999: Atmospheric moisture recycling: role of advection and local evaporation. *J Clim.* **12**, 1368–1381. doi:10.1175/1520-0442(1999)012\1368:AMRROA[2.0.CO;2

Trenberth, K. E., G. W. Branstator, D. Karoly, A. Kumar, N-C. Lau, and C. Ropelewski, 1998: Progress during TOGA in understanding and modeling global teleconnections associated with tropical sea surface temperatures. *J. Geophys. Res.*, **103,** 14291–14324.

Trier, S. B., C. A. Davis, D. A. Ahijevych, M. L. Weisman, and G. H. Bryan, 2006: Mechanisms supporting long-lived episodes of propagating nocturnal convection within a 7-day WRF model simulation. *J. Atmos. Sci.*, **63,** 2437–2461.

Tuttle, J. D., and Carbone, R. E., 2004: Coherent regeneration and the role of water vapor and shear in a long-lived convective episode. *Monthly Weather Review,* **132(1),** 192-208.

Uppala, S. M., D. Dee, S. Kobayashi, and A. Simmons, 2008: Evolution of reanalysis at ECMWF.*Extended Abstracts, Third WCRP Int. Conf. on Reanalysis,* Tokyo, Japan, University of Tokyo, 6 pp.

Ushio, T., S. Heckman, D. J. Boccippio, and H. J. Christian, 2001: A survey of thunderstorm flash rates compared to cloud top height using TRMM satellite data. *J. Geophys. Res.*, **106,** 24089–24095.

Uyeda, H., and Coauthors, 2001: Characteristics of convective clouds observed by a Doppler radar at Naqu on Tibetan Plateau during the GAME-Tibet IOP. *J. Meteor. Soc. Japan*, **79**, 463–474.

van Delden, A., 2001. The synoptic setting of thunderstorms in Western Europe. *Atmos. Res.,* **56**, 89–110.

Velasco I, Frisch M, 1987: Mesoscale convective complexes in the Americas. *J. Geophys. Res.* **92(D8)**, 9591–9613.

Virts KS, and RA Houze., 2016: Seasonal and Intraseasonal Variability of Mesoscale Convective Systems over the South Asian Monsoon Region. *Journal of the Atmospheric Sciences* **73(12):**4753-4774. doi:10.1175/JAS-D-16-0022.1

Virts, K.S., J.M. Wallace, M.L. Hutchins, and R.H. Holzworth, 2013: Highlights of a New Ground-Based, Hourly Global Lightning Climatology. *Bull. Amer. Meteor. Soc.,* **94**,1381–1391.

Walker, G. T., 1925: Correalation in seasonal variations of weather - a further study of world weather. *Mon. Weather Rev.*, **53**, 252–254, doi:10.1175/1520-0493.

Wall, C., E. J. Zipser, and C. Liu, 2014: An investigation of the aerosol indirect effect on convective intensity using satellite observations, J. Atmos. Sci., 71, 430–447.

Wang, B., and H. Rui, 1990: Synoptic climatology of transient tropical intraseasonal convection anomalies: 1975–1985. *Meteor. Atmos. Phys*, **44,** 43–61.

Wang, C., P. J. Crutzen, V. Ramanathan, and S. F. Williams, 1995: The role of a deep convective storm over the tropical Pacific Ocean in the redistribution of atmospheric chemical species. *J. Geophys. Res.*, **100** (D6), 11 509–11 516.

Washington, W. M., and C. L. Parkinson, 2005: An Introduction to Three-dimensional Climate Modeling, Univ. Science Books, Sausalito, Calif.

Webster, P. J., A. Moore, J. Loschnigg, and M. Leban, 1999: Coupled ocean–atmosphere dynamics in the Indian Ocean during 1997–98. *Nature,* **401**, 356–360.

Weisman, M. L., and J. B. Klemp, 1986: Characteristics of isolated convective storms. *Mesoscale Meteorology and Forecasting,* P. S. Ray, Ed., Amer. Meteor. Soc., 331–358.

Weisman, M. L., and R. Rotunno, 2000: The use of vertical wind shear versus helicity in interpreting supercell dynamics. *J. Atmos. Sci.*, **57,** 1452–1472

Weisman, M.L. and J.B. Klemp, 1982: The Dependence of Numerically Simulated Convective Storms on Vertical Wind Shear and Buoyancy. *Mon. Wea. Rev.,* **110**, 504–520.

Weisman, M.L. and R.J. Trapp, 2003: Low-Level Mesovortices within Squall Lines and Bow Echoes. Part I: Overview and Dependence on Environmental Shear. *Mon. Wea. Rev.,* **131**, 2779–2803.

Westermayer, A. T., P. Groenemeijer, G. Pistotnik, R. Sausen, and E. Faust, 2016: Identification of favorable environments for thunderstorms in reanalysis data. *Meteor. Z.*, **26**, 59–70, doi:https://doi.org/10.1127/metz/2016/0754.

Weston, K. J., 1972: The dry-line of Northern India and its role in cumulonimbus convection. *Q.J.R. Meteorol. Soc.,* **98**, 519–531. doi:10.1002/qj.49709841704.

Williams, E. R., 2005: Lightning and climate: A review. *Atmos. Res.*, **76,** 272–287.

Williams, E. R., and S. Stanfill, 2002: The physical origin of the land–ocean contrast in lightning activity. *Comp. Rendus Phys.*, **3,** 1277–1292.

Williams, E. R., C. Cooke, and K. Wright, 1985: Electrical discharge propagation in and around space charge clouds. *J. Geophys. Res.*, **90**, 6059–6070.

Williams, E. R., T. V. Mushtak, D. Rosenfeld, S. Goodman, and D. Boccippio, 2005: Thermodynamic conditions favorable to superlative thunderstorm updraft, mixed phase microphysics and lightning flash rate, *Atmos. Res.*, **76**, 288–306.

Williams, E., and N. Renno, 1993: An analysis of the conditional stability of the tropical atmosphere.*Mon. Wea. Rev.*, **121,** 21–36.

Williams, E., T., Chan, and D., Boccippio, 2004: Islands as miniature continents: Another look at the land-ocean lightning contrast, *J. Geophys. Res.*, **109**, D16206.

Willison, J., W.A. Robinson, and G.M. Lackmann, 2013: The Importance of Resolving Mesoscale Latent Heating in the North Atlantic Storm Track. *J. Atmos. Sci.,* **70**, 2234–2250.

Wilson, J. W., N. A. Crook, C. K. Mueller, J. Sun, and M. Dixon, 1998: Nowcasting thunderstorms: A status report, *Bull. Am. Meteorol. Soc.*, **79**, 2079–2099.

Wolter, K., and M. S. Timlin, 2011: El Niño/Southern Oscillation behaviour since 1871 as diagnosed in an extended multivariate ENSO index (MEI.ext). *Int. J. Climatol.*, **31**, 1074–1087, doi:10.1002/joc.2336.

Xie, S., H. Xu, N.H. Saji, Y. Wang, and W.T. Liu, 2006: Role of Narrow Mountains in Large-Scale Organization of Asian Monsoon Convection. *J. Climate,* **19**, 3420–3429,https://doi.org/10.1175/JCLI3777.1

Xie, S., K. Hu, J. Hafner, H. Tokinaga, Y. Du, G. Huang, and T. Sampe, 2009: Indian Ocean Capacitor Effect on Indo–Western Pacific Climate during the Summer following El Niño. *J. Climate,* **22**, 730–747.

Xu, W., and E. J. Zipser, 2012: Properties of deep convection in tropical continental, monsoon, and oceanic rainfall regimes, *Geophys. Res. Lett*, **39**, doi: 10.1029/2012GL051242.

Xu, W*.,* E. J. Zipser*,* C. Liu*, and* J. Jiang*,* 2010*:* On the relationships between lightning frequency and thundercloud parameters of regional precipitation systems*, J. Geophys. Res.,* **115***, D12203, doi:10.1029/2009JD013385.*

Yamagata, T., S. K. Behera, J.-J. Luo, S. Masson, M. Jury, and S. A. Rao, 2004: Coupled ocean–atmosphere variability in the tropical Indian Ocean. *Earth Climate: The Ocean–Atmosphere Interaction, Geophys. Monogr.*, No. 147, Amer. Geophys. Union, 189– 212.

Yang, X., and T. DelSole, 2012: Systematic comparison of ENSO teleconnection patterns between models and observations. *J. Climate*, **25,** 425–446, doi:10.1175/JCLI-D-11-00175.1.

Yano, J.-I., M. Bister, v. Fuchs, L. Gerard, V. T. J. Phillips, S. Barkidija, and J.-M. Piriou, 2013: Phenomenology of convection-parameterization closure. *Atmos. Chem. Phys.,* **13,** 4111–4131.

Ye, B., A.D. Del Genio, and K.K. Lo, 1998: CAPE Variations in the Current Climate and in a Climate Change. *J. Climate,* **11**, 1997–2015.

Yeo, C. S., 2005: Severe thunderstorms in the Brisbane region and a relationship to the El Niño Southern Oscillation. *Aust. Meteorol. Mag.*, **54**, 197–202.

Yuan, J., and R. A. Houze, 2010: Global variability of mesoscale convective system anvil structure from A-train satellite data. *J. Clim.*, **23**, 5864–5888, doi:10.1175/2010JCLI3671.1.

Zhou, Y., W. K. M. Lau, and C. Liu, 2013: Rain characteristics and large-scale environments of precipitation objects with extreme rain volumes from TRMM observations, *J. Geophys. Res. Atmos.*, **118**, 9673–9689.

Ziegler, C. L., and C. E. Hane, 1993: An observational study of the dryline. *Mon. Wea. Rev.,* **121**, 1134–1151.

Ziegler, C. L., and E. N. Rasmussen, 1998: The initiation of moist convection at the dryline: Forecasting issues from a case study perspective. *Wea. Forecasting*, 13, 1106–1131.

Ziegler, C. L., T. J. Lee, and R. A. Pielke, 1997: Convective initiation at the dryline: A modeling study. *Mon. Wea. Rev.,* **125**, 1001–1026

Zipser, E., C. Liu, D. Cecil, S. W. Nesbitt, and S. Yorty, 2006: Where are the most intense thunderstorms on Earth? *Bull. Am. Meteorol. Soc.,* **87**, 1057–1071.

Zolman, J. L., E. J. Zipser, and K. I. Mohr, 2000: A comparison of tropical mesoscale convective systems in El Nino and La Nina. *J. Clim.*, **13**, 3314–3326, doi:10.1175/1520-0442.

Zuidema, P., 2003: Convective Clouds over the Bay of Bengal. *Mon. Wea. Rev.,* **131**, 780–798, https://doi.org/10.1175/1520-0493(2003)131<0780:CCOTBO>2.0.CO;2

Zuluaga, M., and R. A. Houze, 2015: Extreme convection of the near-equatorial Americas, Africa, and adjoining oceans as seen by TRMM, *Mon. Weather Rev.*, **143**, 298–316.